

UNIVERSIDADE DE SÃO PAULO
INSTITUTO DE GEOCIÊNCIAS

**Intensive (P-T- fO_2) crystallization parameters of Alto Paranaíba
kimberlites and diamond instability: Três Ranchos IV and
Limeira I intrusions**

BRUNA COLDEBELLA

Dissertação apresentada ao Programa de
Geociências (Mineralogia e Petrologia) para
obtenção do título de Mestre em Ciências.

Área de Concentração: Petrologia Ígnea e
Metamórfica

Orientador: Prof. Dr. Rogério Guitarrari
Azzone

SÃO PAULO
2019

Autorizo a reprodução e divulgação total ou parcial deste trabalho, por qualquer meio convencional ou eletrônico, para fins de estudo e pesquisa, desde que citada a fonte.

Serviço de Biblioteca e Documentação do IGc/USP

Ficha catalográfica gerada automaticamente com dados fornecidos pelo(a) autor(a)
via programa desenvolvido pela Seção Técnica de Informática do ICMC/USP

Bibliotecários responsáveis pela estrutura de catalogação da publicação:
Sonia Regina Yole Guerra - CRB-8/4208 | Anderson de Santana - CRB-8/6658

Coldebella, Bruna
Intensive (P-T-fO₂) crystallization parameters
of Alto Paranaíba kimberlites and diamond
instability: Três Ranchos IV and Limeira I
intrusions / Bruna Coldebella; orientador Rogério
Guitarrari Azzone. -- São Paulo, 2019.
198 p.

Dissertação (Mestrado - Programa de Pós-Graduação
em Mineralogia e Petrologia) -- Instituto de
Geociências, Universidade de São Paulo, 2019.

1. Kimberlitos. 2. Província alcalina Alto
Paranaíba. 3. Parâmetros intensivos de cristalização.
4. Fugacidade de Oxigênio. I. Guitarrari Azzone,
Rogério, orient. II. Título.

UNIVERSIDADE DE SÃO PAULO
INSTITUTO DE GEOCIÊNCIAS

**Intensive (P-T-*f*O₂) crystallization parameters of Alto Paranaíba
kimberlites and diamond instability: Três Ranchos IV and
Limeira I intrusions**

BRUNA COLDEBELLA

Orientador: Prof. Dr. Rogério Guitarrari Azzone

Dissertação de Mestrado
Nº 818

COMISSÃO JULGADORA

Dr. Rogério Guitarrari Azzone

Dr^a. Elisa Soares Rocha Barbosa

Dr^a. Fernanda Gervasoni

SÃO PAULO
2019

To my mother, Sandra and
to my husband, Isaac.

ACKNOWLEDGMENTS

I would like to express my special thanks to CAPES and FAPESP for financially supporting the analytical costs (grants 2012/06082-6 and 2017/03768-8) and scholarship (grant 2016/12627-6) involved in this study.

To my advisor, Rogério Guitarrari Azzone, I have no words to express how grateful I am for all your support and for everything that you have taught me since the very first time I walked into your office. Thank you for always being available for help and discussions, and for your patience during my learning process.

I would also like to extend my gratitude to all of the IGc staff who helped me during this study: Vinicius, Zé Paulo, Samuca, Roger, Vasco, Audrey, Isaac, Sônia, and Angélica. In particular, I'd like to thank Marcos and Leandro, who have helped me innumerable times with the mineral chemistry analyses—thank you for all your support and consideration.

Thanks to the wonderful people who welcomed me so dearly at the IGc-USP: professors Renato, Frederico, Excelso, Gergely, Maria Irene, and Gaston; my friends Thereza, Melina, Fabiola, Júlio, Nicholas, Camila, and Dina. Special thanks to Mariana, who was always willing to help and to respond to my emails whenever I had any question.

I would like to dedicate this work to my family, for their unconditional support in every stage of my academic life. To my brother Eduardo, who was the first one to come up with the “why not geology?” idea. Thank you for giving me the best advice that I could ever have received. To my little brother Vitor, who brings so much light and love to my life. And to my mom, thank you for every single thing that you have done for me, thank you for being so understanding whenever I could not come back home: you walked me in every single step of this work and never left me alone. I love you with all my heart.

Finally, I want to express my sincere appreciation to my husband, Isaac, for encouraging me to be better every day. Without you, nothing of this would be possible. Thank you for the happiness you bring to my life, and for being so patient and understanding in my many moments of anxiety. Love you to the moon and back.

“We are all time travelers, traveling together into the future.

But let us make that future a place we want to visit.

Be brave.

Be determined.

Overcome the odds.

It can be done.”

(Stephen Hawking)

RESUMO

Foram estabelecidas as condições de fugacidade de temperatura (T), pressão (P) e fugacidade de oxigênio ($f\text{O}_2$) para os kimberlitos Três Ranchos IV (diamantífero) e Limeira I (LM-I, estéril) do supercampo kimberlítico Coromandel-Três Ranchos (Minas Gerais e Goiás, Brasil), da província alcalina Alto Paranaíba (APAP), com o intuito de determinar uma possível correlação entre tais parâmetros intensivos de cristalização e a instabilidade de diamante daqueles magmas. As intrusões Três Ranchos IV e Limeira I foram classificados como kimberlitos macrocrísticos coerentes, com textura inequigranular evidenciada por megacristais de olivina de até 1 cm parcialmente alterados, macrocristais de flogopita (0.5-10 mm) e xenólitos crustais dispostos em uma matriz muito fina composta principalmente por perovskita, olivina, flogopita, espinélio, serpentina e carbonatos em ambas as intrusões, com adição de apatita, ilmenita e monticelita apenas em LM-I. Macrocrystais de granada e xenocrystais centimétricos de piroxênio e também são fases minerais presentes em Três Ranchos IV e Limeira I, respectivamente. As amostras são todas ricas em MgO, com alto teor de Mg# e são fortemente enriquecidas em elementos incompatíveis.

Concentrações de elementos maiores, menores e traços das principais fases minerais foram obtidas por análises de Microssonda Eletrônica e LA-ICP-MS, com o objetivo de aplicar diferentes geotermo-e-oxibarômetros no cálculo das condições de P-T- $f\text{O}_2$ e caracterizar a variação composicional dos kimberlitos TR-IV e LM-I. Núcleos de olivina de Limeira I apresentam maiores teores de NiO, CaO e menores teores de Cr₂O₃ que os dos cristais de olivina de Três Ranchos IV. O Mg# [(Mg/Mg+FeT), em prop.mol.] calculado a partir das olivinas analisadas varia de 87 a 92 mol.% para TR-IV e de 83 a 92 mol.% para LM-I. O conteúdo de elementos-traço da olivina é semelhante para ambos os kimberlitos, sendo que as concentrações de Li, Zn e Mn parecem ser maiores nas bordas dos cristais de olivina. Nas olivinas das duas intrusões, foram observados tanto um padrão de enriquecimento em Zr, Ga, Nb, Sc, V, P, Al, Ti, Cr, Ca e Mn nas porções de borda, característico do “*melt trend*”, quanto um enriquecimento em Zn, Co, Ni e possivelmente Na nas porções de núcleo, notável no “*mantle trend*”. Os cristais de monticelita de LM-I apresentam Mg # variando de 72 a 93.8 mol.%, com o índice Ca/(Ca + Mg) variando entre 35-58 mol%. A composição dos cristais de perovskita de LM-I e TR-IV analisados permanece próxima do ideal CaTiO₃, mas é notável uma variação dos membros finais dos núcleos (Lop₁₆ e Prv₇₈ médios) às bordas (Lop₁₃ e Prv₈₁ médios) nas amostras de TR-IV. As maiores concentrações de elementos terras raras leves (ETRL), Nb e Fe³⁺ também são observadas nas perovskitas de TR-IV. Os macrocristais de espinélios em amostras de TR-IV

são ricos em Al, enquanto os cristais da matriz variam de magnesiocromita a cromita. Cristais de ilmenita são identificados somente em LM-I, sendo caracterizados pelo alto teor de MgO, com grande variação nas concentrações de Cr₂O₃. As granadas são tipo piropo (62 a 73 mol.%) e estão presentes apenas em TR-IV, com Mg# variando de 72 a 79 mol.%, classificadas como lherzolíticas (G9) e piroxéníticas (G4, G5). O diopsídio ocorre como xenocristais em LM-I e como microfenocristais em TR-IV, com Mg# variando de 85 a 91 mol.% e de 87 a 92 mol.%, respectivamente. Os xenocristais de diopsídio presentes em LM-I apresentam maior concentração de MgO e FeO e são envoltos por coroa de monticelita.

As estimativas de temperatura do kimberlito LM-I foram obtidas utilizando as composições dos xenocristais de diopsídio e as concentrações de Al presentes em cristais de olivina, resultando em um intervalo entre 718 e 985 °C. Enquanto que a pressão varia de 34 a 47 Kbar e foi calculada utilizando uma curva empírica de uma geotermia de 37 mW/m² proposta na literatura para magmas da Província Alcalina do Alto Paranaíba. Para TR-IV foram obtidas temperaturas a partir das concentrações de Al em olivina e de Ni em granada, variando de 975 a 1270 °C. O intervalo de pressão de 18 a 34 Kbar foi obtido a partir da composição dos principais elementos em granada amostrada de TR-IV. A fugacidade de oxigênio registrada em perovskitas (fase cognata de kimberlito) de TR-IV varia de NNO-7 a NNO + 4, e de NNO + 6 a NNO-4 em LM-I. A monticelita, outra fase cognata, também foi utilizada como oxibarômetro, resultando em um intervalo de NNO-4 a NNO + 2 para a intrusão LM-I, onde está presente. Também é notável uma mudança na fugacidade de oxigênio dos núcleos para a borda em perovskitas e em cristais de monticelita. As estimativas de *f*O₂ obtidas neste trabalho foram as primeiras calculadas para magmas da província alcalina do Alto Paranaíba. Todos os resultados de P-T-*f*O₂ obtidos são consistentes com dados da APAP reportados na literatura.

Os xenocristais de clinopiroxênio em LM-I foram classificados como clinopiroxênio de fácies granada de acordo com as composições obtidas neste trabalho. Essa informação, juntamente com os dados de pressão e temperatura, além da presença de Mg-ilmenita em LM-I (conhecido por ser estéril), indica que este magma kimberlítico pode ter ao menos cruzado o campo de estabilidade do diamante, e que é possível que a variação na fugacidade de oxigênio observada em ambos TR-IV e LM-I pode ter-se refletido na instabilidade destes xenocristais nestes magmas, uma vez que Limeira I apresenta condições de oxidação levemente mais altas.

Palavras-chave: Kimberlitos; Província alcalina Alto Paranaíba; Parâmetros intensivos de cristalização; Fugacidade de Oxigênio.

ABSTRACT

Temperature (T), Pressure (P) and Oxygen fugacity ($f\text{O}_2$) conditions were established for the Três Ranchos IV (diamond-bearing) and Limeira I (sterile) kimberlites of the Coromandel-Três Ranchos kimberlite field (Minas Gerais and Goiás, Brazil), Alto Paranaíba Alkaline Province (APAP), in order to draw a possible correlation between these intensive crystallization parameters and diamond instability. Both Três Ranchos IV and Limeira I are classified as coherent macrocrystic kimberlites, with an inequigranular texture formed by partially-to-fully altered olivine, phlogopite megacrysts up to 1 cm wide, macrocrysts (0.5-10 mm-sized), and crustal xenoliths set in a very fine groundmass composed mainly by perovskite, olivine, phlogopite, spinel, serpentine and carbonates identified in both intrusions. Apatite, ilmenite and monticellite are also present, but only in LM-I. Garnet macrocrysts and centimetric pyroxene xenocrysts phases are also present in Três Ranchos IV and Limeira I, respectively. The samples, strongly enriched in incompatible elements, are all MgO-rich, with high Mg# content.

In order to apply different geotherm-and-oxybarometers in the calculation of P-T- $f\text{O}_2$ conditions and to characterize the compositional variation of TR-IV and LM-I kimberlites, major, minor and trace-element concentrations of the main mineral phases were obtained by electron microprobe and LA-ICP-MS. Olivine cores of Limeira I present higher NiO, CaO and lower Cr₂O₃ contents than those from Três Ranchos IV. Mg# [(Mg/Mg+FeT), mol.%) ranges from 87 to 92 mol.% in TR-IV and from 83 to 92 mol.% in LM-I. The trace-element contents of olivine are similar in both kimberlites, the concentrations of Li, Zn and Mn appearing to be higher at olivine rims. In olivines from both intrusions, a pattern of enrichment in Zr, Ga, Nb, Sc, V, P, Al, Ti, Cr, Ca, and Mn in rims regions, is observed in the “melt trend” whereas enrichment in Zn, Co, Ni and possibly Na in cores regions, is found in the “mantle trend.” In monticellite specimens from Limeira I, Mg# ranges from 72 to 93.8, while Ca/(Ca+Mg) ratios range from 35 to 58 mol.%. The perovskite composition in both LM-I and TR-IV remains close to the ideal CaTiO₃, perovskite, but a variation from core endmembers (average Lop₁₆ and Prv₇₈) towards the rims (average Lop₁₃ and Prv₈₁) can be noticed in TR-IV samples. The highest concentrations of light rare earth elements (LREE), Nb, and Fe³⁺ are also observed in perovskites from the TR-IV kimberlite. Macrocrystic spinels of TR-IV kimberlite are Al-rich, whereas the groundmass crystals range from magnesiochromite to chromite. Ilmenites from LM-I are characterized by high MgO values at a given TiO₂, with a large variation in Cr₂O₃. Pyrope garnets (62 to 73 mol.%) are present only in TR-IV, with Mg# ranging from 72 to 79

mol.%, being classified as lherzolitic (G9) and pyroxenitic (G4, G5). Diopside occurs as xenocrysts in LM-I and as microphenocrysts in TR-IV, with Mg# ranging from 85 to 91 and from 87 to 92, respectively. Xenocystic diopsides from LM-I present higher MgO and FeO concentrations with monticellite grains along crystal rims and fractures.

Temperature estimates for the LM-I kimberlite, obtained from the composition of diopside xenocrysts and Al-in olivine concentrations, ranging from 718 to 985 °C. Pressure ranges from 34 to 47 Kbar, as calculated using an empirical curve from a 37-mW/m² geotherm proposed in the literature for Alto Paranaíba magmas. For TR-IV, temperature values ranging from 975 to 1270°C were obtained from Al-in olivine and Ni-in garnet concentrations. Pressures in the range from 18 to 34 Kbar were obtained from major element composition of garnet samples from TR-IV kimberlite. The *f*O₂ of the TR-IV constrained by perovskite (kimberlite cognate phase) oxygen barometry ranges from NNO-7 to NNO+4, while for LM-I values range from NNO+6 to NNO-4. For the LM-I intrusion, monticellite, another cognate phase used as an oxybarometer, yielded a value range of NNO-4 to NNO+2. A change in the oxygen fugacity from cores towards rim recorded in the perovskites and the monticellite crystals is also noticed. The oxygen fugacity estimates of this work are the first ever calculated for magmas of the Alto Paranaíba Alkaline Province. All P-T-*f*O₂ values obtained are consistent with literature data on the APAP.

Clinopyroxene xenocrysts from LM-I were classified as garnet-facies clinopyroxene, according to the compositions obtained in this work. Such results, along with pressure, and temperature data from and the presence of Mg-ilmenite in LM-I (known to be sterile), indicate that the kimberlite magma might have at least crossed the diamond stability field. The variation in oxygen fugacity observed in both kimberlites possibly reflects the instability of diamonds in these magmas since LM-I presents slightly higher oxidation conditions.

Keywords: Kimberlites; Alto Paranaíba Province; Intensive parameters of crystallization, Oxygen Fugacity.

TABLE OF CONTENTS

RESUMO	vii
ABSTRACT	ix
TABLE OF CONTENTS	xi
LIST OF FIGURES	xiii
LIST OF TABLES AND EQUATIONS	xvii
LIST OF APPENDICES	xviii
CHAPTER 1 - INTRODUCTION	1
1.1 Theme Presentation.....	1
1.2 Overview of Kimberlites	3
1.2.1 Mineralogy.....	6
1.2.2 Geochemistry.....	8
1.2.3 Magma generation	10
1.2.4 Pipe formation and models	14
1.2.5 Volatile contents	17
1.3 Research Aims	17
1.4 Study Area Location and Access	18
CHAPTER 2 - MATERIALS AND METHODS	19
2.1 Literature Review	19
2.2 Petrographic Analyses and Imaging	19
2.3 Mineral Chemistry	20
2.3.1 Major and minor element analysis.....	20
2.3.2 Trace element and rare earth element (REE) analysis.....	20
2.4 Whole Rock Geochemistry	22
2.4.1 Major element analyses	22
2.4.2 Trace and rare earth element (REE) analyses.....	22
CHAPTER 3 - BRAZILIAN ALKALINE MAGMATISM	23

3.1	Alto Paranaíba Alkaline Province	23
3.2	Coromandel-Três Ranchos Kimberlitic Field	25
3.2.1	Três Ranchos IV kimberlite	25
3.2.2	Limeira I kimberlite	28
CHAPTER 4 - PETROGRAPHY	29
4.1	Três Ranchos IV	29
4.2	Limeira I.....	33
4.3	Perovskites from Três Ranchos IV and Limeira I.....	36
CHAPTER 5 - MINERAL CHEMISTRY AND GEOCHEMISTRY	42
5.1	Olivine	42
5.2	Monticellite	46
5.3	Perovskite	46
5.4	Spinel.....	48
5.5	Ilmenite.....	48
5.6	Clinopyroxene	53
5.7	Garnet	53
5.8	Bulk Rock Compositions.....	53
5.8.1	Bulk rock composition and mineral chemistry	58
CHAPTER 6 - DISCUSSION	61
6.1	Estimation of Intensive Parameters of Crystallization for the Alto Paranaíba Alkaline Province	61
6.2	Thermobarometry Results for Limeira I and Três Ranchos IV kimberlites... 62	62
6.3	Oxygen Fugacity ($f\text{O}_2$)	66
6.3.1	Possible relations between oxygen fugacity and diamond instability..... 70	70
CHAPTER 7 - SUMMARY AND CONCLUSIONS	74
CHAPTER 8 - REFERENCES	76

LIST OF FIGURES

Figure 1 - Global distribution of diamond bearing Kimberlites after Kjarsgaard (2007)	05
Figure 2 – Schematic model of CO ₂ solubilities in silicic to carbonatitic melts (Brooker et al., 2011; Russell et al., 2012)	12
Figure 3 – Mechanism model of kimberlite ascent.....	13
Figure 4 - Comparison of the three conventional kimberlite pipe models and the preexisting terminology associated with the in-filling deposits (modified from Field and Scott Smith, 1999).....	16
Figure 5 - Components and textural aspects of coherent and fragmental volcanic and high-level intrusive rocks after Cas et al. (2008b)	16
Figure 6 – Alkaline provinces in central-southeastern Brazilian platform and their relationships with major structural features after (Riccomini et al., 2005)	24
Figure 7 – Geological Map of the Alto Paranaíba Alkaline Province after Barbosa et al. (2012)	26
Figure 8 – Geological Map of the Coromandel-Três Ranchos kimberlitic field after Cabral Neto et al. (2017)	27
Figure 9 – Hand sample aspects of Três Ranchos IV intrusion	30
Figure 10 – Petrographic aspects of TRIV olivine crystals. (a) Olivine megacryst with alteration films of serpentine at the boundaries and fractures; (b) recrystallized olivine, preserving the shape of the crystal	30
Figure 11 – Petrographic aspects of TRIV phlogopite crystals (a) pale brown phlogopite macrocryst; (b) phlogopite macrocryst exhibiting “kink-band” deformation and with a reaction rim	30
Figure 12 – BSE images of TRIV spinel crystals. (a) spinel macrocryst with reaction rim of chromite; (b) spinel crystal filling the rims of an olivine macrocryst	32
Figure 13 – Photomicrography of TRIV garnet crystal with a keliphitic rim	32
Figure 14 –Photomicrography of TRIV xenoliths composed mainly by pyroxene and carbonates	32

Figure 15 – Hand sample aspects of LM-I kimberlite (a) General view of a scanned thin section of inequigranular macrocrystic kimberlite texture; (b) autolith in hand sample	34
Figure 16 – Petrographic aspects of LM-I olivine crystals. (a) olivine macrocryst displaying undulose extinction; (b) mega-, macro-, and microcysts of olivine set in a fine-grained groundmass	34
Figure 17 – Petrographic aspects of LM-I phlogopite crystals (a) phlogopite macrocysts and phenocrysts; (b) phlogopite macrocryst with intensive alteration	35
Figure 18 – BSE images of LM-I monticellite crystals: (a) subhedral to euhedral monticellite crystals; (b) monticellite crystals in the autolith as a “garland” around olivine macrocysts	35
Figure 19 - BSE images of LM-I pyroxene crystals (a) pyroxene xenocryst with serpentine rim; (b) monticellite crystals at the boundaries of a pyroxene xenocryst	37
Figure 20 - BSE images of LM-I ilmenite crystals (a) ilmenite macrocryst with reaction rim; (b) ilmenite crystal as inclusion in olivine macrocryst	37
Figure 21 – Petrographic aspects of <i>Limeira I</i> perovskite crystals – (a) photomicrography of zoned perovskite; (b) perovskite as reaction rim in ilmenite crystal	37
Figure 22 – BSE images of TR-IV and LM-I perovskite assemblage	38
Figure 23 - BSE images of TR-IV and LM-I perovskites petrographic aspects	40
Figure 24 – BSE images of TR-IV and LM-I perovskite assemblage	41
Figure 25 – Variation of trace element concentrations in Três Ranchos IV and Limeira I Olivines	43
Figure 26 – Binary plots of EPMA data by mega- and macrocrystic olivines	44
Figure 27 – Median values for minor and trace element of rim and core analyses in olivine from Três Ranchos IV and Limeira I with the mantle and melt trend from Bussweiler et al. (2015)	45
Figure 28 – Olivine diagram showing predominant forsterite (Mg_2SiO_4) and calcic/monticellite ($CaMgSiO_4$) phases for both Três Ranchos IV and Limeira I kimberlites	47
Figure 29 – Perovskite composition in Três Ranchos IV, Limeira I and Alto Paranaíba Alkaline Province (APAP) plotted in the tausonite – perovskite – loparite ternary system	47

Figure 30 – Variation of major and trace element in perovskites from Três Ranchos IV and Limeira I.....	49
Figure 31 – Trace-element distribution patterns for perovskites from TR-IV and LM-1	50
Figure 32 – Composition of Spinel specimens from the Três Ranchos IV kimberlite (this work, red circle - macrocrysts; red diamonds - microcrysts) and Alto Paranaíba Alkaline Province	51
Figure 33 – Cr/(Cr+Al) vs. Mg/(Mg+Fe ²⁺) diagram for Três Ranchos IV (red - this work) spinels macro-, (circle) and microcrysts (diamond) and APAP (gray) data	51
Figure 34 – APAP (data from Guarino et al., 2013) and Limeira I ilmenite diagram, with recommended divisions by Wyatt et al. (2004)	52
Figure 35 – Dashed “parabolic” curves representing compositional trends of kimberlite ilmenite	52
Figure 36 – Clinopyroxenes xenocrysts and microphenocrysts of Limeira I (light blue) and Três Ranchos IV (coral), respectively, plotted in the Morimoto (1990) pyroxene classification diagram.....	54
Figure 37 – Três Ranchos IV rim (diamond) and core (circle) pyrope analyses plotted in the G-number nomenclature classification scheme (after Grüttner et al., 2004)	54
Figure 38 – Major elements (mass%) vs. MgO (mass%) variation diagrams for Três Ranchos IV, Limeira I (analyzed here) and APIP data from literature	56
Figure 39 – Trace element vs. MgO (wt.%) variation diagrams for Limeira I, Três Ranchos IV and APAP rocks (after Guarino et al., 2013; and references therein).	57
Figure 40 – Primitive mantle-normalized (Sun and McDonough, 1989) element and chondrite-normalized rare earth element (Boynton, 1984) pattern for whole-rock data from TR-IV, LM-I, and literature APAP kimberlites	59
Figure 41 – Whole-rock, liquid and mineral phase major element composition: WR - whole rock; Ol - olivine; Pv - perovskite; Mtc - monticellite; Ilm - ilmenite; Spl - spinel; Liq – liquid	60
Figure 42 – Lithospheric geothermal evolution (with APAP samples from Read et al., 2004) P-T conditions and compositions of Limeira I clinopyroxenes with garnet and spinel- facies clinopyroxene samples from Read et al. (2004)	63

Figure 43 – Al versus V concentration of olivine rims and cores from Três Ranchos IV (TR-IV) and Limeira I (LM-I)	65
Figure 44 – Limeira I ilmenite samples plotted in a FeO vs MgO discrimination diagram. Fields proposed by Gurney and Zweistra (1995)	65
Figure 45 – Calculated oxygen fugacities (ΔNNO) for perovskite grains from different samples of Três Ranchos IV and Limeira I, with varying Fe/Nb ratios	68
Figure 46 – XFe of monticellite and bulk composition and ΔNNO estimates for Limeira I kimberlite.....	71

LIST OF TABLES AND EQUATIONS

Table 1 - Summary of Group I and Group II mineralogical characteristics after Howarth et al. (2011).....	07
Table 2 - Calibration routines and patterns for each electron microprobed element and mineral	21
Table 3 - Mass spectrometer operating conditions coupled with the laser used for in-situ trace element analysis of olivine, perovskite, pyroxene, and garnet	21
Equation 1 - C.I = [(SiO ₂ + Al ₂ O ₃ + Na ₂ O) / (MgO + 2K ₂ O)]	9
Equation 2 - ΔNNO = {[0.50 ± (0.021) * Nb - Fe (±0.031) + 0.030 (±0.001)] / 0.004 (±0.0002)}	66
Equation 3 - ΔNNO = {log [0.858 (±0.021) XFe _{Liq} /XFe _{Mtc} - 1] - 0.139 (±0.0222)}/0.193(±0.004)	69
Equation 4 - Ci _{WR} = Ci _{Mt} (1 - Σ v) + Σ (Ci _{Mg} * v)	69
Equation 5 - Ci _{Mt} = {(Ci _{WR} - Ci _{Phl} * v _{Phl} - Ci _{OI} * v _{OI}) / (1 - v _{Phl} * v _{OI})}	70

LIST OF APPENDICES

APPENDIX A – PETROGRAPHIC DESCRIPTIONS	89
Table A01 - Petrographic descriptions of Três Ranchos IV and Limeira I samples.	90
Table A02: Relative abundance of perovskites with different paragenesis from Três Ranchos IV and Limeiras I.....	94
 APPENDIX B – EPMA DATA	96
Table B01 - Major element concentration of olivine from all samples. Structural formula calculated on the basis of 4 oxygens	98
Table B02 - Major element concentration of monticellite from all samples. Structural formula calculated on the basis of 4 oxygens	108
Table B03 - Major element compositions and endmembers for perovskite from all samples. Structural formula calculated on the basis of 3 oxygens.	114
Table B04 - Major element compositions for spinel from TRIV. Structural formula calculated on the basis of 32 oxygens.	139
Table B05 - Major element compositions of ilmenite from LMI all samples. Structural formula calculated on the basis of 6 oxygens.	145
Table B06 - Major element compositions of clinopyroxene from TRIV and LMI all samples. Structural formula calculated on the basis of 6 oxygens.	148
Table B07 - Major element compositions of garnet from TRIV all samples. Structural formula calculated on the basis of 24 oxygens.	151
 APPENDIX C – LA-ICP-MS DATA	154
Table C01 - Standards concentrations from LA-ICP-MS analyses.	155
Table C02 - Trace element concentration, limit of detection and uncertainties (2-sigma error) of olivine megacrysts from all samples.	177
Table C03 - Trace element concentration, limit of detection and uncertainties (2-sigma error) of perovskite from all samples.	185

Table C04 - Trace element concentration, limit of detection and uncertainties (2-sigma error) of clinopyroxene from all samples	191
Table C05 - Trace element concentration, limit of detection and uncertainties (2-sigma error) of garnet from all samples	192
APPENDIX D – XRF AND ICP-MS DATA	193
Table D01 - Whole rock major element concentration in mass.% for Três Ranchos IV and Limeira I kimberlite	194
Table D02 - Whole rock trace element concentration in ppm for Três Ranchos IV and Limeira I kimberlite	195
APPENDIX E – THERMOBAROMETRY DATA	196
Table E01 - Thermobarometry data obtained in this work from Três Ranchos IV and Limeira I kimberlite and compiled from APAP	197

CHAPTER 1 - INTRODUCTION

1.1 Theme Presentation

Kimberlites are ultramafic rocks formed from low-grade partial melting of deep (>150 km) mantle portions under high volatile pressure (Mitchell, 1986). Kimberlites are of remarkable scientific and economic relevance for providing a better understanding about the genesis and evolution of primitive magmas, and for being able to carry diamonds as they are emplaced into the upper crust (Mitchell, 1995).

Kimberlites record the highest known oxygen fugacity values of terrestrial magmas, a phenomenon related to the presence of deep oxidized sources and to the interaction of ferrous iron and carbon-fluid equilibrium during ascent (Canil & Bellis, 2007). The fO_2 of this type of magma mainly reflects the conditions of their source regions (Carmichael, 1991). Thus, kimberlites provide environmental information from depths greater than 200 km, as evidenced by the xenocrysts they bear. Moreover, in some cases the oxygen fugacity of kimberlite magmas can partially control the quality and the presence of diamonds in these rocks (Canil and Fedortchouk, 2001; Fedortchouk et al., 2005).

It is also known that other intensive variables (e.g., P-T) may have an important role in the presence of diamonds in kimberlites. During the ascent of kimberlite magmas, several processes such as decompression (Carmichael and Ghiorso, 1986), cooling, degassing, assimilation of crustal and mantle minerals (Sparks, 2013), crystallization (Carmichael and Nicholls, 1967) and interaction with crustal fluids (Ogilvie-Harris et al., 2009) can cause significant variations in pressure, temperature, volatile content, and oxygen fugacity (Ballhaus and Frost, 1994). Such processes can lead these magmas to experiment changes in mineral assemblages, mineral and melt compositions and physical properties (Ogilvie-Harris et al., 2009).

This research aims to calculate intensive crystallization parameters (pressure, temperature, and fO_2) in Cretaceous kimberlites of the Alto Paranaíba Alkaline Province (APAP) in eastern Brazil separated as either diamond-bearing or sterile occurrences. The APAP is one of the largest potassic-ultrapotassic provinces in the world (>15.000 km³; Gibson et al., 1995; Brod et al., 2000; Araujo et al., 2001; Comin-Chiaromonti and Gomes, 2005), consisting of a diversity of ultrapotassic rock types such as kimberlites, lamproites and large volumes of kamafugite fields, and several plutonic alkaline complexes with associated carbonatites (Brod et al., 2000). The rocks of the province have also been largely studied due to their economic

potential for industrial minerals and elements (e.g. diamonds from the Canastra 1 kimberlite, phosphorus, niobium, titanium and rare earth elements – REE) found as either residual phases or supergene enrichment over Catalão I e II, Salitre and Tapira carbonatite intrusions (Biondi, 2005; Cabral Neto et al., 2017; Comin-Chiaromonti et al., 2005; Guarino et al., 2013).

The ultrabasic potassic rocks generated by the Cretaceous alkaline magmatism that took place in the central and southeastern portions of the Brazilian platform are important in the understanding of the composition and evolution of the lithospheric and sublithospheric mantle in the region, from the study of xenoliths and xenocrysts samples from these magmas (e.g., Araujo et al., 2001; Bizzi et al., 1994; Brod et al., 2000; Carlson et al., 1996; Gonzaga and Tompkins, 1991; Junqueira-Brod et al., 2004, 2002; Leonardos and Meyer, 1991; Meyer et al., 1994; Meyer and Svisero, 1980). Many intrusions exhibit mineralogical and petrographic features of kimberlite or kamafugite but, due to new schemes and the reviewed classification and identification of different crystal populations (Araujo et al., 2001), a reevaluation of these rocks is necessary. Even considering the above-mentioned references, different levels of information correspond to well-known occurrences, especially in the Alto Paranaíba Alkaline Province, where mantle xenoliths and xenocrysts are abundant.

The Alto Paranaíba region is the second largest source of diamonds in Minas Gerais (Karfunkel et al., 2014; Svisero et al., 2017 and references therein). Among its hundreds of known kimberlite intrusions, 18 are estimated to be diamond-bearing occurrences. Examples are Alpha-9, Delta-18, Douradinho-11, Japecanga-6, Limpeza-5, Limpeza-19, Omega-1, Omega-9, Santa Clara-1, Três Ranchos-4, Três Ranchos-101, Três Ranchos-102, Três Ranchos-104 e Vargem-3 (Cabral Neto et al., 2017). Among the reasons that could explain the presence of diamonds only in a few bodies are: i) the depths at which magmas form; ii) variations in oxygen fugacity conditions, which would lead to greater unstabilization of the diamonds carried by these magmas; and (iii) local mantle heterogeneities that would allow sampling of certain minerals (such as diamond) possibly absent in other portions.

As detail study targets, we selected the Três Ranchos IV (TR-IV) intrusion, which is known to be a microdiamond-bearing intrusion, and the sterile Limeira I (LM-I) intrusion. In addition, contrasting the data acquired in this study with those from the literature, we can estimate the variation of the intensive parameters of crystallization for the whole Province. This research aims at understanding the behavior of such parameters in kimberlitic magmas and the reactions of these magmas with mantle xenocrysts (crystal-liquid reactions). Also, we discuss some possible implications associated with the diamond potential of these intrusions. In these

magmas, diamonds are considered xenocrysts that can be preserved in metastable conditions by the rapid ascent and crystallization of kimberlitic liquids (Mitchell, 1986). However, as demonstrated in experimental works, change of certain intensive parameters can lead to greater destabilization and reaction between xenocrysts and the magma (Canil and Bellis, 2007). This is a pioneering study of APAP rocks and the first approach to quantify especially the oxygen fugacity from cognate phases and to discuss the implications of the variation of this intensive parameter.

1.2 Overview of Kimberlites

Kimberlites are ultrabasic hybrid igneous rocks of potassic and ultra-potassic affinity (Mitchell, 1986). These lithotypes are extremely enriched in incompatible elements, occurring mainly in the interior of cratonic regions as undeformed dikes, sills, and pipes (Sparks et al. 2013). However, some aspects of kimberlite petrogenesis, such as the nature of the source, depth of melting, and their relationships with subcontinental-lithospheric mantle (SCLM) remain partially unsolved. This is mostly due to the presence of mantle/crustal xenocrysts and xenoliths that modify the primary composition of kimberlitic magmas, and also because of extensive post-emplacement alteration. (Berg and Allsopp, 1972; Mitchell, 1986; Paton et al., 2007; Kamenetsky et al., 2014). Knowledge of kimberlitic rocks has changed over the past decades. Several authors have attempted to define emplacement models based on petrological, mineralogical, textural and compositional studies (Arndt et al., 2010; Bussweiler et al., 2015; Cas et al., 2008a; Cas et al., 2008b; Clement and Reid, 1989; Jelsma et al., 2009; Kavanagh and Sparks, 2009; Mitchell, 1995; Russell et al., 2012; Scott Smith et al., 2013; Smith, 2017; Sparks et al., 2006; Wilson and Head, 2007). This topic presents a full overview of kimberlite evolution. Classifications, magma generation, and emplacement models are reviewed, and the evolution of their understanding by different authors is discussed.

The term "Kimberlite" was adopted as a reference to porphyritic mica-bearing peridotites first found in Kimberley, South Africa (Mitchell, 1986). Nonetheless, kimberlites from other regions have been more recently studied in an effort to improve the understanding of their genesis on a global scale. Detailed studies of the worldwide distribution of kimberlites demonstrated that they occur in cratonic regions within Archean basements (Dawson, 1989; Janse and Sheahan, 1995), but are also present in off-craton regions in all continents, in different emplacement settings. Diamondiferous members only occur in cratons, mobile belts or shields, underlain by thick subcontinental lithosphere mantle - SCLM (Jelsma et al., 2009). A

compilation of worldwide occurrences of diamond-bearing kimberlites is presented in Figure 1.

Mineralogically, geochemically, isotopically and petrographically, kimberlites can be divided into two main groups, Group I and Group II (Mitchell, 1995; Le Maitre, 2002; Becker and Le Roex, 2006). The first classification of kimberlites recognized two distinct petrographic facies in occurrences in South Africa: the basaltic (Group I) and the micaceous (Group II) types (Wagner, 1914). This classification was first revised by Mitchell (1970), who excluded the term “basaltic kimberlite” on the basis that kimberlites neither contain feldspar nor bear any genetic or mineralogical resemblance with basalts. The current reclassification of kimberlites was proposed by Smith (1983) contrasting two specific patterns of initial Sr, Pr and Nd isotopic compositions, named Group I e Group II Kimberlite.

Group I kimberlites comprise ultrabasic, volatile-rich (CO_2) and potassic rocks whose frequent macrocrysts (0.5-10 mm) and megacrysts (around 1-20 cm) set in a fine-grained matrix constitute a distinctive inequigranular texture (Mitchell, 1995; Le Maitre, 2002; Becker and Le Roex, 2006). In contrast, Group II kimberlites show closer affinity to lamproites and are rarer than Group I ones. They consist in ultrapotassic, peralkaline, and volatile-rich (H_2O) rocks with phlogopite macro- and microphenocrysts, with groundmass micas that vary in composition from “tetraferriphlogopite” to phlogopite (Le Maitre, 2002). Nevertheless, due to the lack of further studies, the definition of Group II kimberlites is not well established yet. Rocks of this clan were also named “orangeites” by Mitchell (1995, 1986) as they might not be classified as kimberlites due to their unique character and occurrence in the Orange Free State, South Africa.

Group II kimberlites are thought to derive from the metasomatized lithospheric mantle, which is unique to each continent, while Group I ones, originated from the asthenospheric mantle, show similar isotopic signature in each occurrence (Mitchell, 2006). Likewise, another difference between the two groups is the composition of the xenoliths and xenocrysts that they include. Group I kimberlites usually contain a broad range of mantle xenoliths (peridotites, metasomatized and shared peridotites), eclogites, MARID (Mica-Amphibole-Rutile-Ilmenite-Diopside) rocks, wherlites and a suite of megacryst minerals. Group II kimberlites incorporate sheared peridotites and metasomatized xenoliths, with rare or absent megacrysts (Field et al., 2008).

In general, the classification used for deposits is not consistent with the volcanology and genetic terminology. Most of it is not descriptive and is difficult to understand, yet kimberlites are volcanic deposits (Cas et al., 2008c). Nowadays, efforts have been made toward a new

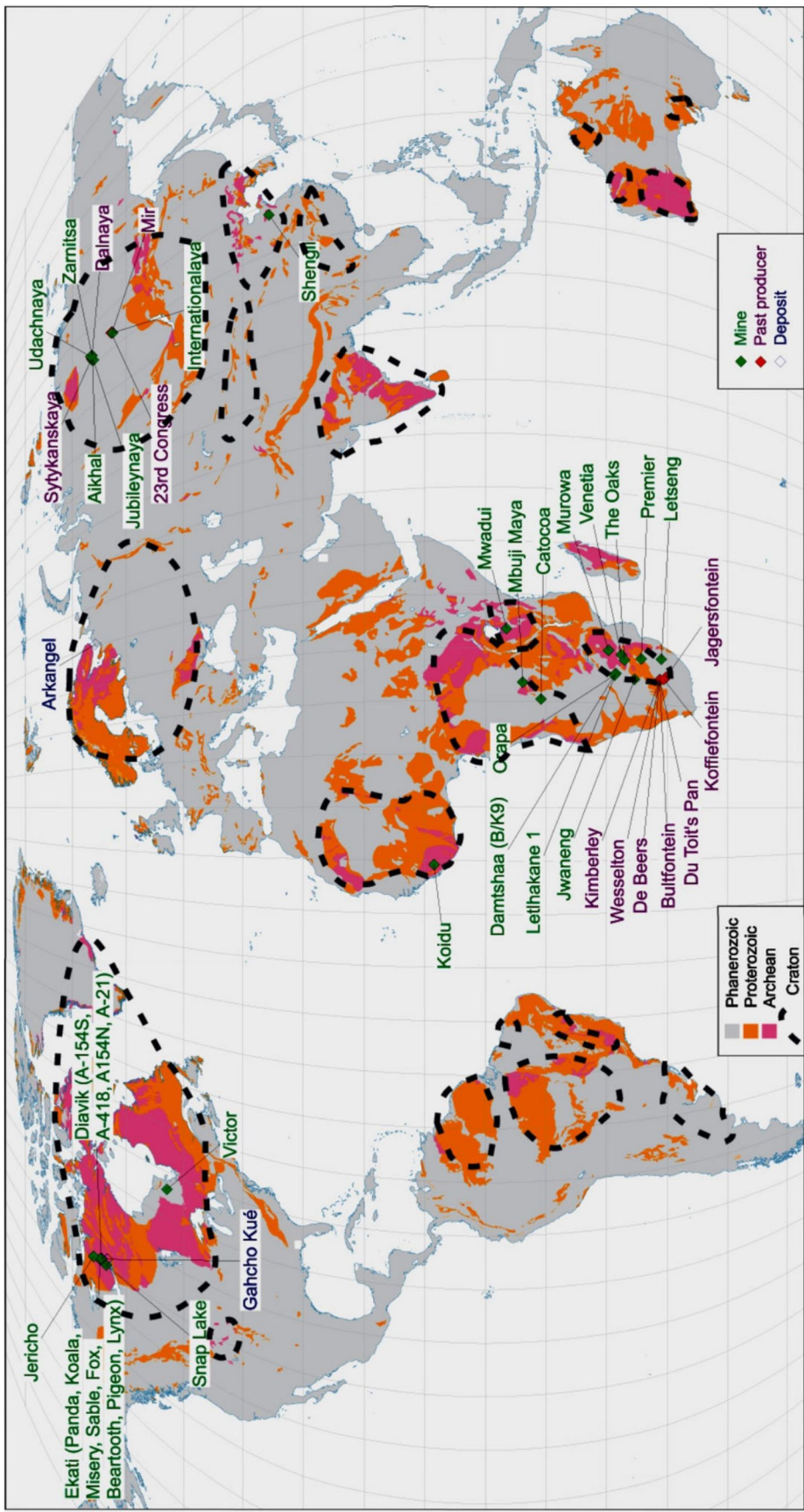


Figure 1 – Global distribution of diamond bearing kimberlites Kjarsgaard (2007).

approach to kimberlite classification (Cas et al., 2008b, 2008c). These terminologies will be described in the “Pipe formation and models” section.

1.2.1 Mineralogy

The broad mineralogical variation of kimberlites is caused by differentiation processes whereby minerals form from three distinct sources: (i) crustal/mantle xenocrysts and xenoliths (e.g. olivine, garnet, spinel, Cr-diopside, phlogopite, and diamond), that may be carried along with the arising magma; (ii) discrete nodule or megacryst suite; and (iii) phases crystallized from the kimberlite (Mitchell, 1986, Le Maitre, 2002). Although the term *xenocrysts* may offer an excellent understanding of mantle processes, most authors do not recommend it to be used in the definition of a kimberlite. The main mineral phases in kimberlitic rocks are olivine, phlogopite, monticellite, calcite, serpentine, ilmenite, diopside, spinels, perovskite, phlogopite, and apatite.

Olivine, volumetrically the most important constituent of kimberlites, is ubiquitous, deriving mainly from disaggregated mantle-derived peridotite or dunite (Clement, 1982; Mitchell, 1986; Arndt et al., 2010). Authors such as Mitchell (1970, 1986, 1995), and Clement et al. (1983) agree that olivine can occur as xenocrysts and ‘primary’ or phenocrysts. As the larger olivine crystals might have evolved from either xenocrysts (i.e. mantle-derived) or phenocrysts (i.e. melt-derived), Clement et al. (1984) proposed the use of the non- genetic term “macrocrysts” for the larger crystal suite (Kjarsgaard et al., 2010; Bussweiler et al., 2015). ‘Macrocrysts’ is used to describe large, sub-angular to rounded, single crystals or crystal aggregates with habit, undulose extinction and recrystallized grains that suggest a different origin to the kimberlite magma (Arndt et al., 2010). Another descriptive term is ‘phenocrystic’ olivine, which refers to smaller grains identified as sub to the euhedral strain-free crystals with planar faces (Arndt et al., 2010). Crystallized olivine corresponds to around 5 vol.% of kimberlites and originates from heterogeneous crystallization (Brett et al., 2009). It occurs mainly as rims on xenocrystic derived olivine. Fine-grained euhedral olivine crystals occur as a minor, up to 0.5% component, being related to homogeneous crystallization (Brett et al., 2009).

In general, both Group I and Group II kimberlites exhibit large rounded-to-anhedral crystals (e.g., olivine, phlogopite) set in a fine-grained matrix composed of several phase minerals (Table 1). The macrocryst and megacryst (some of which possibly xenocrysts) assemblage of Group I kimberlites is composed by anhedral crystals of olivine, diopside,

Table 1 - Summary of Group I and Group II mineralogical characteristics after Howarth et al. (2011).

	<i>Group I</i>	<i>Group II</i>
<i>Olivine</i>		
<i>Macrocryst</i>	Abundant	Common in unevolved kimberlite Rare in evolved kimberlite
<i>Phenocryst</i>	Common-sub/euhedral	Common – minor – sub/euhedral
<i>Mica</i>		
<i>Macrocrysts</i>	Minor phlogopite	Common phlogopite
<i>Microphenocrysts</i>	Rare phlogopite	Common phlogopite
<i>Groundmass</i>	Common phlogopite-kinoshitalite laths	Common phlogopite-tetraferriphlogopite (poikilitic plates)
<i>Spinel</i>	Abundant, large	Minor to rare.
	Typically, Mg-chromite zoned to Mg-ulvöspinel	Mg-chromite rarely zoned to Ti-magnetite
<i>Monticellite</i>	Common, may be pseudomorphed by carbonate or serpentine	Common in unevolved kimberlites, typically pseudomorphed by carbonate or serpentine
<i>Diopside</i>	Primary diopside absent may occur in contaminated groundmass	Microphenocrysts. Common to rare
<i>Perovskite</i>	Common, rounded-euhedral	Rare, subhedral to poikilitic
<i>Apatite</i>	Common to rare, euhedral prisms or acicular radiating aggregates	Common euhedral prisms and poikilitic plates
<i>Melilite</i>	Common - always pseudomorphed	Common — always pseudomorphed
<i>Carbonates</i>	Simple assemblages, common calcite, minor dolomite	Common calcite, common Sr–Mn–Fe dolomites, minor witherite, aegirine, and strontianite
<i>Serpentine</i>	Abundant secondary and primary in segregations	Common secondary
<i>Sanidine</i>	Absent	Groundmass in evolved kimberlite
<i>K-richterite</i>	Absent	Groundmass in evolved kimberlite
<i>Aegirine</i>	Absent	Groundmass in evolved kimberlite
<i>Leucite</i>	Absent	Groundmass in evolved kimberlite
<i>K-Ba hollandite</i>	Very rare	Common
<i>Mn ilmenite</i>	Rare	Common
<i>Zr-silicates</i>	Very rare	Common
<i>Barite</i>	Rare	Common
<i>Megacrysts</i>	Characteristic	Rare to absent
<i>Diamonds</i>	Common	Common

magnesian ilmenite, phlogopite, pyrope, Ti-poor chromite and enstatite, that is normally believed to have disaggregated from mantle-derived eclogite, lherzolite, harzburgite or metasomatized peridotite xenoliths (Table 1). Most diamonds are also found in this suite, but less commonly. Olivine macrocrysts are present in all but fractionated kimberlites (Mitchell, 1995; Le Maitre, 2002). Phases like magnesian ilmenite, diopside, olivine, Ti-pyrope, relatively poor Cr-enstatite (<2% Cr₂O₃) are classified as megacrysts. The fine-grained matrix contains primary euhedral-to-subhedral olivine, together with one or more of following phases: monticellite, phlogopite, perovskite, spinel, carbonate, apatite, and serpentine. Late-stage poikilitic micas of the barian phlogopite kinoshitalite series are also common in this clan of kimberlites. Serpentine and calcite are the most abundant alteration minerals, replacing earlier-formed olivine, monticellite, apatite and phlogopite (Mitchell, 1995; Le Maitre, 2002).

The primary mineralogical difference between Group I and Group II kimberlites is the amount of phlogopite, which is more abundant in Group II ones. This phase occurs as macrocrysts, microphenocrysts, and groundmass, composing around 50% of the assemblage (Mitchell, 1995). The chemical composition of the phlogopites is also distinctive between both types. Group II phlogopite is lower in Al₂O₃ (4-11 mass%) and higher in FeO (10-15 mass%) than Group I phlogopite (Mitchell, 1995).

1.2.2 Geochemistry

Kimberlites are MgO (20-38%) and CaO (5-14%) rich, Al₂O₃ (<3%) and Na₂O (<0.3%) poor ultrabasic rocks (SiO₂ <35%) with high LOI and mg# and potassic to ultrapotassic in character. Their K₂O ratio can reach about 7% in Group II kimberlites due to the increase in the amount of phlogopite (Clement, 1982; Mitchell, 1986, 1995). In general, Group I kimberlites also contain higher TiO₂, CaO, and CO₂, and lower SiO₂ and K₂O contents than Group II ones (Figure 2). Kimberlites also show lower Al₂O₃ and Na₂O amounts than other basic and alkaline rocks (Becker and Le Roex, 2006).

Because of their hybrid nature, the geochemistry of kimberlites is complex. Their primary character is often modified by secondary post-emplacement alteration and by the presence of upper mantle and/or crustal xenoliths (Mitchell, 1986; Le Roex et al., 2003). Thus, whole rock geochemistry results do not represent the rock's primary composition, but that of a mixture with xenoliths (olivine) and alteration phases (serpentine, carbonate). Clement, (1982) proposed a contamination index (C.I) to estimate these combined effects in kimberlites. C.I. is the contamination index expressed by (Equation 1).

$$C.I = [(SiO_2 + Al_2O_3 + Na_2O) / (MgO + 2K_2O)] \quad (1)$$

It is known that crustal contamination raises SiO_2 , Al_2O_3 and Na_2O contents relative to MgO , and that emplacement alteration extracts MgO from the rock to form clay deposits and hydrous phases with SiO_2 and Al_2O_3 (Mitchell, 1986). Likewise, higher contamination ratios lead to a much larger $SiO_2 + Al_2O_3 + Na_2O$ than $MgO + K_2O$, resulting in higher C.I. When C.I. is close to 1, the sample is completely devoid of crustal contamination or alteration (Clement, 1982). Kjarsgaard et al. (2009) also suggested a C.I. = 1.5 as a contamination/alteration brink: samples with $C.I. > 1.5$ will have enough crustal fragments and will have undergone substantial alteration, which compromises the bulk rock geochemical signature (Kjarsgaard et al., 2009).

Both Group I and Group II kimberlites are characterized by extreme incompatible element and light rare element (LREE) enrichment, moderate to heavy rare earth element (HREE) values, which indicates very low degree of partial melting of source, and simple linear (normalized) REE distribution and depletion (Mitchell, 1986; Le Roex et al., 2003; Davies et al., 2004; Harris et al., 2004; Chalapathi Rao et al., 2005; Becker and Le Roex, 2006; Coe et al., 2008; Felgate, 2014). Group II kimberlites are enriched in Pb, Rb, Ba, and LREE and show Cr and Nb depletion compared with Group I ones. As for Group I kimberlite, they are characterized by lower Ba/Nb (<12), Th/Nb (<1.1) and higher Ce/Pb (>22) ratios than the former (Felgate, 2014). The ratios of some trace elements in Group I (e.g. Ce/Pb, Nb/U, La/Nb, Ba/Nb, Th/Nb) indicates affinity to ocean island basalts (OIB). The ratios of some trace elements of Group I kimberlites (e.g. Ce/Pb, Nb/U, La/Nb, Ba/Nb, Th/Nb) indicates affinity to ocean island basalts (OIB). Based on these ratios, Smith (1983) proposed that these rocks and OIB's share the same asthenospheric source in their genesis. Group I kimberlites also show refractory Mg numbers and Ni content akin to SCLM ones, which makes it difficult to attribute them to a simple convecting asthenospheric source (Becker and Le Roex, 2006).

The distinction between both groups of kimberlites in terms of isotope geochemistry is very difficult (Smith, 1983). Sr and Nd isotopic signature of Group I Kimberlites are sometimes slightly depleted, but very similar to the bulk earth, being the most indicative for isotopic studies in both groups (Sarkar, 2011). Group I kimberlites are less radiogenic in Sr (~0.703) and more radiogenic in Nd (~0.51260) as compared to the current Bulk Earth composition, showing OIB affinity. Group II kimberlites, on the other hand, are highly radiogenic in Sr (~0.707-0.712) and Nd (~0.5124-0.5120) compared to the Bulk Earth composition, being associated with SCLM sources (Smith, 1983; Becker and Le Roex, 2006; Felgate, 2014).

Hf isotope geochemistry is an alternative method for differentiating between Group I and Group II kimberlites. Group I ϵHf_i^1 values vary from 5 to -10. In ϵHf_i^1 vs ϵNd_i^1 diagrams, Group I kimberlites plot well below the mantle array.² In Group II kimberlites, ϵHf_i^1 values range from -5 to -25, falling along the mantle array as their ϵNd_i^1 values are more negative (-6 to -12) compared with those of Group I kimberlites. Negative Hf isotope signatures are evidence for sublithospheric kimberlitic source. Along with its megacrysts, the isotopic characteristics of Group I kimberlites require a source with low time-integrated Lu/Hf relative to Sm/Nd, which suggests an ancient source component (>1Ga) represented by deeply subducted oceanic basalts that became incorporated into the convecting mantle source region (Nowell et al., 2004).

On-craton and off-craton tectonic settings exert ambiguous control over the geochemistry of kimberlites. Group II kimberlites are characterized by small systematic differences in major and trace element and Nd-Sr isotope ratios between on-craton and off-craton settings, which suggests that both sources share similar evolutionary trends. Off-craton Group I kimberlites, on the other hand, show lower SiO₂ and MgO, but higher FeO, TiO₂, CaO, and CO₂ values than on-craton occurrences, possibly implying a derivation from more fertile mantle sources (Becker and Le Roex, 2006). Also, authors of experimental studies have proposed that partial melting at lower pressure decreases SiO₂ and MgO while increasing FeO, Al₂O₃, CaO and CO₂ contents (Herzberg, 1992; Dalton and Presnall, 1998; Gudfinnsson and Presnall, 2005; Becker and Le Roex, 2006). Such changes in major element composition are supported by the absence of diamonds in off-craton Group I kimberlites (Clifford, 1966; Becker and Le Roex, 2006), even when both types derive from within the garnet stability field, given similar fractionated HREE patterns.

1.2.3 Magma generation

The mantle conditions under which kimberlites are generated can be determined from experimental studies, geochemistry, xenolith, and xenocryst content, and also from the characterization of mineral inclusions. There are, however, some limitations. Kimberlitic magmas are most likely to undergo compositional changes as they arise, erupt or intrude the upper crust, being also commonly altered in near-surface (Sparks, 2013). Nevertheless, despite these ambiguities, a few concepts are well-established. Given their silica depletion and high incompatible trace elements contents, kimberlites may derive from very low-grade mantle melts. These rocks form at depths that are great enough (~150 Km) for diamond stability conditions to be present, at temperatures higher than the volatile-enriched mantle solidus i.e.,

1.350 to 1.450°C at the base of the lithosphere (Priestley et al., 2006; Sparks, 2013).

High pressures and temperatures in simplified mantle systems restrict kimberlite petrogenesis (Gudfinnsson and Presnall, 2005; Dasgupta and Hirschmann, 2006; Sparks, 2013). At high pressures, carbonated mantle (CMAS-CO₂, Carbonatitic Melts Along with Solidus) initially forms carbonatites as very low-degree melts at the solidus curve (Figure 2). Temperature increases while the accumulation of magma remains very low. From 200°C to 300°C above the solidus curve, magmas of kimberlitic affinity are generated, with the presence of a significant amount of silica (Sparks, 2013). However, kimberlitic magmas require generation temperatures of 1,500°C or higher in simplified experimental systems (Figure 2). Other components added to the experimental systems, such as Fe, alkalis, and water, can reduce the solidus to at least 100°C below the temperatures at which kimberlitic melts are generated. Such conditions are more consistent with temperatures estimated for the base of continental lithosphere (Sparks, 2013). An unresolved issue is that transitional kimberlitic melts with silica contents between those of carbonatites and basalts originate in narrow temperature ranges during the progressive partial melting of similar CMAS mantles. Other components, such as water, K and P may be responsible for the temperature ranges in which kimberlitic melts appear to form (Sparks, 2013).

Russell et al. (2012) suggested that kimberlites are generated by orthopyroxene assimilation during the ascent of the carbonate melts that represent their primary sources (Figure 3). Exsolution of CO₂ “depletes” the magma as it becomes enriched in silica and magnesium. This model explains the common absence of orthopyroxene xenocrysts in kimberlites. Olivine xenocrysts are typically found in kimberlites, being usually interpreted as originated from disaggregation of depleted mantle xenocrysts (harzburgites). Orthopyroxene crystals exhibiting dissolution textures related to reaction with carbonatitic kimberlites may occur (White et al., 2012; Sparks, 2013). Alternative reasons for the absence of orthopyroxene in kimberlites are that olivine xenocrysts originate from rupture of dunite rather than harzburgitic xenoliths and that orthopyroxene is unstable in water-rich kimberlitic melts (Mitchell, 2008; Arndt et al., 2010a; Sparks, 2013).

Carbonatite melts are common products of partial melting in carbonate-rich sources at pressures higher than 2.5 GPa (Russell et al., 2012). A few experimental studies have shown

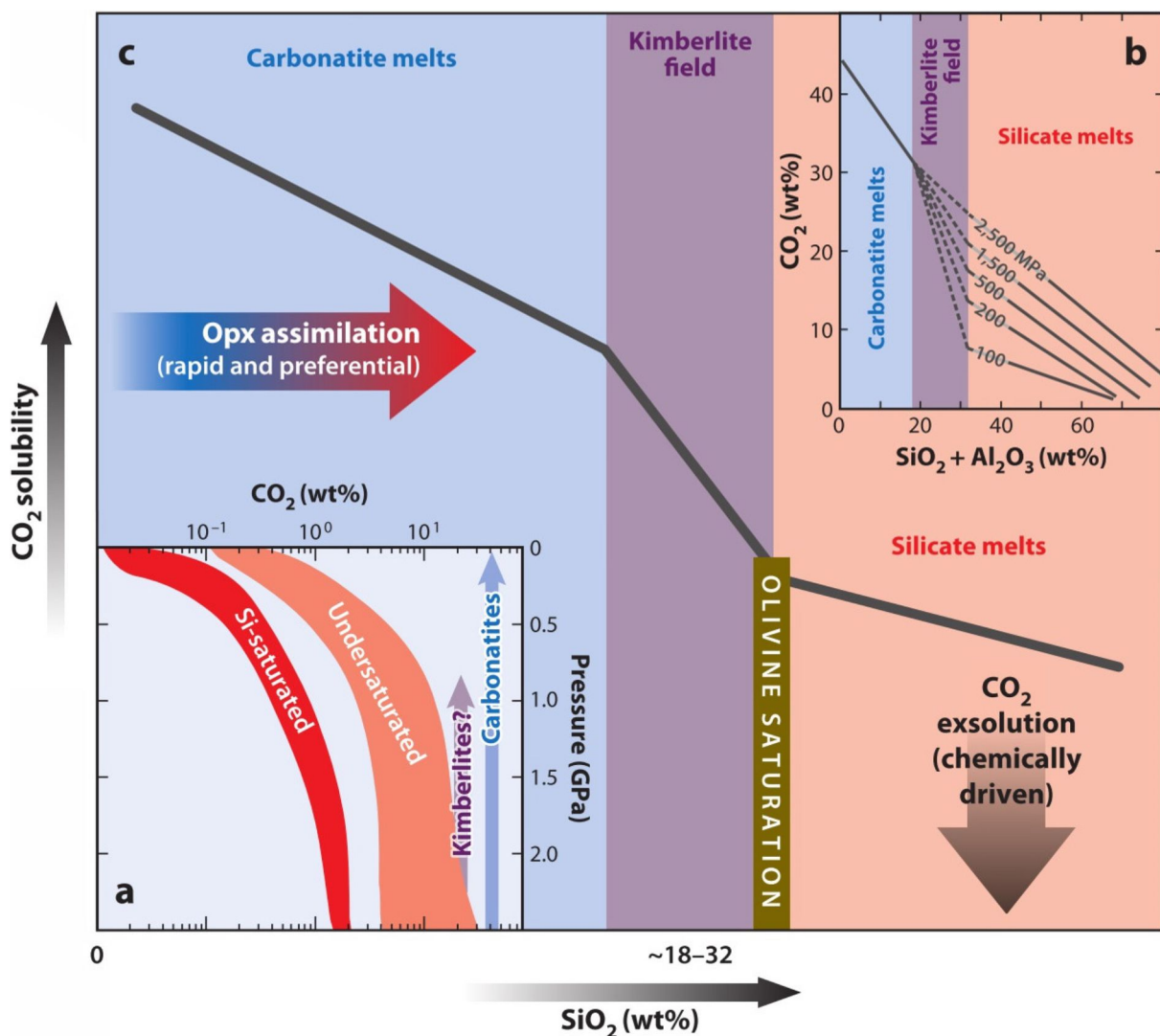


Figure 2 - Schematic model of CO₂ solubilities in silicic to carbonatitic melts (Brooker et al., 2011; Russell et al., 2012): (a) CO₂ solubility limits for silica-saturated and silica-undersaturated melts and hypothetical solubilities of carbonatite and kimberlite melts; (b) Pressure and composition dependence of CO₂ solubility across the carbonate-silicate transition. The effect of pressure (numbers on lines, MPa) on CO₂ solubility is limited compared with the effect of composition (SiO₂ and Al₂O₃). (c) Schematic model (Russell et al. 2012) of assimilation-induced fluid exsolution of carbonatite and proto-kimberlite melts. Orthopyroxene (Opx) assimilation drives non-silicate melts (left-hand side) to more silicic compositions (right-hand side), after Sparks (2013).

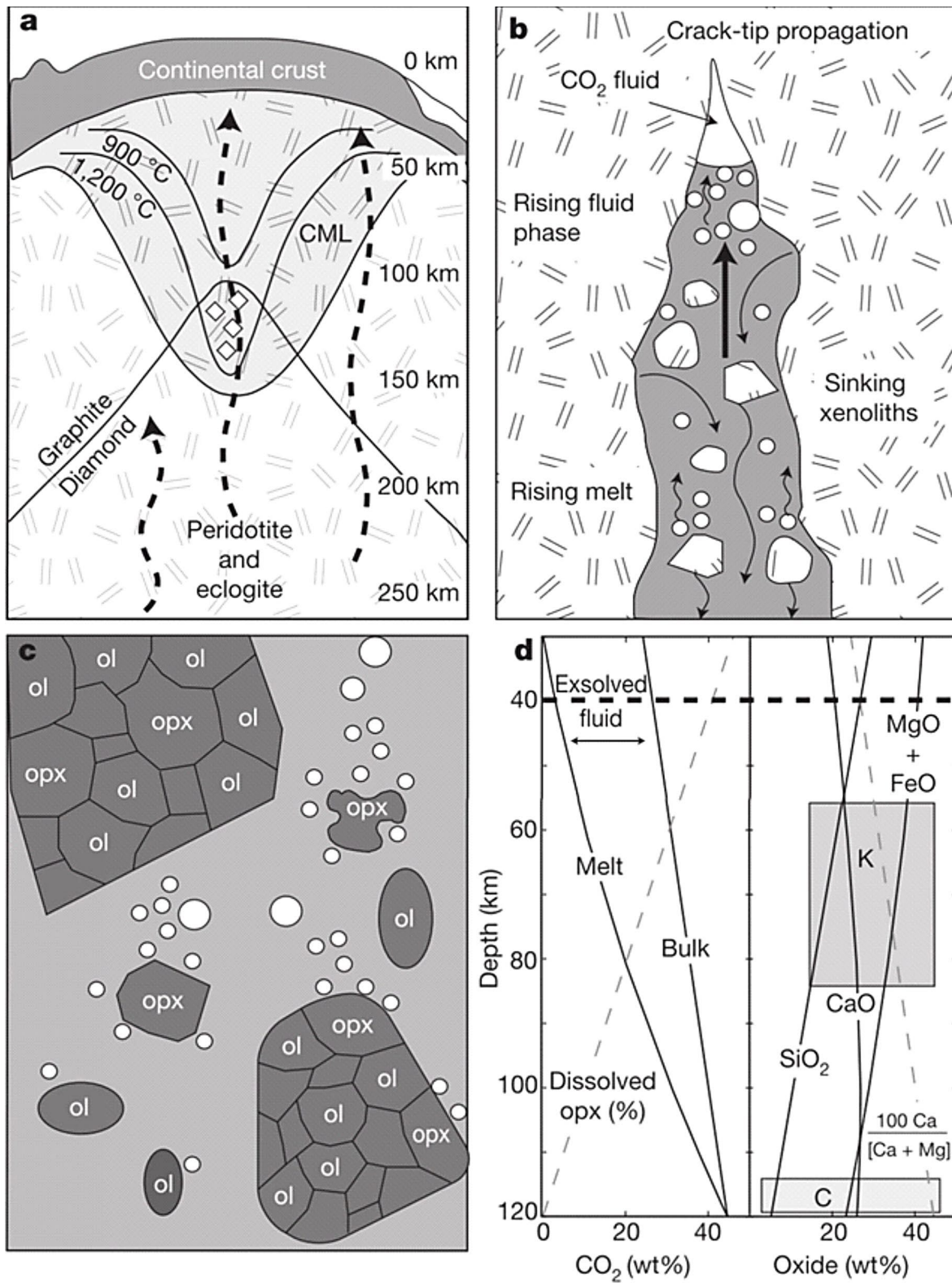


Figure 3 - Mechanism model of kimberlite ascent, showing: (a) Diverse ascent paths through cratonic mantle lithosphere (CML) shown as dashed arrows. Also shown is the line below which diamond is stable relative to graphite; (b) Melts produced by melting of carbonated peridotite transit mantle lithosphere as dykes by crack-tip propagation, liberating dense (sinking) xenoliths to the CO₂-rich silica undersaturated melt, causing effervescence of buoyant (rising) CO₂-fluid; (c) Xenoliths disaggregate and release individual mineral grains (for example, ol) to carbonatitic melt; opx grains are assimilated, preferentially promoting volatile exsolution. Deep-seated volatile production supports continued, crack-propagation-limited magma ascent; (d) Chemical evolution of melt during ascent. After Russel et al. (2012).

that the carbonated peridotite solidus melts at 2.5 GPa, and that it will be enriched in CO₂ but poor in SiO₂ as carbonate is stable in mantle assemblages. Such melts, that have been experimentally produced, contain over 40% dissolved CO₂ and are able to accommodate a large amount of H₂O (Russell et al., 2012). Likewise, Russell et al. (2012), suggested that the onset of kimberlites is marked by the asthenospheric production of such melts, (Figure 2a, b; (Canil and Bellis, 2008). Figure 3 presents a mechanistic ascent model that considers a carbonate-rich-melt and the diversity of kimberlite compositions as the mechanical mixing of mantle olivine (70–80%) (Patterson et al., 2009; Russell et al., 2012). Modeling of the ascending melt chemical evolution is presented in Figure 3, it was interpreted that the amount of orthopyroxene assimilated is linearly related to the distance traveled in the mantle lithosphere, with assimilation and decarbonization essentially instantaneous (Russell et al., 2012). The interpretation of this ascension model is that there is a linear correlation between the amount of orthopyroxene assimilated and the upward displacement of the magma in the mantle lithosphere.

Recent advances in the study of kimberlite (Kavanagh and Sparks, 2009; Lensky et al., 2006; Russell et al., 2012; Sparks et al., 2009, 2007; Wilson and Head, 2007) have focused on the variety of the magma properties and the influence of volatile exsolution on magma ascent. Kimberlites are clustered in space and time (Field et al., 2008), which configures a set of clusters controlled by major structural features (e.g., southern African kimberlites have Jurassic and Cretaceous ages). Such features are unleashed by tectonic triggering mechanisms (Sparks, 2013). Two different approaches explain the spatial/temporal kimberlite clustering: a) kimberlites are generated in pulses as a response to mantle dynamics, the ascent of a deep mantle plume; and/or b) they are generated continuously, and special conditions such as craton deformation provide the trigger for the ascent. Torsvik et al. (2010) proposed that kimberlites are primarily related to old continental craton areas that overlie stable mantle plume sources at the core-mantle boundary (Sparks, 2013).

1.2.4 Pipe formation and models

Kimberlite intrusions are shaped and structurally controlled by the competency of the country rock. Because of their morphological appearance, they are generally referred to as *pipes* (Mitchell, 1986). The different zones that form a kimberlite pipe vary considerably in texture and mineralogy. Clement (1982) and Clement and Reid (1989) provided the basis for a first textural classification of kimberlites. They proposed that a typical kimberlitic pipe is composed

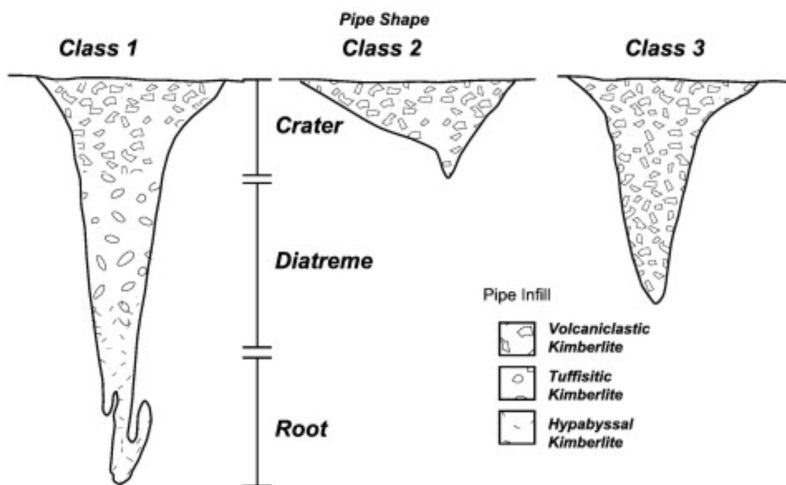
of three distinct zones: crater, diatreme (or pipe), and root. Textural and compositional characteristics specific to each zone separate a given intrusion into crater-facies, diatreme-facies, and hypabyssal-facies kimberlite, respectively. A simple, non-genetic terminology was suggested by Kjarsgaard (2007): volcanoclastic (VK, fragmental rock) kimberlites and hypabyssal (HK, non-fragmental rock) kimberlites (Figure 4). Volcanoclastic kimberlitic rocks, in turn, can be subdivided into pyroclastic kimberlites (PK), resedimented volcanoclastic kimberlites (RVK), and massive volcanoclastic kimberlites (MVK) (Figure 5).

Coherent kimberlites can be either extrusive or intrusive, and their differentiation requires knowledge of their context. Extrusive examples include kimberlite lavas, which are far less abundant than their intrusive counterparts. Intrusive coherent kimberlites are usually restricted to root zones and diatreme facies, being represented by uniform homogeneous rocks, non-fragmental textures. They encompass hypabyssal (Clement and Reid, 1989) and magmatic kimberlites (Sparks et al., 2006). These rocks result of direct crystallization from kimberlitic magmas prior to degassing and fluidization (Clement and Reid, 1989), being well qualified to determine primary kimberlite compositions. Compelling evidence indicates that many examples intrusive coherent kimberlites are pyroclastic in origin and may have formed via welding processes (Brown et al., 2008b, 2008a; Crawford et al., 2009; Buse et al., 2011; Hayman and Cas, 2011; van Straaten et al., 2011).

Volcanoclastic kimberlites subdivide into pyroclastic kimberlites (PK), resedimented volcanoclastic kimberlites (RVK) and epiclastic kimberlites (EVK). These forms are restricted to crater facies and upper diatreme facies of pipes (Cas et al., 2008b; Felgate, 2014; Sparks et al., 2006). Pyroclastic kimberlites originate from explosive volcanic eruptions and are deposited by primary pyroclastic processes, displaying no indication of resedimentation. Generally deposited as tuff rings, they are very unconsolidated and limited in terms of preservation potential (Sparks et al., 2006). Resedimented volcanoclastic kimberlites contain eroded/abraded pyroclastic materials mixed with an-kimberlitic materials eroded from their country rocks. Such kimberlites are located in the peripheral portions of pipes within the crater facies. Epiclastic volcanic kimberlites are the final kimberlite type and the rarest. This type is commonly ascribed to kimberlitic materials (either volcanic or coherent) affected by surface processes, typically formed at the top of pipes within crater facies (Cas et al., 2008a; Felgate, 2014; Sparks et al., 2006).

The formation of a kimberlite pipe is destructive and results in a cavity that connects the upper crust and the Earth's surface. Such conductus usually consist of downward-tapering

Kimberlite Terminology



Kimberlite Pipe Zone, Infill and Facies Terminology

Pipe Zone	Pipe Infill Textural Interpretation	Kimberlite Facies
Crater Zone	+ Volcaniclastic Kimberlite + Pyroclastic Kimberlite + Resedimented Volcaniclastic Kimberlite	= Crater Facies = Crater Facies = Crater Facies
Diatreme Zone	+ Volcaniclastic Kimberlite + Tuffisitic Kimberlite	= ?? Facies = Diatreme Facies
Root Zone	+ Hypabyssal Kimberlite	= Hypabyssal Facies

Figure 4 - Comparison of the three conventional kimberlite pipe models and the preexisting terminology associated with the in-filling deposits (modified from Field and Scott Smith, 1999): (a) Narrow, tapering, steep-sided southern African kimberlite model (Class 1). (b) Open bowl-shaped Canadian Prairies kimberlite body (Class 2). (c) Dual tapering to flaring Lac de Gras type kimberlite pipe model (Class 3). After Cas et al. (2008a).

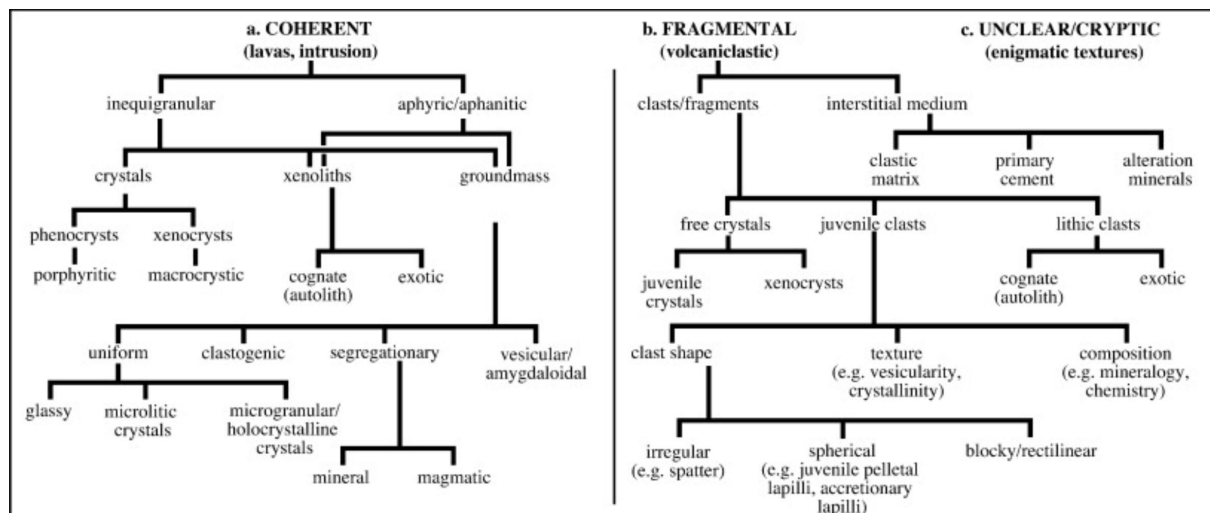


Figure 5 - Components and textural aspects of coherent and fragmental volcanic and high-level intrusive rocks after Cas et al. (2008b).

structures that reach hundreds to thousands square meters in cross sections (Field et al. 2008). Sparks et al. (2006) proposed that kimberlites have an early waxing stage of eruption and that as the erupting magma is initially overpressured at Earth's surface, the cratering explodes. As the kimberlite pipe widens and deepens, the supply rate of explosively erupting magma remains high enough to any rock fragments that reach it from wall rock collapse to be removed by the high-speed magma flows (Sparks, 2013). Therefore, the space that corresponds to the pipe is mostly created before rock fragments are removed from it. Nevertheless, pipe enlargement and infilling may be contemporaneous during the eruptive magma activity (Sparks, 2013).

1.2.5 Volatile contents

Kimberlite magmas are usually assumed to be volatile-rich (Sparks, 2013), and some evidence may help constrain their actual volatile composition. Methods used to define the primary volatile composition of other magmas (e.g., directly from gas emissions from active volcanoes, melt inclusions, mineral assemblages) cannot be applied to kimberlites (Sparks, 2013). Direct evidence for CO₂ comes from the occurrence of igneous carbonate in some kimberlite intrusions and rare lavas, and from phlogopite indicating the presence of water (literature reviewed in Sparks et al. 2006). Kimberlites commonly contain high water and CO₂ contents, but these cannot be taken as primary magmatic volatile contents as they may be of secondary origin (Sparks, 2013). Experimental studies of possible kimberlite compositions at a variety of water, CO₂, and mixed water-CO₂ mixtures at moderate pressures give poor results in terms of reproducing primary mineral assemblages in order to help constrain volatile contents (Sparks et al., 2009; Brooker et al., 2011; Sparks, 2013).

1.3 Research Aims

The main question of this study regards the influence that intensive parameters such as pressure, temperature, and oxygen fugacity (T, P, and O₂) might have on the greater instability of carried (or possibly carried) diamond xenocrysts when sterile and diamond-bearing kimberlite magmas from Alto Paranaiba Alkaline Province are compared with one other. A few specific goals established to support this discussion are: (1) the petrographical characterization of Três Ranchos IV (diamond-bearing) and Limeira I (sterile) kimberlites by focusing on mineral instability textures suggestive of intensive parameters changes during crystallization; (2) the characterization of major, minor and trace elements of TR-IV and LM-I kimberlites (bulk compositions) and their minerals in terms of compositional variation; (3) the

determination of temperature, pressure (through xenocrysts assemblage) and oxygen fugacity (through cognate assemblage) conditions of the kimberlite magmas based on the chemical composition of the main mineral phases of both intrusions; (4) calculation of the same intensive parameters for other intrusions of the province from available chemical data; (5) comparison of textures and reactions with new and available data in order to interpret the petrogenesis of the kimberlite magmas, by comparing them in terms of diamond preservation.

1.4 Study Area Location and Access

Três Ranchos IV and Limeira I intrusions are located in Goiás (GO) and Minas Gerais (MG) states in southeastern Brazil, respectively. TR-IV kimberlite occurs at the former Alagoinha farm, 8 km from Três Ranchos City (GO). From São Paulo (SP) Três Ranchos is mainly accessed through Bandeirantes (SP-348), BR-050 or Gustavo Capanema (GO-030) highways and secondary roads that lead to the intrusion (UTM: W 201787/ S 7972758). LM-I intrusion is located 28 km north of Monte Carmelo City MG. From São Paulo, Monte Carmelo is reached through Bandeirantes (SP-348), BR-050 and MG-190 highways and secondary roads that led to the kimberlite (UTM: W 239626/ S 7946091).

CHAPTER 2 - MATERIALS AND METHODS

2.1 Literature Review

A substantial number of studies have been conducted on the Cretaceous potassic magmatism of Brazil, the majority of which being focused on the APIP kimberlites (Svisero and Chieregati; Svisero et al., 1984; Danni and Scartezini, 1990; Gonzaga et al., 1994; Gibson et al., 1995b; Costa, 1996; Araujo et al., 2001; Melluso et al., 2008; Silva, 2008; Reguir et al., 2009; Thomaz, 2009; Andrade and Chaves, 2011; Nannini, 2011a, 2011b, 2016; Chaves et al., 2012; Guarino et al., 2013; Felgate, 2014; Karfunkel et al., 2014; Lim et al., 2018). The initial stage of this study involved a review of the literature on the geological evolution of the alkaline magmatism that originated the Alto Paranaíba Alkaline Province. Specifically, the Três Ranchos IV (diamond-bearing) and Limeira I (sterile) kimberlites were detailed based on regional and local studies. The main references were accessed from the Geoscience Institute's library using database search systems of the SIBiUSP (Integrated Library System of the University of São Paulo). A systematic search of the topics in this study was accomplished, including mantle petrology and intensive parameters of crystallization (P-T- $f\text{O}_2$) of kimberlite magmas and applied methods, such as scanning electron microscopy (SEM), electron microprobe (EMP), X-ray fluorescence (XRF), inductively coupled plasma-mass spectrometry (ICP-MS), and *in situ* ICP-MS laser ablation analysis.

2.2 Petrographic Analyses and Imaging

Thirty-four thin sections from Limeira I and Três Ranchos IV kimberlites were analyzed in order to identify the mineral assemblages and xenocrysts present and to estimate their modal volumes (Mitchell, 1986, 1995; Le Maitre, 2002). Photomicrographs were taken at the Petrographic Microscopy Laboratory (GeoAnalítica-USP) by using a Zeiss Axio Imager A2m microscope coupled to an AxioCam MRc digital camera.

Five polished thin sections (80 μm -thick) from Três Ranchos IV and seven from Limeira I were analyzed in a FEI Quanta 600F scanning electron microscope under a 20kV accelerating voltage in the Technological Characterization Laboratory of the Department Mining and Petroleum Engineering, Polytechnic School (USP). A 20-25 nm carbon coat was applied to every sample before analysis. High-resolution backscattered electron (BSE) images were taken to identify any zoning or fracturing present and to establish the textural relationships in mineral phases as ilmenite, spinel, olivine, perovskite, magnetite, and monticellite.

2.3 Mineral Chemistry

2.3.1 Major and minor element analysis

Perovskite grains were analyzed under an accelerating voltage of 25 kV and an emission current of 100 nA for better quantification of REEs, minor and trace element analysis. Major elements of monticellite, olivine, pyroxene, spinel, garnet, and ilmenite were measured under an accelerating voltage of 15kV and an emission current of 20nA.

Mineral chemistry data were acquired at the Electron Microprobe Laboratory, NAP-Geoanalítica (USP) with a JXA-8530 HyperProbe Electron Probe Microanalyzer (EPMA). Natural and synthetic standards were applied. 10 samples were covered with a 20-25 nm carbon oat in an EDWARDS AUTO 306 evaporator prior to EPMA analyses. Four spectrometers were used to analyze these elements, which are shown in Table 2.

The data obtained were treated based on structural formula calculations with Microsoft® Excel® 2016 following recommendations of Deer et al. (1992). Matrix corrections were performed with CITZAF (Armstrong, 1985) and ZAF software. The data were used in the determination of intensive parameters of crystallization (P-T-fO₂) and the petrogenetic implications of the evolution of both Três Ranchos IV and Limeira I kimberlites.

2.3.2 Trace element and rare earth element (REE) analysis

The concentrations of the trace elements and rare earth elements (REE) were analyzed at NAP-Geoanalítica (USP) laboratories by laser ablation inductively coupled plasma mass spectrometer (LA-ICP-MS) for more accurate measurement of the elements of lowest concentration in olivine, garnet, perovskite, and pyroxene. A Thermo Scientific™ iCAP™ RQ ICP-MS coupled with a New Wave UP213nm laser was used. Helium was used as a carrier gas of the ablated sample into the Ar plasma. The standard mass spectrometer and laser setup of a typical session are described in Table 3. NIST-612 (glass), BHVO (basalt) and BIR (glass) calibration standards were applied to all samples. Analytical procedures were performed according to Andrade et al. (2014). A total of 8 polished thin sections were selected, four from each kimberlitic intrusion. Primary data reduction and normalization were performed with Glitter v.4.0 (Macquarie University) using reference values from GEOREM website for the calibration standards (Table 03). Ca was used as internal standard for perovskite, and Si was used for garnet, olivine, and pyroxene. The concentrations of the selected elements were analyzed by EPMA.

Table 2 - Calibration routines and patterns for each electron microprobed element and mineral.

Element	X-ray line	Crystal	Standart Olivine/monticellite¹	Standart Perovskite²	Standart Ilmenite¹	Standart Pyroxene¹	Standart Spinel¹
Si	K α	TAP	diopside	anorthite	diopside	olivine	diopside
Al	K α	TAP	anorthite_%ele		Spinel_%ele	microcline	Spinel_%ele
Fe	K α	LIFL	fayalite	ilmenite	ilmenite	fayalite	magnetite_%el
Mn	K α	LIFL	fayalite		fayalite	MnTiO ₃	fayalite
K	K α	PETJ	Ortoclase		Ortoclase		Ortoclase
Ca	K α	PETJ	Wollastonite	Wollastonite	Wollastonite	Wollastonite	Wollastonite
Sr	L α	PETJ		strontianite			
Ti	K α	LIFL	Rutile	Rutile	ilmenite	MnTiO ₃	Rutile
Ba	L α	LIFL		benitoite		MnTiO ₃	
Na	K α	TAPH	Albite	Albite	Albite	Albite	Albite
Mg	K α	TAPH	basalt_#8		diopside	olivine	diopside
Ni	K α	LIFL	glass_rhyolitic_#37		glass_rhyolitic_#37	NiO	
Cr	K α	LIFL	chromite_%ele		chromite_%ele	Cr ₂ O ₃	chromite_%ele
Zn	K α	LIFL			Willemite		Willemite
Nb	L α	PETJ		ilmenite	ilmenite		ilmenite
Nd	L α	LIFL		neodymium-phosphate			
V	K α	LIFL					glass_rhyolitic_#32
La	L α	LIFL		lanthanum-phosphate			
Sm	L α	LIFL		samarium-phosphate			
Pr	L β	LIFL		praseodymium-phosphate			
Zr	L α	PETJ		zircon			
Th	M α	PETJ		glass_rhyolitic_#32			
Ce	L α	LIFL		cerium-phosphate			

Accelerating voltage '15.0 kV' 25.0 kV.

Table 3 - Mass spectrometer operating conditions coupled with the laser used for in-situ trace element analysis of olivine, perovskite, pyroxene, and garnet.

	Olivine	Perovskite	Pyroxene	Garnet
Standart	BHVO	Nist-610	BHVO	Nist-610
Power	80%	78%	80%	75%
Repetition rate	15 Hz	12Hz	12Hz	15Hz
Ablation mode	spot	spot	raster	raster
Spot/raster size	55 μ m	30 μ m	57 μ m	58 μ m

2.4 Whole Rock Geochemistry

Three unweathered samples from each kimberlite intrusion (Três Ranchos IV and Limeira I) were crushed for whole rock geochemical analyses, first in a steel jaw crusher, then in a disk mill of agate. Subsequently, each powdered sample was used to prepare pressed pellets and fused beads for X-ray fluorescence analysis, and chemically dissolved for ICP-MS analyses (Mori et al., 1999). The sample preparation steps are as follows: (1) removal of unweathered surface with a diamond saw or press; (2) pressing for granulometry reduction; (3) quartering of thicker samples and subsequent grinding in an agate mill; (4) separation of about 7.5 g of the pulverized fraction for micronization for 25 minutes and preparation of pressed pellets for X-ray Fluorescence Spectrometry (XFS) trace elements analysis; (5) addition of flux to the pulverized sample in order to prepare fused pellets for major elements analysis.

FRX is one of the most widely used techniques in geochemistry, with many applications in petrology. The chemical characterization of rocks example allowed the use of rock classification, spider and Harker variation diagrams for petrogenetic interpretations. The results were treated with Excel© software prior to geochemical data processing (GCDkit; Janoušek et al., 2006).

2.4.1 Major element analyses

Whole-rock major compositions were obtained using a PANalytical AxiosMAX Advanced spectrometer, following the analytical protocol of (Mori et al., 1999; Sertek et al., 2015) at the X-Ray Fluorescence Laboratory of the Geoanalítica-USP core facility.

2.4.2 Trace and rare earth element (REE) analyses

Chemical analyses were performed at the ICP-MS and Chemistry Laboratory of the Geoanalítica-USP core facility. Trace and REE elements were measured using a Perkin Elmer Plasma Quadrupole MS ELAN 6100DRC, following the analytical protocol of (Navarro et al., 2008).

CHAPTER 3 - BRAZILIAN ALKALINE MAGMATISM

More than one hundred major alkaline clusters and associated bodies of Permian-Triassic to Paleogene age are known in the central and southeastern Brazilian Platform (Figure 6), especially those close to the limits of the Paraná Basin (Riccomini et al. 2005). Most of the alkaline bodies were discovered during a large-scale K-Ar dating program (Amaral et al., 1967a), but it was only in the 1980s and 1990s that the first detailed studies addressing their petrographic-genetic aspects were conducted (Ulbrich and Gomes, 1981; Morbidelli et al., 1995; Comin-Chiaromonti and Gomes, 1996).

Almeida (1983) observed that at latitudes greater than 15°S the Brazilian alkaline rocks outcrop in three different contexts: (i) near the borders of the Paraná Basin; (ii) in a 100 km-wide mobile belt along the onshore Atlantic coast region; and (iii) in the Bolivian territory, within domains of the Amazon Craton. Almeida (1983) introduced the concept of the alkaline province for alkaline bodies clusters of similar petrographic, age and tectonics.

The following alkaline provinces were defined by Almeida (1983): Poços de Caldas, Alto Paranaíba, Rio Verde-Iporá, Ponta do Morro, Eastern Paraguay, Mariscala, Piratini, Santa Catarina, Ponta Grossa Arch and Ipanema, all along the borders of the Paraná Basin; Serra do Mar, on the onshore continental region along the western border of the Santos Basin; and Velasco and Candelaria, in eastern Bolivia, within the Amazon Craton. A most recent classification of the alkaline magmatism in central-southeastern Brazilian Platform into 15 provinces was proposed by Riccomini et al. (2005): (1) Alto Paraguay and the Early Cretaceous Ponta Grossa Arch, Valle Chico, Misiones, Central Paraguay, Amambay and Rio Apa provinces, distributed along the present-day borders of Paraná Basin; (2) Rondonópolis Anteclise and Minas-Goiás provinces adjacent to the Bauru Basin; (3) Serra do Mar and Piratini provinces on the onshore continental region at the western borders of Santos and Pelotas marginal basins, respectively; (4) the Asunción province, related to the Cenozoic evolution of the Asunción Rift; (5) the Cabo Frio Magmatic Lineament province, with at least two phases of alkaline magmatism, from Late Cretaceous to the Paleogene; and (6) Velasco and Candelaria provinces in eastern Bolivia within the Amazon Craton (Riccomini et al., 2005).

3.1 Alto Paranaíba Alkaline Province

The Alto Paranaíba Alkaline Province (APAP) extends over an area of 20,000 km² in southeastern Brazil, over southeastern Minas Gerais and southwestern Goiás (Araujo et al.,

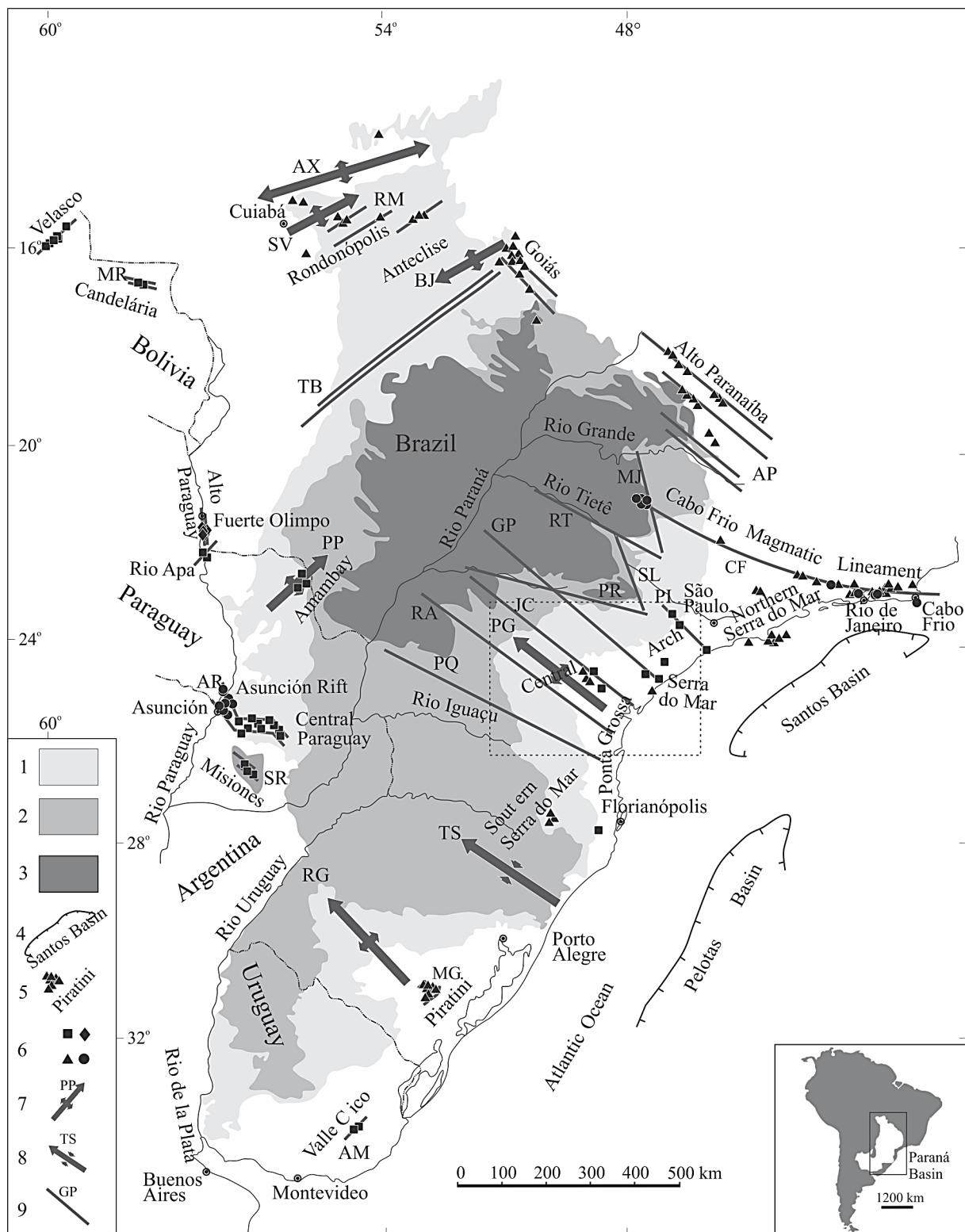


Figure 6 – Alkaline provinces in central-southeastern Brazilian platform and their relationships with major structural features after (Riccomini et al., 2005).

2001; Brod et al., 2000; Comin-Chiaromonti and Gomes, 2005; Felgate, 2014; Guarino et al., 2013; Melluso et al., 2008). The province intrudes the Neoproterozoic Brasília belt and is bounded by the Paraná Basin (to the South) and the São Francisco craton (to the West), including Late Cretaceous alkaline (kamafugites, kimberlites, and lamprophyres) and carbonatitic rocks, lava flows, pyroclastic successions and hypabyssal intrusions (Figure 7; Gibson et al., 1995; Brod et al., 2000; Araújo et al., 2001; Read et al., 2004; Gomes and Comin-Chiaromonti, 2005; Melluso et al., 2008), which occurs along of an NW-SE lineament (Bardet, 1977; Tompkins, 1991; Biondi, 2005). Most of the rocks show an economic potential for precious minerals and industrial applications, as for example diamonds in kimberlite occurrences or P, Nb, Ti, REE elements that occur as residual and supergene enrichments over carbonatite complexes (Biondi, 2005).

3.2 Coromandel-Três Ranchos Kimberlitic Field

The Coromandel-Três Ranchos kimberlitic field covers an area of approximately 11,600 km² between Catalão (GO) and Patrocínio (MG) cities within Alto Paranaíba and Triângulo Mineiro regions. The field is part of the Alto Paranaíba Alkaline Province, including more than five hundred kimberlitic intrusions (Figure 8) that usually show pipes structures up to 300 ha large (as for example, Japecanga-6 kimberlite), as well as hypabyssal, diatreme, and craters facies in severall occurrences. These bodies intrude lower to middle-grade metasedimentary rocks from the Brasília Belt units: Canastra, Vazante, Araxá, Ibiá, and Bambuí groups (Cabral Neto et al., 2017).

3.2.1 Três Ranchos IV kimberlite

The Três Ranchos IV kimberlite occurs as blocks in an area of approximately 0.5 ha, showing hypabyssal facies features (Costa et al., 1997). Its rocks are classified as Group I kimberlite (Le Maitre, 2002), displaying a pseudo-porphyritic serial texture with abundant megacrysts and macrocrysts of phlogopite olivine, spinel, garnet, and microcrysts of serpentine, perovskite, monticellite, magnetite, phlogopite, Cr-spinel and K-richterite (Guarino et al. al., 2013). According to Costa et al. (1997), the Três Ranchos kimberlite intrudes granitic rocks, quartzites, schists, and amphibolites of the Araxá Group, which occur as xenoliths. Microdiamonds were reported by Gonzaga et al. (1994).

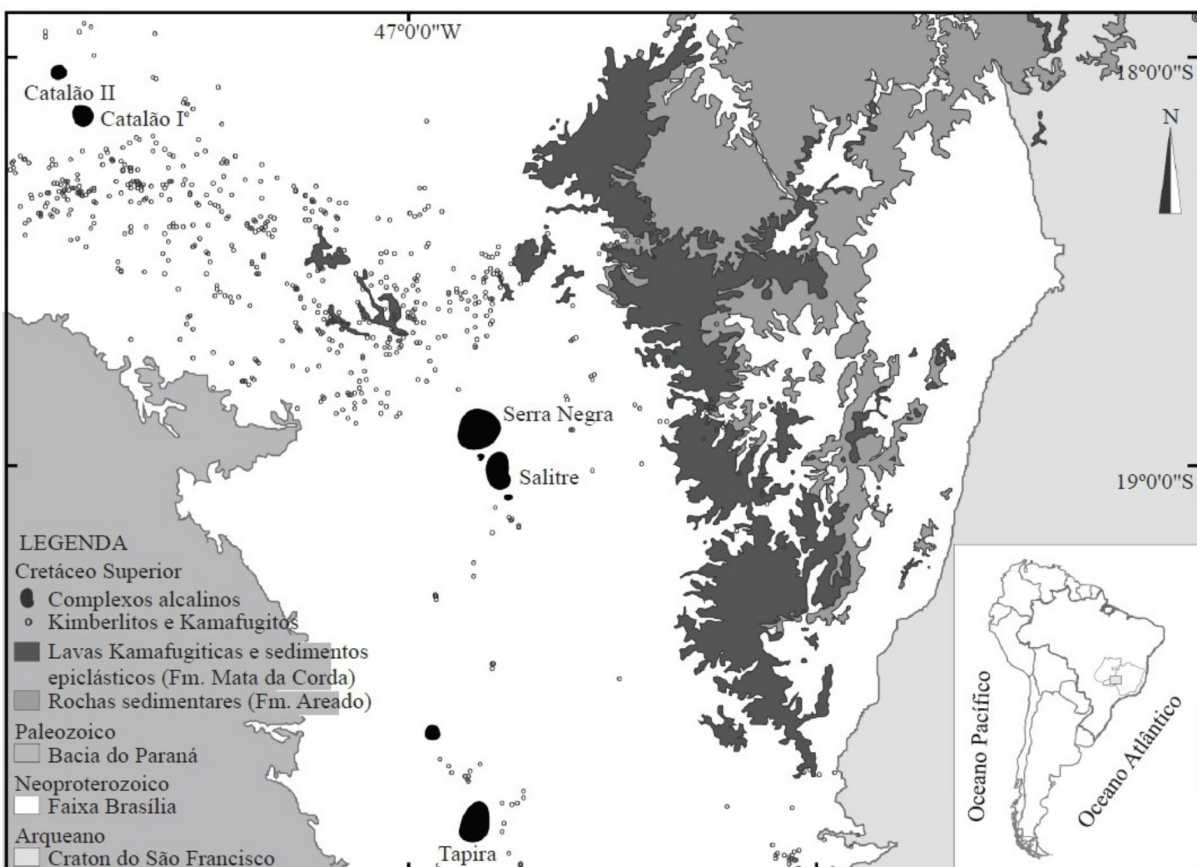


Figure 7 – Geological Map of the Alto Paranaíba Alkaline Province after Barbosa et al. (2012).

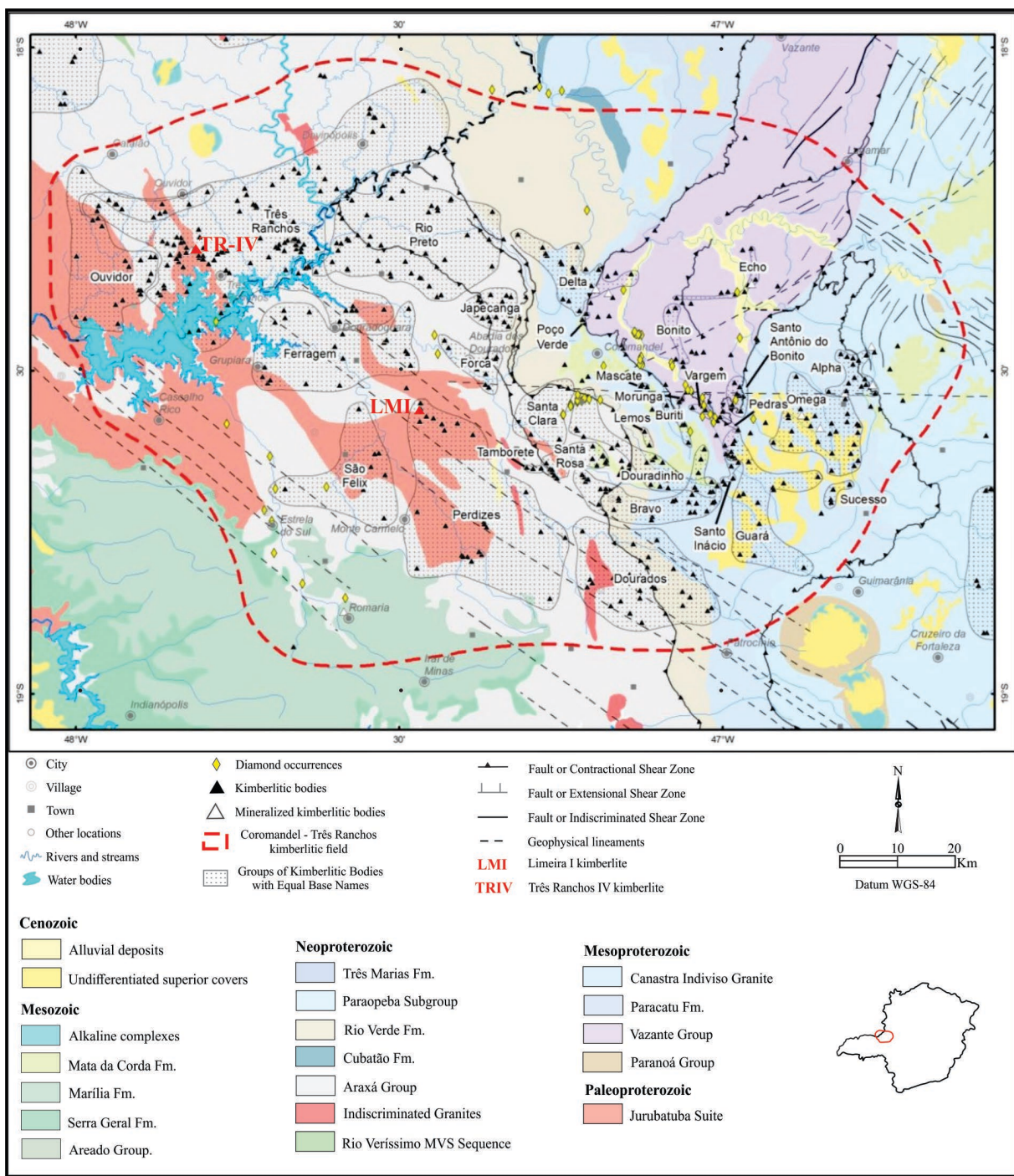


Figure 8 – Geological Map of the Coromandel-Três Ranchos kimberlitic field after Cabral Neto et al. (2017).

3.2.2 Limeira I kimberlite

The Limeira I kimberlite, also named Perdizes 04a (Cabral Neto et al. 2017) occurs as blocks and boulders in an area of ~3.5 ha, exhibiting textural features of hypabyssal facies (Meyer et al. 1994). Its lithotypes, that can also be identified as Group I kimberlites (Meyer et al. 1994), are composed of macrocrysts of olivine, diopside, ilmenite, phlogopite, chromite, and garnet, microcrysts of perovskite, spinel, apatite, monticellite, calcite and serpentine, which constitute the matrix (Meyer et al. 1994). The kimberlite intruded the basement and have not been reported to bear diamond.

CHAPTER 4 - PETROGRAPHY

The Três Ranchos IV (TR-IV) and Limeira I (LM-I) kimberlites have similar mineral assemblages, both including mega- and macrocrysts of olivine and phlogopite set in a fine groundmass of olivine, phlogopite, perovskite, spinel, ilmenite, serpentine, and carbonate. They differ in the absence of ilmenite macrocrysts in TR-IV and in the presence of apatite and monticellite within the groundmass of LM-I. The most distinctive difference, however, is the presence of autholiths and diopside macrocrysts in the LM-I. Estimated modal abundances of all the constituent phases are provided in Table A01 (Appendix A).

4.1 Três Ranchos IV

Três Ranchos IV is identified as a Group I coherent macrocrystic kimberlite (Cas et al., 2008b; Le Maitre, 2002; Mitchell, 1997). The intrusion comprises dark to gray fresh homogenous rocks which exhibit an inequigranular (Figure. 9a-b) texture formed by partially-to-fully altered olivine, phlogopite megacrysts up to 1 cm wide, macrocrysts (0.5-10 mm) and crustal xenoliths set in a very fine greenish groundmass. In hand specimen, millimetric to centimetric, rounded to sub-angular xenoliths or xenocrysts constituted by carbonates, pyroxene microcrysts, phlogopite, perovskites, and opaque minerals are recognized (Figure 9c) that were probably incorporated during magma ascent.

Olivine, the most abundant phase, occurs as mega-, macro-, and microcrysts. The megacrysts, that typically comprise 15-20% of the volume of the rock, are rounded or anhedral and elongated, with sizes between 1.0-3.4 cm, exhibiting extensive alteration, mostly along rims and fractures where serpentine development is present (Figure 10a). Samples of fresh olivine cores are preserved at TR-IV. Some megacrysts are fully recrystallized as clusters of smaller crystals that, as a whole, still retain the shapes of the original megacrysts (Figure 10b). Olivine macrocrysts also show alteration at rims and fractures, and some crystals are fully serpentined. They are typically subhedral and 5-9 mm in size, also showing rounded and anhedral shapes. Many macrocrysts are stained and exhibit undulose extinction (Figure 10c). Microcrysts comprise about 10% of the volume of the samples, down to 1mm in size, are subhedral, usually completely serpentined, with only a few exceptions where minor fresh cores are preserved (Figure 10d).

In Três Ranchos IV kimberlite samples, phlogopite is present as macrocrysts (Figure 11a, b), small euhedral macrocrysts and interstitial phlogopite in the groundmass (Figure 11b).

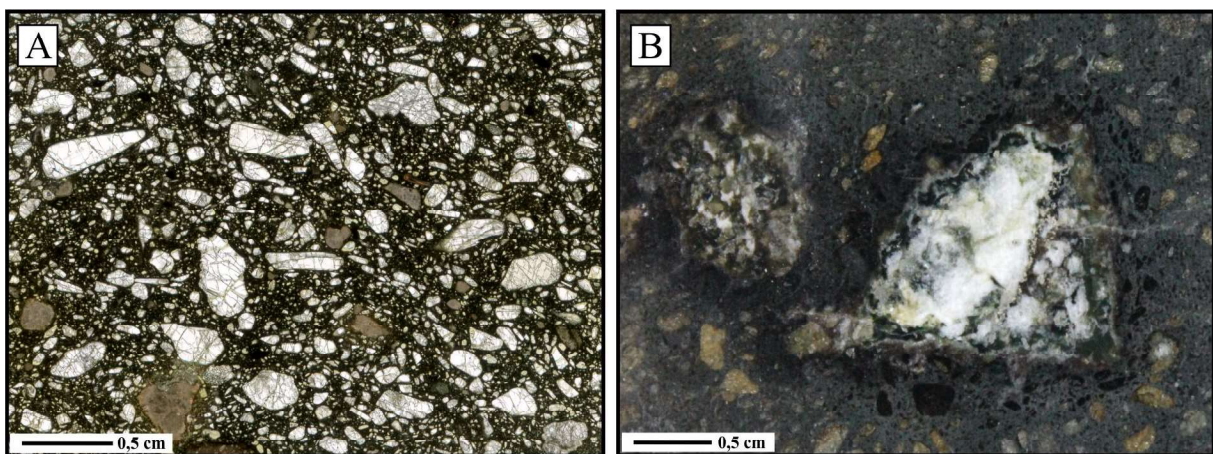


Figure 9 – Hand sample aspects of Três Ranchos IV intrusion. (a) General view of a scanned thin section exhibiting inequigranular macrocrystic texture defined by olivine crystals in olivine and fine-grained groundmass; (b) carbonate segregation, with opaque minerals and phlogopite in hand sample.

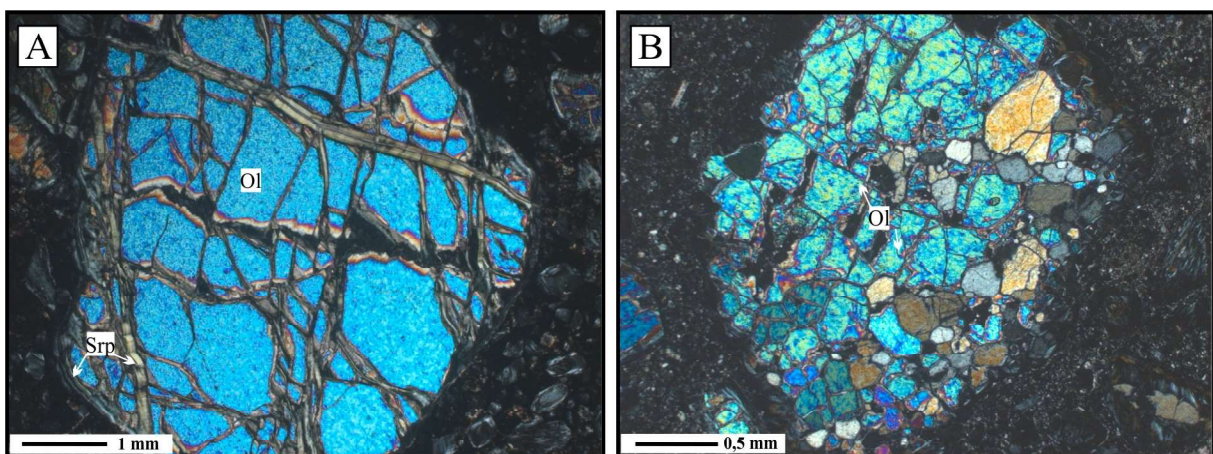


Figure 10 – Petrographic aspects of TRIV olivine crystals. (a) Olivine megacryst with alteration films of serpentine at the boundaries and fractures; (b) recrystallized olivine, preserving the shape of the crystal. Cross-polarized transmitted light in (a) and (b).

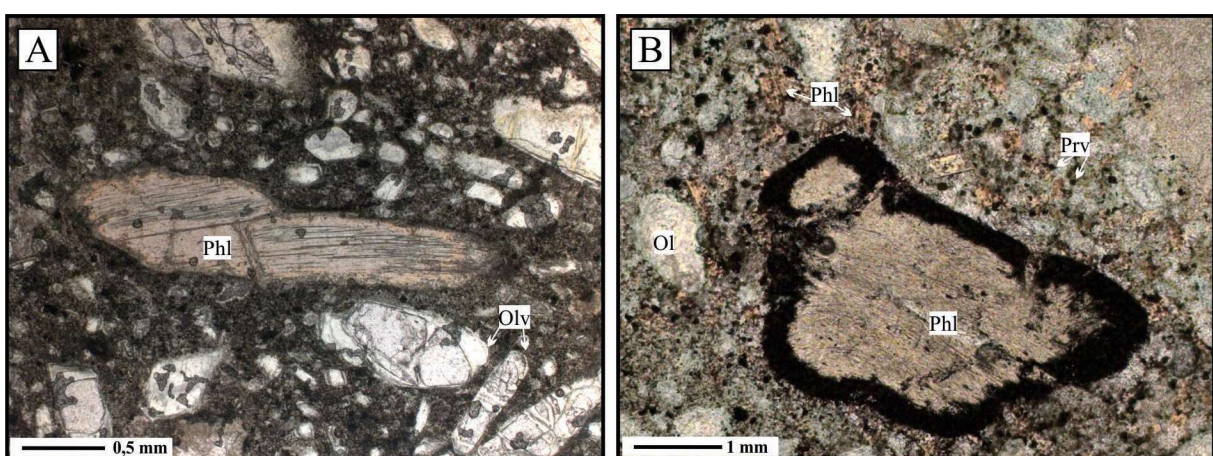


Figure 11 – Petrographic aspects of TRIV phlogopite crystals (a) pale brown phlogopite macrocryst; (b) phlogopite macrocryst exhibiting “kink-band” deformation and with a reaction rim. Plane-polarized transmitted light in (a) and (b).

Macrocrysts typically range in size between 0.2-6 mm, composing 5-10% of the rock volume in TR-IV. Some phlogopite crystals exhibit classic kink banding (Figure 11b), which is indicative of deformation, probably by incorporation of the crystals into the kimberlite magma. The microcrystic phlogopite range in size between 100-200 μm , exhibiting strong pleochroism from colorless/pale yellow to brown, and a range in the state of alteration. Laths are typically fresh, but some extreme chloritization is present. The smaller crystals and interstitial phlogopite show minor alteration, down to 50 μm in size.

Spinel is a constituent of the groundmass, also occurring as macrocrysts. The macrocrysts are translucent red, subhedral to anhedral, with a size between 0.2-0.3 mm, surrounded by an opaque rim of chromite and magnesium-ulvöspinel-magnetite (Figure 12a). Occasionally, spinel also occurs as anhedral to euhedral titanomagnetite in the groundmass, with size down to 0.08 mm. Generally, the grains are distributed evenly and can be seen to be inter-grown with perovskite and/or some other opaque minerals, also around rims of olivine (Figure 12b).

Garnet is only present in Três Ranchos IV, with sizes up to 0.9 mm, invariably with pronounced reaction edges (Figure 13a, b), which indicates that these occurrences represent mantle xenocrysts.

Pyroxene crystals are mainly associated with polymimetic aggregates, that probably represent the interaction of silicate xenoliths with the magma (Figure 14a). These crystals are colorless, prismatic, elongated, with high birefringence, and their dimensions range from 0.02 to 0.04 mm.

Serpentine is common in the groundmass, comprising around 40% of a matrix in which it has almost completely pseudomorphed the original fine grain minerals (Figure 10a). As previously mentioned, serpentinization of mega-, macro-, and microcrystic olivine is common. Serpentinization occurred to varying degrees, ranging from minimal alterations concentrated along fractures to complete replacement with yellow and brown serpentine.

Carbonate is found as segregations within the groundmass, where it has replaced the original groundmass minerals. Sometimes carbonate replacement is so extensive that it can make up 60% of the groundmass, giving thin sections a muddy brown appearance under plane polarized light.

The mantle xenoliths correspond to peridotite, predominantly dunite or metasomatized harzburgite (with phlogopite, secondary clinopyroxene, chromite, ilmenite, and others; Figure 14 a, b).

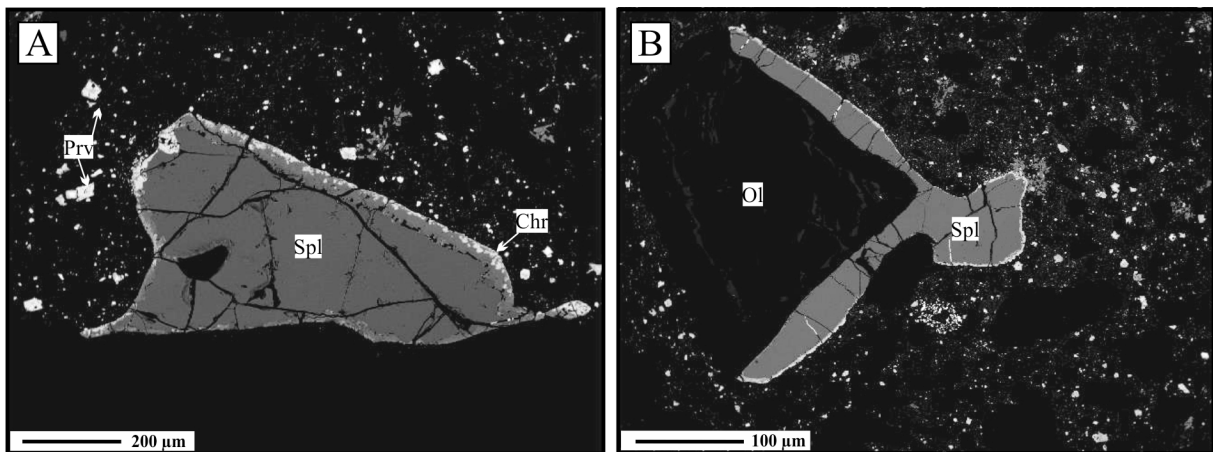


Figure 12 – BSE images of TRIV spinel crystals. (a) spinel macrocryst with reaction rim of chromite; (b) spinel crystal filling the rims of an olivine macrocryst.

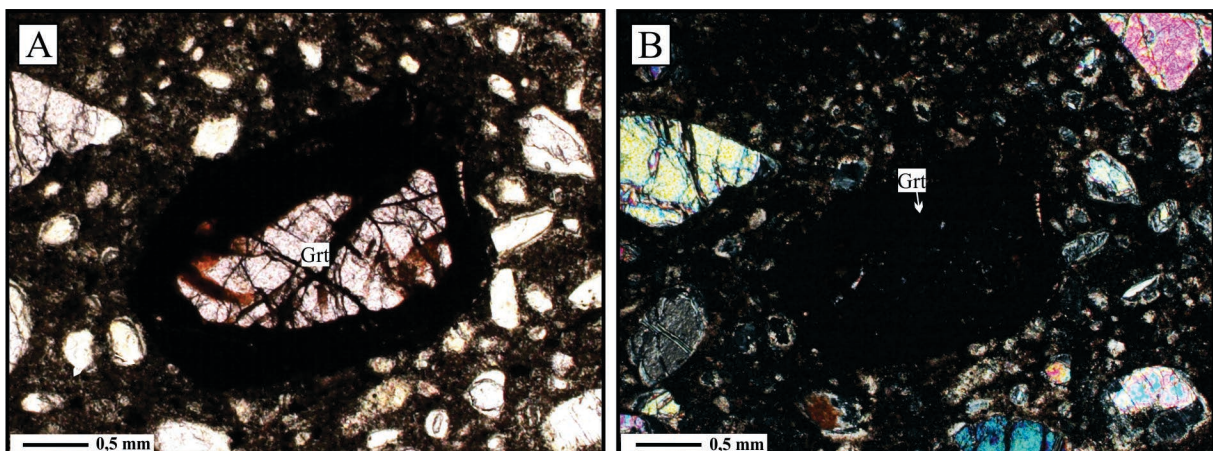


Figure 13 – Photomicrography of TRIV garnet crystal with a keliphitic rim: (a) plane-polarized transmitted light; (b) cross-polarized transmitted light.

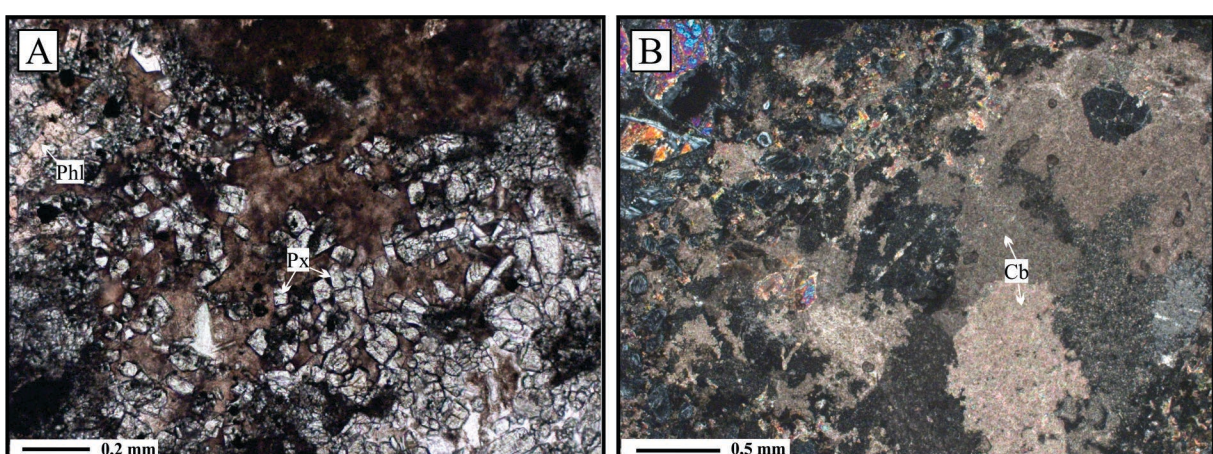


Figure 14 – Photomicrography of TRIV xenoliths composed mainly by pyroxene and carbonates. Plane-polarized transmitted light a) and cross-polarized transmitted light in b).

4.2 Limeira I

Limeira I is classified as Group I hypabyssal coherent macrocristic kimberlite (Cas et al., 2008b; Le Maitre, 2002; Mitchell, 1997). The intrusion includes dark to gray fresh homogenous rocks which exhibit inequigranular (Figure. 15a) texture, formed by partially-to-fully altered olivine, phlogopite megacrysts up to 1 cm wide, macrocysts (0.5-10 mm), and crustal xenoliths set in a very fine greenish groundmass. In hand specimens, Limeira I exhibit rounded fragments of autoliths (Figure 15b) composed by highly serpentinized olivine, perovskite, monticellite, and carbonates set in a serpentine-calcite mesostasis.

Olivine, the most abundant phase, occurs as mega-, macro-, and microcrysts. The megacrysts typically comprise 15-20% of the volume of the rock, are rounded or anhedral and elongated, with a size between 1.0 and 3.4 cm. They exhibit extensive alteration, mostly along rims and fractures, with the development of serpentine (Figure 16a), although samples of fresh olivine cores are preserved. Some megacrysts are fully recrystallized as clusters of smaller crystals that, as a whole, still retain the shape of the original megacryst (Figure 16b). Olivine macrocysts also show alteration at rims and fractures, some crystals being fully serpentinized. They are typically subhedral, 5 to 9 mm in size, also showing rounded and anhedral shapes. Many of the macrocysts are stained, with undulose extinction. Microcrysts compose about 10% of the volume of the samples, down to 1 mm in size. They are subhedral and usually completely serpentinized, with only a few exceptions where minor fresh cores are preserved.

Phlogopite is present as macrocysts (Figure 17a, b), small euhedral microcristic and interstitial phlogopite in the groundmass in Limeira I kimberlites. Macrocrysts typically range between 0.2 and 6 mm in size, composing 5 to 15% of the rock volume. The microcristic phlogopite size ranges between 100 and 200 μm , exhibiting strong pleochroism from colorless/pale yellow to brown, and ranging states of alteration. Typically, laths are fresh, although some of them show extreme chloritization. Smaller crystals and interstitial phlogopite show minor alteration, average 50 μm in sizes.

Monticellite is present as fine-grained (10-30 μm) subhedral to euhedral grains only in the groundmass of Limeira I kimberlites, making up to 15% of the groundmass (Figure 18a). At the autolith, it can occur as a “garland” around olivine macrocysts (Figure 18b).

Pyroxene crystals occur mainly associated with polymimetic aggregates, that probably represent the interaction of silicate xenoliths with the magma. The crystals are colorless, prismatic, elongated, with high birefringence, and their dimensions range from 0.02 to 0.04 mm (Figure 19a). In the Limeira I kimberlite, they also occur as centimetric pyroxene xenocrysts

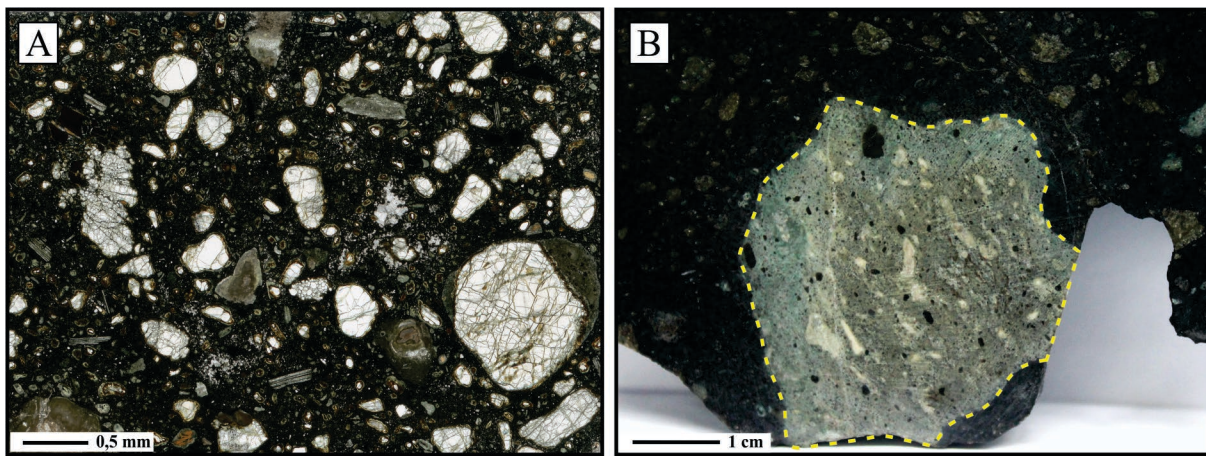


Figure 15 – Hand sample aspects of LM-I kimberlite (a) General view of a scanned thin section of inequigranular macrocristic kimberlite texture; (b) autolith in hand sample.

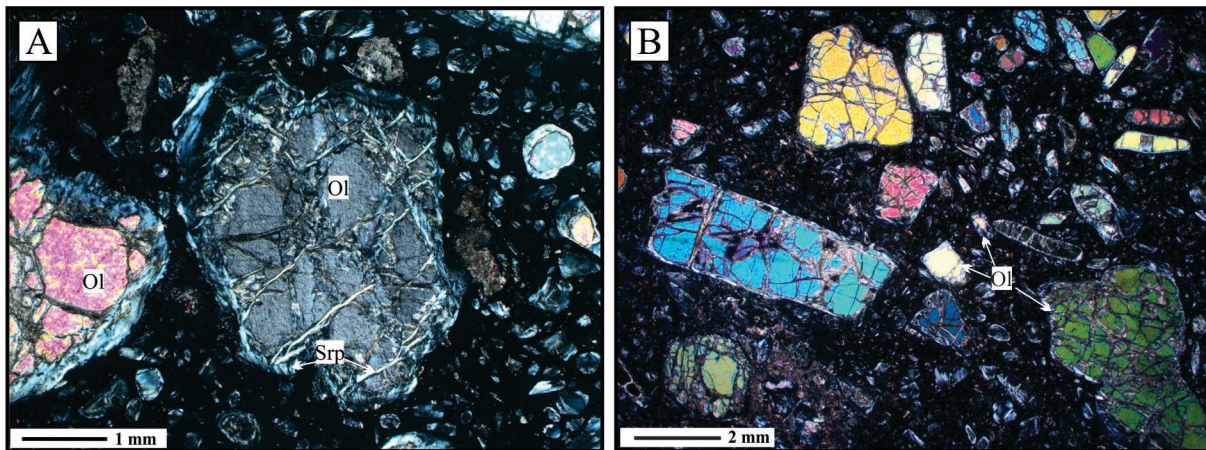


Figure 16 – Petrographic aspects of LM-I olivine crystals. (a) olivine macrocryst displaying undulose extinction; (b) mega-, macro-, and microcrysts of olivine set in a fine-grained groundmass. Cross-polarized transmitted light in (a) and (b).

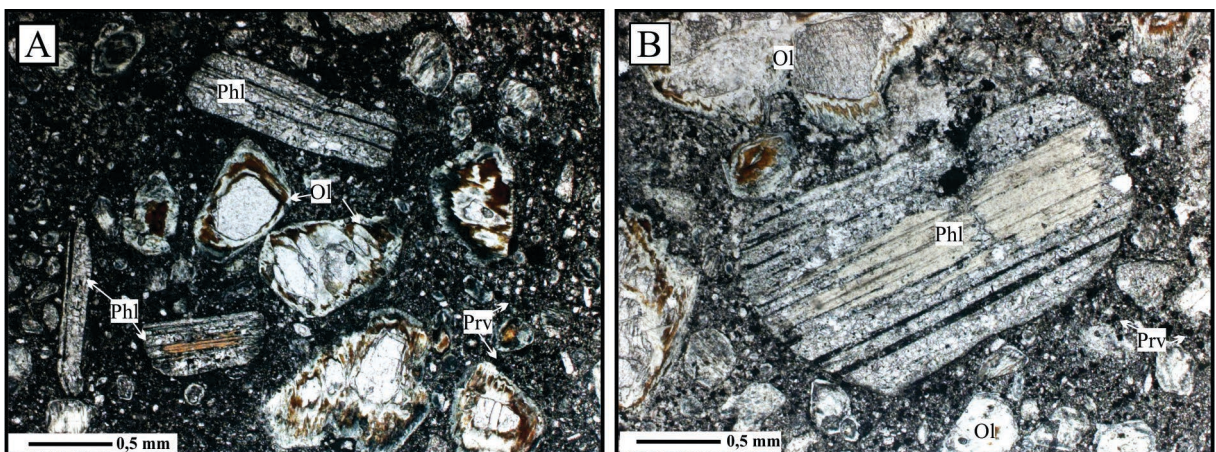


Figure 17 – Petrographic aspects of LM-I phlogopite crystals (a) phlogopite macrocrysts and phenocrysts; (b) phlogopite macrocryst with intensive alteration. Cross-polarized transmitted light in (a) and (b).

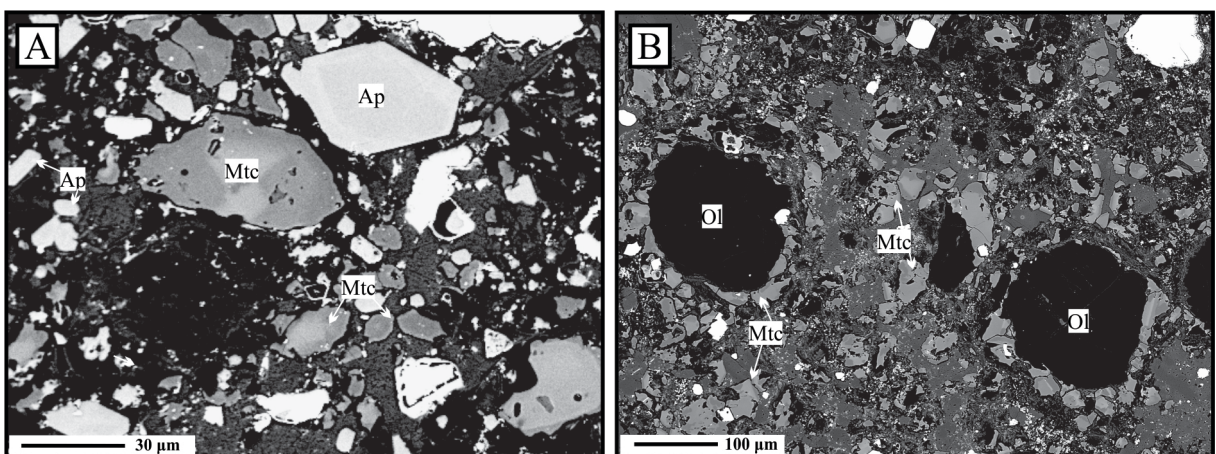


Figure 18 – BSE images of LM-I monticellite crystals: (a) subhedral to euhedral monticellite crystals; (b) monticellite crystals in the autolith as a “garland” around olivine macrocysts.

almost completely altered to serpentine. The presence of monticellite grains is common along crystal rims and fractures (Figure 19b).

Apatite is only observed at the Limeira I kimberlite. It composes about 5% of the groundmass (Figure 18a), as either singular acicular crystals or as its basal section, up to 50 µm in size.

Ilmenite is observed only in the Limeira I kimberlite, as subhedral to anhedral macrocrysts up to 2 mm wide, and in the groundmass ranging from 0.1 to 0.5 mm in size. A perovskite and titanomagnetite or chromite reaction rim are also observed (Figure 20a). Most rarely, inclusions up to 0.1 mm are present in olivine macrocrysts (Figure 20b).

Serpentine is common in the groundmass, composing about 5% of the matrix where it almost completely pseudomorphs the original fine grain minerals (Figure 16a). As previously mentioned, serpentinization of mega-, macro-, and microcrystic olivine is common. Serpentinization occurred to varying degrees, from minimal alterations concentrated along fractures to complete replacement with yellow and brown serpentine.

Carbonate is found as segregations within the groundmass, where it replaces the original groundmass minerals. In some cases, carbonate replacement is so extensive that it can make up 3% of the groundmass, resulting in a muddy brown appearance under plane polarized light.

The mantle xenoliths are peridotites, predominantly the dunites and metasomatized harzburgites (with phlogopite, secondary clinopyroxene, chromite, ilmenite, and others).

4.3 Perovskites from Três Ranchos IV and Limeira I

In Três Ranchos IV and Limeira I kimberlites, perovskite grains are in general similar to the perovskites of another group I kimberlites (Chakhmouradian and Mitchell, 2000). In both kimberlites, perovskite appears as a major groundmass phase that composes about 5-10 vol. % of the rock. The grains are euhedral to subhedral, in sizes that range up to 0.2 mm (Figure 21a; Figure 22 a, b). In Limeira I, some perovskite grains show very distinct zoning, occurring as reaction rims in ilmenite under the petrographic microscope (Figure 21b). Grains are mostly homogeneous, although some of them show normal zonation, with brighter cores. Under the petrographic microscope (Figure 22a), they show oscillatory zoning and relatively darker rims in BSE images (Figure 22 e, f). Complex zonation patterns are also observed where more than one core appears within the same crystal (Figure 22f).

According to the patterns observed in BSE images and suggestions of Sarkar et al. (2013), perovskite crystals were identified as pertaining to the following parageneses: (1)

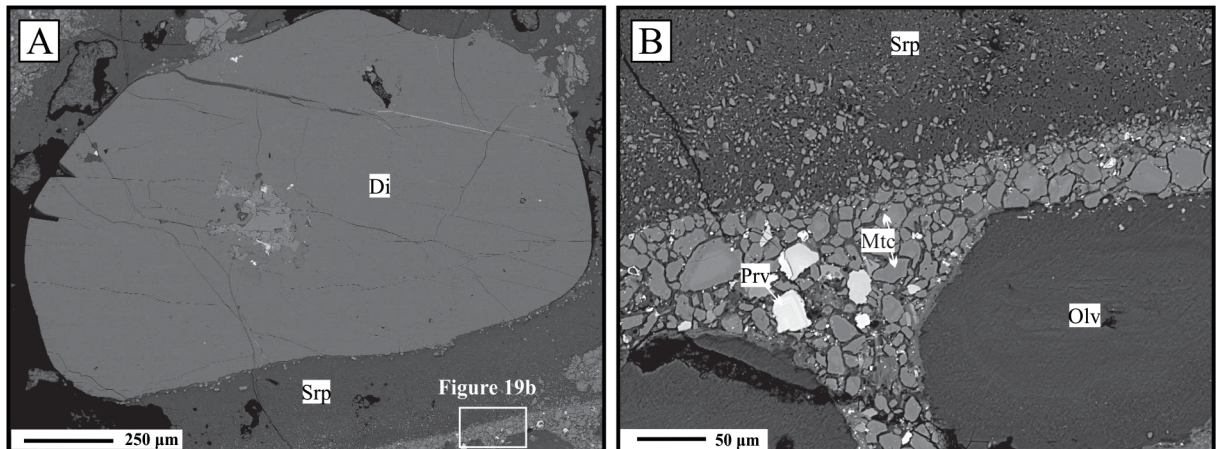


Figure 19 - BSE images of LM-I pyroxene crystals (a) pyroxene xenocryst with serpentine rim; (b) monticellite crystals at the boundaries of a pyroxene xenocryst.

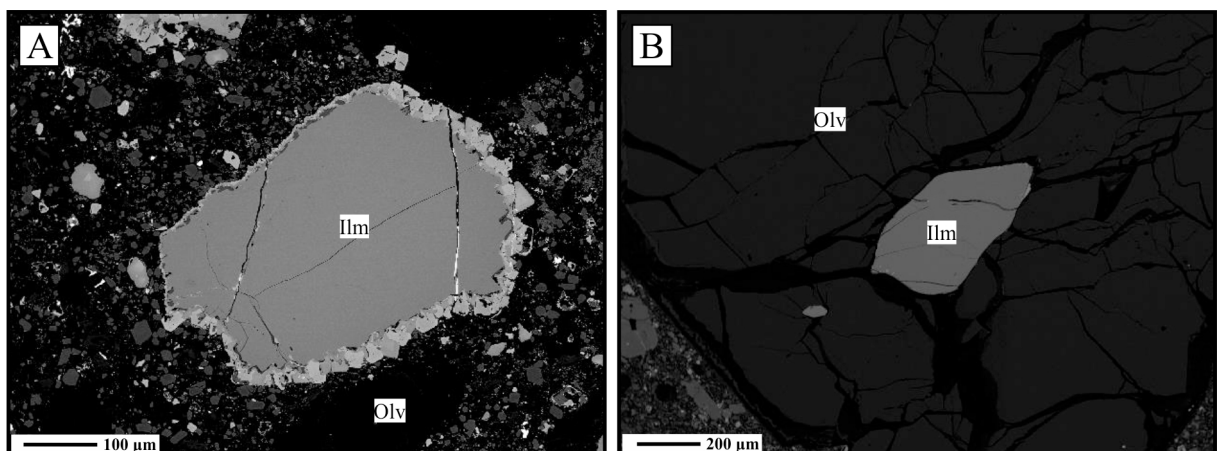


Figure 20 - BSE images of LM-I ilmenite crystals (a) ilmenite macrocryst with reaction rim; (b) ilmenite crystal as inclusion in olivine macrocryst.

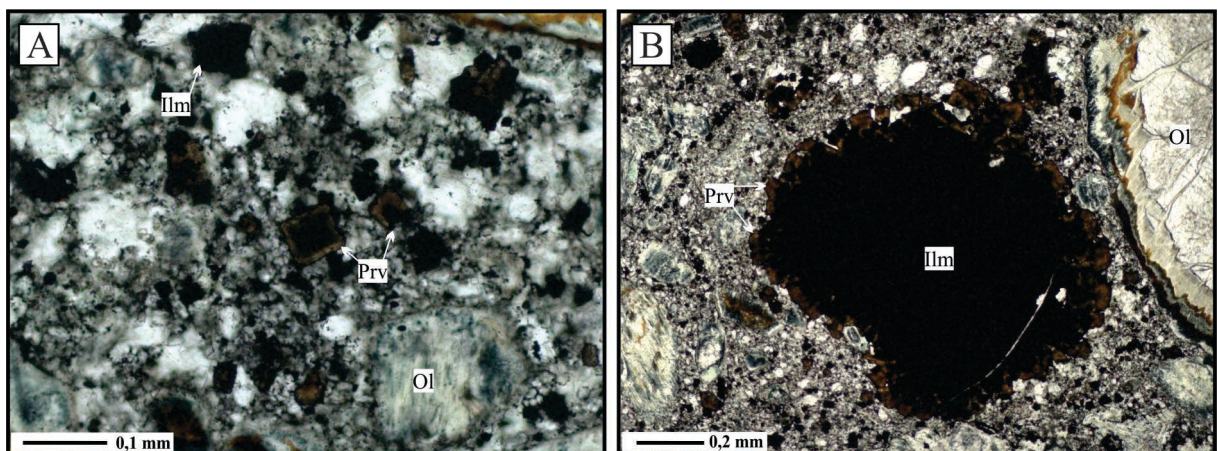


Figure 21 – Petrographic aspects of *Limeira I* perovskite crystals – (a) photomicrography of zoned perovskite; (b) perovskite as reaction rim in ilmenite crystal. Cross-polarized transmitted light in (a) and (b).

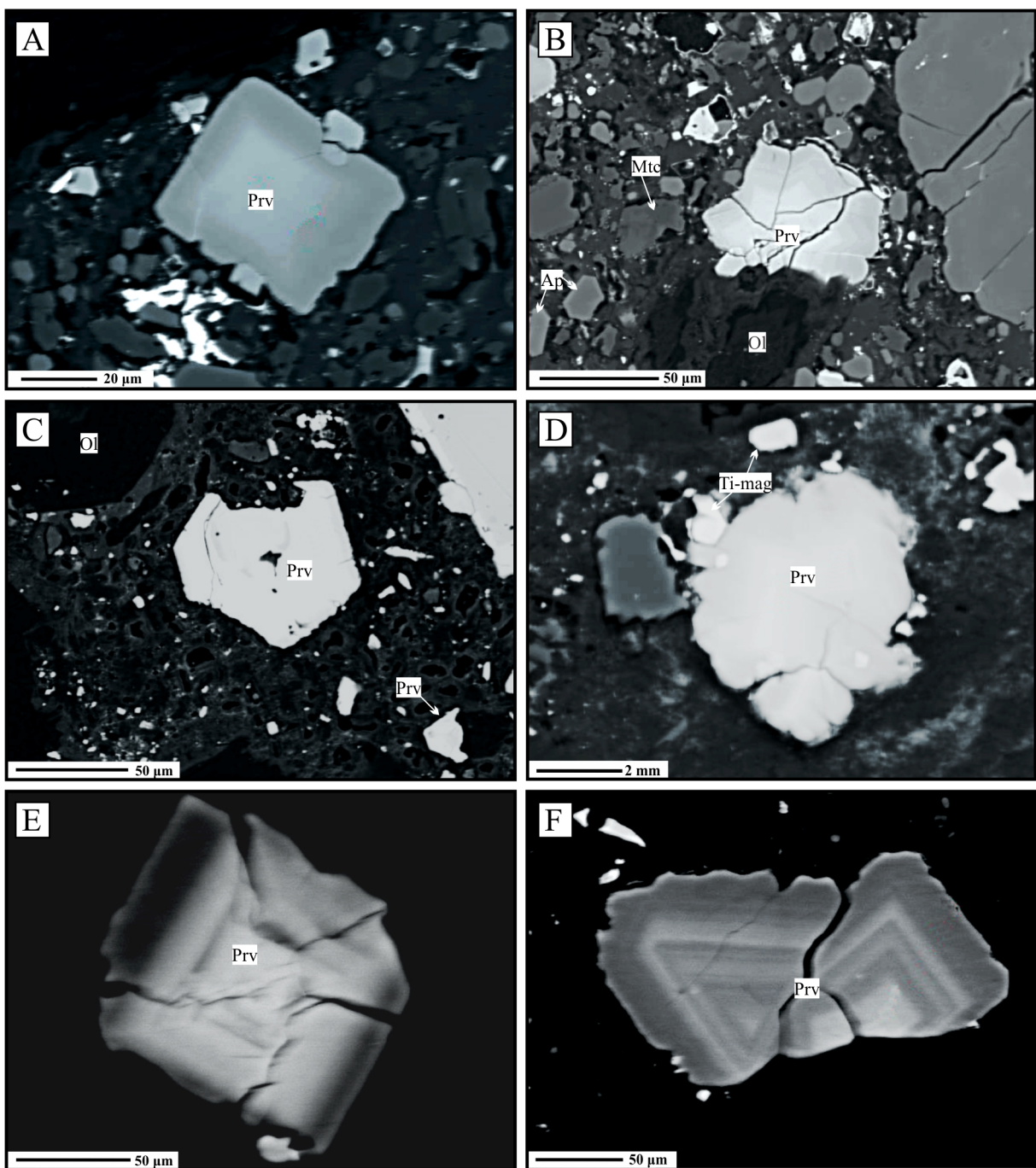


Figure 22 – BSE images of TR-IV and LM-I perovskite assemblage. *Três Ranchos IV* - a) and c) euhedral zoned perovskite crystal; e) perovskite oscillatory zoning; *Limeira I* – b) subhedral zoned perovskite crystal; d) intergrowth of a perovskite crystal with Ti-magnetite; f) perovskite oscillatory zoning.

discrete grains in the groundmass. (Figure 23 a, b); (2) grains along boundaries of olivine macrocysts and macrocysts forming a “garland” or “necklace” texture (Mitchell, 1986, Figure 23 c, d); (3) complex intergrowths with groundmass spinel or titanomagnetite (Figure 23 e, f); (4) a reaction rim around Ti-bearing phases like ilmenite macrocysts (Figure 24 a, b). All four paragenesis were observed in Limeira I. Type (4) is rare in Três Ranchos IV. Euhedral inclusions of serpentinized olivine and phlogopite are common in both intrusions (Figure 24 c, d). Perovskite sometimes is observed as tiny crystal inclusions within larger phlogopite grains, forming a poikilitic texture (Figure 24 e, f). Both kimberlites contain altered and fresh perovskite grains.

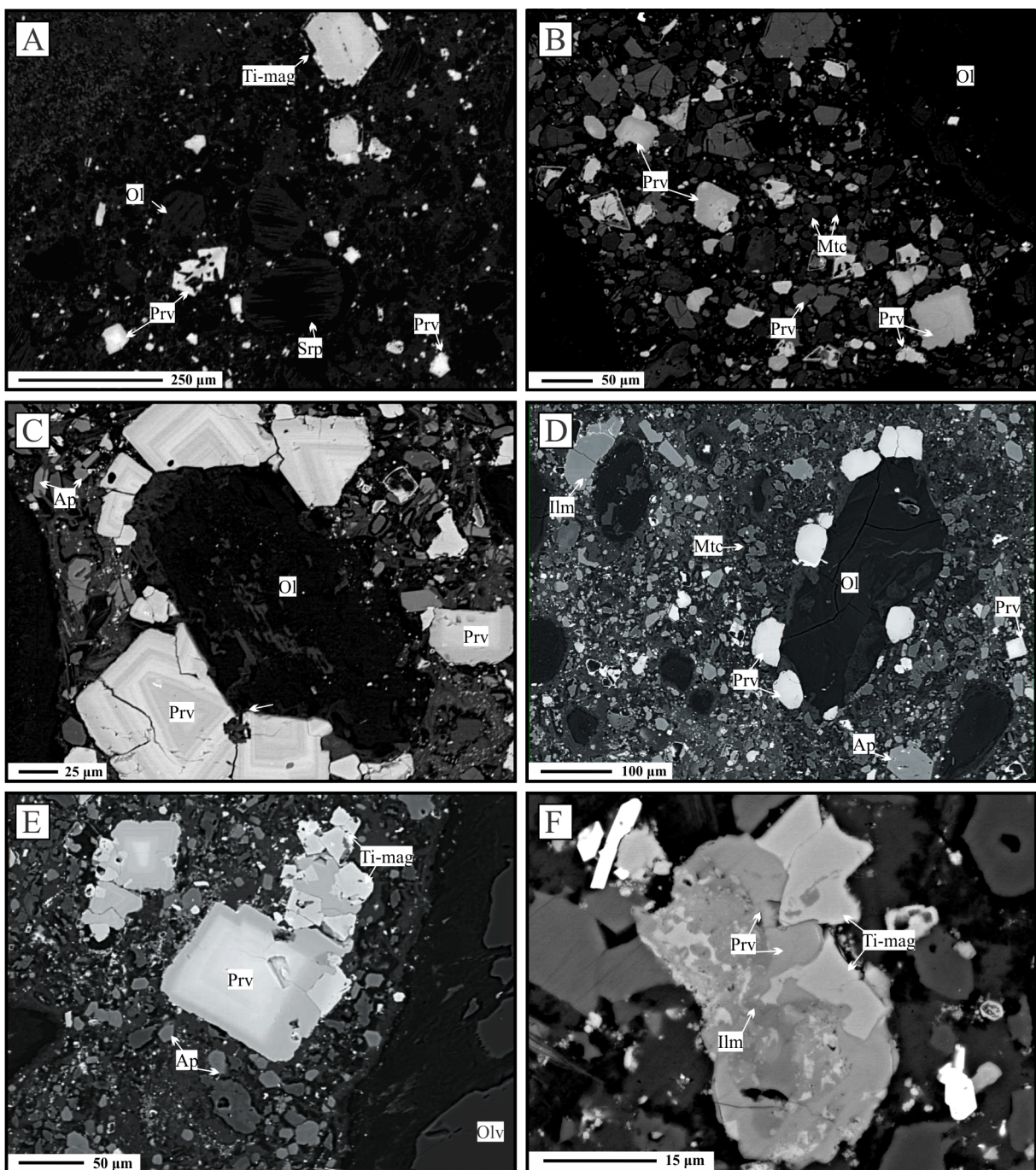


Figure 23 - BSE images of TR-IV and LM-I perovskites petrographic aspects. (a) *Três Ranchos IV* - discrete crystals in the groundmass; *Limeira I*; (b) discrete crystal in the groundmass; (c) and (d) zoned perovskite crystals as “garland” or “necklace” textures in olivine; (e) and (f) complex intergrowths of groundmass titanomagnetite and Ilmenite.

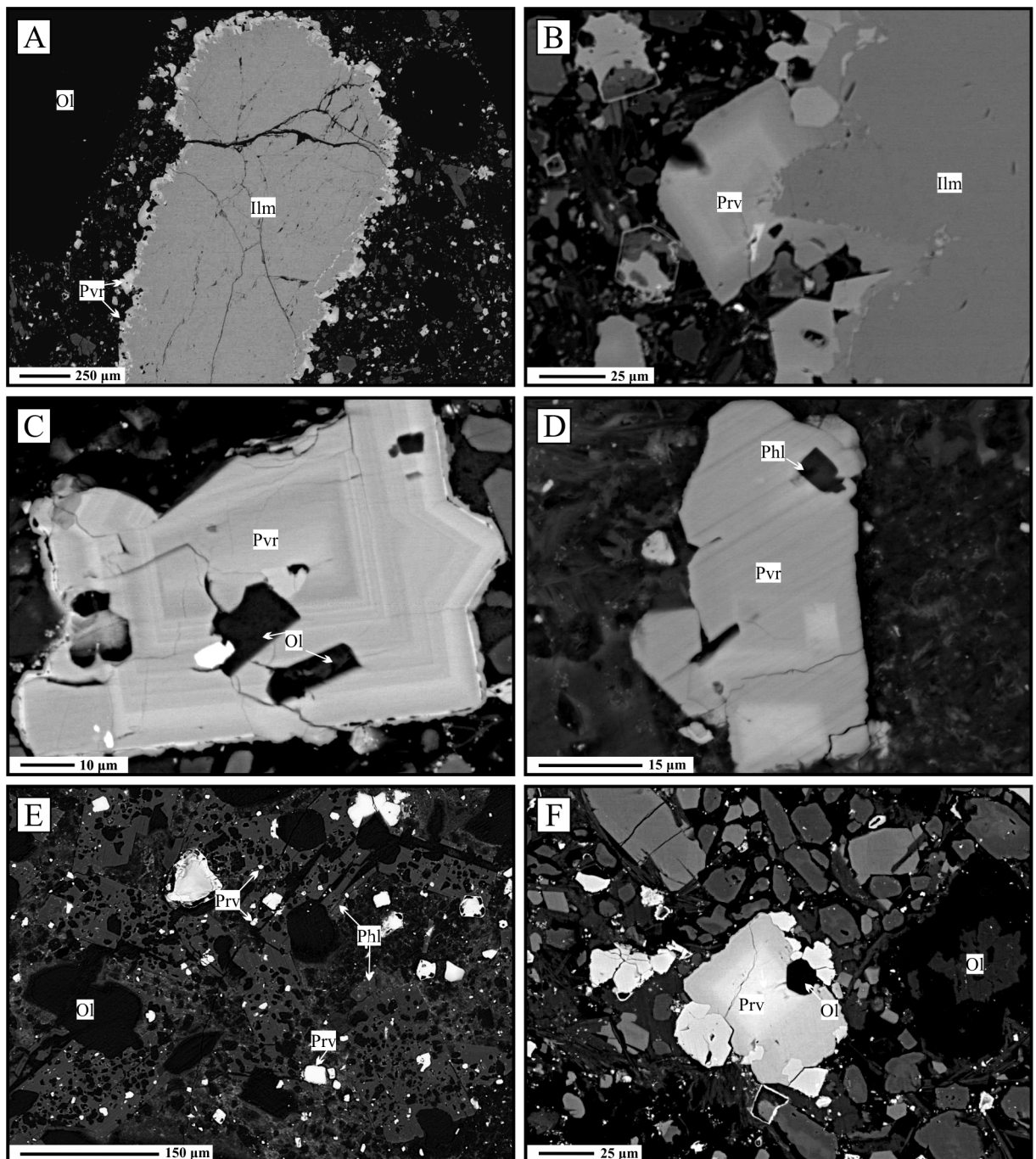


Figure 24 – BSE images of TR-IV and LM-I perovskite assemblage. *Limeira I* – (a) and (b) perovskite as a reaction rim around an ilmenite crystal; (c) and (f) olivine inclusions in zoned perovskite crystal; *Três Ranchos IV* – (d) phlogopite inclusion in perovskite crystal; (e) poikilitic texture of tiny perovskite in a larger phlogopite crystal.

CHAPTER 5 - MINERAL CHEMISTRY AND GEOCHEMISTRY

5.1 Olivine

Olivine compositions (Appendix Table B01) for Três Ranchos IV (Fo₈₇₋₉₂) and Limeira I (Fo₈₃₋₉₂) falls within the compositional range of Alto Paranaíba Alkaline Province (Fo₈₂₋₉₂, Araújo et al., 2001) and worldwide (Fo₈₄₋₉₅; Mitchell, 1986) reported kimberlites. Mega-, macro, and microcrystic olivine present cores with varying Mg# between different grains of both intrusions. In general, the olivine cores of Limeira I present higher NiO (~0.36 mass%), CaO (~0.04 mass%) and lower Cr₂O₃ (~0.02 mass%) contents than those from Três Ranchos IV (up to about 0.19 mass%; 0.04 mass%; and 0.20 mass%, respectively). In both intrusions, intermediary regions between rim and core are defined by the decrease in Mg# (around 0.91) and concentrations of NiO that remain high, while CaO and Cr₂O₃ are low, which reflects the decoupled behavior of major and minor elements (Bussweiler et al., 2015). The trace-element content of olivine (Table B02) is similar in both kimberlites, low Ni and Al, and Li, Zn, and Mn concentrations appear to be higher at the olivine cores (Figure 25, Appendix Table C02).

Distinct NiO, CaO, and Mg# patterns are observed. These components are typically used in the distinction between the mantle and igneous olivine (Bussweiler et al. 2015; Foley et al., 2013). The “mantle trend” represents typical mantle olivine compositions. It is mainly associated with core analyses, with restricted compositions at relatively high NiO (0.3–0.4 mass%) and low CaO (<0.1 mass%) concentrations,” (Bussweiler et al. 2015; Foley et al., 2013). This trend can be separated into different groups as for contents of g#. In a CaO vs. Mg# plot (Figure 26), for example, a group starting at Mg# ≈ 0.9, CaO ≈ 0.04 mass% and ending at Mg# ≈ 0.93, CaO ≈ 0.01 mass% appears to be aligned on a slightly negative slope. According to Bussweiler et al. (2015), the “melt trend” is observed in all rim analyses, being characterized by a decrease in NiO and an increase in CaO concentrations at an almost constant Mg#. However, as the olivines of TR-IV and LM-I show extensive serpentinization along crystals rims, the “melt trend” is identified in only a few samples. As for trace elements, the melt trend is enriched in Zr, Ga, Nb, Sc, V, P, Al, Ti, Cr, Ca, and Mn, whereas Zn, Co, Ni and possibly Na are enriched in the mantle trend. The rim and core analysis of both Três Ranchos IV and Limeira I olivines results closely to the described patterns (Figure 27).

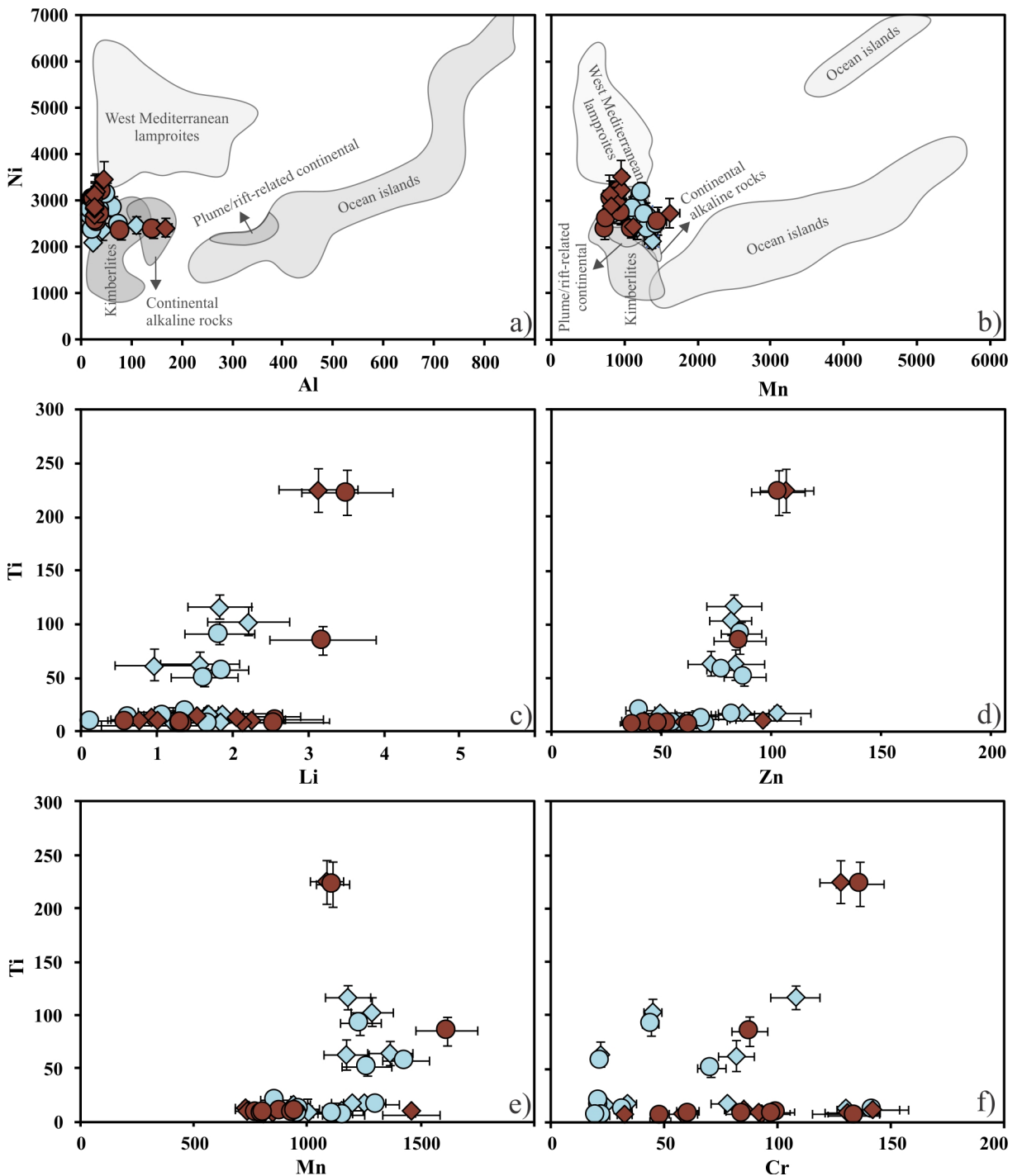


Figure 25 – Variation of trace element concentrations in Três Ranchos IV and Limeira I olivines. a) and b) presents compositional fields of samples compiled in Foley et al. (2013) compared to olivine rims and cores composition from TRIV and LM-I kimberlites (this work). Low Ni contents are characteristic of igneous fractionation, seen best here in kimberlites. A positive correlation of Ti with c) Li, d) Zn, e) Mn and f) Cr is also noticeable. Red symbols are TR-IV and blue symbols are for LM-I; Cores: circle, rims: diamonds.

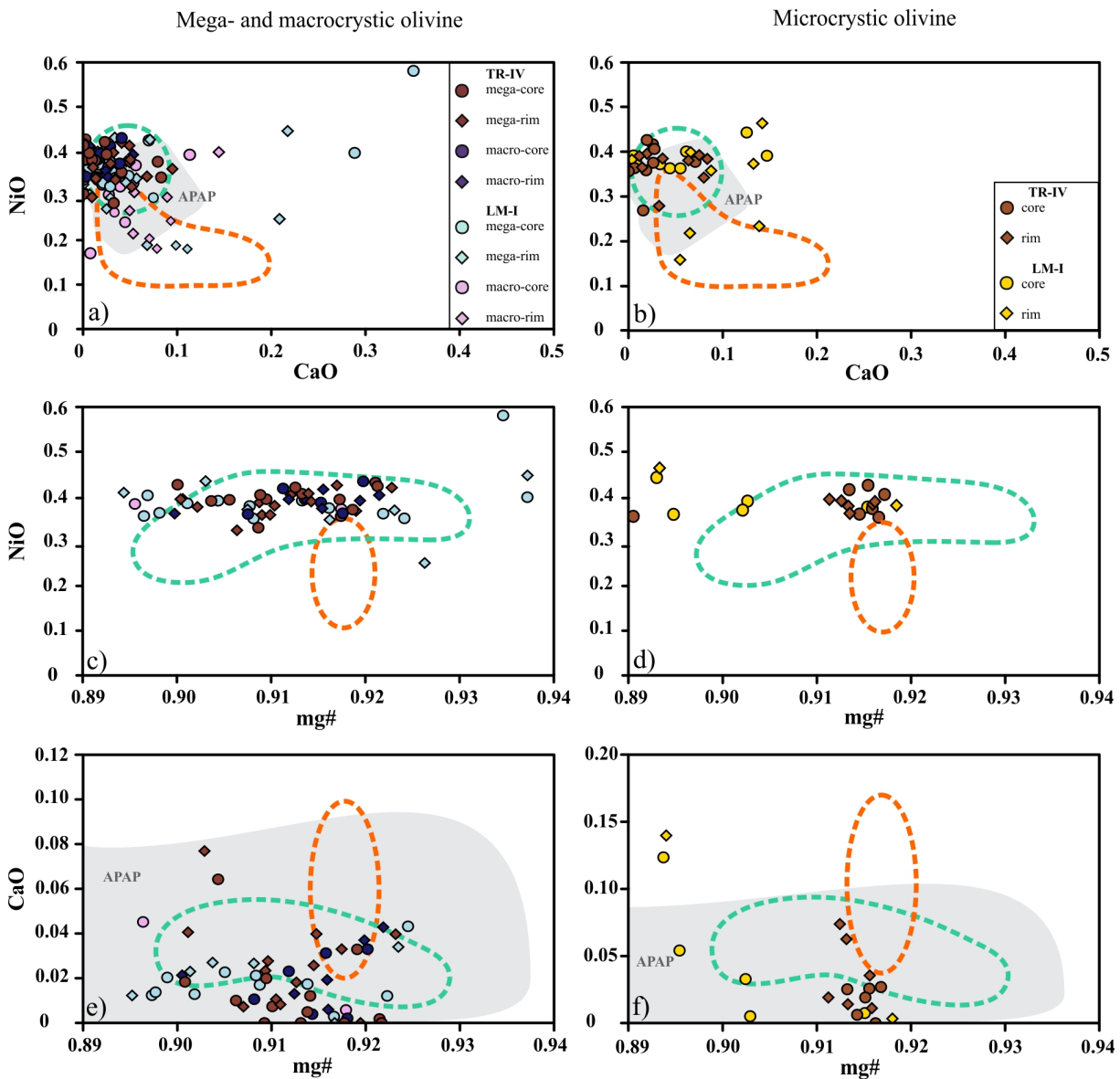


Figure 26 – Binary plots of EPMA data by mega- and macrocrystalline olivines; Três Ranchos IV (TR-IV), Limeira I (LM-I), and a data compilation on Alto Paranaíba Alkaline Province (APAP) kimberlitic intrusions and by rim and core analyses. Mantle trend (green) – compositions at relatively high NiO and low CaO; and Melt trend (orange) – decreasing NiO and increasing CaO at relatively constant Mg# (Bussweiler et al., 2015). Both were determinate according to south African kimberlites compositions. APAP literature data from Melluso et al. (2008), Araújo et al. (2001) and Meyer et al. (1994).

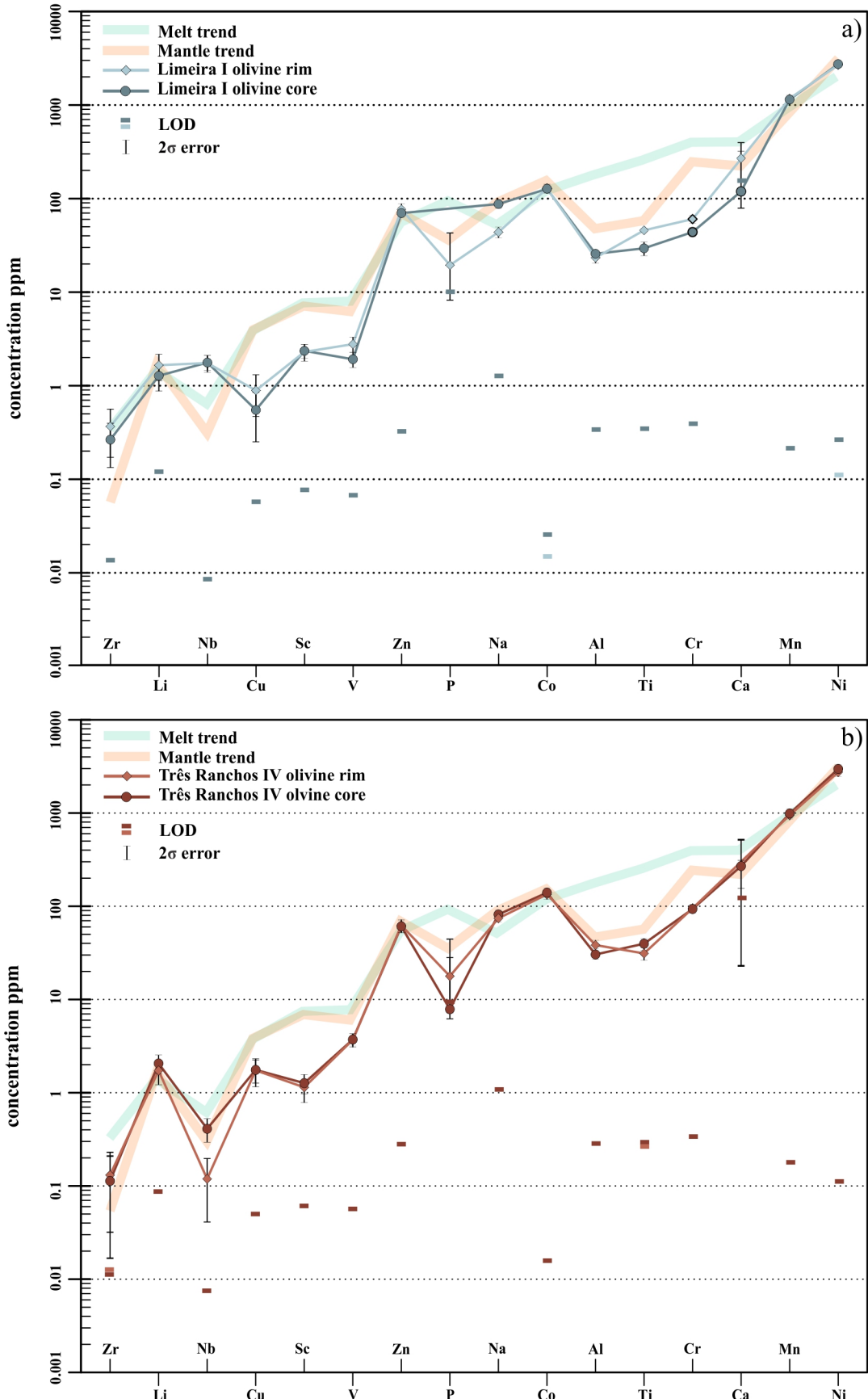


Figure 27 – Median values for minor and trace element of rim and core analyses in olivine from Três Ranchos IV and Limeira I with the mantle and melt trend from Bussweiler et al. (2015). LOD= limits of detection.

5.2 Monticellite

Monticellite was only found in the groundmass of Limeira I kimberlite. Its Mg# ranges from 72 to 93.8, indicating a significant compositional variation (Appendix Table B02, Figure 28) that is in agreement with the literature on kimberlites of the APA Province (74-92; Melluso et al., 2008; Araújo et al., 2001; Meyer et al., 1994; Guarino et al., 2013). Ca/(Ca+Mg) ratios range between 0.35-0.58.

5.3 Perovskite

The major and trace element analyses of perovskite samples from Três Ranchos IV and Limeira I obtained by EPMA, listed in Table B03 (Appendix B), normally remains close to the ideal CaTiO_3 (about 78 and 91 mol.%, respectively). However, a slight variation of the end members compositions of rims (TR-IV: average of 13 mol.% Lop and 81 mol.% Prv; LM-I: average of 4 mol.% Lop and 92 mol.% Prv) and cores (TR-IV: average of 16 mol.% Lop and 78 mol.% Prv; LM-I: average of 5 mol.% Lop and 91 mol.% Prv) is noticed in the analyzed perovskites. Other kimberlite data from APAP reported in the literature also present compositions that are close to the ideal perovskite (91 mol.% CaTiO_3 ; Figure 29).

Both intrusions have relatively minor contents of substituting elements (LREE, Na, Sr, Th, Si, Zr, Al, Fe, Nb, and Ta). The light lanthanides, Na, Th, Nb, and Fe present the most significantly varied concentrations intragranular zonation among the kimberlite the intrusions. Among the samples studied, the highest concentrations of LREE, Nb, and Fe^{3+} (up to 8.8, 4.4 and 5.3 mass% of the respective oxides) are observed in perovskites from the Três Ranchos IV kimberlite, that also present higher Sr and Na (up to 0.86 and 2.8 mass% of the respective oxides) values than those from Limeira I. As for the composition of other APAP kimberlites reported in the literature (Melluso et al., 2008; Felgate, 2014; Araújo et al., 2001; Meyer et al., 1994), the highest LREE concentration (up to 8.15 mass% of the oxide) falls close to one acquired in TR-IV, being higher than in LM-I (4.86 mass% of the respective oxide), whereas Nb, Fe^{3+} , Sr and Na concentrations of APAP (up to 1.05, 2.36, 0.79 and 2.33 mass% of the respective oxides) fall close to the ones of LM-I (up to 1.56, 2.41, 0.49, 1.08 mass% of the respective oxides). In both TR-IV and LM-I, higher LREE, Na and Th contents are observed in cores of zoned perovskite, while rims are slightly higher in Fe.

Perovskite trace element results by LA-ICP-MS analysis were also obtained for Três Ranchos IV and Limeira I kimberlites and are presented in Table C03 (Appendix C). Only trace element composition of central regions of perovskite crystals of both intrusions could be

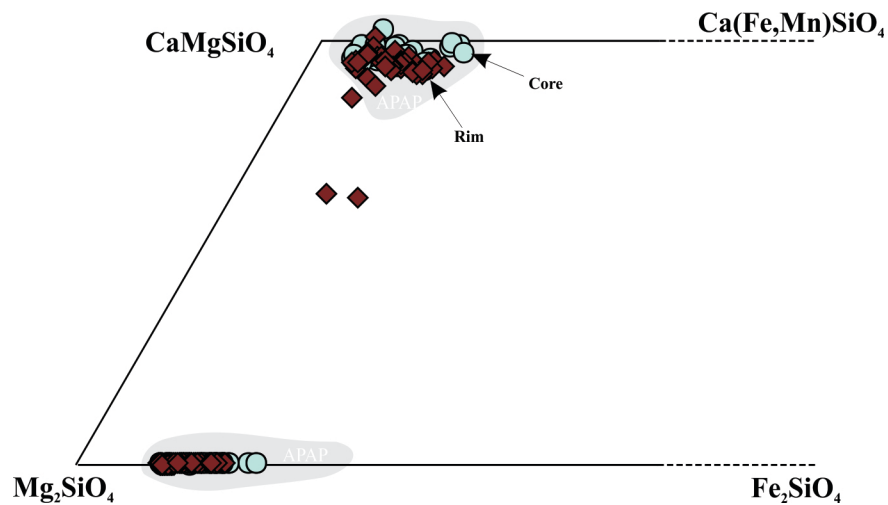


Figure 28 – Olivine diagram showing predominant forsterite (Mg_2SiO_4) and calcic/monticellite (CaMgSiO_4) phases for both Três Ranchos IV and Limeira I kimberlites. Alto Paranaíba Alkaline Province (APAP) literature data from Melluso et al. (2008), Araújo et al. (2001), Meyer et al. (1994), and Guarino et al. (2013).

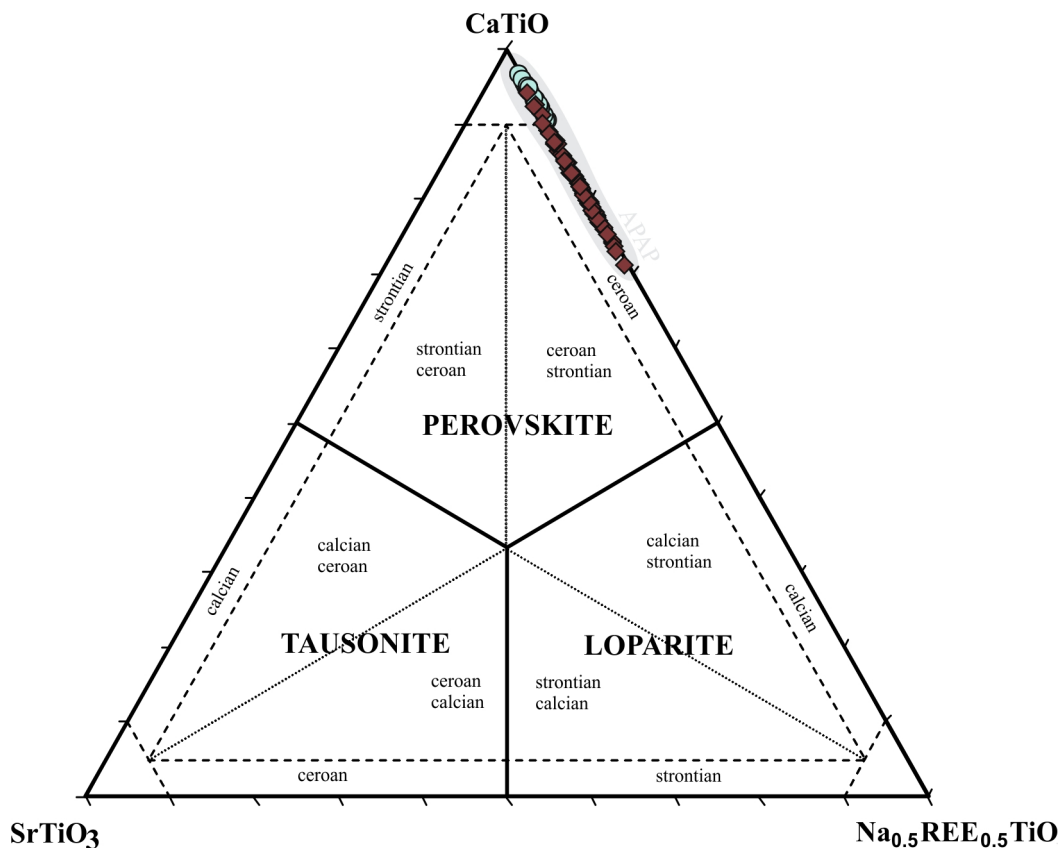


Figure 29 – Perovskite composition in Três Ranchos IV, Limeira I and Alto Paranaíba Alkaline Province (APAP) plotted in the tausonite – perovskite – loparite ternary system, with recommended subdivisions by Mitchell et al. (2017). APAP literature data from Melluso et al. (2008); Felgate (2014); Araújo et al. (2001) and Meyer et al. (1994).

obtained. The average perovskite compositions of TR-IV and LM-I, which are characterized by high concentrations of Sr (LM-I: 3889-2438 ppm; TR-IV: 6816-4919 ppm), Nb (LM-I: 10142-3860 ppm; TR-IV: 11794-5616 ppm), Zr (LM-I: 2207-850 ppm; TR-IV: 2151-463 ppm), and REE (LM-I: 88017-49977 ppm; TR-IV: 108350-87872 ppm), display a strong positive correlation between Nb and Ta; Y and Ho; Zr, and Nb; Mn and Fe (Figure 30). The primitive mantle-normalized REE patterns of the perovskite of the Três Ranchos IV and Limeira I kimberlites show smooth, highly fractionated trends with extreme LREE enrichment and no Eu anomalies. In a primitive mantle-normalized multi-element plot (spidergram), perovskite from both kimberlites shows extreme enrichment in LREE, U, Th, Nb, and Ta, and relative depletion in Ba, Pb, Sr and HFSE (Zr). These patterns fall within the field of previous APIP perovskite data (Figure 31).

5.4 Spinel

Four spinel groups were recognized in the rocks studied: (1) ulvöspinel-magnetite series; (2) Cr-spinel; (3) chromite, and (4) Mg-hercynite (Figure 32). The kimberlites contain Ti-magnetite and Cr-spinel (Figure 33). The macrocrysts spinels of Três Ranchos IV are Al-rich (up to 40.98 mass% Al_2O_3 ; Mg#=70), whereas the groundmass spinel ranges from magnesiochromite to chromite [$\text{Cr}/(\text{Cr}+\text{Al})$] =0.5-0.98; Mg#= 0.39-0.59; Figure 32). The composition obtained for spinels in TR-IV is very close to those reported in the Alto Paranaíba Alkaline Province literature (Araújo et al., 2001; Guarino et al., 2013; Figures 32 and 33). All chemical data regarding spinel is presented in Table B04 (Appendix B).

5.5 Ilmenite

The ilmenites of Limeira I fall into the kimberlitic field (Appendix Table B05), which is in agreement with the literature on data from other APIP kimberlites (Figure 34; Guarino et al., 2013), however being characterized by higher MgO (7.4–20.4 mass%) at a given TiO_2 (45.6–58.3 mass%). There is also a large variation in Cr_2O_3 (0.02-5.1 mass%). Based on these variations, Golubkova et al. (2013) divided Mg-Ilmenites from kimberlites into three different groups showing three different zoning patterns (trends) that define a characteristic parabolic curve (Figure 35). The first two trends are observed in Limeira I ilmenites. *Trend 1* is characterized by reversed zoning patterns with an increase in MgO (up to 14.1 mass%) and Cr_2O_3 (up to 5.1 mass%) toward the rims. An increase in MnO content is also observed towards the rims around 0.7 mass%. *Trend 2* is characterized by an increase in MgO and a decrease in

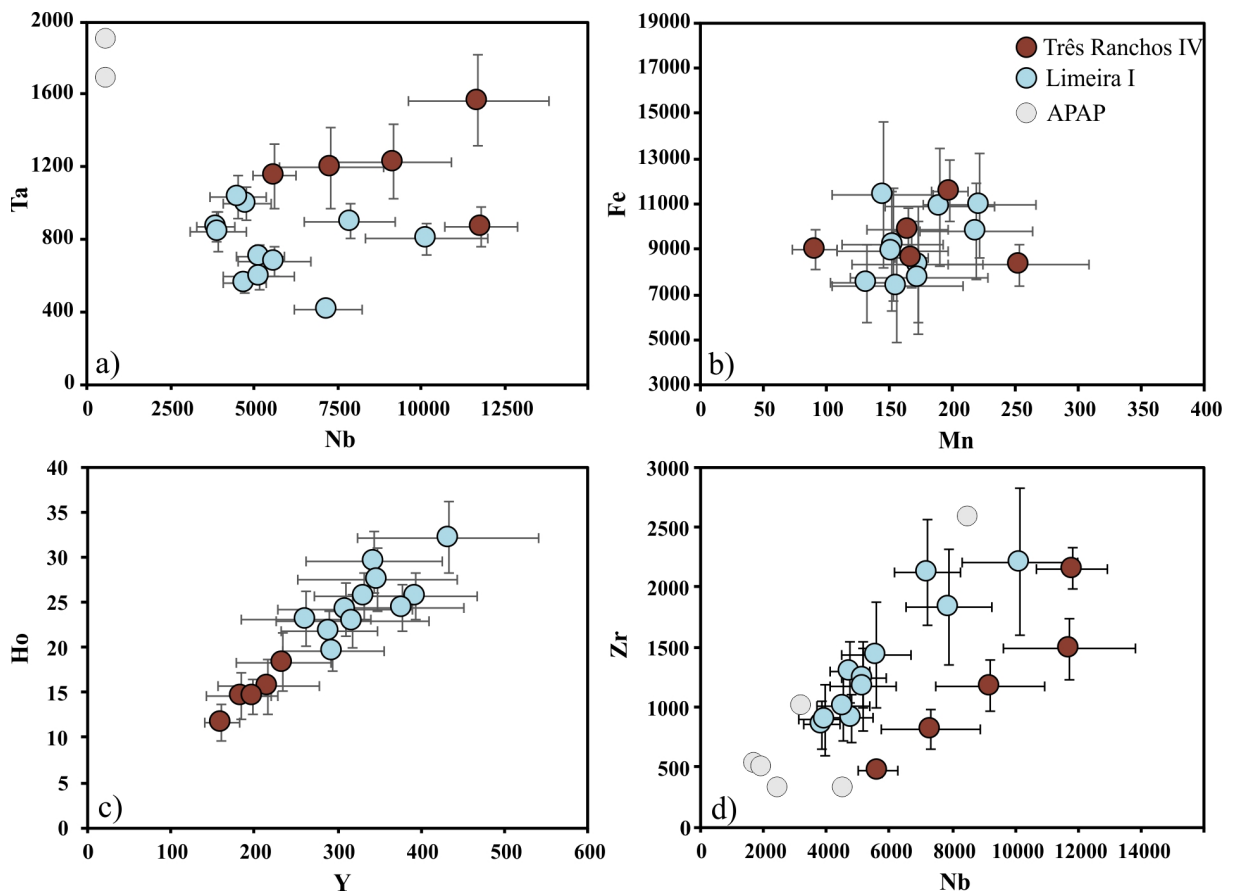


Figure 30 – Variation of major and trace element in perovskites from Três Ranchos IV and Limeira I. Positive correlation is notable between (a) Ta and Nb; c) Ho and Y; d) Nb and Zr. None of the transition elements whose partitioning behavior is sensitive to redox conditions - Mn, Fe: b) exhibit a coherent variation among or within the samples.

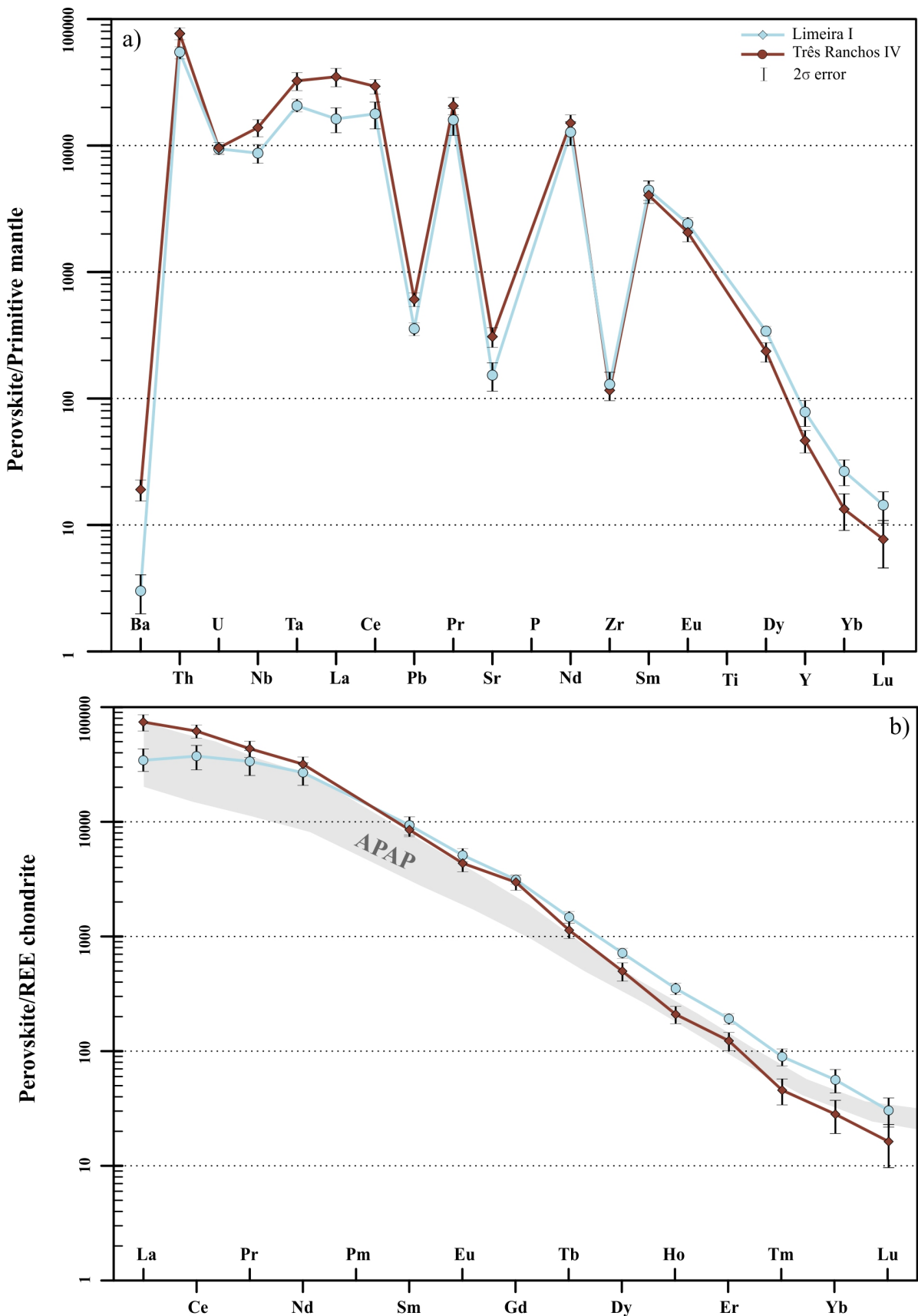


Figure 31 – Trace-element distribution patterns for perovskites from TR-IV and LM-1. Average compositions normalized by the primitive mantle in (a) and by the C1-chondrite in (b). Reservoir compositions from McDonough and Sun (1995). Bars are representative of 2-sigma uncertainties.

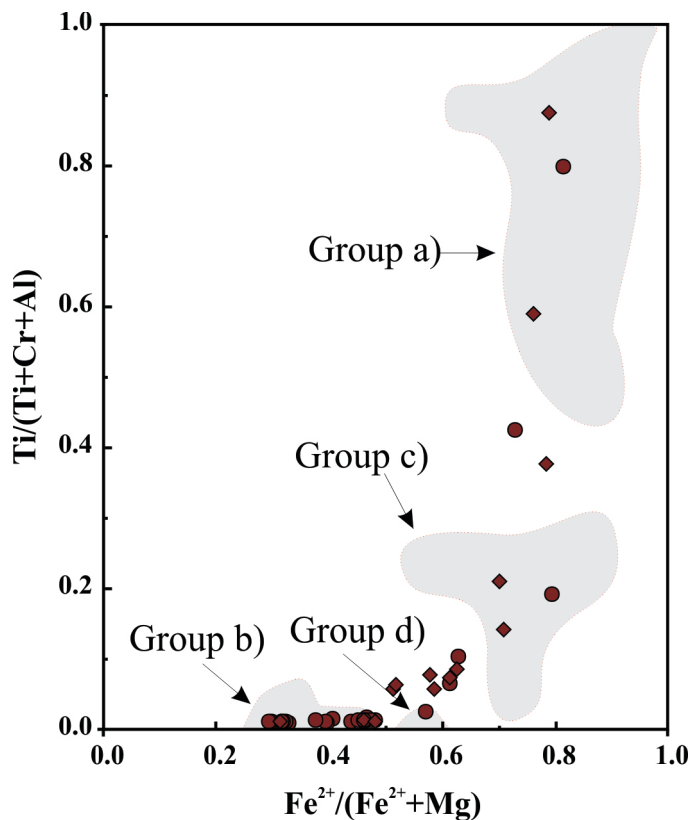


Figure 32 – Composition of Spinel specimens from the Três Ranchos IV kimberlite (this work, red circle - macrocrysts; red diamonds - microcrysts) and Alto Paranaíba Alkaline Province in gray-shaded fields with data from Araújo et al. (2001).

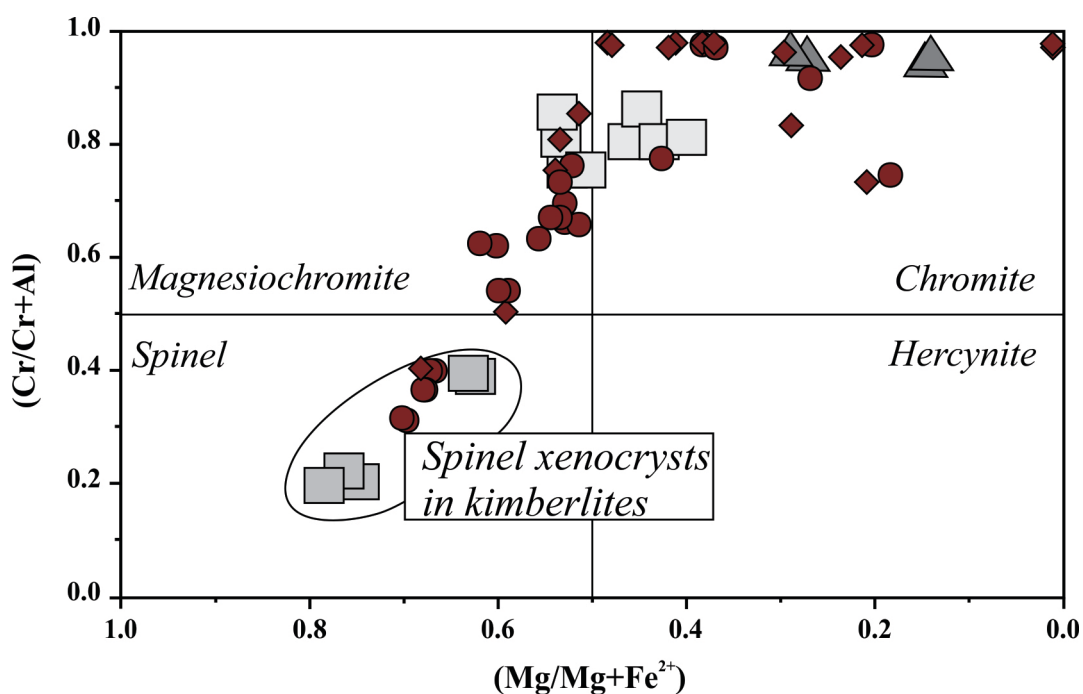


Figure 33 – Cr/(Cr+Al) vs. Mg/(Mg+Fe²⁺) diagram for Três Ranchos IV (red - this work) spinels macro-, (circle) and microcrysts (diamond) and APAP (gray) data from Guarino et al. (2013). Recommended subdivisions by Kapsiotis et al. (2009).

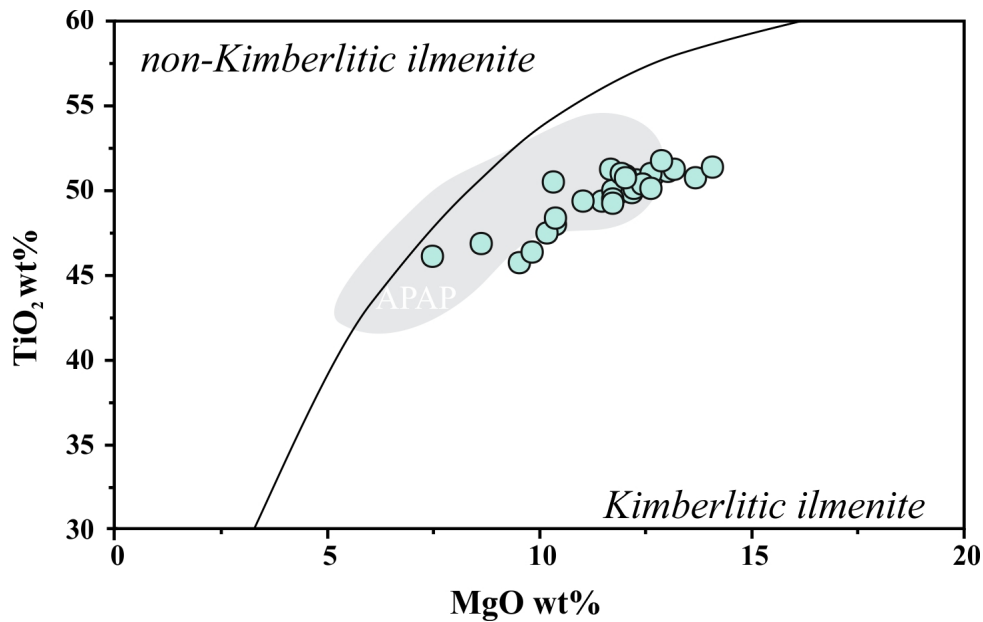


Figure 34 – APAP (data from Guarino et al., 2013) and Limeira I ilmenite diagram, with recommended divisions by Wyatt et al. (2004).

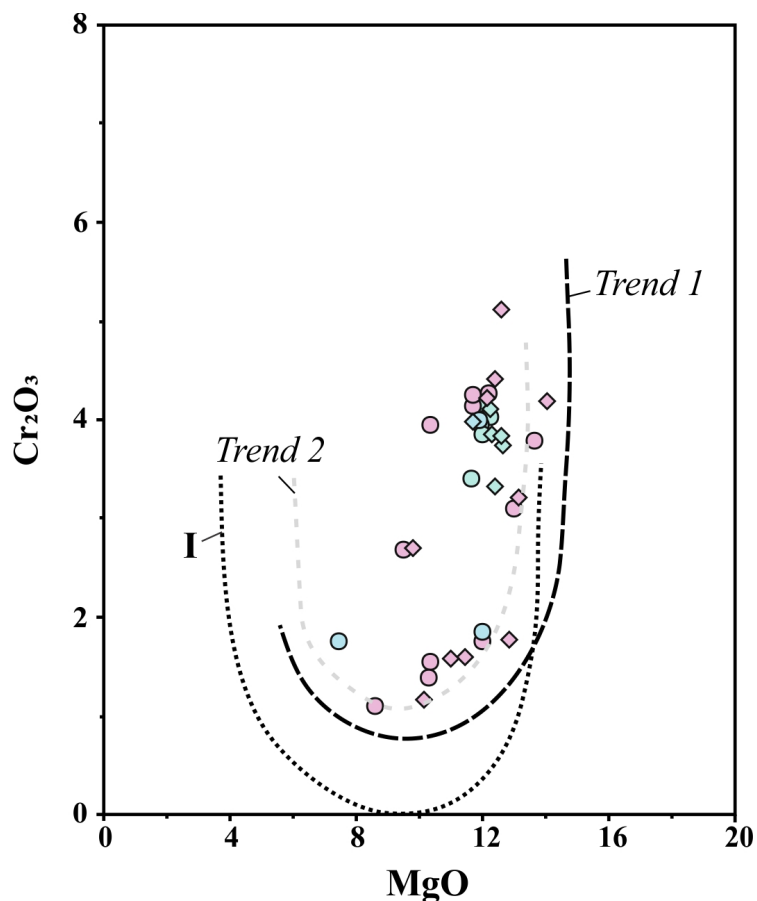


Figure 35 – Dashed “parabolic” curves representing compositional trends of kimberlite ilmenite: I - after Haggerty (1975), “typical” Mg and Cr distribution in ilmenite megacrysts from kimberlites, “parabolic” curve is shifted to the lower MgO concentrations in comparison with samples in the present study; Trend 1 (pink) – increase in MgO and Cr_2O_3 concentration toward rims; Trend 2 (blue) – decrease in Cr_2O_3 and increase in MgO concentrations toward rims.

Cr_2O_3 content towards the rims (Trend 2) in some Mg-ilmenite grains. In terms of MgO and Cr_2O_3 concentration, this trend corresponds to the left side of the parabolic curve in the binary diagram. The third type of zoning patterns, *Trend 3* presents a significant drop in MgO and Cr_2O_3 and an elevation in MnO content, however not observable in LM-I Mg-Ilmenites compositions.

5.6 Clinopyroxene

Xenocrysts and microphenocrysts from Limeira I and Três Ranchos IV, respectively, were subject to EPMA. Concentrations are presented in Table B06 (Appendix B). All the samples from both intrusions plot in the diopside-hedenbergite field in the Es-Wo-Fs diagram (Figure 36). Mg# ranges from 85 to 91 and from 87 to 92 in TR-IV and LM-I samples, respectively. Clinopyroxenes from all samples vary in CaO (TR-IV: 22.67-24.88 mass%; LM-I: 12.83-23.79 mass%), Na_2O (TR-IV: 0.53-1.35 mass%; LM-I: 0.31-0.81 mass%), and Cr_2O_3 (TR-IV: 0.03-0.47 mass%; LM-I: 0.10-1.08 mass%) content. Xenocrystic clinopyroxenes from Limeira I present higher MgO and FeO concentration (17.43-30.36 mass% and 2.78-7.67 mass% respectively) than microcysts clinopyroxenes from Três Ranchos IV (15-47 mass% and 2.77-4.86 mass% respectively).

5.7 Garnet

Major and trace element concentrations of Três Ranchos IV garnet crystals were obtained by EPMA and LA-ICP-MS. The results are listed in Table B07 (Appendix B). All garnet samples are identified as pyrope (62 to 73 mol.%), with Cr_2O_3 contents between 0.67 and 7.20 mass% and CaO contents between 3.99 and 5.67 mass%. TiO_2 is generally low (0.02-0.26 mass%), and Mg# values are variable (72 to 79 mol.%). According to the garnet classification scheme of Grütter et al. (2004), the Três Ranchos IV studied samples can be identified as lherzolitic (G9) and pyroxenitic (G4, G5) (Figure 37).

5.8 Bulk Rock Compositions

Major and trace element concentrations of Três Ranchos IV and Limeira I kimberlites are reported in Table D01 and D2 (Appendix D). For comparison, major elements vs MgO

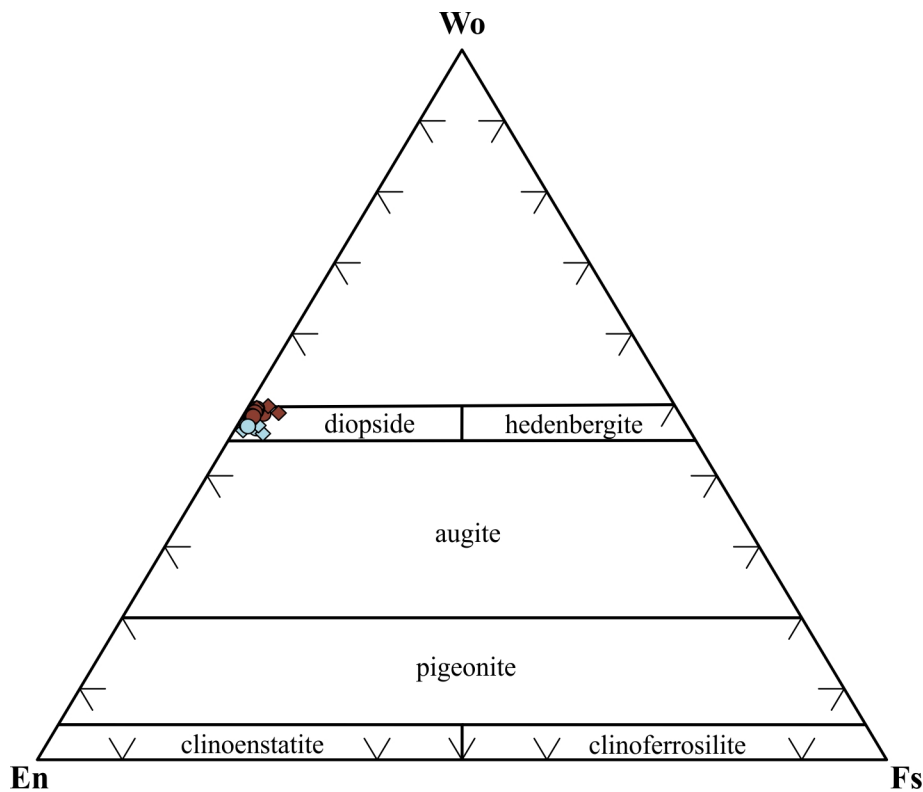


Figure 36 – Clinopyroxenes xenocrysts and microphenocrysts of Limeira I (light blue) and Três Ranchos IV (coral), respectively, plotted in the Morimoto (1990) pyroxene classification diagram. Wo – Wollastonite; En – enstatite; Fs – ferrosilite.

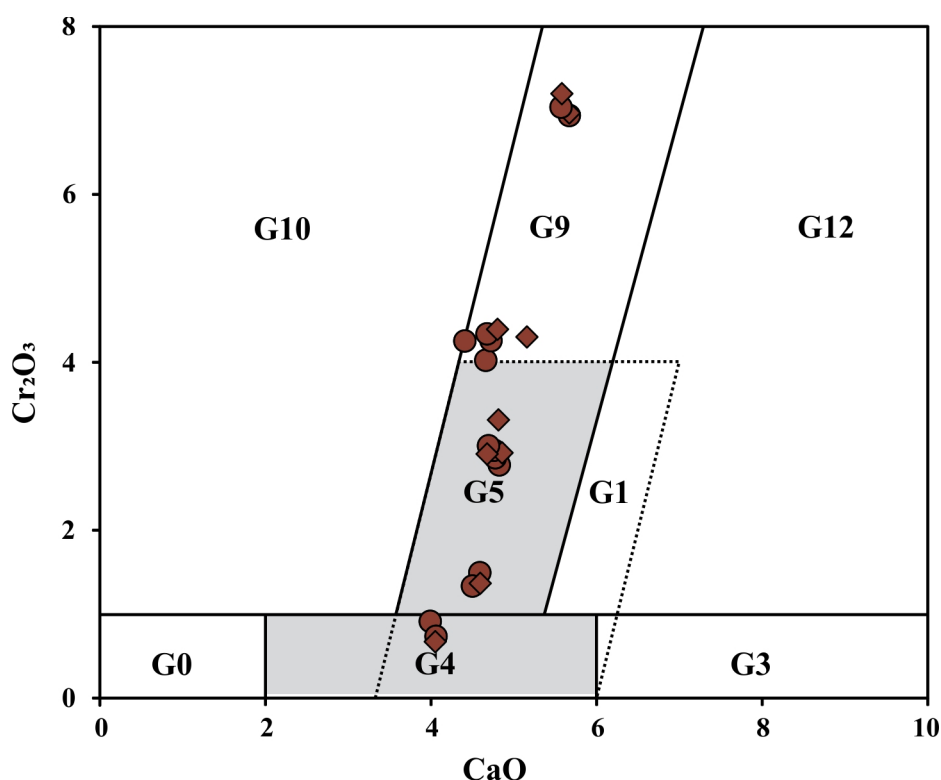


Figure 37 – Três Ranchos IV rim (diamond) and core (circle) pyrope analyses plotted in the G-number nomenclature classification scheme (after Grüttner et al., 2004).

variation diagrams with APAP kimberlite fields are shown in Figure 38. Both Limeira I and Três Ranchos IV kimberlites include ultrabasic rocks (SiO_2 =29.2-30.1 mass% and 32.6-34.6 mass% respectively) that are MgO-rich (MgO = 29.3-30.4 mass% and 31.8-34.6 mass% respectively), high Mg# (Mg# 73-74 and 77-79 respectively), CaO-rich (10.7-12.1 mass% and 3.7-8.3 mass% respectively), Al_2O_3 -poor (1.8-2 mass% and 1.8-2.2 mass% respectively), Na_2O -poor (up to 0.02 mass% and 0.06 mass% respectively) and potassic to ultrapotassic in character (K_2O = 0.9–1.6 mass% and 0.7-1.2 mass% respectively), High LOI (9.2-9.8 mass% and 10.9-11 mass% respectively), largely due to the abundant presence of volatile-bearing phases such as carbonates, serpentine and phlogopite. All major element data are supported by data from the APAP literature (SiO_2 = 25.3-34.2 mass%; MgO = 20.2-32.7 mass%; Mg# 60-86; CaO = 6.5-15.4 mass%; Al_2O_3 = 4-3-3 mass%; Na_2O = 0.02-1.4 mass%; K_2O = 0.54-3 mass%; Gibson et al., 1995; Carl et al., 1995; Melluso et al., 2008; Felgate, 2014; Bazzi et al., 1994; and Meyer et al., 1994). The relatively low K_2O content is a typical characteristic of uncontaminated kimberlites worldwide (Kjarsgaard et al., 2009).

Trace element concentrations are variable for both kimberlites. Concentrations of Ni (Três Ranchos IV: 1469-1634 ppm; Limeira I: 1216-1256 ppm) and Cr (Três Ranchos IV: 1617-1754 ppm; Limeira I: 1390-1523 ppm) are well-correlated with MgO whole-rock concentration (Figure 39 - a and b), with Três Ranchos IV kimberlite being the most enriched in these elements. The high field strength (HFS) elements in both kimberlites show similar concentration ranges and overlapping correlations (e.g., Três Ranchos IV Nb = 311-325 ppm, Zr = 342-363 ppm and Hf = 6.1-6.44 ppm; Limeira I Nb = 209-227 ppm, Zr = 629-688 ppm, Hf = 11.8-13.1 ppm). Within the TR-IV kimberlite, Th concentrations range from 31.6 to 33 ppm in moderate correlation with U (7.3-7.8 ppm), despite the known mobility of U, but in stronger correlation with La (U/Th = 0.23; La/Th = 12.3). The Limeira I kimberlite shows U and Th ranges similar to the TR-IV kimberlite (U = 4.9-5.2; Th = 19.8-21.5 ppm) ones, but lacks a good correlation between these elements. La/Th ratio (La/Th = 14 ± 1.9) is slightly higher. Limeira I kimberlites tend to show higher Rb, and Sr (Rb = 103-124 ppm; Sr = 2221-2304 ppm), and lower Ba (Ba = 2342-2476 ppm) concentrations than Três Ranchos IV (Rb = 60.9-104 ppm; Sr = 2039-2174 ppm; Ba = 3422-4863 ppm) ones (Figure 39). Compared to APAP kimberlites, the Limeira I and Três Ranchos IV kimberlites are depleted in Rb (APAP, Sr = 506-4502 ppm), however, supported by all the other elements (e.g. APAP, Sr = 355-3727 ppm; Ba = 506-4502 ppm; U = 3-7.7 ppm; Th = 10.4-42 ppm). Rare earth elements show considerable variation among Três Ranchos IV and Limeira I kimberlites (e.g., TR-IV La =

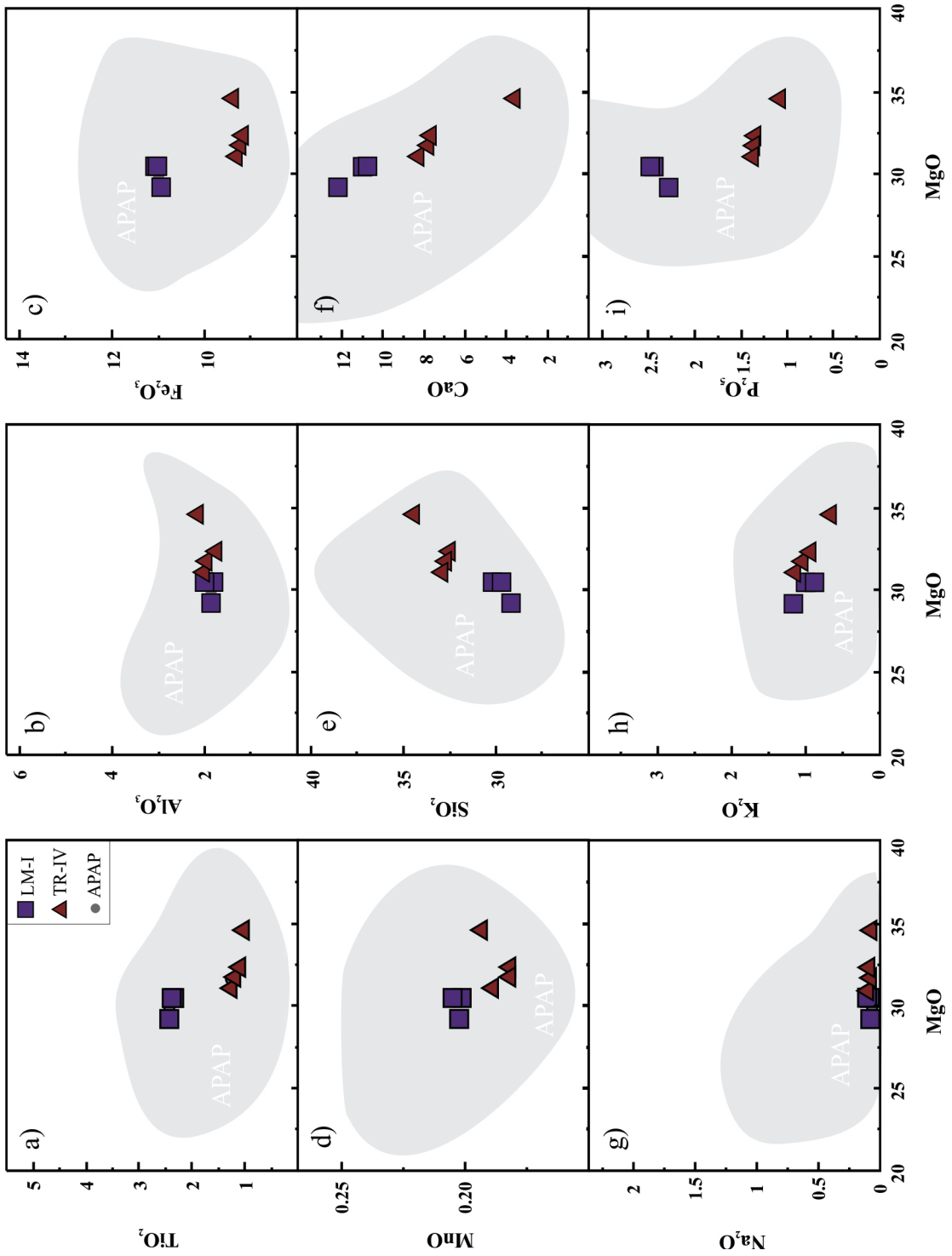


Figure 38 – Major elements (mass%) vs. MgO (mass%) variation diagrams for Três Ranchos IV, Limeira I (analyzed here) and APIP data from literature (Gibson et al., 1995; Carl et al., 1995; Melluso et al., 2008; Feijate, 2014; Melluso et al., 2014; Buzzi et al., 1994; and Meyer et al., 1994).

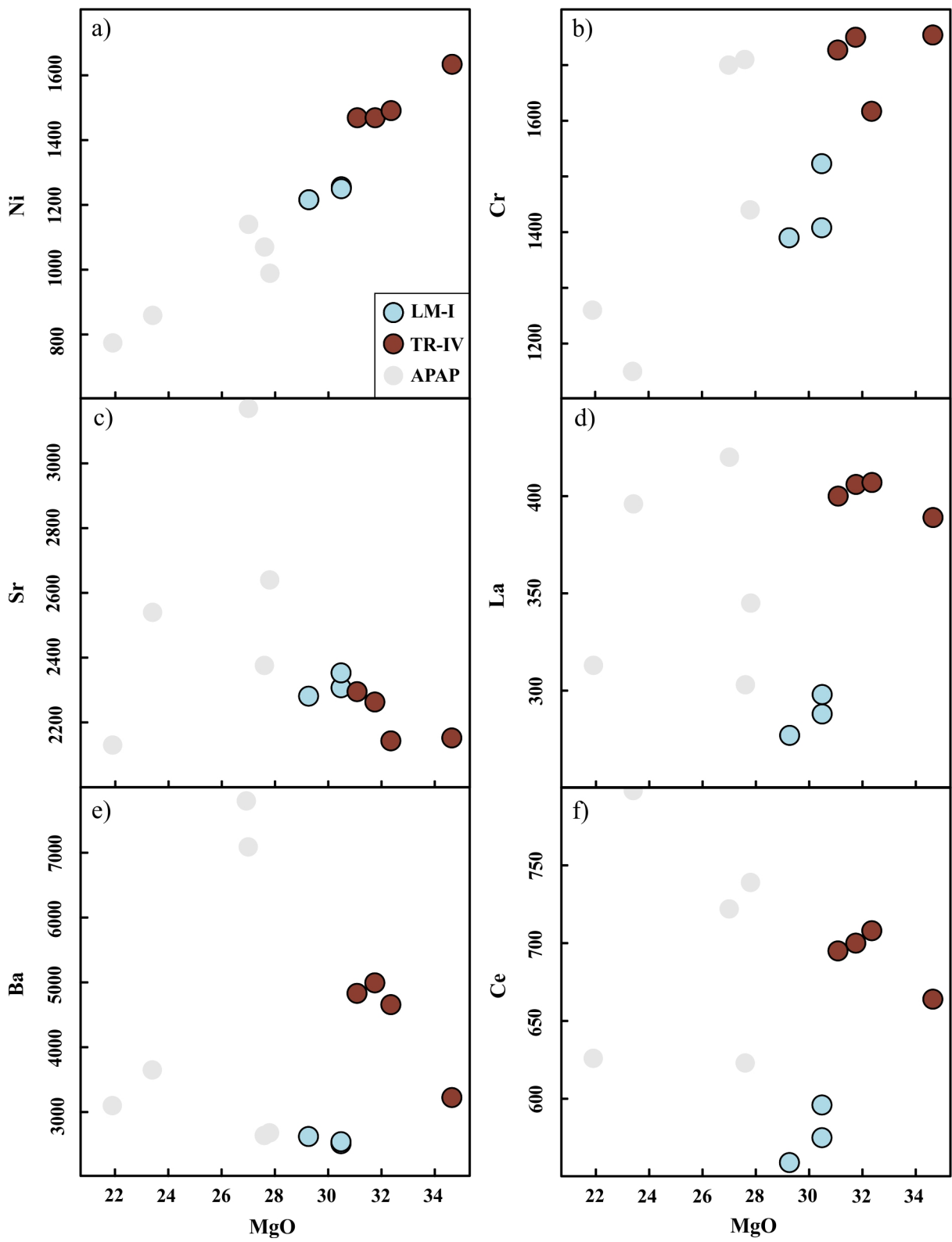


Figure 39 – Trace element vs. MgO (mass.%) variation diagrams for Limeira I, Três Ranchos IV and APAP rocks (after Guarino et al., 2013; and references therein).

389-407 ppm; LM-I La = 277-298 ppm, Figure 39). Both kimberlites samples show highly fractionated REE patterns and relatively low HREE abundance chondrite normalized, these and the primitive mantle-normalized incompatible element patterns are near to other Alto Paranaíba Alkaline Province kimberlites (Melluso et al. 2013) (Figure 40).

5.8.1 Bulk rock composition and mineral chemistry

Whole-rock, mineral and estimatives of liquid compositions are plotted together in binary major element diagrams (Figure 41). The samples of the kimberlitic intrusions studied (TR-IV and LM-I) show whole-rock compositions for many major elements. In SiO₂ vs MgO plots, monticellite and olivine are the major controller minerals, olivine thus presenting higher MgO concentrations. This feature is due to olivine being the most abundant phase, constituting about 40% of the rock volume. Likewise, olivine is the mineral phase that most contributes to the concentration of MgO in the global compositions of both intrusions (from 29.6 to 32.25 mass%). In MnO vs MgO plots, the concentration of MnO in both Três Ranchos IV and Limeira I kimberlite is strongly controlled by the presence of monticellite spinel and olivine. The concentrations of CaO and TiO₂ are controlled by perovskite, spinel, and ilmenite, and monticellite in the former. Aluminous phases like spinel and ilmenite are responsible for the rise in Al₂O₃ content. In Na₂O vs MgO plots, the whole rock composition of both intrusions is balanced between similar Na₂O variations between spinel, ilmenite, and olivine, with a respectively increase in MgO content in these phases.

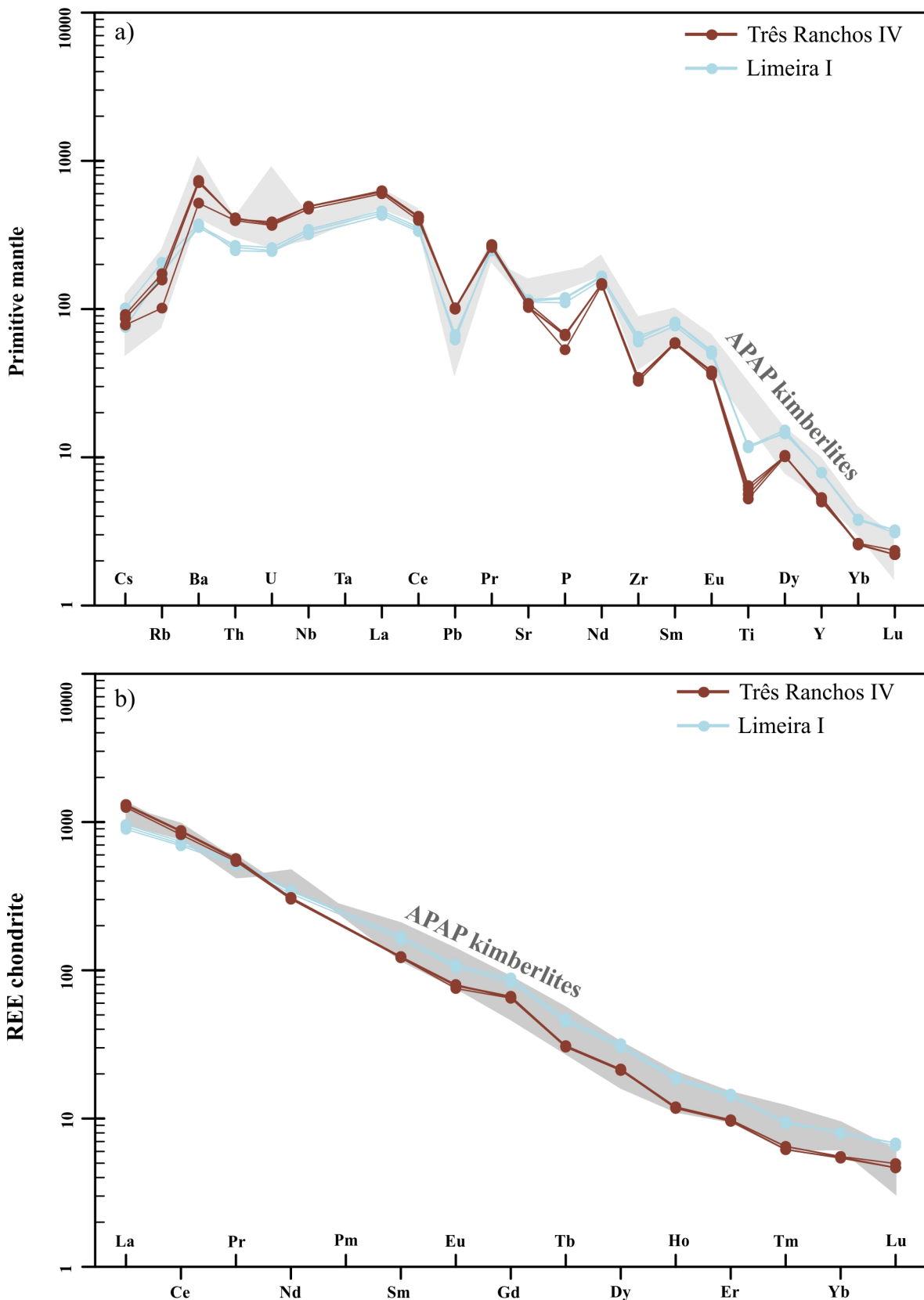


Figure 40 – Primitive mantle-normalized (Sun and McDonough, 1989) element and chondrite-normalized rare earth element (Boynton, 1984) pattern for whole-rock data from TR-IV, LM-I and literature APAP kimberlites (Guarino et al., 2013; and references therein).

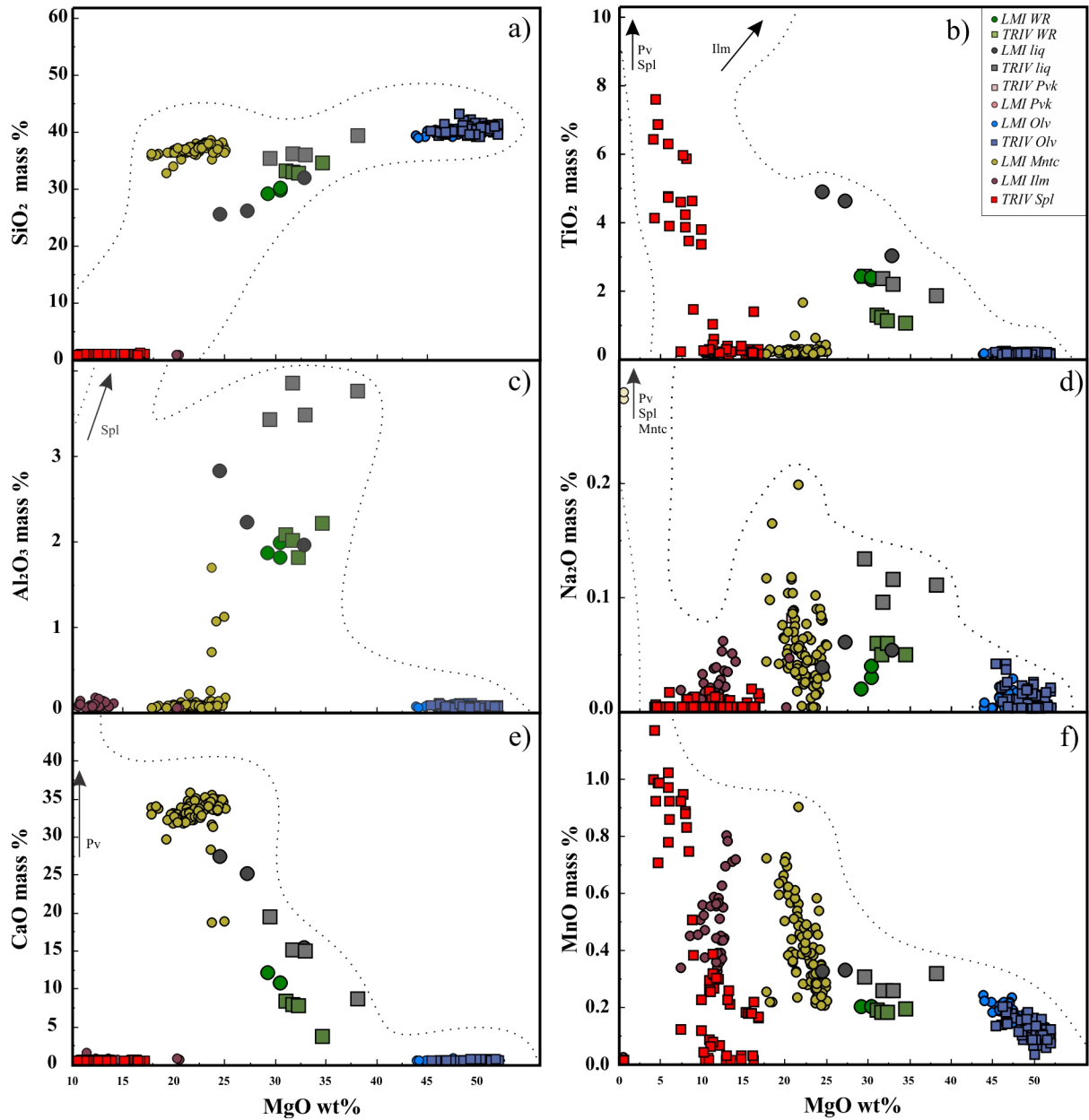


Figure 41 – Whole rock, liquid and mineral phase major element composition: WR - whole rock; Ol - olivine; Pv - perovskite; Mtc - monticellite; Ilm - ilmenite; Spl - spinel; Liq - liquid.

CHAPTER 6 - DISCUSSION

6.1 Estimation of Intensive Parameters of Crystallization for the Alto Paranaíba Alkaline Province

Mineral phases like garnet, olivine, clinopyroxene, and spinel are among the most important constituents of the upper mantle, and they are all sampled from kimberlites. In most cases, the composition of these minerals is controlled by subsurface reactions, which are influenced by pressure (P) and temperature (T) conditions. These specific reactions can be calculated by experimental and/or theoretical methods that allow the determination of the equilibrium conditions of minerals. The resulting T and P support several geological interpretations, such as the construction of paleogeotherms, which reflect the reigning thermal conditions of the mantle during a kimberlitic intrusion. Pressure values obtained from xenocrysts are also important in the evaluation of the potential of these kimberlite magmas as diamond carriers. The application of thermobarometric techniques to xenoliths allows discriminating among natural pressure and temperature (P-T) of xenolithic occurrences up to 3.0 Kbar (Pearson et al., 1994; Grütter et al., 2004). This error margin on both sides of the diamond stability curve ($P [Kbar] = 19.4 + 0.025 * T [^{\circ}C]$, Kennedy and Kennedy, 1976) allows for the assignment of mantle xenoliths to the graphite $P < 16.4 + 0.025 * T$) or diamond ($P > 22.4 + 0.025 * T$; Grütter et al., 2004) stability fields. Besides, clinopyroxene is a common mineral phase in kimberlites of the APAP, and xenocystic clinopyroxene compositions can also provide information on the relative abundance of spinel-facies or garnet-facies peridotite carried from the upper mantle by kimberlite magmas (Read et al., 2004).

Several works have reported pressure and temperature estimations obtained from xenoliths of the Alto Paranaíba Alkaline Province. Leonardos et al. (1993) presented the first studies on the Três Ranchos IV kimberlite, with temperatures of 977 to 1273°C, a pressure ranging from 55.5 to 78 Kbar and a geotherm of 40 W/m², using diopside and Cr-diopside from a garnet lherzolite xenolith. By applying several geothermobarometers from TR-IV xenoliths, Costa (2008) presented a temperature range of 974 to 1139°C, a pressure range of 36 to 51 Kbar and geotherms of about 38 and 63 mW/m². For Limeira I kimberlite xenoliths, Almeida (2009) presented temperatures ranging from 622 to 921°C, obtained from orthopyroxene, clinopyroxene, olivine and spinel geothermometers (Appendix Table E01). A compilation of geochemical data from several publications on the APAP allowed Cabral Neto et al. (2017) to determine, from a Nimis and Taylor (2000) clinopyroxene geothermobarometer, a geotherm

from range from 40 to 50 mW/m² for the Limeira I kimberlite and 35 to 40 mW/m² for Três Ranchos IV. Read et al. (2004) presented the first approach to single grain thermobarometric methods for mantle-derived xenocrystic clinopyroxene derived from kimberlite samples of the Alto Paranaíba Alkaline Province. Spinel-facies clinopyroxenes occur predominantly in the temperature interval between 625 and 875 °C, overlapping the lower end of the 700–1000 °C temperature range in which garnet-facies clinopyroxenes predominate (Read et al., 2004). A geotherm close to 37 mW/m² is proposed that is approximated to the heat flow model for steady-state conductive lithosphere (Pollack and Chapman, 1977). All the thermobarometric data presented on the APAP relate to xenoliths or single grain thermobarometry. The present work is the first one to estimate P-T conditions of xenocrysts and *fO*₂ from cognate mineral phases from fresh samples of two distinct kimberlites, one recognized as diamondiferous and the other one sterile.

6.2 Thermobarometry Results for Limeira I and Três Ranchos IV kimberlites.

The application of different geothermobarometers was due to the presence of distinct paragenesis in Três Ranchos IV and Limeira I kimberlites. The geothermometer of Nimis and Taylor (2000), which is based on enstatite-in-cpx, was applied to diopside xenocrysts from LM-I, as were Nimis and Grütter (2010) recommendations for a safer selection of clinopyroxenes i.e., that temperatures should be sufficiently reliable (a cut-off at T > 700 °C). The calculated temperature ranges from 718 to 986°C, calculated for a constant pressure of 40 Kbar, which is an average pressure value reported in the literature for several APAP kimberlites (Table E01). The uncertainties related to the geothermometer used are considered equivalent, or better than, most of the widely used thermobarometers for garnet peridotites (Nimis and Taylor, 2000). The Limeira I clinopyroxene xenocrysts analyzed in this work are identified as garnet-facies clinopyroxene (Mg-rich chromium diopsides with moderate Al and low tschermacks contents), which can be interpreted as mantle xenocrysts derived from disaggregated garnet-facies lherzolite xenoliths (Read et al., 2004, Figure 42). Read et al. (2004) proposed a single empirical curve for all APAP garnet-facies clinopyroxene that falls within a 600 to 1000°C temperature range, that represents the lithospheric geotherm at the time of kimberlite eruption (37-mW/m²). Based on the calculated temperature, an estimation of pressure with such a geotherm empirical curve resulted in a variation of 37 to 47 Kbar for clinopyroxene from the Limeira I kimberlite. Another approach to temperature calculations is the Bussweiler et al. (2017) Al-in-olivine thermometer for mantle peridotites. This version of the Al-in-olivine thermometer is applicable

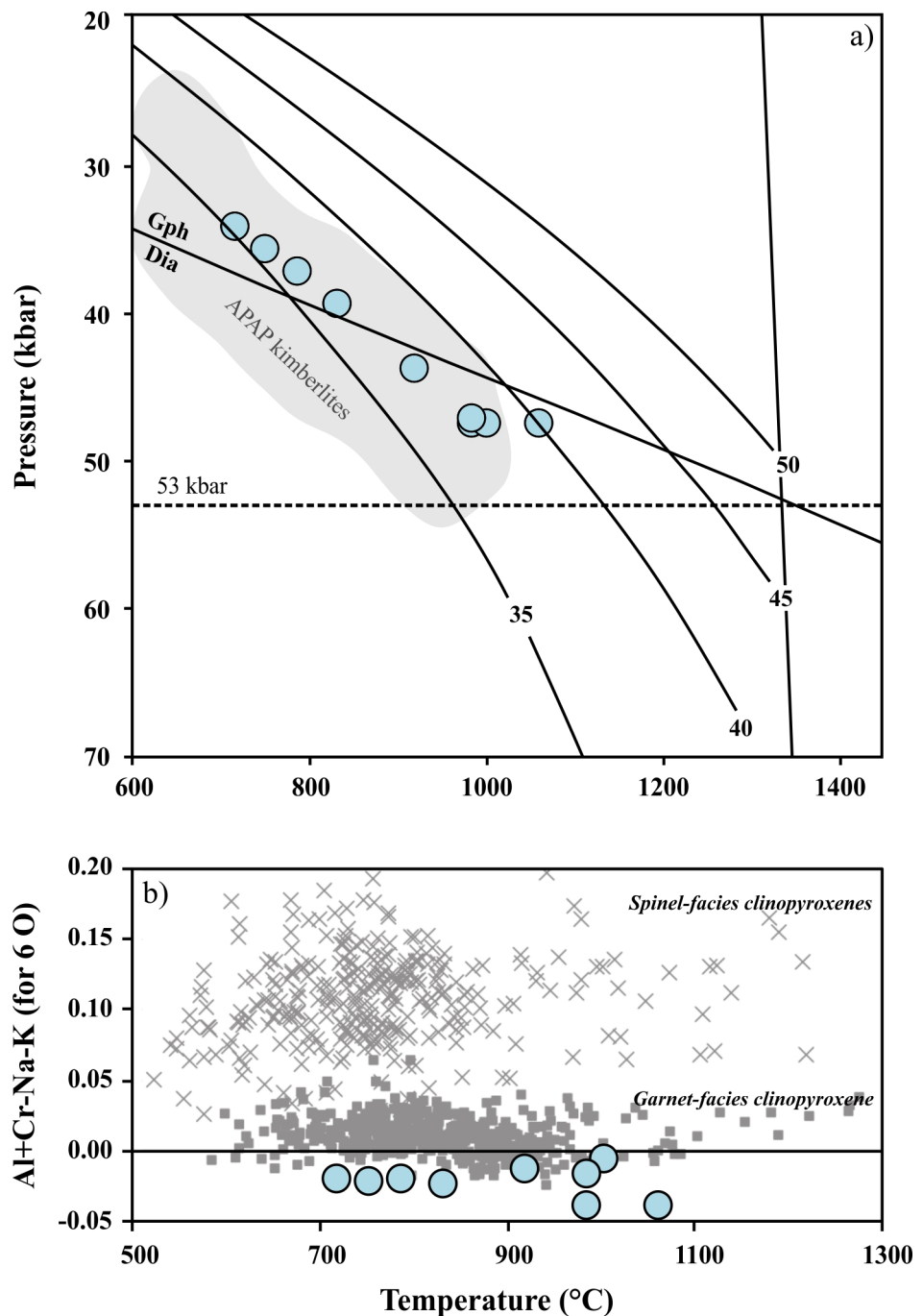


Figure 42 – Lithospheric geothermal evolution (with APAP samples from Read et al., 2004) P-T conditions and compositions of Limeira I clinopyroxenes with garnet- facies clinopyroxene samples from Read et al. (2004).

to garnet peridotites (lherzolites and harzburgites) and is not applicable to spinel-bearing peridotites (Bussweiler et al., 2017). One olivine core from an LM-I sample falls within the garnet peridotite field (high Al and high V, Figure 43) which was used in the Al-in-olivine thermometer with a constant pressure of 47Kbar, calculated with the empirical geotherm curve of reading et al (2004). The application of this geothermometer resulted in a temperature range from $985 \pm 13^{\circ}\text{C}$. The 2σ error presented in the Ni content is considered.

In pyrope xenocrysts from Três Ranchos IV kimberlite, the application of chromium in the pyrope geobarometer of Grüitter et al. (2006) yields pressures that range from 18 to 34 Kbar. Using the same barometer, an estimation using available chemical data (in Cabral Neto et al., 2017) in garnets from other APAP kimberlites resulted in 18 to 42 Kbar. Canil (1999) Ni-in-garnet geothermometers, that use partitioning of Ni between olivine and garnet were applied to a sample of Três Ranchos IV kimberlite using a constant pressure of 34 Kbar. This partition is temperature-dependent and can constitute a useful geothermometer in the interpretation of mantle-derived garnets (Canil, 1999). With this thermometer, calculations for Três Ranchos IV yield a temperature range from 975 ± 19 to $1050 \pm 24^{\circ}\text{C}$. One olivine core from a TR-IV sample presented the chemical characteristics of a garnet peridotite (Figure 43). The Al-in-olivine thermometer (Bussweiler et al., 2017) under constant pressure of 36 Kbar estimates from garnets of the same rock sample yielded a temperature of $1270 \pm 13^{\circ}\text{C}$ (considering analytic aluminum 2σ error). Limeira I, Três Ranchos IV and other pressure and temperature estimations for several APAP kimberlite xenoliths available in the literature are summarized in Table E01.

The P-T data acquired from Limeira I samples show that, even though the kimberlite is known to be sterile, the garnet-lherzolite facies clinopyroxene and olivine xenocrysts analyzed in this work indicate that the magma may have at least crossed the diamond stability field (Figure 42). Mg-ilmenite, an important mineral indicator used in diamond exploration, is also present as xenocrystic phases in LM-I samples (Figure 44). On the other hand, garnet data from samples of the diamond-bearing Três Ranchos IV kimberlite in this work indicate a much lower pressure than the ones from the diamond stability field. However, the Cr-in-pyrope barometer is related to a minimum pressure estimate for such xenocrysts. Therefore, it does not rule out the relationship with the diamond field. It is also possible that these specific sampled xenocrysts have formed at shallower horizons, so the comparison of pressure and temperature in Três Ranchos IV and Limeira I and its relation with diamond stability in these magmas is inconclusive. It is known that besides P-T conditions, diamond stability is also dependent on

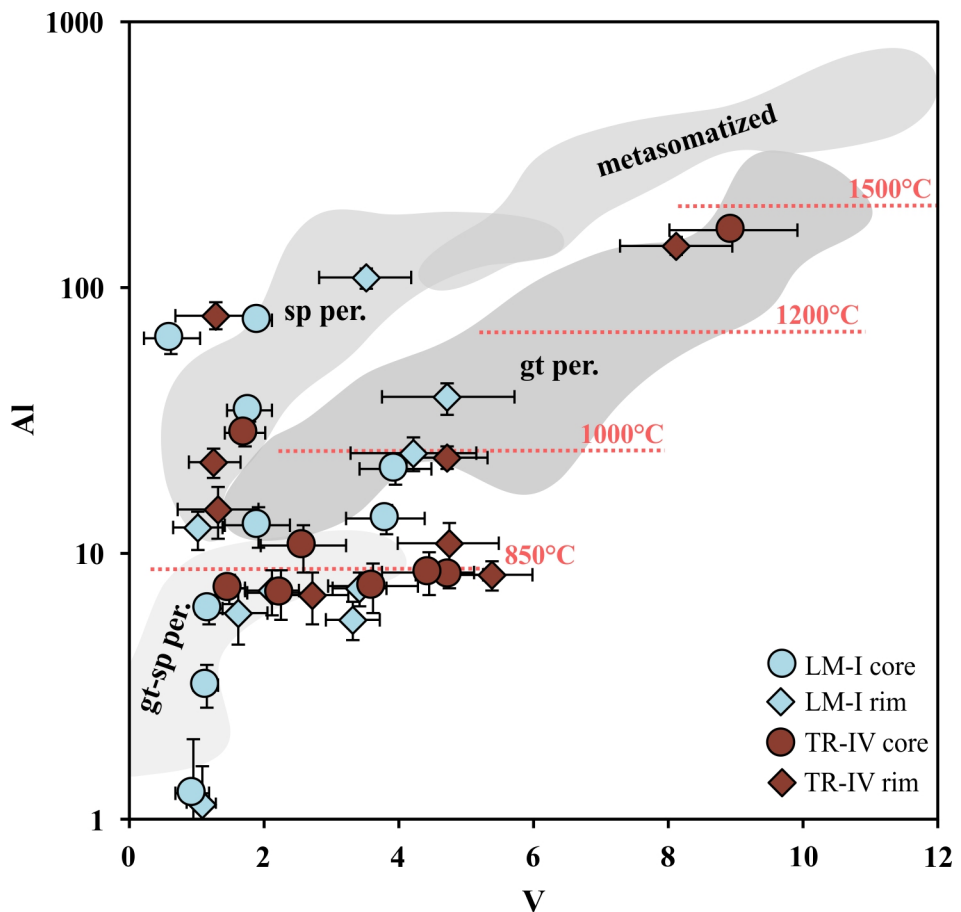


Figure 43 – Al versus V concentration of olivine rims and cores from Três Ranchos IV (TR-IV) and Limeira I (LM-I) including compositional facies fields based on data presented by Bussweiler et al. (2017) and 2σ error (uncertainties) bars for the olivine analyzed.

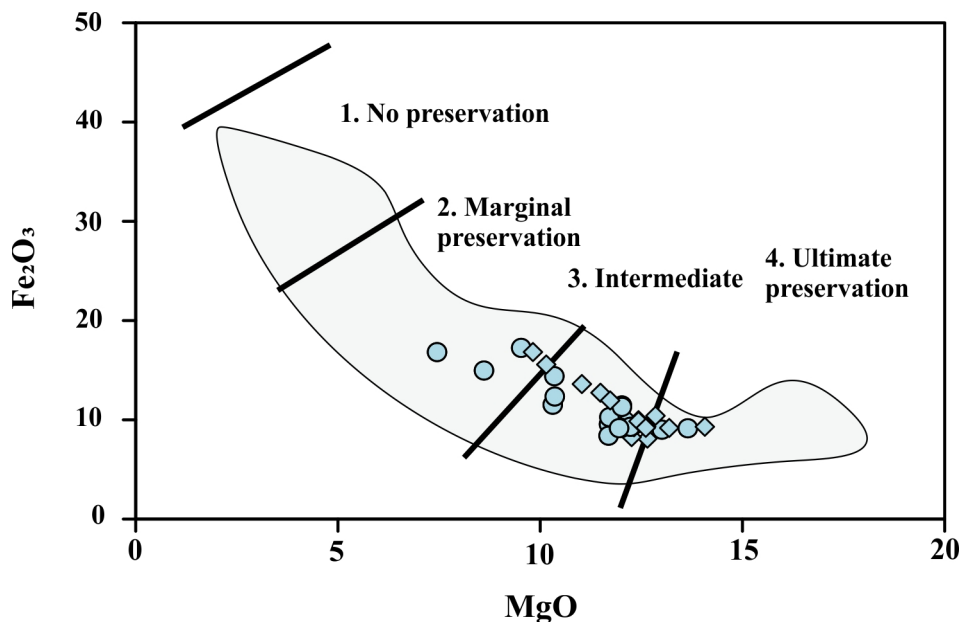


Figure 44 – Limeira I ilmenite samples plotted in a FeO vs MgO discrimination diagram. Fields proposed by Gurney and Zweistra (1995) define the diamond grade of a kimberlite from the composition of its ilmenite xenocrysts.

oxygen fugacity, and that this may affect the properties, textures and possibly the preservation of this phase in the kimberlite magma (Bellis and Canil, 2007; Nowicki et al., 2007).

6.3 Oxygen Fugacity ($f\text{O}_2$)

Petrographic and compositional analyses performed for the present study indicate that perovskite occurs as a discrete groundmass phase in both Três Ranchos IV and Limeira I kimberlites. Perovskite crystallization follows most macrocrystic phases, such as olivine and Cr-spinel (Clement, 1982; Mitchell, 1986, 2008; Chakhmouradian and Mitchell, 2000; Sarkar et al., 2013), but it can also coexist with Fe-Ti spinel and magnetite, which suggests simultaneous crystallization. This cognate phase becomes very unstable during the final magma evolution stages when there is excess CO_2 in the system (Mitchell and Chakhmouradian, 1998). This leads to the reaction of perovskite with the CO_2 -rich fluid, forming a TiO_2 polymorph (rutile) and calcite that precipitate in the vicinities of the perovskite, giving the grains a spongy appearance (Sarkar et al., 2013). However, some TR-IV and LM-I perovskite crystals appear to have remained very fresh and not converted into rutile, suggesting that a reaction with a CO_2 fluid did not take place.

Several studies have used the composition of perovskite, a common cognate phase in kimberlites, (Mitchell, 1972) to estimate oxygen fugacity through Nb and Fe content (Fedortchouk & Canil, 2004). Perovskite is one of the minerals that most incorporate incompatible elements in kimberlites, and its occurrences invariably show zonation, with different types of microstructures and even reactional features. Because perovskite can crystallize in kimberlites of different generations (Chakhmouradian and Mitchell, 2000), this oxybarometer can potentially indicate, in great detail, the $f\text{O}_2$ recorded during the formation and emplacement of the kimberlite in different eruption phases. Perovskite is common in most kimberlites, crystallizing generally after chromite, olivine, and monticellite (Mitchell, 1973). Bellis & Canil (2007) experimentally calibrated the compositional variation of perovskite as an oxygen barometer, using an empirical relation (2) to describe the covariation of Fe and Nb cations in the mineral with $f\text{O}_2$ relative to the NNO variation (uncertainties at 2α , besides Nb and Fe as cations by three oxygens).

$$\Delta\text{NNO} = \frac{[0.50 (\pm 0.021) \times \text{Nb} - \text{Fe} (\pm 0.031) + 0.030 (\pm 0.001)]}{0.004 (\pm 0.0002)} \quad (2)$$

In kimberlite perovskites, the concentration of Fe shows a large variation of oxygen fugacity (NNO -5 to +6), the highest compared to any other types of magma. The Bellis & Canil (2006) experiment demonstrates that the determining factor in the variation of the Fe_2O_3 concentration in perovskite is $f\text{O}_2$ and not the total Fe content in the system. This indication is supported by the lack of correlation between Fe content of in perovskite (and the calculated $f\text{O}_2$) and the total geochemical composition of the kimberlite. Also, kimberlites show restricted variation of total Fe (~ 8 mass% FeO).

The variation in nickel-nickel oxide buffer (ΔNNO , $f\text{O}_2$ relative to that of the Nickel-bunsenite NNO buffer) also varies in core-rim analyses. Perovskite samples from Limeira I present relative oxygen fugacity that ranges from -3.58 to 4.12 (core); -2.45 to -1.91 (intermediate region between core and rim); and -3.15 to 5.53 (rim). In Três Ranchos IV, NNO ranges from -4.96 to -3.84 (core); -4.80 to -1.87 (intermediate region); and -6.20 to 2.48 (rim). Both $f\text{O}_2$ ranges are the same as in other kimberlites from the Alto Paranaíba Alkaline Province (Melluso et al., 2008; Felgate, 2014; Araújo et al., 2001; and Meyer et al., 1994) and worldwide (Bellis and Canil, 2007; Trickett, 2007) as recorded in literature (Figure 45). Thus, it is likely that Três Ranchos IV perovskite crystallization probably started under slightly more oxidizing conditions than the IW buffer (~ -5 NNO) and continued until FMQ (fayalite-magnetite-quartz) buffer (* -1 NNO) and beyond, whereas the perovskites from Limeira I might have crystallized in conditions close to FMQ (Figure 46).

As mentioned, Três Ranchos IV perovskites present a wide $f\text{O}_2$ range, some grains being highly reduced (lower than IW buffer, < -5 NNO). It is known that such values probably limit the applicability of this oxygen barometer, as metallic iron is formed under such reducing conditions, which is unlikely to be achieved in kimberlite magmas (Sarkar et al., 2013). This variability in the oxygen fugacity values can be caused by several processes such as degassing, decompression (Carmichael and Ghiorso, 1986; Sparks et al., 2006) crystallization (Carmichael and Nicholls, 1967) and magma mixing (Sarkar et al., 2013).

Another oxygen fugacity calculation procedure involves the estimation of Fe composition in kimberlite liquid and monticellite. Studies by Le Pioufle and Canil (2012) demonstrated the use of an oxybarometer for kimberlite magmas based on the amount of Fe in monticellite (CaMgSiO_4) in equilibrium with kimberlite liquids in experiments at 100 kPa, with temperatures from 1,230 to 1,350 °C and $\log f\text{O}_2$ from NNO -4.1 to NNO +5.3 (where NNO is the nickel-nickel oxide variation). Monticellite is a mineral of the kirschsteinite-monticellite series (CaFeSiO_4 - CaMgSiO_4) that is present in the kimberlite groundmasses (Le Pioufle and

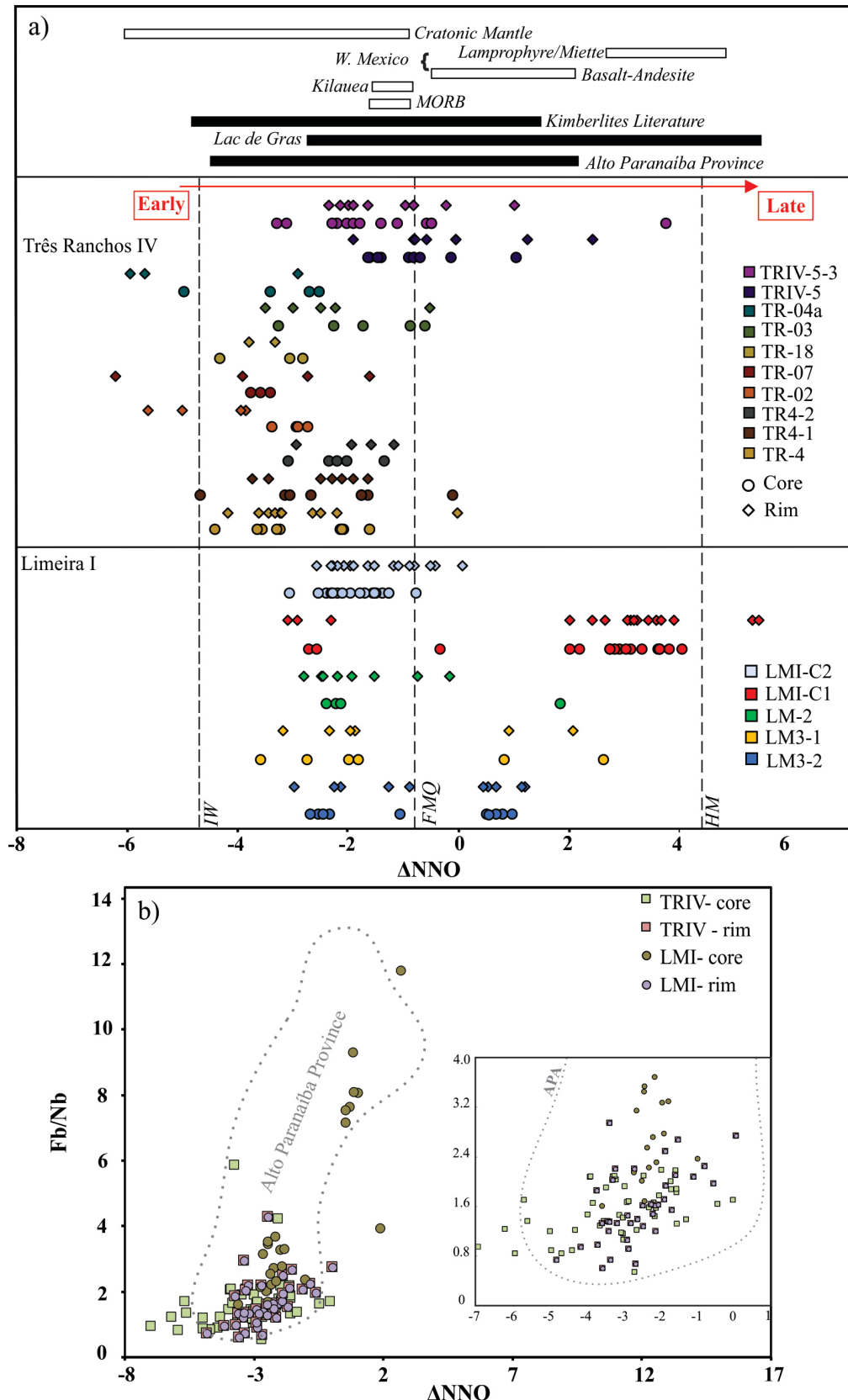


Figure 45 – Calculated oxygen fugacities (ΔNNO) for perovskite grains from different samples of Três Ranchos IV and Limeira I, with varying Fe/Nb ratios. Oxygen fugacity of global kimberlite bodies, other mantle-derived magmas and the Alto Paranaíba Alkaline Province (calculated with mineral chemical data from Melluso et al., 2008; Felgate, 2014; Araújo et al., 2001; and Meyer et al., 1994) are also plotted for reference. FMQ - fayalite-quartz-magnetite; IW - ironwustite.

Canil, 2012). This phase can form up to 80% of the matrix (Mitchell, 1986), and it crystallizes at low pressures (<0.5 GPa), usually after spinel and perovskite, but before calcite and serpentine (Mitchell, 1986). The equation proposed for this oxybarometer (2) is:

$$\Delta NNO = \frac{\left\{ \log \left[0.858(\pm 0.021) \frac{x_{Fe}^{Liq}}{x_{Fe}^{Mtc}} - 1 \right] - 0.139(\pm 0.022) \right\}}{0.193 (\pm 0.004)} \quad (3)$$

where x_{Fe}^{Liq} and x_{Fe}^{Mtc} correspond to the molar fraction of Fe in the liquid and monticellite, respectively (Le Pioufle & Canil, 2012). The global analysis of the matrix of such samples can be considered a good approximation of such liquid since a large number of xenocrysts are carried by kimberlitic magmas. This oxybarometer was applied only to Limeira I kimberlite since monticellite was not found in Três Ranchos IV, probably replaced with serpentine. All bulk compositions were recalculated on a volatile-free basis. x_{Fe}^{Liq} was determined for three LM-I samples from bulk composition data. An average value was therefore applied to different samples of the same pipe.

The calculation of Fe present in the liquid composition was carried out based on whole rock chemical concentrations and the amount of olivine (the -5% considered to have crystallized from the magma itself, Brett et al., 2009) and phlogopite macrocrysts. These proportions are in the petrographic data sheet of Table C01. Ubide et al. (2012) suggest Equation 4 yields quantitative proof that the proportions of each member (groundmass and mega-, macrocrysts) reflect its proportions in the rock.

$$C_{WR}^i = C_{Mt}^i (1 - \sum v) + \sum (C_{Mg}^i \times v) \quad (4)$$

Where C_{WR}^i , C_{Mt}^i , C_{Mg}^i is the concentration of an ‘ i ’ element in the whole rock composition, in both matrix and mega-, macrocrysts, respectively, and ‘ v ’ is the modal volume of the mega-, macrocrysts crystals of olivine and phlogopite. Likewise, the following equation was applied to the kimberlites studied:

$$C_{Mt}^i = \frac{C_{WR}^i - C_{Phl}^i \times v_{Phl} - C_{Ol}^i \times v_{Ol}}{1 - v_{Phl} - v_{Ol}} \quad (5)$$

All elements were then recalculated on an anhydrous basis (C_{Mt}^i mass% / sum. x100).

In Limeira I, XFe_{Mtc} ranges from 0.020 to 0.087. XFe_{Liq} averages to 0.120 (Figure 46).

The same molar fractions were calculated based on APAP monticellite data reported in the literature, with XFe_{Mtc} and XFe_{Liq} ranging from 0.022 to 0.077 and from 0.090 to 0.184, respectively (Figure 46). The fO_2 for LM-I monticellite calculated using Eq. 3 varies from NNO -4.23 to NNO +2.4. As calculated from literature data, it varies from NNO -4.50 to NNO +2.60 (Figure 46). Because perovskite generally crystallizes after chromite, olivine, and spinel (Mitchell, 1986), the kimberlite magmas of Três Ranchos IV and Limeira I pipes are suggested to have experienced oxidation during differentiation and emplacement (Canil and Bellis, 2007).

Bellis and Canil's (2007) perovskite oxybarometer yields fO_2 values that range from NNO-4 to NNO+6 for Limeira I kimberlite. For the Três Ranchos IV kimberlite, values range from NNO+4 to NNO-6.20. While the monticellite oxybarometer of Le Pioufle & Canil (2012), yields fO_2 values that range from -4 to +2, only one pipe (Limeira I) in that detailed study was able to be compared given the absence of monticellite in Três Ranchos IV. This represents the first limitation of the monticellite oxybarometer, as this mineral can be altered and replaced with serpentine in kimberlite intrusions. Calibration of the perovskite oxybarometer bears a large uncertainty, of ± 1 log fO_2 unit (Bellis and Canil, 2006), but it has the potential advantage of being applicable to discrete evolution stages of kimberlite magmas that are recognized by their different compositional types of perovskite in kimberlite intrusions (Canil and Bellis, 2007).

6.3.1 Possible relations between oxygen fugacity and diamond instability.

It is widely recognized that many diamonds are partially reabsorbed during the ascension of magma from the upper mantle to the Earth's surface (Robinson, 1989; first by oxidation). This is a common process from which it can be deduced that many diamonds exhibit the rounded dodecahedral morphology from their original octahedral shapes, which implies a mass loss of at least 45% (Nowicki et al., 2007), under which oxidation is considered likely to cause many microdiamonds (> 0.5mm) to be completely reabsorbed. Thus, a proposition was made that microdiamonds may constitute a separate population, that crystallizes prior to intrusion, and unreliable to macrodiamond populations, which appears to be much more

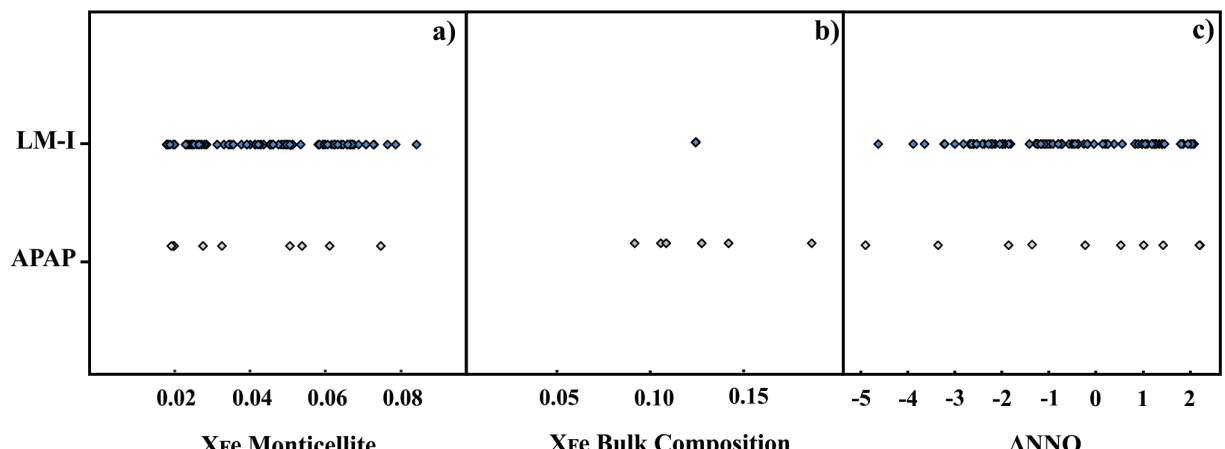


Figure 46 – XFe of monticellite and bulk composition and ΔNNO estimates for Limeira I kimberlite (a) XFe of monticellite expressed as molar fraction, (b) XFe of the bulk composition expressed as molar fraction, and (c) ΔNNO calculated with equation 3 for Limeira I and other kimberlites from Alto Paranaíba Alkaline Province (calculated with mineral chemical data from Melluso et al., 2008; Meyer et al., 1994 and Guarino et al., 2008).

previous (Haggerty, 1986). However, microdiamonds appear to carry inclusions similar to those of macrodiamonds, which indicates that they share a common origin (Nowicki et al., 2007).

High-temperature kimberlitic melts are very reactive, and this may possibly be the cause of diamond re-absorption. Considering that co-crystallization of olivine-spinel occurs below 1.0 GPa, the maximum oxygen fugacity values of kimberlitic magmas (in a silica-buffered activity and diopside-monticellite) are in the graphite stability field, very close to the D/GCO (Diamond/Graphite and CO₂) buffer (Fedortchouk and Canil, 2004). With the increase of the pressure, *fO*₂ values reach the CO₂ stability field. Thereby, any diamond released from depth xenoliths will have undergone dissolution in the graphite stability field, while those coming into contact with the magma in the final stages of eruption are possibly reabsorbed in the CO₂ stability field (Fedortchouk and Canil, 2004). Although the degree of diamond is probably a result of the amount of these samples in the mantle by ascending kimberlitic magma, it is estimated that the *fO*₂ of the kimberlites may be of some utility in predicting the quality or the properties of such diamonds (Fedortchouk and Canil, 2004). Kimberlite pipes with higher oxygen fugacity display the largest proportions of strongly absorbed diamonds, while pipes with lower *fO*₂ values show lower degrees of diamond absorption (Canil and Bellis, 2007). This suggests that oxygen fugacity affects the properties and textures of the diamonds preserved in the magma (Canil and Bellis, 2007).

Studies have demonstrated that all reabsorbed natural diamonds undergo powerful condition-controlled dissolution, which overwhelms the effects of internal factors on diamond resorption (Fedortchouk et al., 2005; Fedortchouk and Canil, 2009; Zhang, 2016). Resorption can reduce the content and the quality of diamonds in a kimberlite pipe (Fedortchouk and Canil, 2009). In the lithospheric mantle, diamonds are stable at T = 900 – 1400 °C, P = 4 to 7 GPa, and *fO*² at NNO-5 to NNO-1 (Stagno et al., 2013; Stachel and Luth, 2015). Kimberlites are believed to form at 1450 °C (Kavanagh and Sparks, 2009) and their average crystallization T is ~ 1030 °C estimated by olivine-spinel thermometry (Fedortchouk and Canil, 2004). The *fO*² of the Três Ranchos IV constrained by perovskite oxygen barometry ranges from NNO-7 to NN+4, while in Limeira I values reach NNO+6 to NNO-4. It is possible that the variation in oxygen fugacity in both kimberlites may have reflected in the instability of diamonds in their magmas, since LM-I presents slightly higher oxidation conditions, thus being not diamondiferous. However, diamond oxidation during groundmass crystallization may be too slow due to lower T (Mitchel, 1986) and short emplacement time for the kimberlite (Canil and Fedortchouk, 1999; Kelley and Wartho, 2000) to show notable diamond preservation. It is also

known that the P effect on diamond dissolution determined in experiments suggests that the final stages of kimberlite eruption ($P < 1$ GPa) play the major role in diamond preservation (Zhang, 2016). Kimberlite crystallization conditions during this stage (T , fO_2 , the presence of fluids, and ascent rate) could have a significant effect on diamond grade (Zhang, 2016). Fast cooling of kimberlite after pipe emplacement would promote diamond preservation (Fedortchouk and Canil, 2009; Zhang et al., 2015; Zhang, 2016).

CHAPTER 7 - SUMMARY AND CONCLUSIONS

In the Alto Paranaíba Alkaline Province, especially regarding relations between P-T- $f\text{O}_2$ conditions, the main mineral phases chemistry and bulk rock geochemistry allowed for the differentiation of two kimberlite intrusions, one sterile and the other a diamond-bearing one (Limeira I and Três Ranchos IV, respectively). Several geothermobarometers were used in the calculation of these intensive parameters of crystallization, resulting in temperatures ranging from 718 to 985°C for Limeira I and from 975 to 1270°C for Três Ranchos IV. Pressure ranges in intervals of 34 to 47 Kbar and 18 to 34 Kbar for the kimberlites, respectively. In Três Ranchos IV, $f\text{O}_2$ constrained by the perovskite oxygen barometry ranges from NNO-7 to NN+4, while in Limeira I it ranges from NNO+6 to NNO-4. The results are compatible with those available of APAP in literature.

The Três Ranchos IV and Limeira I are coherent macrocrystic kimberlites, with an inequigranular texture formed by partially-to-fully altered olivine, phlogopite megacrysts up to 1 cm wide, macrocrysts (0.5-10 mm-sized), and crustal xenoliths set in a very fine groundmass composed mainly of perovskite, olivine, phlogopite, spinel, serpentine and carbonates, and also apatite, ilmenite and monticellite in LM-I. Garnet macrocrysts and centimetric pyroxene xenocrysts are also bearing phases in Três Ranchos IV and Limeira I, respectively.

Both Limeira I and Três Ranchos IV kimberlites are ultrabasic rocks that are MgO-rich, high Mg#, CaO-rich, Al_2O_3 -poor, Na_2O -poor and potassic to ultrapotassic in composition ($\text{K}_2\text{O} = 0.9\text{--}1.6$ mass% and 0.7-1.2 mass% respectively). The high LOI is largely due to the abundant presence of volatile-bearing phases such as carbonates, serpentine, and phlogopite. All major element values are supported by literature data. The relatively low K_2O is a typical characteristic of uncontaminated kimberlites worldwide. The kimberlites are strongly enriched in incompatible elements.

The olivine Mg# values, which range from 87 to 92 mol.% in Três Ranchos IV and from 83 to 92 mol.% in Limeira I, are consistent with the olivine compositions from APAP kimberlites (82-92 mol.%). Olivine cores of Limeira I present higher NiO, CaO and lower Cr_2O_3 contents than those of Três Ranchos IV. Most cores fall within the “mantle trend”. Although rim compositions are representative from “melt trends”, this trend is only identified in a few olivines of TR-IV and LM-I, that show extensive serpentinization around crystals, with rims that may not be preserved. The “melt trend” shows enrichment in Zr, Ga, Nb, Sc, V, P, Al, Ti, Cr, Ca, and Mn, whereas enrichment in Zn, Co, Ni and possibly Na in the “mantle trend” is

observed in both kimberlites. In Limeira I, monticellite Mg# ranges from 72 to 93.8 mol.%, while Ca/(Ca+Mg) ratios range between 0.35-0.58 mol.%.

Perovskite compositions in both Limeira I and Três Ranchos IV remain close to ideal CaTiO_3 , yet a variation in endmember compositions from cores is noticeable (TR-IV: average Lop_{16} and Prv_{78} ; LM-I: average Lop_5 and Prv_{91}) towards the rims (TR-IV: average Lop_{13} and Prv_{81} ; LM-I: average Lop_4 and Prv_{92}). In TR-IV and LM-I, perovskite compositions are characterized by relatively high concentrations of Sr, Nb, Zr, and REE and a strong positive correlation between Nb and Ta; Nb and Zr; Mn and Fe. The primitive mantle-normalized REE patterns of the perovskite from both kimberlites have smooth, highly fractionated trends, with extreme LREE enrichment and no Eu anomalies.

The macrocrystic spinels of the Três Ranchos IV kimberlite are Al-rich, whereas groundmass crystals range from magnesiochromite to chromite. The ilmenite from Limeira I is characterized by its high MgO content at a given TiO_2 , with a large variation in Cr_2O_3 . Garnet is present only in Três Ranchos IV, identified as pyrope (62 to 73 mol.%) with Mg# ranging from 72 to 79 mol.%. The crystals correspond to lherzolitic (G9) and pyroxenitic (G4, G5) garnets according to the Cr_2O_3 and CaO contents. Clinopyroxene occurs as xenocrysts in Limeira I and as microphenocrysts in Três Ranchos IV, and are identified as diopside with Mg# ranging from 85 to 91 and from 87 to 92, respectively. The xenocystic clinopyroxene from Limeira I presents higher MgO and FeO concentrations.

The Limeira I clinopyroxene xenocrysts analyzed in this work are identified as garnet-facies ones (Mg-rich chromium diopsides with moderate Al and low tschermack contents), which can be interpreted as mantle xenocrysts derived from disaggregated garnet-facies lherzolite xenoliths.

This indicates that the magma that originated the intrusion, which is known to be sterile, must at least have crossed the diamond stability field. It is possible that the variation in oxygen fugacity observed in Limeira I and Três Ranchos IV kimberlites may have reflected in the instability of diamonds in these magmas since LM-I presents slightly higher oxidation conditions, thus not being diamondiferous. However, diamond oxidation during groundmass crystallization may have been too slow due to the lower T and the short time for kimberlite emplacement to have notable effects on diamond preservation.

CHAPTER 8 - REFERENCES

- Almeida, V.V. de, 2009, Mineralogia e Petrologia de Xenólitos Mantélicos das Regiões de Ubatuba (SP) e Monte Carmelo (MG): Evidências de Fusão Parcial e Metassomatismo no Manto Superior do Sudeste do Brasil: , p. 112.
- Andrade, K.W., and Chaves, M.L. de S.C., 2011, Geologia E Mineralogia Do Kimberlito Grotá Do Cedro (Coromandel, MG): Geonomos, v. 19, p. 39–45.
- Araujo, A.L.N., Carlson, R.W., Gaspar, J.C., and Bizzi, L.A., 2001, Petrology of kamafugites and kimberlites from the Alto Paranaíba Alkaline Province, Minas Gerais, Brazil: Contributions to Mineralogy and Petrology, v. 142, p. 163–177, doi:10.1007/s004100100280.
- Arndt, N.T., Guitreau, M., Boullier, A.M., Le Roex, A.P., Tommasi, A., Cordier, P., and Sobolev, A., 2010a, Olivine, and the origin of kimberlite: Journal of Petrology, v. 51, p. 573–602, doi:10.1093/petrology/egp080.
- Arndt, N.T., Guitreau, M., Boullier, A.M., Le Roex, A., Tommasi, A., Cordier, P., and Sobolev, A., 2010b, Olivine, and the origin of kimberlite: Journal of Petrology, v. 51, p. 573–602, doi:10.1093/petrology/egp080.
- Ballhaus, C., and Frost, B.R., 1994, The generation of oxidized CO₂-bearing basaltic melts from reduced CH₄-bearing upper mantle sources: Geochimica et Cosmochimica Acta, v. 58, p. 4931–4940, doi:10.1016/0016-7037(94)90222-4.
- Barbosa, E.S.R., Brod, J.A., Junqueira-Brod, T.C., Dantas, E.L., Cordeiro, P.F. de O., and Gomide, C.S., 2012, Bebedourite from its type area (Salitre I complex): A key petrogenetic series in the Late-Cretaceous Alto Paranaíba kamafugite-carbonatite-phoscorite association, Central Brazil: Lithos, v. 144–145, p. 56–72, doi:10.1016/j.lithos.2012.04.013.
- Becker, M., and Le Roex, A.P., 2006, Geochemistry of South African on- and off-craton, group I and group II kimberlites: Petrogenesis and source region evolution: Journal of Petrology, v. 47, p. 673–703, doi:10.1093/petrology/egi089.
- Bellis, A.J., and Canil, D., 2007, Ferric Iron in CaTiO₃ perovskite as an oxygen barometer for kimberlitic magmas I: Experimental calibration: Journal of Petrology, v. 48, p. 219–230, doi:10.1093/petrology/egl054.
- Berg, G.W., and Allsopp, H.L., 1972, Low⁸⁷Sr/⁸⁶Sr ratios in fresh South African kimberlites: Earth and Planetary Science Letters, v. 16, p. 27–30, doi:10.1016/0012-821X(72)90233-6.

- Biondi, J.C., 2005, Brazilian mineral deposits associated with alkaline and alkaline-carbonatite complexes, *in* Comin-Chiaromonti, P. and Gomes, C.B. eds., Mesozoic to Cenozoic Alkaline Magmatism in the Brazilian Platform, São Paulo, Brazil, FAPESP, p. 707–750.
- Bizzi, L.A., Smith, C.B., Wit, M.J., Armstrong, R.A.A., and Meyer, H.O.A., 1994, Mesozoic kimberlites and related alkalic rocks in south-western São Francisco Craton, Brazil: a case for local mantle reservoirs and their interaction, *in* Proceedings of the Fifth International Kimberlite Conference, p. 156–171.
- Brod, J.A., Gibson, S.A., Thompson, R.N., Junqueira-Brod, T.C., Seer, H.J., Moraes, L.C., and Boaventura, G.R., 2000, The Kamafugite-Carbonatite association in the Alto Paranaíba Igneous Province (APIP) Southeastern Brazil: Revista Brasileira de Geociências, v. 30, p. 408–412.
- Brooker, R.A., Sparks, R.S.J., Kavanagh, J.L., and Field, M., 2011, The volatile content of hypabyssal kimberlite magmas: Some constraints from experiments on natural rock compositions: Bulletin of Volcanology, v. 73, p. 959–981, doi:10.1007/s00445-011-0523-7.
- Brown, R.J., Buse, B., Sparks, R.S.J., and Field, M., 2008a, On the Welding of Pyroclasts from Very Low-Viscosity Magmas: Examples from Kimberlite Volcanoes: The Journal of Geology, v. 116, p. 354–374, doi:10.1086/588832.
- Brown, R.J., Field, M., Gernon, T., Gilbertson, M., and Sparks, R.S.J., 2008b, Problems with an in-vent column collapse model for the emplacement of massive volcaniclastic kimberlite.: Journal of Volcanology and Geothermal Research, v. 178, p. 847–850, doi:10.1016/j.jvolgeores.2008.06.002.
- Buse, B., Sparks, R.S.J., Field, M., Schumacher, J.C., Chisi, K., and Tlhaodi, T., 2011, Geology of the BK9 kimberlite (Damtshaa, Botswana): Implications for the formation of dark volcaniclastic kimberlite: Bulletin of Volcanology, v. 73, p. 1029–1045, doi:10.1007/s00445-011-0491-y.
- Bussweiler, Y., Brey, G.P., Pearson, D.G., Stachel, T., Stern, R.A., Hardman, M.F., Kjarsgaard, B.A., and Jackson, S.E., 2017, The aluminum-in-olivine thermometer for mantle peridotites—Experimental versus empirical calibration and potential applications: Lithos, v. 272–273, p. 301–314, doi:10.1016/j.lithos.2016.12.015.
- Bussweiler, Y., Foley, S.F., Prelevic, D., and Jacob, D.E., 2015, The olivine macrocryst problem: New insights from minor and trace element compositions of olivine from Lac de Gras kimberlites, Canada: Lithos, v. 220–223, p. 238–252, doi:10.1016/j.lithos.2015.02.016.

Cabral Neto, I., Nannini, F., Silveira, F. V., and Cunha, L.M., 2017, Áreas kimberlíticas e diamantíferas do Estado de Minas Gerais.:

Canil, D., 1999, The Ni-in-garnet geothermometer: Calibration at natural abundances: Contributions to Mineralogy and Petrology, v. 136, p. 240–246, doi:10.1007/s004100050535.

Canil, D., and Bellis, A.J., 2007, Ferric iron in CaTiO₃ perovskite as an oxygen barometer for kimberlite magmas II: Applications: Journal of Petrology, v. 48, p. 231–252, doi:10.1093/petrology/egl067.

Canil, D., and Bellis, A.J., 2008, Phase equilibria in a volatile-free kimberlite at 0.1??MPa and the search for primary kimberlite magma: Lithos, v. 105, p. 111–117, doi:10.1016/j.lithos.2008.02.011.

Canil, D., and Fedortchouk, Y., 1999, Garnet dissolution and the emplacement of kimberlites: v. 167, p. 227–237, doi:10.1016/S0012-821X(99)00019-9.

Canil, D., and Fedortchouk, Y., 2001, Olivine-liquid partitioning of vanadium and other trace elements, with applications to modern and ancient picrites: Canadian Mineralogist, v. 39, p. 319–330, doi:10.2113/gscanmin.39.2.319.

Carlson, R.W., Esperança, S., and Svisero, D.P., 1996, Chemical and Os isotopic study of Cretaceous potassic rocks from Southern Brazil: Contributions to Mineralogy and Petrology, v. 125, p. 393–405, doi:10.1007/s004100050230.

Carmichael, I.S.E., 1991, The redox states of basic and silicic magmas: a reflection of their source regions? Contributions to Mineralogy and Petrology, v. 106, p. 129–141, doi:10.1007/BF00306429.

Carmichael, I.S.E., and Ghiorso, M.S., 1986, Oxidation-reduction relations in basic magma: a case for homogeneous equilibria: Earth and Planetary Science Letters, v. 78, p. 200–210, doi:10.1016/0012-821X(86)90061-0.

Carmichael, I.S.E., and Nicholls, J., 1967, Iron-titanium oxides and oxygen fugacities in volcanic rocks: Journal of Geophysical Research, v. 72, p. 4665–4687, doi:10.1029/JZ072i018p04665.

Cas, R.A.F., Hayman, P., Pittari, A., and Porritt, L., 2008a, Some major problems with existing models and terminology associated with kimberlite pipes from a volcanological perspective, and some suggestions: Journal of Volcanology and Geothermal Research, v. 174, p. 209–225, doi:10.1016/j.jvolgeores.2007.12.031.

Cas, R.A.F., Hayman, P., Pittari, A., and Porritt, L., 2008b, Some major problems with existing

- models and terminology associated with kimberlite pipes from a volcanological perspective, and some suggestions: *Journal of Volcanology and Geothermal Research*, v. 174, p. 209–225, doi:10.1016/j.jvolgeores.2007.12.031.
- Cas, R.A.F., Porritt, L., Pittari, A., and Hayman, P., 2008c, A new approach to kimberlite facies terminology using a revised general approach to the nomenclature of all volcanic rocks and deposits: Descriptive to genetic: *Journal of Volcanology and Geothermal Research*, v. 174, p. 226–240, doi:10.1016/j.jvolgeores.2007.12.018.
- Chakhmouradian, A.R., and Mitchell, R.H., 2000, Occurrence, alteration patterns and compositional variation of perovskite in kimberlites: *Canadian Mineralogist*, v. 38, p. 975–994, doi:10.2113/gscanmin.38.4.975.
- Chalapathi Rao, N. V., Gibson, S.A., Pyle, D.M., and Dickin, A.P., 2005, Petrogenesis of Proterozoic lamproites and kimberlites from the Cuddapah Basin and Dharwar Craton, southern India: *Journal of Petrology*, v. 46, p. 907–948, doi:10.1093/petrology/egi040.
- Chaves, M.L. de S.C., Andrade, K.W., Dussin, I.A., and Azzi, A. de A., 2012, *Geologia, Geoquímica e Mineralogia Comparativa Entre as Intrusões Diamantíferas Canastras-1 e Abel Régis (Minas Gerais)*: Geociencias, v. 31, p. 516–533.
- Clement, C.R., 1982, A Comparative Geological Study of Some Major Kimberlite Pipes in the Northern Cape and Orange Free State: University of Cape Town, 432 p.
- Clement, C.R., and Reid, A.M., 1989, The origin of kimberlite pipes; an interpretation based on a synthesis of geological features displayed by Southern African occurrences, *in* Ross, J. ed., *Proceedings of the Fourth International Kimberlite Conference, Volume 1. Kimberlites and Related Rocks: Their Composition, Occurrence, Origin and Emplacement*, Oxford, Blackwell Scientific Publications, p. 632 – 646.
- Clifford, T.N., 1966, Tectono-metallogenic provinces: *Earth and Planetary Science Letters*, v. 1, p. 421–434, doi:10.1016/0012-821X(66)90039-2.
- Coe, N., Roex, A., Gurney, J., Pearson, G.D., and Nowell, G., 2008, Petrogenesis of the Swartruggens and Star Group II kimberlite dyke swarms, South Africa: Constraints from whole rock geochemistry: *Contributions to Mineralogy and Petrology*, v. 156, p. 627–652, doi:10.1007/s00410-008-0305-1.
- Comin-Chiaromonti, P., and Gomes, C.B., 2005, Mesozoic to Cenozoic Alkaline Magmatism in the Brazilian Platform: São Paulo, Edusp/Fapesp, 750 p.
- Comin-Chiaromonti, P., Gomes, C.B., Marques, L.S., Censi, P., Ruberti, E., and Antonini, P., 2005, Carbonatites from southeastern Brazil: geochemistry, O-C, Sr-Nd-Pb isotopes and relationships with the magmatism from the Paraná-Angola-Namibia Province, *in* Comin-

- Chiaramonti, P. and Gomes, C.B. eds., Mesozoic to Cenozoic Alkaline Magmatism in the Brazilian Platform, São Paulo, Edusp/Fapesp, p. 651–682.
- Costa, V.S., 1996, Estudos Mineralógicos e Químicos do Kimberlito Batovi 6 (MT) em Comparaçao com as Intrusões Três Ranchos 4 (GO) e Limeira I (MG): Universidade Estadual de Campinas, 112 p.
- Costa, G.V., 2008, Química Mineral e Geotermobarometria de Xenólitos Mantélicos do Kimberlito Canastra-01: , p. 137.
- Crawford, B., Hetman, C., Nowicki, T., Baumgartner, M., and Harrison, S., 2009, The geology and emplacement history of the Pigeon kimberlite, EKATI Diamond Mine, Northwest Territories, Canada: *Lithos*, v. 112, p. 501–512, doi:10.1016/j.lithos.2009.06.032.
- Dalton, J. a, and Presnall, D.C., 1998, Carbonatitic melts along the solidus of model lherzolite in the system CaO-MgO-Al₂O₃-SiO₂-CO₂ from 3 to 7 GPa: Contributions to Mineralogy and Petrology, v. 131, p. 123–135, doi:10.1007/s004100050383.
- Danni, J.C.M., and Scartezini, A.A., 1990, O Olivina Leucitito de Pântano e a Natureza do Vulcanismo da Formação Mata da Corda, MG: Revista Brasileira de Geociências, v. 20, p. 83–87.
- Dasgupta, R., and Hirschmann, M.M., 2006, Melting in the Earth's deep upper mantle caused by carbon dioxide: *Nature*, v. 440, p. 659–662, doi:10.1038/nature04612.
- Davies, R.M., Griffin, W.L., O'Reilly, S.Y., and McCandless, T.E., 2004, Inclusions in diamonds from the K14 and K10 kimberlites, Buffalo Hills, Alberta, Canada: Diamond growth in a plume? *Lithos*, v. 77, p. 99–111, doi:10.1016/j.lithos.2004.04.008.
- Dawson, J., 1989, Geographic and time distribution of kimberlites and lamproites: relationships to tectonic processes, *in* Ross, J., Jaques, A.L., and Ferguson, J. eds., Kimberlites and related rocks : Proceedings of the Fourth International Kimberlite Conference., Perth, Blackwell Scientific Publications, p. 323.
- Fedortchouk, Y., and Canil, D., 2009, Diamond oxidation at atmospheric pressure: development of surface features and the effect of oxygen fugacity: European Journal of Mineralogy, v. 21, p. 623–635, doi:10.1127/0935-1221/2009/0021-1929.
- Fedortchouk, Y., Canil, D., and Carlson, J.A., 2005, Dissolution forms in Lac de Gras diamonds and their relationship to the temperature and redox state of kimberlite magma: Contributions to Mineralogy and Petrology, v. 150, p. 54–69, doi:10.1007/s00410-005-0003-1.
- Felgate, M.R., 2014, Improved Geochemical and Geochronological Constraints on Magmatism

in Rondonia and The Alto Paranaiba Igneous Province: The University of Melbourne, 275 p.

- Field, M., Stiefenhofer, J., Robey, J., and Kurszlaukis, S., 2008, Kimberlite-hosted diamond deposits of southern Africa: A review: *Ore Geology Reviews*, v. 34, p. 33–75, doi:10.1016/j.oregeorev.2007.11.002.
- Gibson, S.A., Thompson, R.N., Dickin, A.P., and Leonardos, O.H., 1995a, High-Ti and low-Ti mafic potassic magmas: Key to plume - lithosphere interactions and continental flood-basalt genesis.: *Earth and Planetary Science Letters*, v. 136, p. 149–165.
- Gibson, S.A., Thompson, R.N., Leonardos, O.H., Dickin, A.P., and Mitchell, J.G., 1995b, The late cretaceous impact of the trindade mantle plume: Evidence from large-volume, mafic, potassic magmatism in SE Brazil: *Journal of Petrology*, v. 36, p. 189–229, doi:10.1093/petrology/36.1.189.
- Gonzaga, G.M., Teixeira, N.A., Gaspar, J.C., and Apt, B.J., 1994, The origin of diamonds in western Minas Gerais, Brazil: *Mineralium Deposita*, v. 421, p. 414–421.
- Gonzaga, G.M., and Tompkins, L.A., 1991, Geologia do diamante, *in* Schobbenhaus, C., Queiroz, E.T. de;, and Coelho, C.E.S. eds., *Principais depósitos minerais do Brasil - Gemas e rochas ornamentais*, v. IV - A, Brasília, DNPM/CPRM, p. 53–116.
- Grütter, H.S., Gurney, J.J., Menzies, A.H., and Winter, F., 2004, An updated classification scheme for mantle-derived garnet, for use by diamond explorers: *Lithos*, v. 77, p. 841–857, doi:10.1016/j.lithos.2004.04.012.
- Grütter, H., Latti, D., and Menzies, A., 2006, Cr-saturation arrays in concentrate garnet compositions from kimberlite and their use in mantle barometry: *Journal of Petrology*, v. 47, p. 801–820, doi:10.1093/petrology/egi096.
- Guarino, V., Wu, F.Y., Lustrino, M., Melluso, L., Brotzu, P., Gomes, C.B., Ruberti, E., Tassinari, C.C.G., and Svisero, D.P., 2013, U-Pb ages, Sr-Nd- isotope geochemistry, and petrogenesis of kimberlites, kamafugites and phlogopite-picrites of the Alto Parana??ba Igneous Province, Brazil: *Chemical Geology*, v. 353, p. 65–82, doi:10.1016/j.chemgeo.2012.06.016.
- Gudfinnsson, G.H., and Presnall, D.C., 2005, Continuous gradations among primary carbonatitic, kimberlitic, melilititic, basaltic, picritic, and komatiitic melts in equilibrium with garnet lherzolite at 3-8 GPa: *Journal of Petrology*, v. 46, p. 1645–1659, doi:10.1093/petrology/egi029.
- Haggerty, S.E., 1986, Diamond genesis in a multiply-constrained model: *Nature*, v. 320, p. 34–38, doi:10.1038/320034a0.

- Harris, M., le Roex, A., and Class, C., 2004, Geochemistry of the Uintjiesberg kimberlite, South Africa: Petrogenesis of an off-craton, group I, kimberlite: *Lithos*, v. 74, p. 149–165, doi:10.1016/j.lithos.2004.02.001.
- Hayman, P.C., and Cas, R.A.F., 2011, Criteria for interpreting kimberlite as coherent: Insights from the Muskox and Jericho kimberlites (Nunavut, Canada): *Bulletin of Volcanology*, v. 73, p. 1005–1027, doi:10.1007/s00445-011-0512-x.
- Herzberg, C., 1992, Depth and degree of melting of komatiites: *Journal of Geophysical Research*, v. 97, p. 4521, doi:10.1029/91JB03066.
- Janse, A.J.A., and Sheahan, P.A., 1995, Catalogue of world wide diamond and kimberlite occurrences: a selective and annotative approach: *Journal of Geochemical Exploration*, v. 53, p. 73–111, doi:10.1016/0375-6742(94)00017-6.
- Jelsma, H., Barnett, W., Richards, S., and Lister, G., 2009, Tectonic setting of kimberlites: *Lithos*, v. 112, p. 155–165, doi:10.1016/j.lithos.2009.06.030.
- Kamenetsky, V.S., Golovin, A. V., Maas, R., Giuliani, A., Kamenetsky, M.B., and Weiss, Y., 2014, Towards a new model for kimberlite petrogenesis: Evidence from unaltered kimberlites and mantle minerals: *Earth-Science Reviews*, v. 139, p. 145–167, doi:10.1016/j.earscirev.2014.09.004.
- Karfunkel, J., Hoover, D., Fernandes, A.F., Sgarbi, G.N.C., Kambrock, K., and Oliveira, G.D., 2014, Diamonds from the Coromandel Area, West Minas Gerais State, Brazil: an update and new data on surface sources and origin: *Brazilian Journal of Geology*, v. 44, p. 325–338, doi:10.5327/Z2317-4889201400020011.
- Kavanagh, J.L., and Sparks, R.S.J., 2009a, Temperature changes in ascending kimberlite magma: *Earth and Planetary Science Letters*, v. 286, p. 404–413, doi:10.1016/j.epsl.2009.07.011.
- Kavanagh, J.L., and Sparks, R.S.J., 2009b, Temperature changes in ascending kimberlite magma: *Earth and Planetary Science Letters*, v. 286, p. 404–413.
- Kelley, S.P., and Wartho, J.A., 2000, Rapid kimberlite ascent and the significance of Ar-Ar ages in xenolith phlogopites: *Science*, v. 289, p. 609–611, doi:10.1126/science.289.5479.609.
- Kennedy, C.S., and Kennedy, G.C., 1976, The equilibrium boundary between graphite and diamond: *Journal of Geophysical Research*, v. 81, p. 2467–2470, doi:10.1029/JB081i014p02467.
- Kjarsgaard, B.A., 2007, Kimberlite Pipe Models : Significance for Exploration: *Ore Deposits*

- and Exploration Technology, p. 667–677.
- Kjarsgaard, B.A., Pearson, D.G., and Malarkey, J., 2010, The Kimberlite Olivine Phenocryst / Macrocryst / Xenocryst Problem , Re-Visited, *in* GeoCanada 2010, Cratons, Kimberlites and Diamonds plenary session, Calgary, p. 1–2.
- Kjarsgaard, B.A., Pearson, D.G., Tappe, S., Nowell, G.M., and Dowall, D.P., 2009, Geochemistry of hypabyssal kimberlites from Lac de Gras, Canada: Comparisons to a global database and applications to the parent magma problem: *Lithos*, v. 112, p. 236–248, doi:10.1016/j.lithos.2009.06.001.
- Lensky, N.G., Niebo, R.W., Holloway, J.R., Lyakhovsky, V., and Navon, O., 2006, Bubble nucleation as a trigger for xenolith entrapment in mantle melts: *Earth and Planetary Science Letters*, v. 245, p. 278–288, doi:10.1016/j.epsl.2005.11.064.
- Leonardos, O.H., Carvalho, J.B., Tallarico, F.H.B., Gibson, S.A., Thompson, R.N., Meyer, H.O.A., and Dickin, A.P., 1993, O xenolito de granada Iherzolito de Tres Ranchos 4: uma rocha matriz do diamante na província magmática cretacea do Alto Paranaíba, *in* Annais de Simpósio de Geologia do Diamanteo, p. 3–16.
- Leonardos, O.H., and Meyer, H.O.A., 1991, Outline of the geology of western minas gerais.pdf, *in* Fifth International Kimberlite Conference, p. 8.
- Lim, E., Giuliani, A., Phillips, D., and Goemann, K., 2018, Origin of complex zoning in olivine from diverse, diamondiferous kimberlites and tectonic settings: Ekati (Canada), Alto Paranaiba (Brazil) and Kaalvallei (South Africa): *Mineralogy and Petrology*, p. 1–16, doi:10.1007/s00710-018-0607-6.
- Le Maitre, R.W., 2002, Classification and nomenclature, *in* Igneous Rocks: a Classification and Glossary of Terms: Recommendations of the International Union of Geological Sciences Subcommission on the Systematics of Igneous Rocks, Cambridge, Cambridge University Press, p. 3–42.
- Melluso, L., Lustrino, M., Ruberti, E., Brotzu, P., Gomes, C.B., Morbidelli, L., Morra, V., Svisero, D.P., and Amelio, F.D., 2008, Major- and trace-element composition of olivine, perovskite, clinopyroxene, cr–fe–ti oxides, phlogopite and host kamafugites and kimberlites, alto paranaíba, brazil: *The Canadian Mineralogist*, v. 46, p. 19–40.
- Meyer, H.O.A., Garwood, B.L., Svisero, D.P., and Smith, C.B., 1994, Alkaline ultrabasic intrusions in western minas gerais brazil.pdf, *in* Proceedings of the Fifth International Kimberlite Conference, p. 140–155.
- Meyer, H.O.A., and Svisero, D.P., 1980, Kimberlites and diamonds in Brazil: Windows to the upper mantle: *Anais da Academia Brasileira de Ciências*, v. 52, p. 819–825.

- Mitchell, R.H., 1997, Kimberlite, Orangeites, Lamproites, Melilitites and Minettes: A Petrographic Atlas: Winnipeg, Almaz Press Inc, 243 p.
- Mitchell, R.H., 1970, Kimberlite and Related Rocks: A Critical Reappraisal: The Journal of Geology, v. 78, p. 686–704.
- Mitchell, R.H., 1995, Kimberlites, Orangeites, and Related Rocks: New York, NY, Springer Science+Business Media, 410 p.
- Mitchell, R.H., 1986, Kimberlites: mineralogy, geochemistry, and petrology: New York, NY, Springer Science+Business Media, 442 p., doi:10.1007/978-1-4899-0568-0.
- Mitchell, R.H., 2008, Petrology of hypabyssal kimberlites: Relevance to primary magma compositions: Journal of Volcanology and Geothermal Research, v. 174, p. 1–8, doi:10.1016/j.jvolgeores.2007.12.024.
- Mitchell, R.H., and Chakhmouradian, A.R., 1998, Th-rich loparite from the Khibina alkaline complex, Kola Peninsula: isomorphism and paragenesis: Mineralogical Magazine, v. 62, p. 341–353, doi:10.1180/002646198547738.
- Mori, P.E., Shane, R., Correia, C.T., and Haukka, M., 1999, Development of a fused glass disc XRF Facility and comparison with the pressed powder pellet technique at Instituto de: Revista Brasileira de Geociências, v. 29, p. 441–446, doi:10.5327/rbg.v29i3.715.
- Nannini, F., 2016, Geologia e Petrologia de Xenólitos Mantélicos da Província Ígnea do Alto Paranaíba, Minas Gerais: Universidade de São Paulo, 288 p.
- Nannini, F., 2011a, Petrografia e Química Mineral de Xenólitos Mantélicos da Intrusão Kimberítica Indaiá, Monte Carmelo, MG: Universidade de São Paulo, 100 p.
- Nannini, F., 2011b, Petrografia e química mineral de xenólitos mantélicos de região de Indaiá, Monte Carmelo, MG.: Universidade de São Paulo.
- Navarro, M.S., Andrade, S., Ulbrich, H., Gomes, C.B., and Girardi, V.A.V., 2008, The direct determination of rare earth elements in basaltic and related rocks using ICP-MS: Testing the efficiency of microwave oven sample decomposition procedures: Geostandards and Geoanalytical Research, v. 32, p. 167–180, doi:10.1111/j.1751-908X.2008.00840.x.
- Nimis, P., and Grütter, H., 2010, Internally consistent geothermometers for garnet peridotites and pyroxenites: Contributions to Mineralogy and Petrology, v. 159, p. 411–427, doi:10.1007/s00410-009-0455-9.
- Nimis, P., and Taylor, W.R., 2000, Single clinopyroxene thermobarometry for garnet peridotites. Part I. Calibration and testing of a Cr-in-Cpx barometer and an enstatite-in-Cpx thermometer: Contributions to Mineralogy and Petrology, v. 139, p. 541–554,

doi:10.1007/s004100000156.

- Nowell, G.M., Pearson, D.G., Bell, D.R., Carlson, R.W., Smith, C.B., Kempton, P.D., and Noble, S.R., 2004, Hf isotope systematics of kimberlites and their megacrysts: New constraints on their source regions: *Journal of Petrology*, v. 45, p. 1583–1612, doi:10.1093/petrology/egh024.
- Nowicki, T.E., Moore, R.O., Gurney, J.J., and Baumgartner, M.C., 2007, Diamonds and Associated Heavy Minerals in Kimberlite: A Review of Key Concepts and Applications, in *Developments in Sedimentology*, v. 58, p. 1235–1267, doi:10.1016/S0070-4571(07)58046-5.
- Ogilvie-Harris, R.C., Field, M., Sparks, R.S.J., and Walter, M.J., 2009, Perovskite from the Dutoitspan kimberlite, Kimberley, South Africa: implications for magmatic processes: *Mineralogical Magazine*, v. 73, p. 915–928, doi:10.1180/minmag.2009.073.6.915.
- Paton, C., Hergt, J.M., Phillips, D., Woodhead, J.D., and Shee, S.R., 2007, New insights into the genesis of Indian kimberlites from the Dharwar Craton via in situ Sr isotope analysis of groundmass perovskite: *Geology*, v. 35, p. 1011–1014, doi:10.1130/G24040A.1.
- Patterson, M.D., Francis, D., and McCandless, T.E., 2009, Kimberlites: Magmas or mixtures? *Lithos*, v. 112, p. 191–200, doi:10.1016/j.lithos.2009.06.004.
- Pearson, D.G., Boyd, F.R., Haggerty, S.E., Pasteris, J.D., Field, S.W., Nixon, P.H., and Pokhilenko, N.P., 1994, The characterisation and origin of graphite in cratonic lithospheric mantle: a petrological carbon isotope and Raman spectroscopic study: *Contributions to Mineralogy and Petrology*, v. 115, p. 449–466, doi:10.1007/BF00320978.
- Pollack, H.N., and Chapman, D.S., 1977, On the regional variation of heat flow, geotherms, and lithospheric thickness: *Tectonophysics*, v. 38, p. 279–296, doi:10.1016/0040-1951(77)90215-3.
- Priestley, K., McKenzie, D., and Debayle, E., 2006, The state of the upper mantle beneath southern Africa: *Tectonophysics*, v. 416, p. 101–112, doi:10.1016/j.tecto.2005.11.024.
- Read, G., Grutter, H., Winter, S., Luckman, N., Gaunt, F., and Thomsen, F., 2004, Stratigraphic relations, kimberlite emplacement and lithospheric thermal evolution, Quirico Basin, Minas Gerais State, Brazil: *Lithos*, v. 77, p. 803–818, doi:10.1016/j.lithos.2004.04.011.
- Reguir, E.P., Chakhmouradian, A.R., Halden, N.M., Malkovets, V.G., and Yang, P., 2009, Major- and trace-element compositional variation of phlogopite from kimberlites and carbonatites as a petrogenetic indicator: *Lithos*, v. 112, p. 372–384, doi:10.1016/j.lithos.2009.05.023.
- Riccomini, C., Velázquez, V.F., and Gomes, C.B., 2005, Tectonic controls of the Mesozoic and

- Cenozoic alkaline magmatism in central-southeastern Brazilian platform.: Mesozoic to Cenozoic Alkaline Magmatism in the Brazilian Platform, p. 31–55.
- Robinson, D.N., 1989, Surface Textures and Other Features of Diamonds: University of Cape Town, 161 p.
- Le Roex, A.P., Bell, D.R., and Davis, P., 2003, Petrogenesis of Group I Kimberlites from Kimberley, South Africa: Evidence from Bulk-rock Geochemistry: Journal of Petrology, v. 44, p. 2261–2286, doi:10.1093/petrology/egg077.
- Russell, J.K., Porritt, L.A., Lavallée, Y., and Dingwell, D.B., 2012, Kimberlite ascent by assimilation-fuelled buoyancy: Nature, v. 481, p. 352–356, doi:10.1038/nature10740.
- Sarkar, C., 2011, Trace Element and Isotope Geochemistry of Perovskite From Kimberlites of Southern: University of Bristol, 360 p.
- Sarkar, C., Storey, C.D., and Hawkesworth, C.J., 2013, Detailed Protracted Crystallization History of Perovskite in Orapa Kimberlite, *in* 10th International Kimberlite Conference, p. 211–224, doi:10.1007/978-81-322-1170-9.
- Scott Smith, B.H., Nowick, T.E., Russell, J.K., Webb, K.J., Mithcell, R.H., Hetman, C.M., Harder, M., Skinner, E.M.W., and Robey, J.A., 2013, Kimberlite Terminology and Classification, *in* Pearson, D.G. ed., Proceedings of 10th International Kimberlite Conference, v.2. Special Issue of the Journal of the Geological Society of India, Springer India, p. 1–17, doi:10.1007/978-81-322-1173-0.
- Sertek, J.P., Andrade, S., and Ulbrich, H.H., 2015, An Evaluation of the Effects of Primary and Cross-Contamination during the Preparation of Rock Powders for Chemical Determinations: Geostandards and Geoanalytical Research, v. 39, p. 381–397, doi:10.1111/j.1751-908X.2014.00324.x.
- Silva, S. da, 2008, Petrografia e Química Mineral das Intrusões Indaiá I e Indaiá II, Oeste do Estado de Minas Gerais: Universidade de São Paulo, 113 p.
- Smith, B.H.S., 2017, Kimberlites – from Mantle to Mine: , p. 2–4.
- Smith, C.B., 1983, Pb, Sr and Nd isotopic evidence for sources of southern African Cretaceous kimberlites: Nature, v. 304, p. 51–54, doi:10.1038/304051a0.
- Sparks, R.S.J., 2013, Kimberlite Volcanism: Annual Review of Earth and Planetary Sciences, v. 41, p. 497–528, doi:10.1146/annurev-earth-042711-105252.
- Sparks, R.S.J., Baker, L., Brown, R.J., Field, M., Schumacher, J., Stripp, G., and Walters, A., 2006, Dynamical constraints on kimberlite volcanism: Journal of Volcanology and Geothermal Research, v. 155, p. 18–48, doi:10.1016/j.jvolgeores.2006.02.010.

- Sparks, R.S.J., Brooker, R.A., Field, M., Kavanagh, J.L., Schumacher, J.C., Walter, M.J., and White, J., 2009, The nature of erupting kimberlite melts: *Lithos*, v. 112S, p. 429–438.
- Sparks, R.S.J., Brown, R.J., Field, M., and Gilbertson, M., 2007, Kimberlite ascent and eruption: *Nature*, v. 450, p. E21–E21, doi:10.1038/nature06435.
- Stachel, T., and Luth, R.W., 2015, Diamond formation - Where, when and how? *Lithos*, v. 220–223, p. 200–220, doi:10.1016/j.lithos.2015.01.028.
- Stagno, V., Ojwang, D.O., Mccammon, C.A., and Frost, D.J., 2013, The oxidation state of the mantle and the extraction of carbon from Earth's interior: *Nature*, v. 493, p. 84–90, doi:10.1038/nature11679.
- van Straaten, B.I., Kopylova, M.G., Russell, J.K., and Smith, B.H.S., 2011, A rare occurrence of a crater-filling clastogenic extrusive coherent kimberlite, Victor Northwest (Ontario, Canada): *Bulletin of Volcanology*, v. 73, p. 1047–1062, doi:10.1007/s00445-011-0507-7.
- Svisero, D.P., and Chieregati, L.A. Contexto Geológico de Kimberlitos, Lamproítos e Ocorrências Diamantíferas do Brasil: , p. 75–81.
- Svisero, D.P., Meyer, H.O.A., Haralyi, N.L.E., and Hasui, Y., 1984, A Note on the Geology of Some Brazilian Kimberlites: *The Journal of Geology*, v. 92, p. 331–338.
- Svisero, D.P., Shigley, J.E., and Weldon, R., 2017, Brazilian diamonds: a historical and recent perspective: *Gems & Gemology*, v. 53, p. 2–33.
- Thomaz, L. V, 2009, Estudo Petrográfico e Química Mineral da Intrusão Kimberlítica Régis, no Oeste de Minas Gerais: Universidade de São Paulo, 143 p.
- Torsvik, T.H., Burke, K., Steinberger, B., Webb, S.J., and Ashwal, L.D., 2010, Diamonds sampled by plumes from the core–mantle boundary: *Nature*, v. 466, p. 352–355, doi:10.1038/nature09216.
- Trickett, S.K., 2007, Mapping lithofacies within the D/K1 kimberlite Pipe at Lethakane, Botswana: An assessment of petrgraphic, geochemical and mineralogical indicators: University of London.
- Ubide, T., Arranz, E., Lago, M., Galé, C., and Larrea, P., 2012, The influence of crystal settling on the compositional zoning of a thin lamprophyre sill: A multi-method approach: *Lithos*, v. 132–133, p. 37–49, doi:10.1016/j.lithos.2011.11.012.
- Wagner, P., 1914, The diamond fields of South Africa: Johannesburg, South Africa, Transvaal Leader.
- White, J.L., Sparks, R.S.J., Bailey, K., Barnett, W.P., Field, M., and Windsor, L., 2012, Kimberlite sills and dykes associated with the Wesselton kimberlite pipe, Kimberley, South Africa: *South African Journal of Geology*, v. 115, p. 1–32,

doi:10.2113/gssajg1151.1.

Wilson, L., and Head III, J.W., 2007, An integrated model of kimberlite ascent and eruption: Nature, v. 447, p. 53–57, doi:10.1038/nature05692.

Zhang, Z., 2016, Diamond resorption morphology as a fluid proxy in diamond- bearing environments: constraints from empirical and experimental studies: Dalhousie University.

Zhang, Z., Fedortchouk, Y., and Hanley, J.J., 2015, Evolution of diamond resorption in a silicic aqueous fluid at 1 – 3 GPa: Application to kimberlite emplacement and mantle metasomatism: Lithos, v. 227, p. 179–193.

APPENDIX A

PETROGRAPHIC DESCRIPTIONS

Table A01: Petrographic descriptions of Três Ranchos IV and Limeira I samples.

	Olivine			Phlogopite			Spinel			
	Megacrysts (> 1cm)	Macrocrysts (1,0 - 10 mm)		Macrocrysts (0,2-0,5 mm)		Macrocrysts (>1 mm)				
	size mm	vol.%	Description	size mm	vol.%	Description	size mm	vol.%	Description	
TR-IV 14 samples	1-3,4	10-15	anhedral, rounded crystals, with fractures and boundaries filled with serpentine, some exhibit undulose extinction and fresh cores.	subhedral to anhedral or rounded and elongated crystals, with rims and fractures filled with serpentine films, sometimes exhibit undulose extinction and be completely serpentinised.	0,2-0,5	5-10	euhedral crystals, exhibits strong from colorless/pale yellow to brown pleochroism, some with kink banding extensive chloritisation	1-	2-4	reaction rims and sometimes with intergrown with perovskite
LM-I 18 samples	1-3	15-20	anhedral and rounded crystals, with fresh cores, and minor to extensive greenish serpentine alteration along fractures and boundaries, some can exhibit undulose extinction	subhedral to rounded and elongated crystals, with greenish serpentinite alteration along rims and fractures, sometimes completely serpentinised	0,2-0,5	5-10	euhedral crystals, exhibits strong from colorless/pale yellow to brown pleochroism, some with kink banding extensive chloritisation	1-9	3-5	translucent red subhedral to anhedral crystals

Table A01: Cont. Petrographic descriptions of Três Ranchos IV and Limeira I samples.

	Ilmenite			Pyroxene			Garnet		
	Macrocrysts (>1 mm)			Macrocrysts (>1 mm)			Macrocrysts (>1 mm)		
	size mm	vol.%	Description	size mm	vol.%	Description	size mm	vol.%	Description
TR-IV	14	-	-	absent in Três Ranchos IV	-	-	absent in Três Ranchos IV	>1	>2
LM-I	18	1-5	3-6	subhedral to anhedral, with perovskite and titanomagnetite or crhomite reaction rim, can also occur as complex intergrowth with Prv and Ti-mag	1-1,5	>1	anhedral to rounded crystals, almost completely altered to serpentine and carbonates, at the crystals rims and fractures its very common the presence of monticellite grains	-	-

Table A01: Cont. Petrographic descriptions of Três Ranchos IV and Limeira I samples.

Intrusion	Groundmass phases*													
	Olivine			Perovskite			Phlogopite			Spinel			Ilmenite	
size mm	vol.%	Description	size mm	vol.%	Description	size mm	vol.%	Description	size mm	vol.%	Description	size mm	vol.%	Description
TR-IV 14 samples	0,05- 0,2	subhedral to rounded anhdral crystals, most completely pseudomorphed by serpentine	1-9	5-10	euhedral to subhedral crystals, with dark brown pleochorism, sometimes with olivine inclusions and can occur as complex intergrowth with Ilm and Ti-mag	0,08- 0,2	20-25	subhedral to anhedral, associated with other groundmass phases	0,2- 0,3	5-8	translucent red subhedral to anhedral	-	-	absent in Três Ranchos IV
LM-I 18 samples	0,01- 0,09	subhedral to anhedral crystals, most completely pseudomorphed by serpentine	0,06- 0,3	5-10	euhedral to subhedral crystals, with dark brown pleochorism, sometimes with olivine inclusions and can occur as complex intergrowth with Ilm and Ti-mag, as reaction rims in Ilm, "necklace" texture in olivine megacrysts	0,04- 0,2	20-25	subhedral to anhedral, associated with other groundmass phases	0,2- 0,3	2-5	translucent red subhedral to anhedral	0,4- 0,5	3-5	subhedral to anhedral, with perovskite and titanomagnetic or crhomite reaction rim

*Proportion of groundmass phases in TR-IV: 49-66% and LM-I: 38-63%.

Table A01: Cont. Petrographic descriptions of Três Ranchos IV and Limeira I samples.

	Groundmass phases*						Alteration phases					
	Montcellite			Apatite			Carbonate			Serpentine		
Intrusion	size mm	vol. %	Description	size mm	vol. %	Description	size mm	vol. %	Description	size mm	vol. %	Description
TR-IV 14 samples	-	-	absent in Três Ranchos IV	-	-	absent in Três Ranchos IV	<0,01	<2		<0,01	4-8	common in the groundmass, where it has most completely pseudomorphed the original fine grain mineralogy; serpentinisation of mega-, macro-, and microcrysttic olivine is common and has occurred to varying degrees, ranging from minimal alterations concentrated along fractures to complete replacement by yellow and brown serpentine.
LM-I 18 samples	0,01- 0,03	10- 15	subhedral to euhedral zoned grains. At the aoutolith it can occur as a “garland” around olivine macrocrysts.	>0,05	5%	singular acicular crystals or as its basal section	<0,01	<2		<0,01	4-8	common in the groundmass, where it has most completely pseudomorphed the original fine grain mineralogy; serpentinisation of mega-, macro-, and microcrysttic olivine is common and has occurred to varying degrees, ranging from minimal alterations concentrated along fractures to complete replacement by yellow and brown serpentine.

*Proportion of groundmass phases in TR-IV: 49-66% and LM-I: 38-63%.

Table A02: Relative abundance of perovskites with different paragenesis from Três Ranchos IV and Limeiras I.

Perovskite paragenesis		Limeira I	
		Frequency	Description
Major parageneses	Discrete groundmass	Abundant	10-30µm, zoned and non-zoned, sub- to euhedral.
	Along olivine grain boundary	Intermediate	20-50µm, non zoned or with weak zoning, sub- to euhedral.
	Intergrowth with spinel	Very rare	Not registered
	Reaction mantle around Ilmenite	Abundant	10µm, zoned and non-zoned, sub- to euhedral.
Minor parageneses	Pvs with Olv and Cr spinel inclusion	Intermediate	50µm, zoned, sub- to euhedral.
	Pvs inclusion within phlogopite	Very rare	Not registered
	Pvs containing inclusions of mica and apatite	Very rare	Not registered
	Pvs rim around resorbed Fe-Ti spinel	Very rare	Not registered
Perovskites with resorbed grain boundary		Intermediate	10-20µm, zoned and non-zoned, sub- to euhedral.
Fresh perovskites		Abundant	10-60µm, zoned and non-zoned, sub- to euhedral.
Perovskites with alteration features		Intermediate	20-30µm, zoned and non-zoned, sub- to euhedral.

Table A02: Cont. Relative abundance of perovskites with different paragenesis from Três Ranchos IV and Limeiras I.

Perovskite paragenesis		Três Ranchos IV	
		Frequency	Description
Major parageneses	Discrete groundmass	Abundant	10-30µm, zoned and non-zoned, sub- to euhedral.
	Along olivine grain boundary	Intermediate	20-50µm, non zoned, sub- to euhedral.
	Intergrowth with spine	Intermediate	30µm, with weak zoning, sub-to anhedral
	Reaction mantle around Ilmenite	Very rare	Not registered
Minor parageneses	Pvs with Olv and Cr spinel inclusion	Intermediate	20µm, zoned, sub- to euhedral.
	Pvs inclusion within phlogopite	Very rare	Not registered
	Pvs containing inclusions of mica and apatite	Very rare	Not registered
	Pvs rim around resorbed Fe-Ti spinel	Rare	Not registered
Perovskites with resorbed grain boundary		Intermediate	30-50µm, zoned, sub- to euhedral.
Fresh perovskites		Abundant	10-50µm, zoned and non-zoned, sub- to euhedral.
	Perovskites with alteration features	Intermediate	10-30µm, with weak zoning, sub-to anhedral

APPENDIX B

EPMA DATA

TABELA B01 - Major element concentration of olivine from all samples. Structural formula calculated on the basis of 4 oxygens. C - core; R - rim; I - intermediated; mega - megacrystals, macro - macrocrysts, micro - microcrysts.

Sample	LM-2	LM-2	LM-2	LM-2	LM-2	LM-2	LM-2	LM-2	LM-2	LM-2	LM-2	LM-2	LM-2	LM-2	LM-2	LM-2
Grain/Analysis	01/01	02/03	02/04	03/05	03/06	04/07	04/08	05/09	05/10	06/11	06/12	07/13	07/14	08/15	08/16	09/17
Location	C	R	C	R	C	R	C	R	C	R	C	R	C	R	C	C
Crystal type	mega	mega	mega	mega	mega	mega	macro	macro	macro	macro	macro	macro	macro	macro	macro	micro
SiO ₂	40.17	40.46	40.61	40.40	40.19	39.86	39.71	40.66	40.23	39.82	40.63	40.04	40.45	40.16	40.06	40.07
Al ₂ O ₃	0.01	0.00	0.00	0.01	0.00	0.00	0.00	0.01	0.00	0.00	0.01	0.05	0.04	0.00	0.00	0.04
FeO	8.50	9.67	10.04	10.31	9.89	13.50	13.33	10.13	11.78	13.61	9.57	12.77	10.37	10.38	12.51	12.43
MnO	0.16	0.15	0.15	0.14	0.17	0.21	0.21	0.15	0.17	0.19	0.16	0.21	0.11	0.12	0.24	0.22
NiO	0.39	0.39	0.35	0.41	0.36	0.20	0.21	0.38	0.34	0.24	0.39	0.16	0.44	0.46	0.33	0.39
CaO	0.02	0.02	0.01	0.01	0.02	0.06	0.07	0.05	0.02	0.09	0.01	0.05	0.13	0.14	0.02	0.04
K ₂ O	0.01	0.00	0.00	0.01	0.01	0.02	0.00	0.00	0.01	0.01	0.02	0.00	0.00	0.02	0.00	0.01
TiO ₂	0.00	0.03	0.00	0.00	0.02	0.02	0.00	0.04	0.09	0.01	0.00	0.06	0.02	0.00	0.05	0.06
Cr ₂ O ₃	0.01	0.00	0.08	0.00	0.00	0.05	0.03	0.00	0.10	0.00	0.01	0.06	0.12	0.00	0.01	0.09
MgO	50.34	49.19	48.79	48.94	46.02	46.21	48.72	47.57	45.89	49.62	46.80	48.53	48.73	47.32	47.15	47.54
Na ₂ O	0.01	0.00	0.01	0.00	0.01	0.01	0.00	0.01	0.01	0.02	0.00	0.01	0.00	0.01	0.01	0.03
Total:	99.60	99.92	100.06	100.22	99.58	99.89	99.83	100.12	100.17	100.06	100.41	100.07	100.20	100.47	100.32	100.30
Si	0.986	0.994	0.997	0.992	0.996	0.993	0.998	0.995	0.995	0.993	0.995	0.994	0.994	0.988	0.993	0.993
Al	0.000	0.000	0.000	0.000	0.000	0.000	0.000	0.000	0.000	0.000	0.000	0.000	0.000	0.001	0.000	0.001
Fe	0.174	0.199	0.206	0.212	0.204	0.282	0.279	0.208	0.244	0.284	0.196	0.265	0.213	0.214	0.259	0.241
Mn	0.003	0.003	0.003	0.003	0.004	0.004	0.005	0.003	0.003	0.004	0.003	0.004	0.002	0.003	0.005	0.003
Ni	0.008	0.008	0.007	0.008	0.007	0.004	0.004	0.008	0.007	0.005	0.008	0.003	0.009	0.009	0.006	0.008
Ca	0.000	0.001	0.000	0.001	0.001	0.002	0.002	0.001	0.000	0.002	0.000	0.001	0.003	0.004	0.001	0.004
K	0.000	0.000	0.000	0.000	0.000	0.001	0.001	0.000	0.000	0.001	0.000	0.000	0.001	0.000	0.000	0.000
Ti	0.000	0.001	0.000	0.000	0.000	0.000	0.000	0.000	0.001	0.001	0.002	0.000	0.001	0.000	0.001	0.001
Cr	0.000	0.000	0.002	0.000	0.000	0.000	0.001	0.001	0.000	0.002	0.000	0.000	0.001	0.002	0.000	0.002
Mg	1.842	1.801	1.786	1.792	1.800	1.714	1.722	1.783	1.754	1.709	1.807	1.734	1.778	1.788	1.742	1.751
Na	0.000	0.000	0.001	0.000	0.000	0.000	0.000	0.000	0.001	0.000	0.001	0.000	0.000	0.000	0.001	0.001
Cations:	3.014	3.006	3.002	3.008	3.008	3.004	3.007	3.002	3.007	3.003	3.005	3.007	3.003	3.010	3.009	3.005
<i>Fayalite</i>	0.09	0.10	0.10	0.11	0.10	0.14	0.10	0.12	0.14	0.10	0.13	0.11	0.13	0.13	0.12	0.12
<i>Forsterite</i>	0.91	0.90	0.90	0.89	0.90	0.86	0.86	0.90	0.88	0.86	0.90	0.87	0.89	0.87	0.87	0.88

TABLEA B01 – Cont. Major element concentration of olivine from all samples. Structural formula calculated on the basis of 4 oxygens. C - core; R - rim; I - intermediately; mega - megacrystals, macro - macrocrysts, micro - microcrysts.

Sample	LM-2	LM3-1	LM3-1	LM3-1	LM3-1	LM3-1	LM3-1	LM3-1	LM3-1	LM3-1	LM3-1	LM3-1	LM3-1	LM3-1	LM3-1	
Grain/Analysis	09/18	10/19	10/20	11/21	11/22	12/23	12/24	13/25	13/26	14/27	14/28	15/29	15/30	16/31	16/32	
Location	R	C	R	C	R	C	R	C	R	C	R	C	R	C	R	
Crystal type	micro	mega	mega	mega	mega	mega	mega	macro	macro	macro	macro	macro	macro	macro	micro	
SiO ₂	40.45	40.32	39.55	40.90	41.10	40.20	40.73	40.22	39.93	40.47	39.89	40.25	39.86	39.91	39.99	
Al ₂ O ₃	0.04	0.00	0.00	0.01	0.00	0.02	0.01	0.01	0.00	0.05	0.05	0.00	0.00	0.02	0.01	0.01
FeO	11.61	10.10	12.22	7.46	7.53	12.18	11.79	8.18	13.91	11.29	10.89	13.15	13.01	12.31	12.48	11.57
MnO	0.16	0.18	0.17	0.12	0.13	0.16	0.16	0.10	0.20	0.13	0.16	0.15	0.22	0.15	0.15	0.16
NiO	0.37	0.40	0.29	0.35	0.37	0.31	0.36	0.37	0.19	0.39	0.40	0.34	0.31	0.40	0.40	0.36
CaO	0.13	0.01	0.02	0.04	0.03	0.07	0.05	0.01	0.08	0.11	0.14	0.03	0.08	0.06	0.07	0.04
K ₂ O	0.00	0.01	0.00	0.00	0.00	0.00	0.02	0.00	0.00	0.00	0.02	0.00	0.00	0.01	0.01	0.00
TiO ₂	0.00	0.01	0.03	0.01	0.05	0.02	0.00	0.00	0.02	0.06	0.03	0.04	0.03	0.00	0.03	0.04
Cr ₂ O ₃	0.08	0.00	0.03	0.03	0.01	0.00	0.00	0.01	0.04	0.11	0.08	0.01	0.02	0.02	0.06	0.01
MgO	47.46	49.29	48.12	51.20	50.91	47.50	47.15	51.15	45.79	48.22	47.90	47.18	46.37	46.85	47.51	48.06
Na ₂ O	0.02	0.02	0.00	0.00	0.01	0.00	0.01	0.00	0.01	0.01	0.02	0.01	0.00	0.02	0.01	0.00
Total:	100.32	100.33	100.42	100.13	100.14	100.46	99.91	100.55	100.45	100.32	100.16	100.80	100.29	99.70	100.64	100.24
Si	0.998	0.989	0.979	0.992	0.997	0.993	1.000	0.988	1.000	0.986	0.997	0.987	0.999	0.994	0.987	0.988
Al	0.001	0.000	0.000	0.000	0.000	0.001	0.000	0.000	0.000	0.002	0.001	0.000	0.000	0.001	0.000	0.000
Fe	0.240	0.207	0.253	0.151	0.153	0.252	0.244	0.166	0.289	0.233	0.224	0.272	0.270	0.257	0.258	0.239
Mn	0.003	0.004	0.004	0.002	0.003	0.003	0.003	0.002	0.004	0.003	0.003	0.003	0.005	0.003	0.003	0.003
Ni	0.007	0.008	0.006	0.007	0.006	0.007	0.007	0.007	0.004	0.008	0.008	0.007	0.006	0.008	0.008	0.007
Ca	0.004	0.000	0.001	0.001	0.001	0.002	0.001	0.000	0.002	0.003	0.004	0.001	0.002	0.002	0.001	0.001
K	0.000	0.000	0.000	0.000	0.000	0.000	0.001	0.000	0.000	0.000	0.001	0.000	0.000	0.000	0.000	0.000
Ti	0.000	0.000	0.000	0.001	0.000	0.000	0.000	0.000	0.000	0.001	0.001	0.001	0.001	0.001	0.001	0.001
Cr	0.002	0.000	0.001	0.000	0.000	0.000	0.000	0.000	0.001	0.001	0.002	0.002	0.000	0.000	0.001	0.000
Mg	1.746	1.802	1.776	1.852	1.841	1.749	1.742	1.849	1.698	1.774	1.760	1.741	1.716	1.741	1.751	1.770
Na	0.001	0.000	0.000	0.000	0.000	0.000	0.001	0.000	0.001	0.001	0.001	0.000	0.000	0.001	0.001	0.000
Cations:	3.001	3.020	3.007	3.002	3.006	3.000	3.012	2.999	3.012	3.001	3.012	3.000	3.006	3.012	3.011	3.012
<i>Fayalite</i>	0.12	0.10	0.12	0.08	0.08	0.13	0.12	0.08	0.15	0.12	0.11	0.14	0.14	0.13	0.12	0.12
<i>Forsterite</i>	0.88	0.90	0.88	0.92	0.92	0.87	0.88	0.92	0.85	0.88	0.89	0.86	0.86	0.87	0.87	0.88

TABLEA B01 – Cont. Major element concentration of olivine from all samples. Structural formula calculated on the basis of 4 oxygens. C - core; R - rim; I - intermediated; mega - megacrystals, macro - macrocrysts, micro - microcrysts.

Sample	LM3-1	LM3-1	LM3-1	LM3-2	LM3-2	LM3-2	LM3-2	LM3-2	LM3-2	LM3-2	LM3-2	LM3-2	LM3-2	LM3-2	LM3-2
Grain/Analysis	17/34	18/35	18/36	19/37	19/38	20/39	20/40	21/41	21/42	22/43	22/44	23/45	23/46	24/47	24/48
Location	R	C	R	C	R	C	R	C	R	C	R	C	R	C	R
Crystal type	micro	micro	micro	micro	micro	micro	micro	micro	micro	micro	micro	micro	micro	macro	macro
SiO ₂	40.18	40.79	40.38	39.77	39.91	40.58	39.69	40.26	40.20	40.53	39.57	39.88	39.59	39.12	39.07
Al ₂ O ₃	0.02	0.01	0.00	0.02	0.01	0.01	0.00	0.01	0.00	0.02	0.00	0.00	0.01	0.00	0.00
FeO	13.78	8.43	8.22	12.79	12.76	10.29	13.39	11.41	13.45	7.72	13.55	13.57	13.31	16.01	12.89
MnO	0.18	0.13	0.13	0.14	0.15	0.15	0.19	0.17	0.20	0.09	0.22	0.16	0.18	0.22	0.19
NiO	0.23	0.38	0.38	0.43	0.43	0.36	0.36	0.36	0.19	0.36	0.19	0.24	0.22	0.17	0.23
CaO	0.14	0.01	0.00	0.06	0.06	0.09	0.04	0.11	0.01	0.09	0.04	0.05	0.01	0.41	0.03
K ₂ O	0.01	0.00	0.00	0.02	0.01	0.00	0.01	0.00	0.00	0.03	0.01	0.00	0.01	0.00	0.01
TiO ₂	0.02	0.00	0.02	0.05	0.00	0.03	0.00	0.00	0.06	0.03	0.01	0.00	0.05	0.02	0.03
Cr ₂ O ₃	0.08	0.00	0.00	0.01	0.01	0.04	0.01	0.08	0.03	0.05	0.00	0.02	0.00	0.00	0.00
MgO	45.08	50.77	51.48	46.77	46.90	49.05	45.88	48.32	46.28	51.31	47.09	46.75	46.84	44.85	47.50
Na ₂ O	0.00	0.00	0.01	0.01	0.02	0.00	0.01	0.01	0.01	0.02	0.00	0.00	0.01	0.00	0.01
Total:	99.72	100.51	100.62	100.28	100.54	99.67	100.59	100.59	100.59	100.67	100.80	100.67	100.41	100.32	100.67
Si	1.006	0.990	0.980	0.990	0.991	0.993	0.995	0.990	0.997	0.986	0.982	0.990	0.986	0.985	0.973
Al	0.001	0.000	0.000	0.001	0.001	0.000	0.000	0.000	0.000	0.001	0.000	0.000	0.000	0.000	0.000
Fe	0.289	0.171	0.167	0.266	0.265	0.211	0.281	0.235	0.279	0.157	0.281	0.282	0.277	0.337	0.197
Mn	0.004	0.003	0.003	0.003	0.003	0.003	0.004	0.004	0.004	0.002	0.005	0.003	0.004	0.005	0.003
Ni	0.005	0.007	0.007	0.009	0.009	0.009	0.007	0.007	0.007	0.004	0.007	0.004	0.005	0.003	0.007
Ca	0.004	0.000	0.000	0.002	0.001	0.002	0.001	0.001	0.003	0.000	0.003	0.001	0.001	0.011	0.001
K	0.000	0.000	0.000	0.001	0.000	0.000	0.000	0.000	0.000	0.001	0.000	0.000	0.000	0.000	0.000
Ti	0.000	0.000	0.000	0.001	0.000	0.001	0.000	0.000	0.001	0.001	0.000	0.000	0.001	0.001	0.000
Cr	0.002	0.000	0.000	0.000	0.000	0.000	0.000	0.001	0.000	0.002	0.000	0.001	0.000	0.000	0.000
Mg	1.683	1.837	1.862	1.736	1.737	1.789	1.714	1.772	1.711	1.860	1.742	1.729	1.739	1.683	1.810
Na	0.000	0.000	0.000	0.001	0.001	0.000	0.001	0.000	0.001	0.000	0.000	0.000	0.000	0.000	0.000
Cations:	2.993	3.020	3.009	3.009	3.006	3.005	3.010	3.001	3.014	3.017	3.011	3.013	3.014	3.026	3.009
<i>Fayalite</i>	0.15	0.09	0.08	0.13	0.13	0.11	0.14	0.12	0.14	0.08	0.14	0.14	0.17	0.13	0.10
<i>Forsterite</i>	0.85	0.91	0.92	0.87	0.87	0.89	0.86	0.88	0.86	0.92	0.86	0.86	0.83	0.87	0.90

TABLEA B01 – Cont. Major element concentration of olivine from all samples. Structural formula calculated on the basis of 4 oxygens. C - core; R - rim; I - intermediately; mega - megacrystals, macro - macrocrysts, micro - microcrysts.

Sample	LMI-C1 33/65	LMI-C1 33/66	LMI-C1 34/67	LMI-C1 34/68	LMI-C1 35/69	LMI-C1 35/70	LMI-C1 36/71	LMI-C2 36/72	LMI-C2 37/73	LMI-C2 37/74	TR-4 01/01	TR-4 01/02	TR-4 02/03	TR-4 02/04	TR-4 03/05
Grain/Analysis	C	R	C	R	C	R	C	R	C	R	C	R	C	R	C
Location															
Crystal type	mega	mega	mega	mega	micro	macro									
SiO ₂	40.72	39.55	40.40	40.22	40.01	39.28	40.54	39.55	40.16	41.26	41.04	40.75	41.38	41.63	40.86
Al ₂ O ₃	0.01	0.00	0.01	0.00	1.36	1.59	0.03	0.00	0.00	0.00	0.00	0.00	0.01	0.02	0.00
FeO	11.40	11.26	11.55	11.30	4.65	4.55	8.98	9.22	12.40	12.83	8.06	7.89	8.19	8.03	8.02
MnO	0.18	0.20	0.18	0.18	0.22	0.21	0.14	0.16	0.16	0.17	0.12	0.09	0.08	0.09	0.11
NiO	0.41	0.40	0.34	0.33	0.58	0.45	0.38	0.37	0.36	0.35	0.35	0.37	0.38	0.39	0.36
CaO	0.02	0.01	0.02	0.01	0.35	0.22	0.02	0.03	0.03	0.04	0.00	0.00	0.03	0.04	0.00
K ₂ O	0.00	0.01	0.01	0.00	0.03	0.02	0.00	0.00	0.01	0.01	0.02	0.00	0.00	0.00	0.00
TiO ₂	0.00	0.00	0.00	0.00	0.04	0.00	0.01	0.03	0.03	0.01	0.00	0.00	0.00	0.00	0.05
Cr ₂ O ₃	0.02	0.00	0.05	0.03	0.13	0.05	0.00	0.01	0.03	0.04	0.02	0.01	0.03	0.00	0.00
MgO	48.21	49.38	48.36	49.29	37.54	38.38	49.63	50.82	47.00	45.06	50.38	50.39	49.64	48.70	50.25
Na ₂ O	0.00	0.02	0.01	0.01	0.03	0.03	0.00	0.01	0.01	0.00	0.00	0.00	0.00	0.00	0.00
Total:	100.97	100.84	100.93	101.36	84.94	84.77	99.72	100.20	100.17	99.77	100.00	99.50	99.74	98.89	99.65
Si	0.997	0.973	0.991	0.982	1.115	1.097	0.994	0.970	0.996	1.025	0.999	0.996	1.009	1.021	0.998
Al	0.000	0.000	0.000	0.000	0.045	0.052	0.001	0.000	0.000	0.000	0.000	0.000	0.000	0.000	0.000
Fe	0.233	0.232	0.237	0.231	0.108	0.106	0.184	0.189	0.257	0.267	0.164	0.161	0.167	0.165	0.164
Mn	0.004	0.004	0.004	0.004	0.005	0.005	0.005	0.003	0.003	0.003	0.002	0.002	0.002	0.002	0.002
Ni	0.008	0.008	0.007	0.006	0.013	0.010	0.007	0.007	0.007	0.007	0.007	0.007	0.008	0.007	0.007
Ca	0.001	0.000	0.001	0.000	0.010	0.007	0.001	0.001	0.001	0.001	0.000	0.000	0.001	0.001	0.000
K	0.000	0.000	0.000	0.000	0.001	0.001	0.000	0.000	0.000	0.000	0.001	0.000	0.000	0.000	0.000
Ti	0.000	0.000	0.000	0.000	0.001	0.000	0.000	0.001	0.000	0.000	0.000	0.000	0.000	0.000	0.001
Cr	0.000	0.000	0.001	0.001	0.003	0.001	0.000	0.000	0.001	0.001	0.000	0.000	0.001	0.000	0.000
Mg	1.760	1.810	1.768	1.794	1.559	1.598	1.815	1.858	1.738	1.669	1.828	1.837	1.804	1.781	1.829
Na	0.000	0.001	0.000	0.000	0.002	0.001	0.000	0.001	0.000	0.001	0.000	0.000	0.000	0.000	0.000
Cations:	3.003	3.028	3.009	3.018	2.862	2.878	3.005	3.030	3.003	2.975	3.001	3.004	2.991	2.978	3.001
<i>Fayalite</i>	1.000	0.818	0.933	0.932	0.751	0.779	1.000	0.843	0.948	0.873	0.08	0.08	0.08	0.08	0.08
<i>Forsterite</i>	0.000	0.182	0.067	0.068	0.249	0.221	0.000	0.157	0.052	0.127	0.92	0.92	0.92	0.92	0.92

TABELA B01 – Cont. Major element concentration of olivine from all samples. Structural formula calculated on the basis of 4 oxygens. C - core; R - rim; I - intermediately
 mega - megacrystals, macro - macrocrysts, micro - microcrysts.

TABELA B01 – Cont. Major element concentration of olivine from all samples. Structural formula calculated on the basis of 4 oxygens. C - core; R - rim; I - intermediately; mega - megacrystals, macro - macrocrysts, micro - microcrysts.

Sample	TR-4	TR-4	TR-4	TR-4	TR-4	TR-4	TR-4	TR-4	TR-4	TR-4	TR-4	TR-4	TR-4	TR-4	TR-4
Grain/Analysis	03/06	04/07	04/08	05/09	05/10	06/11	06/12	07/13	07/14	08/15	08/16	09/17	09/18	10/19	10/20
Location	R	C	R	C	R	C	R	C	R	C	R	C	R	C	R
Crystal type	macro	micro	macro	micro	macro	micro	macro	macro	macro	macro	macro	macro	macro	macro	macro
SiO ₂	39.97	40.48	41.10	39.29	40.18	41.21	42.15	41.03	41.16	40.68	40.74	41.13	41.43	40.70	41.40
Al ₂ O ₃	0.00	0.01	0.04	0.02	0.01	0.01	0.01	0.01	0.01	0.01	0.02	0.01	0.02	0.00	0.00
FeO	8.03	8.46	8.63	13.53	13.47	8.11	8.10	8.38	9.41	9.36	8.60	8.36	8.38	8.16	8.85
MnO	0.09	0.11	0.11	0.14	0.13	0.11	0.11	0.11	0.14	0.13	0.09	0.10	0.12	0.11	0.14
NiO	0.39	0.42	0.40	0.38	0.38	0.41	0.39	0.39	0.40	0.37	0.39	0.42	0.39	0.41	0.33
CaO	0.04	0.03	0.02	0.07	0.08	0.03	0.01	0.01	0.02	0.08	0.07	0.02	0.01	0.00	0.01
K ₂ O	0.00	0.00	0.01	0.00	0.00	0.01	0.01	0.01	0.00	0.00	0.01	0.03	0.01	0.01	0.02
TiO ₂	0.04	0.00	0.00	0.00	0.04	0.00	0.01	0.00	0.00	0.06	0.00	0.03	0.00	0.03	0.04
Cr ₂ O ₃	0.00	0.03	0.01	0.02	0.02	0.04	0.00	0.01	0.00	0.03	0.02	0.03	0.00	0.02	0.04
MgO	51.58	49.74	49.46	46.19	45.40	49.97	49.27	49.82	48.88	48.72	49.29	49.65	48.63	49.96	49.75
Na ₂ O	0.01	0.00	0.01	0.02	0.04	0.00	0.00	0.00	0.00	0.01	0.01	0.02	0.01	0.01	0.00
Total:	100.13	99.26	99.75	99.67	99.78	99.88	100.05	99.78	99.97	99.53	100.02	100.01	98.99	99.61	99.92
Si	0.975	0.995	1.005	0.986	1.005	1.004	1.022	1.002	1.012	1.001	0.998	1.003	1.018	0.997	1.008
Al	0.000	0.000	0.000	0.001	0.001	0.000	0.000	0.000	0.000	0.000	0.000	0.000	0.000	0.000	0.000
Fe	0.164	0.174	0.176	0.284	0.282	0.165	0.164	0.171	0.172	0.194	0.192	0.175	0.172	0.172	0.166
Mn	0.002	0.002	0.002	0.003	0.003	0.002	0.002	0.002	0.002	0.003	0.003	0.002	0.002	0.002	0.003
Ni	0.008	0.008	0.008	0.008	0.008	0.008	0.008	0.008	0.008	0.007	0.008	0.008	0.008	0.008	0.007
Ca	0.001	0.001	0.001	0.002	0.002	0.001	0.000	0.000	0.000	0.002	0.001	0.000	0.000	0.000	0.000
K	0.000	0.000	0.000	0.000	0.000	0.000	0.000	0.000	0.000	0.000	0.000	0.001	0.000	0.000	0.000
Ti	0.001	0.000	0.000	0.000	0.001	0.000	0.000	0.000	0.000	0.001	0.000	0.000	0.001	0.001	0.001
Cr	0.000	0.001	0.000	0.000	0.000	0.001	0.000	0.000	0.000	0.001	0.000	0.001	0.000	0.001	0.000
Mg	1.875	1.823	1.803	1.728	1.692	1.814	1.781	1.814	1.792	1.787	1.800	1.781	1.805	1.824	1.821
Na	0.000	0.000	0.000	0.001	0.002	0.000	0.000	0.000	0.000	0.000	0.000	0.001	0.000	0.000	0.000
Cations:	3.025	3.004	2.995	3.014	2.995	2.996	2.978	2.998	2.997	3.002	2.997	2.983	3.003	2.992	3.007
<i>Fayalite</i>	0.08	0.09	0.09	0.14	0.14	0.08	0.08	0.09	0.09	0.10	0.10	0.09	0.09	0.08	0.09
<i>Forsterite</i>	0.92	0.91	0.91	0.86	0.86	0.92	0.92	0.91	0.91	0.90	0.90	0.91	0.91	0.92	0.91

TABELA B01 – Cont. Major element concentration of olivine from all samples. Structural formula calculated on the basis of 4 oxygens. C - core; R - rim; I - intermediately; mega - megacrystals, macro - macrocrysts, micro - microcrysts.

Sample	TR4-1	TR4-2	TR4-2	TR4-2													
Grain/Analysis	12/23	12/24	13/25	13/26	14/27	14/28	15/29	15/30	16/31	16/32	17/33	17/34	18/35	18/36	19/37	19/38	20/39
Location	C	R	C	R	C	R	C	R	C	R	C	R	C	R	C	R	C
Crystal type	mega	mega	mega	mega	micro	micro	macro	macro	micro	macro	micro	macro	micro	macro	macro	mega	mega
SiO ₂	40.72	39.82	40.34	40.42	39.62	39.50	40.81	40.45	40.29	40.53	40.11	39.70	40.17	39.94	41.06	40.53	40.84
Al ₂ O ₃	0.00	0.00	0.00	0.01	0.00	0.01	0.00	0.00	0.02	0.01	0.00	0.01	0.04	0.01	0.01	0.00	0.00
FeO	7.68	11.24	7.96	8.29	12.75	12.98	8.24	8.41	8.48	10.44	12.18	8.96	9.76	7.79	7.71	8.22	
MnO	0.12	0.18	0.09	0.11	0.19	0.20	0.08	0.12	0.11	0.16	0.18	0.12	0.16	0.09	0.11	0.10	
NiO	0.43	0.34	0.37	0.39	0.27	0.28	0.38	0.37	0.36	0.38	0.36	0.34	0.36	0.42	0.42	0.39	
CaO	0.00	0.04	0.03	0.04	0.02	0.03	0.03	0.02	0.01	0.06	0.02	0.08	0.01	0.02	0.00	0.04	0.00
K ₂ O	0.00	0.00	0.02	0.00	0.01	0.02	0.00	0.00	0.02	0.01	0.00	0.01	0.00	0.00	0.00	0.00	0.00
TiO ₂	0.00	0.04	0.02	0.00	0.01	0.00	0.00	0.01	0.04	0.00	0.00	0.03	0.00	0.00	0.02	0.00	0.01
Cr ₂ O ₃	0.01	0.02	0.03	0.03	0.01	0.00	0.02	0.02	0.00	0.03	0.06	0.08	0.00	0.02	0.01	0.00	0.00
MgO	50.46	47.36	50.59	49.71	46.49	46.80	50.07	50.16	50.12	49.80	47.65	46.73	49.41	49.17	51.34	51.91	51.28
Na ₂ O	0.02	0.01	0.02	0.01	0.02	0.01	0.00	0.00	0.00	0.00	0.00	0.00	0.04	0.01	0.01	0.00	0.01
Total:	99.44	99.06	99.48	99.01	99.38	99.83	99.64	99.39	99.38	99.42	98.80	99.39	99.07	99.46	100.74	100.71	100.84
Si	0.996	0.994	0.988	0.996	0.993	0.987	0.998	0.993	0.998	0.995	1.000	0.993	0.992	0.987	0.992	0.980	1.003
Al	0.000	0.000	0.000	0.000	0.000	0.000	0.000	0.000	0.001	0.000	0.000	0.000	0.001	0.000	0.000	0.000	0.000
Fe	0.157	0.235	0.163	0.171	0.267	0.271	0.168	0.169	0.173	0.174	0.218	0.255	0.185	0.202	0.157	0.156	0.164
Mn	0.003	0.004	0.002	0.002	0.004	0.004	0.002	0.002	0.003	0.003	0.004	0.003	0.003	0.003	0.002	0.002	0.003
Ni	0.008	0.007	0.007	0.008	0.005	0.006	0.008	0.007	0.007	0.008	0.007	0.007	0.007	0.007	0.008	0.008	
Ca	0.000	0.001	0.001	0.000	0.001	0.001	0.001	0.001	0.000	0.002	0.000	0.002	0.000	0.001	0.000	0.001	0.001
K	0.000	0.000	0.001	0.000	0.001	0.000	0.000	0.000	0.000	0.000	0.000	0.000	0.000	0.000	0.000	0.000	
Ti	0.000	0.001	0.000	0.000	0.000	0.000	0.000	0.000	0.001	0.000	0.000	0.001	0.000	0.000	0.000	0.000	
Cr	0.000	0.000	0.001	0.001	0.000	0.000	0.000	0.000	0.000	0.000	0.001	0.001	0.002	0.000	0.000	0.000	
Mg	1.840	1.763	1.848	1.825	1.736	1.743	1.825	1.835	1.835	1.823	1.770	1.742	1.819	1.811	1.848	1.872	1.816
Na	0.001	0.001	0.001	0.000	0.001	0.001	0.000	0.000	0.000	0.000	0.002	0.000	0.001	0.000	0.000	0.000	
Cations:	3.004	3.005	3.012	3.004	3.008	3.013	3.002	3.007	3.010	3.005	3.000	3.007	3.008	3.013	3.008	3.020	2.996
<i>Fayalite</i>	0.08	0.12	0.08	0.09	0.13	0.13	0.08	0.08	0.09	0.11	0.13	0.09	0.10	0.08	0.08	0.08	
<i>Forsterite</i>	0.92	0.88	0.92	0.91	0.87	0.87	0.92	0.92	0.91	0.91	0.89	0.87	0.91	0.90	0.92	0.92	

TABLE A B01 – Cont. Major element concentration of olivine from all samples. Structural formula calculated on the basis of 4 oxygens. C - core; R - rim; I - intermediately; mega - megacrystals, macro - macrocrysts, micro - microcrysts.

Sample	TR4-2	TR4-2	TRIV-5	TRIV-5	TRIV-5	TRIV-5	TRIV-5	TRIV-5	TRIV-5	TRIV-5						
Grain/Analysis	21/41	21/42	22/43	22/44	23/45	23/46	24/47	24/48	25/49	25/50	26/51	26/52	27/53	27/54	28/55	28/56
Location	C	R	C	R	C	R	C	R	C	R	C	R	C	R	C	R
Crystal type	macro	macro	macro	macro	micro	micro	micro	micro	mega	mega	mega	mega	mega	mega	mega	mega
SiO ₂	40.03	39.40	41.07	40.57	40.87	41.46	40.85	41.84	40.79	40.41	40.77	41.39	40.80	40.77	40.96	41.64
Al ₂ O ₃	0.01	0.00	0.00	0.01	0.01	0.00	0.00	0.00	0.00	0.00	0.00	0.00	0.00	0.01	0.01	0.00
FeO	11.63	11.11	7.93	7.87	8.32	8.46	8.45	8.35	9.26	8.91	8.88	8.86	11.06	11.20	8.49	8.68
MnO	0.13	0.14	0.10	0.09	0.13	0.09	0.12	0.13	0.09	0.10	0.11	0.18	0.22	0.12	0.09	0.09
NiO	0.40	0.42	0.43	0.40	0.36	0.37	0.43	0.39	0.39	0.38	0.39	0.36	0.31	0.35	0.40	0.36
CaO	0.01	0.01	0.03	0.04	0.00	0.01	0.02	0.08	0.01	0.02	0.01	0.03	0.03	0.03	0.01	0.01
K ₂ O	0.00	0.00	0.00	0.00	0.01	0.00	0.01	0.00	0.02	0.01	0.01	0.00	0.00	0.02	0.01	0.03
TiO ₂	0.03	0.04	0.00	0.01	0.00	0.01	0.01	0.05	0.00	0.00	0.06	0.02	0.02	0.04	0.03	0.03
Cr ₂ O ₃	0.01	0.02	0.01	0.02	0.01	0.02	0.00	0.00	0.02	0.00	0.01	0.02	0.03	0.00	0.05	0.03
MgO	48.47	49.01	51.18	52.00	50.87	49.78	50.93	48.60	49.88	49.86	50.15	49.75	48.32	47.99	50.28	49.26
Na ₂ O	0.00	0.01	0.01	0.02	0.01	0.00	0.00	0.00	0.00	0.01	0.00	0.01	0.00	0.01	0.00	0.00
Total:	100.71	100.14	100.75	101.05	100.54	100.24	100.79	99.42	100.51	99.70	100.38	100.55	100.75	100.64	100.37	100.12
Si	0.975	0.992	0.979	0.991	1.007	0.989	1.022	0.987	0.994	0.991	0.993	1.004	0.999	1.000	0.996	1.013
Al	0.000	0.000	0.000	0.000	0.000	0.000	0.000	0.000	0.000	0.000	0.000	0.000	0.000	0.000	0.000	0.000
Fe	0.230	0.160	0.159	0.169	0.172	0.171	0.171	0.182	0.189	0.183	0.181	0.180	0.226	0.230	0.173	0.177
Mn	0.003	0.002	0.002	0.002	0.003	0.002	0.002	0.003	0.003	0.002	0.002	0.002	0.004	0.005	0.003	0.002
Ni	0.008	0.008	0.008	0.007	0.007	0.008	0.008	0.008	0.008	0.008	0.008	0.008	0.007	0.006	0.007	0.007
Ca	0.000	0.001	0.001	0.000	0.000	0.001	0.002	0.000	0.000	0.001	0.000	0.001	0.001	0.000	0.000	0.000
K	0.000	0.000	0.000	0.000	0.000	0.000	0.000	0.000	0.001	0.000	0.000	0.000	0.000	0.000	0.000	0.001
Ti	0.001	0.000	0.000	0.000	0.000	0.000	0.000	0.001	0.000	0.000	0.001	0.000	0.000	0.001	0.001	0.001
Cr	0.000	0.000	0.000	0.000	0.000	0.000	0.000	0.000	0.006	0.000	0.000	0.000	0.000	0.000	0.001	0.001
Mg	1.807	1.843	1.870	1.839	1.803	1.839	1.770	1.830	1.812	1.824	1.821	1.800	1.764	1.755	1.822	1.786
Na	0.000	0.000	0.001	0.000	0.000	0.000	0.000	0.000	0.000	0.000	0.000	0.001	0.000	0.000	0.000	0.000
Cations:	3.025	3.008	3.021	3.009	2.992	3.011	2.977	3.009	3.006	3.006	3.009	3.001	2.995	3.001	2.999	3.003
<i>Fayalite</i>	0.11	0.08	0.08	0.09	0.09	0.09	0.09	0.09	0.09	0.09	0.09	0.09	0.11	0.12	0.09	0.09
<i>Forsterite</i>	0.89	0.92	0.92	0.91	0.91	0.91	0.91	0.91	0.91	0.91	0.91	0.91	0.91	0.88	0.91	0.91

TABELA B01 – Cont. Major element concentration of olivine from all samples. Structural formula calculated on the basis of 4 oxygens. C - core; R - rim; I - intermediately
 mega - megacrystals, macro - macrocrysts, micro - microcrysts.

TABLEA B01 – Cont. Major element concentration of olivine from all samples. Structural formula calculated on the basis of 4 oxygens. C - core; R - rim; I - intermediated; mega - megacrystals, macro - macrocrysts, micro - microcrysts.

Sample	TR-04B	TR-04B	TR-04B	TR-04B	TR-07	TR-07	TR-07	TR-07	TR-02	TR-04A	TR-04A	TR-04A	TR-04A	TR-04A	TR-04B	
Grain/Analysis	04/08	05/09	05/10	06/11	06/12	07/13	07/14	01/01	02/02	03/04	04/05	05/06	06/07	07/08		
Location	R	C	R	C	R	C	R	C	R	C	C	C	C	C		
Crystal type	macro	macro	macro	macro	macro	macro	macro	macro	macro	macro	macro	macro	macro	macro		
SiO ₂	40.83	41.23	41.14	40.51	40.49	39.91	39.52	40.71	40.96	40.52	40.13	40.48	40.38	40.68		
Al ₂ O ₃	0.01	0.01	0.00	0.00	0.01	0.00	0.00	0.01	0.00	0.02	0.00	0.00	0.00	0.00	0.02	
FeO	8.01	7.61	7.45	7.72	7.79	8.58	8.90	7.65	7.81	9.68	7.66	8.38	9.43	8.72	8.56	
MnO	0.12	0.07	0.12	0.11	0.09	0.07	0.10	0.12	0.10	0.17	0.10	0.13	0.14	0.09	0.13	
NiO	0.03	0.00	0.05	0.03	0.00	0.04	0.00	0.04	0.00	0.03	0.07	0.00	0.02	0.00	0.01	
CaO	0.03	0.01	0.02	0.01	0.02	0.01	0.03	0.01	0.01	0.04	0.00	0.00	0.03	0.01	0.01	
K ₂ O	0.00	0.02	0.01	0.01	0.02	0.00	0.00	0.01	0.00	0.01	0.01	0.01	0.01	0.01	0.00	
TiO ₂	0.01	0.00	0.02	0.01	0.00	0.03	0.00	0.00	0.02	0.02	0.02	0.01	0.00	0.01	0.00	
Cr ₂ O ₃	0.35	0.38	0.40	0.41	0.40	0.37	0.35	0.37	0.35	0.37	0.35	0.37	0.34	0.39	0.39	
MgO	50.56	52.00	51.50	51.10	49.74	49.95	50.30	52.06	50.75	49.14	51.12	50.30	49.36	49.87	50.30	
Na ₂ O	0.01	0.02	0.02	0.00	0.00	0.02	0.00	0.00	0.00	0.00	0.00	0.01	0.00	0.01	0.01	
Total:	99.95	101.32	100.71	99.90	98.56	99.59	99.61	99.76	99.79	100.40	99.89	99.34	99.87	99.47	100.12	
Si	0.988	0.992	0.987	0.998	0.992	0.981	0.966	0.992	0.999	0.987	0.986	0.993	0.991	0.991	1.003	
Al	0.000	0.000	0.000	0.000	0.000	0.000	0.000	0.000	0.000	0.001	0.000	0.000	0.000	0.000	0.000	
Fe	0.153	0.150	0.157	0.161	0.176	0.183	0.156	0.159	0.197	0.156	0.172	0.193	0.179	0.174	0.210	
Mn	0.001	0.002	0.002	0.001	0.002	0.001	0.003	0.002	0.004	0.002	0.003	0.003	0.002	0.003	0.003	
Ni	0.000	0.001	0.001	0.000	0.001	0.000	0.001	0.000	0.001	0.001	0.000	0.000	0.000	0.000	0.000	
Ca	0.000	0.000	0.000	0.001	0.000	0.001	0.000	0.000	0.001	0.000	0.001	0.001	0.000	0.001	0.001	
K	0.001	0.000	0.000	0.001	0.000	0.000	0.000	0.000	0.000	0.000	0.000	0.000	0.000	0.000	0.000	
Ti	0.000	0.000	0.000	0.000	0.001	0.000	0.000	0.000	0.000	0.000	0.000	0.000	0.000	0.000	0.000	
Cr	0.007	0.007	0.008	0.008	0.008	0.007	0.007	0.007	0.007	0.007	0.007	0.008	0.007	0.008	0.007	
Mg	1.858	1.851	1.855	1.828	1.824	1.842	1.897	1.843	1.788	1.855	1.842	1.805	1.825	1.827	1.768	
Na	0.001	0.001	0.000	0.000	0.001	0.000	0.000	0.000	0.000	0.000	0.000	0.001	0.000	0.001	0.001	
Cations:	3.009	3.010	2.998	3.004	3.016	3.030	3.004	2.997	3.009	3.011	3.003	3.005	3.005	2.994		
<i>Fayalite</i>	0.08	0.08	0.08	0.09	0.09	0.08	0.08	0.08	0.10	0.08	0.09	0.10	0.09	0.09	0.11	
<i>Forsterite</i>	0.92	0.92	0.92	0.92	0.91	0.91	0.92	0.92	0.90	0.92	0.91	0.90	0.91	0.91	0.89	

TABELA B01 – Cont. Major element concentration of olivine from all samples. Structural formula calculated on the basis of 4 oxygens. C - core; R - rim; I - intermediately; mega - megacrystals, macro - macrocrysts, micro - microcrysts.

Sample	TR-04B	TR-04B	TR-04B	TR-04B	TR-07	TR-07	TR-07	TR-07	TR-07	TR-07	TR-07	TR-07
Grain/Analysis	07/09	08/10	09/11	10/12	11/13	11/14	12/15	12/16	13/17	14/18		
Location	R	C	C	C	R	C	R	C	R	C		
Crystal type	micro	micro	micro	micro	micro	micro	micro	micro	micro	micro	micro	micro
SiO ₂	41.08	40.83	40.18	39.02	39.44	39.96	40.13	41.34	39.39	39.47		
Al ₂ O ₃	0.00	0.01	0.02	0.00	0.01	0.03	0.01	0.00	0.01	0.00	0.00	0.00
FeO	10.28	7.85	12.29	8.35	8.71	10.55	10.55	10.05	9.15	9.32		
MnO	0.16	0.09	0.15	0.09	0.09	0.20	0.16	0.15	0.18	0.16		
NiO	0.01	0.00	0.09	0.00	0.00	0.03	0.01	0.04	0.06	0.06		
CaO	0.05	0.01	0.12	0.03	0.03	0.09	0.08	0.03	0.01	0.03		
K ₂ O	0.01	0.00	0.02	0.00	0.00	0.01	0.00	0.00	0.00	0.00	0.00	0.00
TiO ₂	0.02	0.02	0.07	0.04	0.00	0.00	0.03	0.05	0.05	0.03		
Cr ₂ O ₃	0.37	0.45	0.36	0.41	0.38	0.32	0.30	0.29	0.33	0.37		
MgO	48.58	51.65	46.68	50.20	49.80	46.25	48.51	46.75	49.25	49.21		
Na ₂ O	0.02	0.00	0.04	0.00	0.02	0.01	0.00	0.00	0.02	0.02		
Total:	100.56	100.91	100.02	98.14	98.46	97.45	99.77	98.70	98.43	98.67		
Si	0.985	0.997	0.972	0.980	1.009	0.991	1.025	0.981	0.982	0.996		
Al	0.000	0.001	0.000	0.000	0.001	0.000	0.000	0.000	0.000	0.000	0.000	0.000
Fe	0.158	0.255	0.174	0.181	0.223	0.218	0.208	0.191	0.194	0.253		
Mn	0.002	0.003	0.002	0.002	0.004	0.003	0.003	0.004	0.003	0.003		
Ni	0.000	0.002	0.000	0.000	0.001	0.000	0.001	0.001	0.001	0.001	0.001	0.001
Ca	0.000	0.003	0.001	0.001	0.002	0.002	0.002	0.001	0.000	0.002		
K	0.000	0.000	0.000	0.000	0.000	0.000	0.000	0.000	0.000	0.000	0.000	0.000
Ti	0.000	0.001	0.001	0.000	0.000	0.000	0.001	0.001	0.001	0.001	0.000	0.000
Cr	0.009	0.007	0.008	0.007	0.006	0.006	0.006	0.006	0.006	0.007	0.006	
Mg	1.857	1.727	1.865	1.845	1.741	1.785	1.727	1.829	1.825	1.739		
Na	0.000	0.002	0.000	0.001	0.000	0.000	0.000	0.000	0.001	0.001	0.001	0.001
Cations:	3.011	2.999	3.023	3.017	2.988	3.006	2.972	3.015	3.015	3.001		
<i>Fayalite</i>	0.08	0.13	0.09	0.09	0.11	0.11	0.11	0.09	0.10	0.13		
<i>Forsterite</i>	0.92	0.87	0.91	0.91	0.89	0.89	0.89	0.91	0.90	0.87		

TABLE B02 - Major element concentration of monticellite from all samples. Structural formula calculated on the basis of 4 oxygens. C - core; R - rim; I - intermediately.

Sample	LM-2	LM-2	LM-2	LM-2	LM-2	LM-2											
Grain/Analysis	01/01	02/02	02/03	03/04	04/05	05/06	05/07	06/08	07/09	08/11	09/12	10/13	11/14	12/15	13/16	14/17	15/18
Location	C	C	R	C	C	C	R	C	C	C	C	C	C	C	C	C	C
SiO ₂	36.63	36.44	37.02	36.13	36.36	35.76	36.41	35.85	36.63	36.92	36.50	37.40	38.19	37.93	37.59	37.22	36.67
Al ₂ O ₃	0.01	0.03	0.01	0.02	0.02	0.00	0.01	0.01	0.03	0.02	0.07	0.02	0.06	0.11	0.04	0.11	0.03
FeO	8.86	8.72	6.29	10.82	9.21	11.71	9.36	10.83	8.77	6.49	8.97	3.01	3.74	2.95	3.88	2.97	4.44
MnO	0.38	0.38	0.23	0.22	0.40	0.25	0.36	0.22	0.33	0.32	0.39	0.54	0.35	0.48	0.27	0.26	0.32
NiO	0.00	0.03	0.02	0.03	0.03	0.03	0.01	0.04	0.03	0.03	0.02	0.04	0.04	0.04	0.04	0.06	0.02
CaO	32.55	32.71	34.68	33.75	32.27	33.76	32.66	33.92	32.58	33.74	32.66	34.84	34.79	34.39	34.54	34.31	34.44
K ₂ O	0.04	0.02	0.05	0.05	0.00	0.02	0.04	0.02	0.05	0.00	0.02	0.18	0.04	0.09	0.03	0.13	0.04
TiO ₂	0.11	0.10	0.06	0.09	0.12	0.04	0.06	0.15	0.04	0.03	0.12	0.14	0.06	0.07	0.15	0.26	0.14
Cr ₂ O ₃	0.00	0.01	0.00	0.04	0.04	0.00	0.03	0.04	0.02	0.00	0.00	0.04	0.01	0.03	0.03	0.04	0.05
MgO	20.90	21.14	21.45	18.48	20.90	17.87	20.98	18.23	21.36	21.39	21.20	24.18	23.15	23.69	24.94	23.70	24.36
Na ₂ O	0.08	0.09	0.05	0.16	0.12	0.12	0.09	0.10	0.06	0.03	0.08	0.02	0.06	0.04	0.06	0.02	0.03
Total:	99.55	99.66	99.85	99.78	99.47	99.54	99.99	99.42	99.85	99.04	99.96	100.26	100.61	99.92	100.78	99.81	100.74
Si	0.995	0.989	0.995	0.992	0.990	0.990	0.988	0.990	0.991	0.999	0.999	0.988	0.987	1.005	1.002	0.985	0.993
Al	0.000	0.001	0.000	0.001	0.001	0.000	0.000	0.000	0.000	0.001	0.001	0.002	0.001	0.002	0.004	0.001	0.001
Fe	0.201	0.198	0.141	0.249	0.210	0.271	0.212	0.250	0.198	0.147	0.203	0.066	0.082	0.070	0.065	0.086	0.098
Mn	0.009	0.009	0.005	0.005	0.009	0.006	0.008	0.005	0.007	0.007	0.009	0.012	0.008	0.011	0.006	0.007	0.009
Ni	0.000	0.001	0.001	0.001	0.001	0.001	0.000	0.001	0.001	0.001	0.001	0.001	0.001	0.001	0.001	0.001	0.001
Ca	0.947	0.951	0.999	0.993	0.941	1.001	0.949	1.003	0.945	0.979	0.947	0.985	0.981	0.973	0.970	0.976	0.973
K	0.001	0.001	0.002	0.000	0.001	0.000	0.001	0.001	0.001	0.002	0.000	0.001	0.001	0.006	0.001	0.003	0.001
Ti	0.002	0.002	0.001	0.002	0.001	0.001	0.003	0.001	0.001	0.003	0.003	0.003	0.001	0.001	0.005	0.003	0.002
Cr	0.000	0.000	0.000	0.001	0.001	0.000	0.001	0.001	0.000	0.000	0.000	0.000	0.000	0.001	0.001	0.001	0.001
Mg	0.846	0.855	0.859	0.757	0.848	0.737	0.848	0.750	0.862	0.863	0.856	0.951	0.908	0.933	0.974	0.967	0.924
Na	0.004	0.005	0.003	0.009	0.006	0.006	0.005	0.005	0.003	0.002	0.004	0.001	0.003	0.002	0.003	0.001	0.001
Cations:	3.006	3.011	3.005	3.010	3.010	3.013	3.013	3.010	3.010	3.011	3.010	2.997	2.997	3.013	3.006	3.022	3.005
Mg#	81.20	85.87	75.27	80.17	73.11	79.97	74.99	81.27	85.45	80.81	93.47	91.69	93.06	93.77	91.58	93.60	90.42
XFe _{liq}	0.12	0.12	0.12	0.12	0.12	0.12	0.12	0.12	0.12	0.12	0.12	0.12	0.12	0.12	0.12	0.12	0.12
XFe _{Mtc}	0.06	0.06	0.08	0.06	0.08	0.06	0.05	0.06	0.05	0.06	0.05	0.06	0.05	0.02	0.03	0.02	0.03
ΔNNO	-1.54	-1.42	0.03	-2.83	-1.74	-3.49	-1.81	-2.82	-1.45	-0.12	-1.57	2.41	1.73	2.24	1.66	2.47	1.24

TABLE A B02 – Cont. Major element concentration of monticellite from all samples. Structural formula calculated on the basis of 4 oxygens. C - core; R - rim; I – intermediately.

Sample	LM-2	LM-2	LM-2	LM-2	LM-2	LM-2	LM-2	LM-2	LM-2	LM-2	LM-2	LM-2	LM-2	LM-2	LM-2	LM-2
Grain/Analysis	16/19	17/20	17/21	18/22	19/23	19/24	20/25	21/26	21/27	22/28	23/30	24/31	25/32	25/33	26/34	27/35
Location	C	C	R	C	C	R	C	C	R	C	C	R	C	C	R	C
SiO ₂	37.15	36.18	37.20	37.96	36.63	37.30	36.78	36.52	37.94	36.97	37.33	37.81	36.98	36.25	37.19	35.16
Al ₂ O ₃	0.09	0.00	0.00	0.12	0.03	0.06	0.10	0.02	0.03	0.01	0.03	0.01	0.02	0.02	0.03	0.12
FeO	3.27	12.37	6.08	5.19	9.75	3.75	7.45	9.88	5.35	9.49	6.85	3.95	9.77	10.09	4.49	7.85
MnO	0.25	0.72	0.90	0.45	0.66	0.26	0.49	0.61	0.36	0.61	0.46	0.23	0.73	0.60	0.31	0.57
NiO	0.06	0.01	0.03	0.04	0.01	0.00	0.04	0.04	0.01	0.02	0.04	0.06	0.00	0.02	0.04	0.04
CaO	34.55	32.93	34.48	32.82	33.03	35.05	32.92	32.10	33.59	32.60	33.39	34.75	32.10	33.03	34.82	33.87
K ₂ O	0.05	0.00	0.02	0.05	0.02	0.06	0.03	0.02	0.00	0.03	0.05	0.03	0.04	0.05	0.04	0.07
TiO ₂	0.16	0.03	0.14	0.08	0.06	0.04	0.12	0.06	0.00	0.11	0.08	0.09	0.04	0.07	0.06	0.14
Cr ₂ O ₃	0.06	0.05	0.00	0.00	0.04	0.04	0.00	0.06	0.02	0.03	0.00	0.01	0.01	0.00	0.05	0.03
MgO	24.50	17.82	21.66	22.17	19.90	23.87	22.15	20.46	23.05	20.59	21.84	23.92	20.13	20.38	23.20	20.73
Na ₂ O	0.08	0.04	0.03	0.03	0.06	0.05	0.03	0.05	0.03	0.04	0.05	0.03	0.04	0.01	0.04	0.04
Total:	100.21	100.16	100.53	98.90	100.20	100.49	100.11	99.83	100.38	100.50	100.13	99.84	100.55	100.19	98.63	100.72
Si	0.981	0.996	0.994	1.017	0.995	0.985	0.988	0.994	1.004	0.997	1.000	0.993	1.004	0.983	0.988	0.969
Al	0.003	0.000	0.000	0.004	0.001	0.002	0.003	0.001	0.001	0.000	0.001	0.000	0.001	0.001	0.004	0.000
Fe	0.072	0.285	0.136	0.116	0.221	0.083	0.167	0.225	0.118	0.214	0.153	0.087	0.222	0.229	0.100	0.181
Mn	0.006	0.017	0.020	0.010	0.015	0.006	0.011	0.014	0.008	0.014	0.010	0.005	0.017	0.014	0.007	0.013
Ni	0.001	0.000	0.001	0.001	0.000	0.000	0.001	0.001	0.000	0.000	0.001	0.001	0.000	0.001	0.001	0.001
Ca	0.978	0.971	0.987	0.942	0.961	0.992	0.947	0.936	0.952	0.942	0.958	0.978	0.934	0.960	0.992	1.000
K	0.002	0.000	0.001	0.002	0.001	0.002	0.001	0.001	0.000	0.002	0.001	0.001	0.002	0.001	0.001	0.003
Ti	0.003	0.001	0.003	0.002	0.001	0.001	0.002	0.001	0.000	0.002	0.002	0.001	0.001	0.001	0.003	0.003
Cr	0.001	0.001	0.000	0.000	0.001	0.000	0.001	0.000	0.001	0.001	0.000	0.000	0.000	0.000	0.001	0.001
Mg	0.965	0.731	0.862	0.886	0.806	0.940	0.887	0.830	0.909	0.828	0.872	0.937	0.815	0.824	0.919	0.852
Na	0.004	0.002	0.001	0.003	0.002	0.002	0.003	0.001	0.002	0.003	0.001	0.002	0.002	0.000	0.002	0.005
Cations:	3.016	3.004	3.005	2.981	3.015	3.010	3.006	2.996	3.002	3.001	3.006	2.996	3.017	3.010	3.028	3.003
Mg#	93.03	71.96	86.39	88.39	78.43	91.90	84.12	78.68	88.47	79.45	85.03	91.52	78.59	78.25	90.20	82.47
XFe _{liq}	0.12	0.12	0.12	0.12	0.12	0.12	0.12	0.12	0.12	0.12	0.12	0.12	0.12	0.12	0.12	0.12
XFe _{mtc}	0.02	0.09	0.04	0.07	0.03	0.05	0.07	0.04	0.07	0.05	0.03	0.07	0.07	0.03	0.05	0.07
ΔNN _O	2.19	4.23	0.13	0.63	-2.12	1.79	-0.67	-2.20	0.59	-1.97	-0.35	-1.61	-2.19	-0.84	-2.02	

TABELA B02 – Cont. Major element concentration of monticellite from all samples. Structural formula calculated on the basis of 4 oxygens. C - core; R - rim; I – intermediately.

Sample	LM3-1	LM3-1	LM3-1	LM3-1	LM3-1	LM3-1	LM3-1	LM3-1	LM3-1	LM3-1	LM3-1	LM3-1	LM3-1	LM3-1	LM3-1	LM3-1
Grain/Analysis	27/36	28/37	29/38	30/39	31/40	32/41	32/42	33/43	34/44	35/45	36/46	37/47	37/48	38/49	38/50	39/51
Location	R	C	R	C	C	R	C	C	C	C	R	C	R	C	R	C
SiO ₂	36.57	37.40	37.14	37.78	37.29	33.92	37.94	38.01	36.28	36.60	37.66	36.52	35.83	36.38	37.83	36.53
Al ₂ O ₃	0.03	0.03	0.06	0.13	0.04	0.01	0.13	0.02	1.06	0.01	0.01	0.02	0.11	0.02	0.02	0.03
FeO	6.72	7.53	3.24	4.35	4.12	7.23	2.97	2.99	3.98	10.09	4.25	9.38	3.84	8.04	4.12	9.02
MnO	0.38	0.56	0.35	0.38	0.56	0.50	0.22	0.21	0.40	0.44	0.28	0.36	0.28	0.58	0.23	0.58
NiO	0.02	0.03	0.04	0.03	0.01	0.02	0.04	0.06	0.02	0.02	0.04	0.03	0.05	0.04	0.05	0.01
CaO	34.11	33.93	34.87	34.14	35.78	31.71	35.45	34.92	33.74	32.53	34.78	32.79	34.97	33.64	34.97	33.07
K ₂ O	0.02	0.03	0.04	0.13	0.13	1.91	0.14	0.08	0.05	0.01	0.16	0.04	0.10	0.08	0.02	0.00
TiO ₂	0.07	0.06	0.10	0.10	0.07	0.13	0.13	0.07	0.38	0.06	0.01	0.09	1.65	0.67	0.09	0.10
Cr ₂ O ₃	0.02	0.00	0.00	0.00	0.01	0.07	0.09	0.04	0.08	0.03	0.01	0.00	0.00	0.02	0.00	0.00
MgO	22.59	21.53	24.47	23.50	21.65	19.94	23.83	24.81	24.23	20.83	22.76	20.95	22.19	21.26	23.91	21.18
Na ₂ O	0.08	0.02	0.05	0.02	0.20	1.17	0.09	0.03	0.09	0.12	0.07	0.10	0.06	0.08	0.02	0.06
Total:	100.62	101.12	100.35	100.57	99.86	96.59	101.02	101.24	100.31	100.74	100.01	100.30	99.08	100.81	101.29	100.59
Si	0.978	0.996	0.981	0.997	0.997	0.965	0.993	0.991	0.960	0.988	1.001	0.988	0.965	0.977	0.991	0.985
Al	0.001	0.001	0.002	0.004	0.001	0.000	0.004	0.001	0.033	0.000	0.000	0.001	0.003	0.001	0.001	0.001
Fe	0.150	0.168	0.072	0.096	0.092	0.172	0.065	0.065	0.088	0.228	0.094	0.212	0.087	0.181	0.090	0.203
Mn	0.009	0.013	0.008	0.009	0.013	0.012	0.005	0.005	0.009	0.010	0.006	0.008	0.006	0.013	0.005	0.013
Ni	0.001	0.001	0.001	0.001	0.000	0.000	0.001	0.001	0.000	0.001	0.001	0.001	0.001	0.001	0.001	0.000
Ca	0.977	0.968	0.987	0.965	1.025	0.966	0.994	0.975	0.957	0.941	0.990	0.950	1.009	0.968	0.982	0.955
K	0.001	0.001	0.001	0.005	0.004	0.069	0.005	0.003	0.002	0.000	0.005	0.002	0.003	0.003	0.001	0.000
Ti	0.001	0.001	0.002	0.002	0.001	0.003	0.002	0.001	0.008	0.001	0.000	0.002	0.033	0.014	0.002	0.002
Cr	0.000	0.000	0.000	0.000	0.000	0.000	0.002	0.002	0.001	0.002	0.001	0.000	0.000	0.000	0.000	0.000
Mg	0.900	0.855	0.963	0.924	0.863	0.845	0.930	0.964	0.956	0.838	0.901	0.845	0.891	0.851	0.934	0.851
Na	0.004	0.001	0.002	0.001	0.010	0.064	0.005	0.002	0.005	0.006	0.003	0.005	0.003	0.004	0.001	0.003
Cations:	3.022	3.003	3.018	3.002	3.008	3.006	3.009	3.018	3.014	3.003	3.013	3.003	3.012	3.008	3.014	3.014
Mg#	85.69	83.59	93.08	90.59	90.35	83.09	93.46	93.66	91.56	78.62	90.51	79.92	91.15	82.49	91.18	80.71
XFeliq	0.12	0.12	0.12	0.12	0.12	0.12	0.12	0.12	0.12	0.12	0.12	0.12	0.12	0.12	0.12	0.12
XFeMtc	0.05	0.05	0.02	0.03	0.05	0.02	0.03	0.07	0.03	0.07	0.03	0.07	0.03	0.06	0.03	0.06
ΔANNO	-0.18	-0.74	2.22	1.28	1.45	-0.58	2.42	1.59	-2.29	1.36	-1.83	1.67	-1.02	-1.49	-1.59	

TABELA B02 – Cont. Major element concentration of monticellite from all samples. Structural formula calculated on the basis of 4 oxygens. C - core; R - rim; I – intermediately.

Sample	LM3-1	LM3-1	LM3-1	LM3-1	LM3-1	LM3-1	LM3-1	LM3-1	LM3-1	LM3-1	LM3-1	LM3-1	LM3-1	LM3-1	LM3-2	LM3-2
Grain/Analysis	40/52	41/53	42/54	42/55	42/56	43/57	44/58	45/59	46/60	46/61	47/62	47/63	48/64	49/65	50/66	51/67
Location	C	C	C	C	C	R	C	C	R	R	C	C	C	C	C	C
SiO ₂	37.11	36.31	37.89	36.31	36.69	36.27	36.72	36.62	36.29	37.68	32.73	36.05	35.19	36.54	37.25	37.41
Al ₂ O ₃	0.01	0.07	0.00	0.03	0.17	0.02	0.21	0.03	0.02	0.06	0.00	0.03	1.69	0.01	0.01	0.01
FeO	6.35	10.23	4.24	11.31	3.77	10.54	7.34	7.58	9.91	5.08	9.25	6.88	5.24	7.76	5.46	3.91
MnO	0.39	0.64	0.29	0.63	0.22	0.70	0.54	0.49	0.71	0.39	0.59	0.45	0.21	0.52	0.39	0.29
NiO	0.03	0.02	0.00	0.01	0.05	0.03	0.03	0.01	0.00	0.05	0.00	0.03	0.03	0.02	0.03	0.01
CaO	34.69	32.91	35.18	32.19	33.73	32.44	33.18	33.61	32.64	34.15	29.64	32.12	31.60	33.12	33.66	33.62
K ₂ O	0.04	0.04	0.08	0.03	0.14	0.02	0.02	0.05	0.00	0.01	2.90	0.04	1.42	0.07	0.03	0.06
TiO ₂	0.02	0.07	0.01	0.04	0.22	0.10	0.07	0.08	0.10	0.15	0.12	0.14	0.61	0.06	0.03	0.00
Cr ₂ O ₃	0.01	0.00	0.00	0.01	0.04	0.02	0.00	0.03	0.00	0.04	0.00	0.02	0.16	0.01	0.00	0.00
MgO	22.12	19.77	23.16	19.35	25.14	20.27	21.57	22.08	20.07	23.10	19.33	22.02	23.76	21.54	22.58	23.69
Na ₂ O	0.00	0.08	0.01	0.04	0.06	0.05	0.04	0.05	0.06	0.04	1.48	0.05	0.10	0.04	0.03	0.01
Total:	100.77	100.14	100.85	99.94	100.23	100.45	99.72	100.62	99.80	100.76	96.05	97.83	100.03	99.69	99.48	99.01
Si	0.989	0.989	0.998	0.994	0.971	0.986	0.991	0.982	0.990	0.995	0.951	0.989	0.943	0.998	0.999	0.999
Al	0.000	0.002	0.000	0.001	0.005	0.001	0.007	0.001	0.001	0.002	0.000	0.001	0.053	0.000	0.000	0.000
Fe	0.141	0.233	0.093	0.259	0.083	0.240	0.166	0.170	0.226	0.112	0.225	0.158	0.117	0.176	0.122	0.087
Mn	0.009	0.015	0.006	0.015	0.005	0.016	0.012	0.011	0.016	0.009	0.015	0.010	0.005	0.012	0.009	0.006
Ni	0.001	0.000	0.000	0.000	0.001	0.001	0.001	0.000	0.000	0.001	0.000	0.001	0.001	0.001	0.000	0.000
Ca	0.990	0.961	0.993	0.944	0.956	0.944	0.959	0.965	0.954	0.966	0.922	0.944	0.907	0.960	0.966	0.962
K	0.001	0.001	0.003	0.001	0.005	0.001	0.001	0.002	0.000	0.000	0.107	0.001	0.049	0.002	0.001	0.002
Ti	0.000	0.001	0.000	0.001	0.004	0.002	0.001	0.002	0.003	0.003	0.003	0.003	0.012	0.001	0.001	0.000
Cr	0.000	0.000	0.000	0.000	0.001	0.000	0.000	0.001	0.001	0.000	0.000	0.000	0.003	0.000	0.000	0.000
Mg	0.879	0.803	0.909	0.790	0.991	0.821	0.867	0.882	0.816	0.910	0.837	0.900	0.949	0.869	0.902	0.943
Na	0.000	0.004	0.001	0.002	0.003	0.002	0.003	0.002	0.003	0.002	0.083	0.003	0.005	0.002	0.001	0.001
Cations:	3.011	3.011	3.003	3.006	3.026	3.013	3.006	3.018	3.009	3.002	3.142	3.010	3.044	3.012	3.002	3.002
Mg#	86.12	77.49	90.68	75.30	92.24	77.41	83.96	83.84	78.30	89.01	78.83	85.08	88.99	83.18	88.05	91.52
XFe _{liq}	0.12	0.12	0.12	0.12	0.12	0.12	0.12	0.12	0.12	0.12	0.12	0.12	0.12	0.12	0.12	0.12
XFe _{Mc}	0.04	0.07	0.03	0.08	0.03	0.07	0.05	0.07	0.04	0.06	0.05	0.04	0.05	0.04	0.03	0.03
ΔNNO	0.01	-2.42	1.38	-3.24	1.79	-2.60	-0.62	-0.71	-2.20	0.78	-1.81	-0.33	0.65	-0.85	0.53	1.63

TABELLA B02 – Cont. Major element concentration of monticellite from all samples. Structural formula calculated on the basis of 4 oxygens. C - core; R - rim; I – intermediately.

Sample	LM3-2																
Grain/Analysis	52/68	53/69	54/70	54/71	55/72	56/73	57/74	57/75	58/76	58/77	59/78	60/79	61/80	61/81	62/82	63/83	63/84
Location	C	C	C	R	C	C	R	C	C	R	C	C	R	C	C	R	
SiO ₂	37.49	37.79	37.58	36.86	36.27	37.29	37.30	38.42	36.83	36.52	37.20	36.61	36.87	37.52	37.79	37.25	
Al ₂ O ₃	0.01	0.04	0.02	0.01	1.11	0.70	0.02	0.24	0.01	0.07	0.03	0.01	0.04	0.12	0.07	0.01	
FeO	4.00	3.66	5.91	7.68	6.54	8.99	7.53	4.58	8.89	6.99	5.73	9.40	8.99	3.23	3.04	6.85	
MnO	0.31	0.58	0.42	0.50	0.29	0.28	0.49	0.23	0.51	0.42	0.40	0.36	0.61	0.21	0.35	0.48	
NiO	0.03	0.05	0.01	0.01	0.03	0.03	0.05	0.03	0.02	0.03	0.03	0.00	0.01	0.01	0.03	0.04	
CaO	34.47	33.50	33.06	32.17	18.89	18.61	32.54	28.34	31.97	32.63	32.82	31.72	31.89	33.91	33.31	32.70	
K ₂ O	0.04	0.03	0.04	0.01	0.07	0.31	0.02	0.07	0.02	0.05	0.05	0.01	0.02	0.16	0.03	0.03	
TiO ₂	0.00	0.17	0.06	0.08	0.42	0.27	0.07	0.18	0.13	0.22	0.03	0.07	0.04	0.11	0.21	0.03	
Cr ₂ O ₃	0.03	0.06	0.00	0.06	0.05	0.11	0.02	0.03	0.04	0.01	0.04	0.00	0.00	0.07	0.00	0.00	
MgO	23.49	23.91	22.54	21.74	25.02	23.83	21.62	23.70	21.07	22.14	22.54	20.98	21.24	24.45	24.34	22.40	
Na ₂ O	0.00	0.05	0.03	0.06	0.03	0.02	0.06	0.03	0.07	0.04	0.05	0.09	0.03	0.08	0.04	0.02	
Total:	99.87	99.83	99.68	99.18	88.70	90.47	99.71	95.86	99.56	99.10	98.90	99.26	99.73	99.31	99.27	99.81	
Si	0.995	1.000	1.004	0.998	1.047	1.067	1.004	1.043	0.998	0.989	1.002	0.997	0.998	0.992	1.001	0.999	
Al	0.000	0.001	0.001	0.000	0.038	0.024	0.001	0.008	0.000	0.002	0.001	0.000	0.001	0.004	0.002	0.000	
Fe	0.089	0.081	0.132	0.174	0.158	0.215	0.169	0.104	0.202	0.158	0.129	0.214	0.203	0.071	0.067	0.154	
Mn	0.007	0.013	0.009	0.011	0.007	0.011	0.005	0.012	0.010	0.009	0.014	0.005	0.008	0.011	0.007	0.007	
Ni	0.001	0.001	0.000	0.000	0.001	0.001	0.001	0.001	0.001	0.001	0.001	0.000	0.000	0.001	0.001	0.001	
Ca	0.981	0.950	0.947	0.933	0.584	0.570	0.938	0.824	0.929	0.946	0.947	0.925	0.925	0.961	0.945	0.939	
K	0.001	0.001	0.001	0.000	0.003	0.011	0.001	0.003	0.001	0.002	0.000	0.001	0.005	0.001	0.001	0.000	
Ti	0.000	0.003	0.001	0.002	0.009	0.006	0.001	0.004	0.003	0.004	0.001	0.001	0.001	0.002	0.004	0.001	
Cr	0.001	0.001	0.000	0.001	0.001	0.003	0.000	0.001	0.001	0.000	0.001	0.000	0.000	0.001	0.000	0.000	
Mg	0.930	0.943	0.898	0.878	1.077	1.016	0.867	0.959	0.851	0.894	0.905	0.852	0.857	0.964	0.961	0.895	
Na	0.000	0.003	0.002	0.003	0.001	0.002	0.003	0.001	0.004	0.002	0.003	0.005	0.002	0.004	0.002	0.000	
Cations:	3.005	2.997	2.996	3.001	2.926	2.921	2.996	2.952	3.001	3.007	2.999	3.004	3.002	3.008	2.994	3.002	
Mg#	91.28	92.09	87.17	83.45	87.21	82.53	83.65	90.21	80.85	84.95	87.51	79.91	80.80	93.10	93.45	85.35	
XFeLi _q	0.12																
XFeMtc	0.03	0.03	0.04	0.05	0.07	0.05	0.03	0.06	0.05	0.04	0.07	0.06	0.02	0.02	0.05	0.03	
ΔNNO	1.57	1.80	0.22	-0.84	-0.52	-2.24	-0.78	0.95	-1.59	-0.40	-1.89	-1.64	2.20	-0.34	1.44		

TABELA B02 – Cont. Major element concentration of monticellite from all samples. Structural formula calculated on the basis of 4 oxygens. C - core; R - rim; I - intermediate.

Sample	LM3-2	LM3-2	LM3-2	LM3-2	LM3-2	LM3-2	LM3-2
Grain/Analysis	64/85	65/86	65/87	66/88	67/89	68/90	
Location	C	C	R	C	C	C	
SiO ₂	36.35	37.16	36.91	36.94	37.08	37.10	
Al ₂ O ₃	0.07	0.01	0.00	0.07	0.02	0.05	
FeO	6.55	9.68	6.99	3.67	5.98	6.39	
MnO	0.45	0.62	0.49	0.24	0.43	0.45	
NiO	0.05	0.01	0.04	0.02	0.03	0.05	
CaO	31.35	31.82	32.47	33.52	33.31	32.77	
K ₂ O	0.02	0.06	0.03	0.05	0.01	0.02	
TiO ₂	0.07	0.02	0.07	0.21	0.05	0.14	
Cr ₂ O ₃	0.07	0.00	0.01	0.02	0.03	0.01	
MgO	23.94	20.44	22.60	24.38	22.43	22.72	
Na ₂ O	0.03	0.07	0.04	0.08	0.03	0.04	
Total:	98.95	99.89	99.64	99.20	99.40	99.76	
Si	0.981	1.007	0.992	0.985	0.996	0.994	
Al	0.002	0.000	0.000	0.002	0.000	0.001	
Fe	0.148	0.219	0.157	0.082	0.134	0.143	
Mn	0.010	0.014	0.011	0.005	0.010	0.010	
Ni	0.001	0.000	0.001	0.000	0.001	0.001	
Ca	0.906	0.923	0.935	0.958	0.959	0.941	
K	0.001	0.002	0.001	0.002	0.000	0.001	
Ti	0.001	0.000	0.001	0.004	0.001	0.003	
Cr	0.001	0.000	0.000	0.001	0.001	0.000	
Mg	0.963	0.825	0.906	0.969	0.899	0.907	
Na	0.001	0.004	0.002	0.004	0.001	0.002	
Cations:							
Mg#	3.017	2.996	3.008	3.013	3.003	3.004	
XFe _{liq}	0.12	0.12	0.12	0.12	0.12	0.12	
XFe _{mfc}	0.05	0.07	0.05	0.03	0.04	0.04	
ΔNNO	-0.10	-2.14	-0.40	1.84	0.21	-0.05	

ABELA B03 – Major element compositions and endmembers for perovskite from all samples. Structural formula calculated on the basis of 3 oxygens. C - core; R - rim; I – intermediated.

Sample Grain/Analysis Location	LM-2 01/01	LM-2 01/02	LM-2 02/03	LM-2 02/04	LM-2 03/05	LM-2 03/06	LM-2 04/07	LM-2 04/08	LM-2 05/09	LM-2 05/10	LM-2 06/11	LM-2 06/12
	R	C	C	R	C	R	C	R	C	R	C	R
SiO ₂	0.00	0.00	0.00	0.00	0.00	0.00	0.00	0.00	0.00	0.00	0.00	0.00
Fe ₂ O ₃	2.07	1.97	2.05	2.10	1.93	1.93	1.46	1.33	1.82	1.81	1.49	1.76
La ₂ O ₃	1.21	1.05	0.93	0.90	1.24	1.20	1.49	1.34	1.59	1.51	1.27	1.43
Sm ₂ O ₃	0.16	0.13	0.11	0.10	0.16	0.16	0.24	0.18	0.21	0.21	0.18	0.21
Pr ₂ O ₃	0.37	0.31	0.24	0.24	0.40	0.39	0.59	0.39	0.51	0.47	0.39	0.47
CaO	35.99	36.91	37.84	37.95	35.87	36.14	33.14	35.43	34.19	34.52	35.34	32.72
Nb ₂ O ₅	0.44	0.35	0.42	0.45	0.45	0.42	1.21	1.06	1.28	1.15	1.12	1.32
SrO	0.41	0.43	0.49	0.46	0.41	0.43	0.35	0.38	0.39	0.37	0.37	0.35
ZrO ₂	0.09	0.08	0.09	0.11	0.08	0.09	0.15	0.16	0.28	0.25	0.18	1.29
ThO ₂	0.35	0.21	0.07	0.09	0.45	0.39	0.97	0.05	0.21	0.30	0.08	0.33
TiO ₂	52.48	53.17	53.76	53.86	52.98	53.14	52.12	53.36	52.26	52.13	53.20	51.27
BaO	0.00	0.00	0.00	0.00	0.00	0.00	0.00	0.00	0.00	0.00	0.00	0.00
Ce ₂ O ₃	3.29	2.85	2.16	2.11	3.46	3.38	4.86	3.63	4.46	4.18	3.50	4.12
Nd ₂ O ₃	1.41	1.22	0.87	0.83	1.52	1.50	2.22	1.48	1.90	1.82	1.49	1.76
Na ₂ O	0.48	0.40	0.27	0.28	0.52	0.52	1.08	0.81	0.83	0.76	0.80	1.01
MgO	0.00	0.00	0.00	0.00	0.00	0.00	0.00	0.00	0.00	0.00	0.00	0.00
Al ₂ O ₃	0.00	0.00	0.00	0.00	0.00	0.00	0.00	0.00	0.00	0.00	0.00	0.00
Ta ₂ O ₅	0.00	0.00	0.00	0.00	0.00	0.00	0.00	0.00	0.00	0.00	0.00	0.00
Total	98.75	99.06	99.32	99.49	99.47	99.69	99.87	99.61	99.93	99.48	99.40	98.04
Si	0.000	0.000	0.000	0.000	0.000	0.000	0.000	0.000	0.000	0.000	0.000	0.000
Fe	0.037	0.035	0.036	0.037	0.035	0.035	0.027	0.024	0.033	0.033	0.027	0.032
La	0.011	0.009	0.008	0.008	0.011	0.011	0.013	0.012	0.014	0.013	0.011	0.013
Sm	0.001	0.001	0.001	0.001	0.001	0.001	0.002	0.002	0.002	0.002	0.002	0.002
Pr	0.003	0.003	0.002	0.002	0.003	0.003	0.005	0.003	0.005	0.004	0.003	0.004
Ca	0.927	0.941	0.956	0.956	0.918	0.922	0.860	0.904	0.880	0.891	0.903	0.858
Nb	0.005	0.004	0.005	0.005	0.005	0.004	0.013	0.011	0.014	0.012	0.012	0.015
Sr	0.006	0.006	0.007	0.006	0.006	0.006	0.005	0.005	0.005	0.005	0.005	0.005
Zr	0.001	0.001	0.001	0.001	0.001	0.001	0.002	0.002	0.003	0.003	0.002	0.015
Th	0.002	0.001	0.000	0.000	0.002	0.002	0.005	0.000	0.001	0.002	0.000	0.002
Ti	0.949	0.952	0.953	0.953	0.952	0.952	0.949	0.956	0.944	0.944	0.955	0.944
Ba	0.000	0.000	0.000	0.000	0.000	0.000	0.000	0.000	0.000	0.000	0.000	0.000
Ce	0.029	0.025	0.019	0.018	0.030	0.029	0.043	0.032	0.039	0.037	0.031	0.037
Nd	0.012	0.010	0.007	0.007	0.013	0.013	0.019	0.013	0.016	0.016	0.013	0.015
Na	0.022	0.019	0.013	0.013	0.024	0.024	0.051	0.037	0.039	0.036	0.037	0.048
Mg	0.000	0.000	0.000	0.000	0.000	0.000	0.000	0.000	0.000	0.000	0.000	0.000
Al	0.000	0.000	0.000	0.000	0.000	0.000	0.000	0.000	0.000	0.000	0.000	0.000
Ta	0.000	0.000	0.000	0.000	0.000	0.000	0.000	0.000	0.000	0.000	0.000	0.000
Cations	2.005	2.008	2.008	2.008	2.002	2.004	1.994	2.001	1.995	1.998	2.000	1.989
<i>lueshite</i>	0.00	0.00	0.00	0.00	0.00	0.01	0.01	0.01	0.01	0.01	0.01	0.01
<i>loparite</i>	0.04	0.03	0.02	0.02	0.04	0.04	0.08	0.05	0.05	0.05	0.05	0.07
<i>REEFeO₃</i>	0.04	0.03	0.03	0.03	0.04	0.03	0.03	0.02	0.03	0.03	0.03	0.03
<i>tausonite</i>	0.01	0.01	0.01	0.01	0.01	0.01	0.00	0.01	0.01	0.01	0.01	0.01
<i>REE₂Ti₂O₇</i>	0.00	0.00	0.00	0.00	0.00	0.00	0.01	0.01	0.01	0.01	0.00	0.00
<i>lakargiite</i>	0.00	0.00	0.00	0.00	0.00	0.00	0.00	0.00	0.00	0.00	0.00	0.02
<i>perovskite</i>	0.91	0.93	0.94	0.94	0.91	0.91	0.87	0.90	0.88	0.89	0.90	0.86
Fe/Nb	7.83	9.30	8.07	7.74	7.17	7.69	2.01	2.09	2.37	2.63	2.22	2.23
ANNO	1.26	0.85	1.03	1.19	0.57	0.59	-2.50	-2.95	-1.01	-0.86	-2.32	-1.22

TABELA B03 – Cont. Major element compositions and endmembers for perovskite from all samples. Structural formula calculated on the basis of 3 oxygens. C - core; R - rim; I – intermediately.

Sample Grain/Analysis Location	LM-2 07/13 C	LM-2 07/14 R	LM-2 08/15 C	LM-2 08/16 R	LM-2 09/17 C	LM-2 09/18 R	LM-2 10/19 C	LM-2 10/20 R	LM3-1 11/21 C	LM3-1 11/22 R	LM3-1 12/23 C
SiO ₂	0.00	0.00	0.00	0.00	0.00	0.00	0.00	0.00	0.00	0.00	0.00
Fe ₂ O ₃	1.28	1.38	1.58	1.48	1.96	1.96	1.92	1.91	1.24	1.24	1.98
La ₂ O ₃	1.21	0.94	1.66	1.29	1.12	1.15	1.13	1.09	1.54	1.31	1.18
Sm ₂ O ₃	0.21	0.12	0.21	0.17	0.14	0.14	0.15	0.14	0.24	0.20	0.17
Pr ₂ O ₃	0.44	0.26	0.48	0.36	0.33	0.34	0.33	0.28	0.61	0.46	0.39
CaO	35.13	36.99	33.86	35.52	36.71	36.55	36.50	36.86	32.98	34.55	36.15
Nb ₂ O ₅	0.67	0.56	1.56	1.03	0.43	0.42	0.42	0.42	1.29	0.97	0.41
SrO	0.34	0.35	0.39	0.30	0.42	0.47	0.42	0.42	0.37	0.38	0.43
ZrO ₂	0.13	0.16	0.18	0.20	0.08	0.10	0.10	0.10	0.13	0.11	0.10
ThO ₂	0.47	0.01	0.02	0.00	0.26	0.33	0.23	0.22	0.83	0.53	0.35
TiO ₂	52.96	54.10	51.78	53.13	53.00	53.01	53.07	53.11	51.64	52.43	52.78
BaO	0.00	0.00	0.00	0.00	0.00	0.00	0.00	0.00	0.00	0.00	0.00
Ce ₂ O ₃	3.82	2.41	4.44	3.21	2.90	3.08	2.91	2.83	4.93	3.96	3.23
Nd ₂ O ₃	1.79	1.00	1.81	1.27	1.25	1.30	1.23	1.21	2.23	1.78	1.42
Na ₂ O	0.74	0.52	0.99	0.78	0.41	0.46	0.42	0.44	1.07	0.87	0.49
MgO	0.00	0.00	0.00	0.00	0.00	0.00	0.00	0.00	0.00	0.00	0.00
Al ₂ O ₃	0.00	0.00	0.00	0.00	0.00	0.00	0.00	0.00	0.00	0.00	0.00
Ta ₂ O ₅	0.00	0.00	0.00	0.00	0.00	0.00	0.00	0.00	0.00	0.00	0.00
Total	99.18	98.82	98.97	98.74	99.02	99.30	98.82	99.03	99.10	98.80	99.09
Si	0.000	0.000	0.000	0.000	0.000	0.000	0.000	0.000	0.000	0.000	0.000
Fe	0.023	0.025	0.029	0.027	0.035	0.035	0.035	0.034	0.023	0.023	0.036
La	0.011	0.008	0.015	0.011	0.010	0.010	0.010	0.010	0.014	0.012	0.010
Sm	0.002	0.001	0.002	0.001	0.001	0.001	0.001	0.001	0.002	0.002	0.001
Pr	0.004	0.002	0.004	0.003	0.003	0.003	0.003	0.002	0.005	0.004	0.003
Ca	0.904	0.939	0.879	0.910	0.938	0.933	0.934	0.941	0.863	0.895	0.927
Nb	0.007	0.006	0.017	0.011	0.005	0.005	0.005	0.004	0.014	0.011	0.004
Sr	0.005	0.005	0.005	0.004	0.006	0.006	0.006	0.006	0.005	0.005	0.006
Zr	0.001	0.002	0.002	0.002	0.001	0.001	0.001	0.001	0.002	0.001	0.001
Th	0.003	0.000	0.000	0.000	0.001	0.002	0.001	0.001	0.005	0.003	0.002
Ti	0.957	0.964	0.944	0.956	0.951	0.951	0.954	0.952	0.949	0.954	0.951
Ba	0.000	0.000	0.000	0.000	0.000	0.000	0.000	0.000	0.000	0.000	0.000
Ce	0.034	0.021	0.039	0.028	0.025	0.027	0.025	0.025	0.044	0.035	0.028
Nd	0.015	0.008	0.016	0.011	0.011	0.011	0.010	0.010	0.019	0.015	0.012
Na	0.035	0.024	0.047	0.036	0.019	0.021	0.019	0.020	0.051	0.041	0.023
Mg	0.000	0.000	0.000	0.000	0.000	0.000	0.000	0.000	0.000	0.000	0.000
Al	0.000	0.000	0.000	0.000	0.000	0.000	0.000	0.000	0.000	0.000	0.000
Ta	0.000	0.000	0.000	0.000	0.000	0.000	0.000	0.000	0.000	0.000	0.000
Cations	2.001	2.004	1.999	2.002	2.007	2.007	2.004	2.008	1.995	2.001	2.006
<i>lueshite</i>	0.01	0.01	0.02	0.01	0.00	0.00	0.00	0.00	0.01	0.01	0.00
<i>loparite</i>	0.06	0.04	0.06	0.05	0.03	0.03	0.03	0.03	0.07	0.06	0.04
<i>REEFeO₃</i>	0.02	0.02	0.03	0.03	0.04	0.04	0.03	0.03	0.02	0.02	0.04
<i>tausonite</i>	0.00	0.00	0.01	0.00	0.01	0.01	0.01	0.01	0.01	0.01	0.01
<i>REE₂Ti₂O₇</i>	0.01	0.00	0.01	0.00	0.00	0.00	0.00	0.00	0.01	0.01	0.00
<i>lakargiite</i>	0.00	0.00	0.00	0.00	0.00	0.00	0.00	0.00	0.00	0.00	0.00
<i>perovskite</i>	0.90	0.93	0.88	0.90	0.92	0.92	0.92	0.92	0.87	0.89	0.91
<i>Fe/Nb</i>	3.14	4.08	1.69	2.40	7.63	7.73	7.54	7.65	1.60	2.15	8.08
<i>ANNO</i>	-2.65	-2.10	-2.43	-2.23	0.72	0.72	0.56	0.50	-3.58	-3.15	0.87

TABELA B03 – Cont. Major element compositions and endmembers for perovskite from all samples. Structural formula calculated on the basis of 3 oxygens. C - core; R - rim; I – intermediated.

Sample Grain/Analysis Location	LM3-1 12/24 R	LM3-1 13/26 R	LM3-1 14/27 R	LM3-1 15/28 C	LM3-1 16/29 C	LM3-1 16/30 R	LM3-1 17/31 C	LM3-1 17/32 R	LM3-2 18/33 C	LM3-2 18/34 I
SiO ₂	0.00	0.01	0.00	0.00	0.00	0.00	0.00	0.00	0.00	0.00
Fe ₂ O ₃	2.01	1.47	1.53	1.40	1.48	1.50	2.37	2.27	1.44	1.51
La ₂ O ₃	1.07	1.14	1.11	1.21	1.35	1.28	1.04	1.04	1.30	1.37
Sm ₂ O ₃	0.14	0.17	0.12	0.17	0.22	0.21	0.13	0.12	0.20	0.22
Pr ₂ O ₃	0.33	0.38	0.21	0.39	0.49	0.47	0.33	0.32	0.46	0.51
CaO	36.48	35.66	36.71	35.89	34.32	34.09	36.58	36.63	34.79	34.06
Nb ₂ O ₅	0.42	0.73	1.22	1.08	0.75	0.92	0.33	0.42	0.88	0.91
SrO	0.44	0.37	0.37	0.34	0.36	0.35	0.45	0.47	0.36	0.36
ZrO ₂	0.08	0.19	0.28	0.14	0.18	0.17	0.08	0.11	0.17	0.18
ThO ₂	0.22	0.17	0.00	0.34	0.77	0.79	0.28	0.20	0.32	0.72
TiO ₂	53.06	52.85	53.73	53.48	52.40	52.37	52.87	52.89	53.10	52.82
BaO	0.00	0.00	0.00	0.00	0.00	0.00	0.00	0.00	0.00	0.00
Ce ₂ O ₃	2.84	3.22	2.19	3.33	4.17	3.99	2.91	2.67	3.95	4.36
Nd ₂ O ₃	1.21	1.43	0.78	1.45	1.91	1.88	1.23	1.08	1.78	2.01
Na ₂ O	0.42	0.72	0.61	0.65	0.85	0.79	0.36	0.34	0.87	0.96
MgO	0.00	0.00	0.00	0.00	0.00	0.00	0.00	0.00	0.00	0.00
Al ₂ O ₃	0.00	0.00	0.00	0.00	0.00	0.00	0.00	0.00	0.00	0.00
Ta ₂ O ₅	0.00	0.00	0.00	0.00	0.00	0.00	0.00	0.00	0.00	0.00
Total	98.72	98.50	98.84	99.85	99.25	98.81	98.96	98.57	99.62	99.99
Si	0.000	0.000	0.000	0.000	0.000	0.000	0.000	0.000	0.000	0.000
Fe	0.036	0.027	0.027	0.025	0.027	0.027	0.043	0.041	0.026	0.027
La	0.009	0.010	0.010	0.011	0.012	0.011	0.009	0.009	0.011	0.012
Sm	0.001	0.001	0.001	0.001	0.002	0.002	0.001	0.001	0.002	0.002
Pr	0.003	0.003	0.002	0.003	0.004	0.004	0.003	0.003	0.004	0.005
Ca	0.934	0.918	0.931	0.913	0.889	0.885	0.935	0.938	0.892	0.876
Nb	0.004	0.008	0.013	0.012	0.008	0.010	0.004	0.005	0.010	0.010
Sr	0.006	0.005	0.005	0.005	0.005	0.005	0.006	0.007	0.005	0.005
Zr	0.001	0.002	0.003	0.002	0.002	0.002	0.001	0.001	0.002	0.002
Th	0.001	0.001	0.000	0.002	0.004	0.004	0.002	0.001	0.002	0.004
Ti	0.954	0.955	0.957	0.955	0.953	0.955	0.949	0.951	0.956	0.954
Ba	0.000	0.000	0.000	0.000	0.000	0.000	0.000	0.000	0.000	0.000
Ce	0.025	0.028	0.019	0.029	0.037	0.035	0.025	0.023	0.035	0.038
Nd	0.010	0.012	0.007	0.012	0.016	0.016	0.010	0.009	0.015	0.017
Na	0.020	0.034	0.028	0.030	0.040	0.037	0.017	0.016	0.040	0.045
Mg	0.000	0.000	0.000	0.000	0.000	0.000	0.000	0.000	0.000	0.000
Al	0.000	0.000	0.000	0.000	0.000	0.000	0.000	0.000	0.000	0.000
Ta	0.000	0.000	0.000	0.000	0.000	0.000	0.000	0.000	0.000	0.000
Cations	2.005	2.005	2.002	1.998	1.999	1.994	2.005	2.005	2.000	1.997
<i>lueshite</i>	0.00	0.01	0.01	0.01	0.01	0.01	0.00	0.00	0.01	0.01
<i>loparite</i>	0.03	0.05	0.03	0.04	0.06	0.05	0.03	0.02	0.06	0.07
<i>REEFeO₃</i>	0.03	0.03	0.02	0.03	0.03	0.03	0.04	0.03	0.03	0.03
<i>tausonite</i>	0.01	0.01	0.01	0.00	0.01	0.00	0.01	0.01	0.01	0.01
<i>REE₂Ti₂O₇</i>	0.00	0.00	0.00	0.01	0.01	0.01	0.00	0.00	0.01	0.01
<i>lakargiite</i>	0.00	0.00	0.00	0.00	0.00	0.00	0.00	0.00	0.00	0.00
<i>perovskite</i>	0.92	0.90	0.93	0.91	0.89	0.89	0.93	0.93	0.89	0.88
<i>Fe/Nb</i>	8.06	3.37	2.08	2.15	3.30	2.70	11.80	9.07	2.72	2.77
<i>ANNO</i>	0.97	-1.84	-2.32	-2.72	-1.79	-1.93	2.69	2.14	-2.21	-1.91

TABELA B03 – Cont. Major element compositions and endmembers for perovskite from all samples. Structural formula calculated on the basis of 3 oxygens. C - core; R - rim; I – intermediately.

Sample Grain/Analysis Location	LM3-2 18/35 R	LM3-2 19/36 C	LM3-2 19/37 I	LM3-2 19/38 I	LM3-2 19/39 I	LM3-2 19/40 R	LM3-2 20/41 C	LM3-2 20/42 R	LM3-2 21/45 C	LM3-2 21/46 R
SiO ₂	0.00	0.00	0.00	0.00	0.00	0.00	0.00	0.00	0.00	0.00
Fe ₂ O ₃	1.73	1.41	1.32	1.32	1.39	1.55	2.41	1.39	1.54	1.89
La ₂ O ₃	0.95	1.23	1.07	1.11	1.17	0.92	1.31	1.26	1.25	0.94
Sm ₂ O ₃	0.14	0.20	0.16	0.19	0.18	0.13	0.18	0.18	0.18	0.11
Pr ₂ O ₃	0.25	0.46	0.33	0.38	0.38	0.25	0.39	0.41	0.37	0.21
CaO	37.18	34.47	36.25	36.02	36.00	37.42	34.93	35.52	35.78	37.18
Nb ₂ O ₅	0.65	0.92	0.64	0.62	0.63	0.60	1.02	1.10	1.11	0.71
SrO	0.37	0.33	0.34	0.35	0.32	0.35	0.35	0.36	0.36	0.38
ZrO ₂	0.21	0.14	0.12	0.11	0.12	0.19	0.14	0.16	0.26	0.24
ThO ₂	0.03	0.75	0.13	0.23	0.28	0.02	0.05	0.17	0.08	0.01
TiO ₂	54.04	52.64	54.07	53.87	53.87	55.10	53.22	54.02	53.36	54.66
BaO	0.00	0.00	0.00	0.00	0.00	0.00	0.00	0.00	0.00	0.00
Ce ₂ O ₃	2.33	3.89	3.00	3.26	3.38	2.27	3.51	3.63	3.39	2.11
Nd ₂ O ₃	0.96	1.79	1.35	1.50	1.54	0.92	1.53	1.58	1.45	0.81
Na ₂ O	0.54	0.87	0.68	0.68	0.75	0.50	0.89	0.88	0.78	0.56
MgO	0.00	0.00	0.00	0.00	0.00	0.00	0.00	0.00	0.00	0.00
Al ₂ O ₃	0.00	0.00	0.00	0.00	0.00	0.00	0.00	0.00	0.00	0.00
Ta ₂ O ₅	0.00	0.00	0.00	0.00	0.00	0.00	0.00	0.00	0.00	0.00
Total	99.39	99.10	99.46	99.65	100.00	100.22	99.92	100.68	99.92	99.79
Si	0.000	0.000	0.000	0.000	0.000	0.000	0.000	0.000	0.000	0.000
Fe	0.031	0.026	0.024	0.024	0.025	0.027	0.043	0.025	0.027	0.033
La	0.008	0.011	0.009	0.010	0.010	0.008	0.011	0.011	0.011	0.008
Sm	0.001	0.002	0.001	0.002	0.002	0.001	0.001	0.002	0.001	0.001
Pr	0.002	0.004	0.003	0.003	0.003	0.002	0.003	0.004	0.003	0.002
Ca	0.939	0.891	0.920	0.916	0.913	0.934	0.888	0.897	0.909	0.932
Nb	0.007	0.010	0.007	0.007	0.007	0.006	0.011	0.012	0.012	0.007
Sr	0.005	0.005	0.005	0.005	0.004	0.005	0.005	0.005	0.005	0.005
Zr	0.002	0.002	0.001	0.001	0.001	0.002	0.002	0.002	0.003	0.003
Th	0.000	0.004	0.001	0.001	0.002	0.000	0.000	0.001	0.000	0.000
Ti	0.958	0.955	0.963	0.962	0.960	0.966	0.950	0.958	0.952	0.962
Ba	0.000	0.000	0.000	0.000	0.000	0.000	0.000	0.000	0.000	0.000
Ce	0.020	0.034	0.026	0.028	0.029	0.019	0.031	0.031	0.029	0.018
Nd	0.008	0.015	0.011	0.013	0.013	0.008	0.013	0.013	0.012	0.007
Na	0.025	0.041	0.031	0.031	0.034	0.023	0.041	0.040	0.036	0.025
Mg	0.000	0.000	0.000	0.000	0.000	0.000	0.000	0.000	0.000	0.000
Al	0.000	0.000	0.000	0.000	0.000	0.000	0.000	0.000	0.000	0.000
Ta	0.000	0.000	0.000	0.000	0.000	0.000	0.000	0.000	0.000	0.000
Cations	2.006	1.999	2.003	2.002	2.004	2.001	2.000	2.000	2.002	2.003
<i>lueshite</i>	0.01	0.01	0.01	0.01	0.01	0.01	0.01	0.01	0.01	0.01
<i>loparite</i>	0.04	0.06	0.05	0.05	0.06	0.03	0.06	0.06	0.05	0.04
<i>REEFeO₃</i>	0.02	0.03	0.02	0.02	0.02	0.02	0.03	0.02	0.03	0.02
<i>tausonite</i>	0.01	0.00	0.00	0.00	0.00	0.00	0.00	0.00	0.01	0.01
<i>REE₂Ti₂O₇</i>	0.00	0.01	0.00	0.00	0.00	0.00	0.00	0.00	0.00	0.00
<i>lakargiite</i>	0.00	0.00	0.00	0.00	0.00	0.00	0.00	0.00	0.00	0.00
<i>perovskite</i>	0.93	0.89	0.91	0.91	0.90	0.93	0.89	0.90	0.90	0.93
<i>Fe/Nb</i>	4.40	2.55	3.45	3.54	3.69	4.31	3.94	2.10	2.31	4.46
<i>ANNO</i>	-0.70	-2.36	-2.45	-2.43	-2.16	-1.49	1.90	-2.79	-2.12	-0.12

TABELA B03 – Cont. Major element compositions and endmembers for perovskite from all samples. Structural formula calculated on the basis of 3 oxygens. C - core; R - rim; I – intermediated.

Sample Grain/Analysis Location	LMIC1 22/47	LMIC1 23/48	LMIC1 24/49	LMIC1 25/50	LMIC1 25/51	LMIC1 26/52	LMIC1 26/53	LMIC1 27/54	LMIC1 27/55	LMIC1 28/56
	C	C	C	C	R	R	C	R	C	R
SiO ₂	0.00	0.00	0.00	0.00	0.00	0.11	0.00	0.15	0.00	0.00
Fe ₂ O ₃	2.70	2.60	2.59	2.63	2.67	2.55	2.28	2.35	2.53	2.48
La ₂ O ₃	0.94	0.95	0.99	1.00	1.00	0.82	1.01	1.02	0.95	0.96
Sm ₂ O ₃	0.13	0.12	0.11	0.12	0.11	0.09	0.11	0.14	0.12	0.12
Pr ₂ O ₃	0.27	0.28	0.31	0.33	0.29	0.18	0.27	0.32	0.28	0.27
CaO	37.40	37.75	37.47	37.33	37.42	38.22	37.60	36.98	37.54	37.38
Nb ₂ O ₅	0.28	0.25	0.25	0.25	0.27	0.33	0.27	0.23	0.25	0.24
SrO	0.17	0.16	0.15	0.16	0.16	0.21	0.17	0.21	0.19	0.18
ZrO ₂	0.10	0.08	0.08	0.08	0.08	0.12	0.08	0.08	0.08	0.06
ThO ₂	0.21	0.17	0.23	0.20	0.23	0.07	0.17	0.20	0.18	0.15
TiO ₂	53.44	53.46	53.33	53.21	53.50	54.13	53.84	52.77	53.56	53.88
BaO	0.00	0.00	0.00	0.00	0.00	0.00	0.00	0.00	0.00	0.00
Ce ₂ O ₃	2.52	2.46	2.68	2.67	2.72	1.70	2.46	2.68	2.55	2.43
Nd ₂ O ₃	1.03	1.00	1.13	1.11	1.12	0.63	0.94	1.13	1.05	1.02
Na ₂ O	0.34	0.32	0.36	0.32	0.34	0.32	0.32	0.40	0.32	0.33
MgO	0.00	0.00	0.00	0.00	0.00	0.00	0.00	0.00	0.00	0.00
Al ₂ O ₃	0.00	0.00	0.00	0.00	0.00	0.00	0.00	0.00	0.00	0.00
Ta ₂ O ₅	0.00	0.00	0.00	0.00	0.00	0.00	0.00	0.00	0.00	0.00
Total	99.52	99.60	99.67	99.41	99.89	99.48	99.53	98.64	99.62	99.50
Si	0.000	0.000	0.000	0.000	0.000	0.003	0.000	0.004	0.000	0.000
Fe	0.048	0.046	0.046	0.047	0.047	0.045	0.040	0.042	0.045	0.044
La	0.008	0.008	0.009	0.009	0.009	0.007	0.009	0.009	0.008	0.008
Sm	0.001	0.001	0.001	0.001	0.001	0.001	0.001	0.001	0.001	0.001
Pr	0.002	0.002	0.003	0.003	0.003	0.002	0.002	0.003	0.002	0.002
Ca	0.946	0.953	0.948	0.947	0.944	0.957	0.949	0.945	0.948	0.943
Nb	0.003	0.003	0.003	0.003	0.003	0.003	0.003	0.003	0.003	0.003
Sr	0.002	0.002	0.002	0.002	0.002	0.003	0.002	0.003	0.003	0.002
Zr	0.001	0.001	0.001	0.001	0.001	0.001	0.001	0.001	0.001	0.001
Th	0.001	0.001	0.001	0.001	0.001	0.000	0.001	0.001	0.001	0.001
Ti	0.949	0.948	0.947	0.948	0.948	0.952	0.954	0.947	0.950	0.955
Ba	0.000	0.000	0.000	0.000	0.000	0.000	0.000	0.000	0.000	0.000
Ce	0.022	0.021	0.023	0.023	0.023	0.015	0.021	0.023	0.022	0.021
Nd	0.009	0.008	0.010	0.009	0.009	0.005	0.008	0.010	0.009	0.009
Na	0.015	0.015	0.016	0.015	0.015	0.014	0.015	0.018	0.014	0.015
Mg	0.000	0.000	0.000	0.000	0.000	0.000	0.000	0.000	0.000	0.000
Al	0.000	0.000	0.000	0.000	0.000	0.000	0.000	0.000	0.000	0.000
Ta	0.000	0.000	0.000	0.000	0.000	0.000	0.000	0.000	0.000	0.000
Cations	2.007	2.010	2.009	2.008	2.007	2.009	2.006	2.009	2.008	2.005
<i>lueshite</i>	0.00	0.00	0.00	0.00	0.00	0.00	0.00	0.00	0.00	0.00
<i>loparite</i>	0.03	0.02	0.03	0.02	0.03	0.02	0.02	0.03	0.02	0.03
<i>REEFeO₃</i>	0.03	0.03	0.03	0.03	0.03	0.02	0.03	0.03	0.03	0.03
<i>tausonite</i>	0.00	0.00	0.00	0.00	0.00	0.00	0.00	0.00	0.00	0.00
<i>REE₂Ti₂O₇</i>	0.00	0.00	0.00	0.00	0.00	0.00	0.00	0.00	0.00	0.00
<i>lakargiite</i>	0.00	0.00	0.00	0.00	0.00	0.00	0.00	0.00	0.00	0.00
<i>perovskite</i>	0.94	0.94	0.93	0.94	0.94	0.95	0.94	0.93	0.94	0.94
<i>Fe/Nb</i>	16.30	17.56	17.05	17.44	16.66	13.06	14.19	16.80	16.62	17.21
<i>ANNO</i>	4.12	3.70	3.67	3.88	3.98	3.29	2.25	2.73	3.38	3.17

TABELA B03 – Cont. Major element compositions and endmembers for perovskite from all samples. Structural formula calculated on the basis of 3 oxygens. C - core; R - rim; I – intermediated.

Sample Grain/Analysis Location	LMIC1 28/57 C	LMIC1 29/58 C	LMIC1 29/59 R	LMIC1 30/60 C	LMIC1 30/61 R	LMIC1 31/62 R	LMIC1 31/63 C	LMIC1 32/64 C	LMIC1 32/65 R	LMIC1 33/66 C
SiO ₂	0.00	0.00	0.00	0.00	0.00	0.00	0.00	0.01	2.03	0.00
Fe ₂ O ₃	2.39	1.39	1.19	2.04	1.22	1.36	1.31	2.44	3.08	2.26
La ₂ O ₃	0.94	1.69	1.01	1.52	1.00	1.27	1.40	1.03	0.84	1.03
Sm ₂ O ₃	0.11	0.22	0.11	0.23	0.12	0.21	0.24	0.13	0.09	0.12
Pr ₂ O ₃	0.27	0.59	0.23	0.51	0.25	0.50	0.53	0.34	0.21	0.30
CaO	37.53	33.53	36.96	34.17	37.16	34.90	33.92	37.27	37.16	37.59
Nb ₂ O ₅	0.23	1.11	0.65	1.50	0.63	0.63	0.72	0.26	0.39	0.33
SrO	0.19	0.14	0.14	0.12	0.13	0.12	0.13	0.18	0.26	0.18
ZrO ₂	0.07	0.14	0.14	0.34	0.16	0.15	0.14	0.10	0.15	0.08
ThO ₂	0.14	0.28	0.14	0.42	0.09	0.57	1.09	0.22	0.13	0.16
TiO ₂	53.71	52.57	54.24	51.79	54.51	53.90	52.71	53.52	52.00	53.86
BaO	0.00	0.00	0.00	0.00	0.00	0.00	0.00	0.00	0.00	0.00
Ce ₂ O ₃	2.27	4.99	2.35	4.43	2.25	4.10	4.45	2.74	1.92	2.57
Nd ₂ O ₃	0.93	2.17	0.89	1.88	0.83	1.90	2.09	1.14	0.77	1.04
Na ₂ O	0.28	0.99	0.66	0.83	0.58	0.81	0.92	0.35	1.21	0.32
MgO	0.00	0.00	0.00	0.00	0.00	0.00	0.00	0.00	0.00	0.00
Al ₂ O ₃	0.00	0.00	0.00	0.00	0.00	0.00	0.00	0.00	0.00	0.00
Ta ₂ O ₅	0.00	0.00	0.00	0.00	0.00	0.00	0.00	0.00	0.00	0.00
Total	99.06	99.81	98.70	99.78	98.94	100.41	99.65	99.72	100.23	99.83
Si	0.000	0.000	0.000	0.000	0.000	0.000	0.000	0.000	0.047	0.000
Fe	0.042	0.025	0.021	0.037	0.022	0.024	0.024	0.043	0.054	0.040
La	0.008	0.015	0.009	0.013	0.009	0.011	0.012	0.009	0.007	0.009
Sm	0.001	0.002	0.001	0.002	0.001	0.002	0.002	0.001	0.001	0.001
Pr	0.002	0.005	0.002	0.005	0.002	0.004	0.005	0.003	0.002	0.003
Ca	0.950	0.866	0.938	0.881	0.939	0.888	0.877	0.942	0.921	0.947
Nb	0.002	0.012	0.007	0.016	0.007	0.007	0.008	0.003	0.004	0.004
Sr	0.003	0.002	0.002	0.002	0.002	0.002	0.002	0.002	0.003	0.002
Zr	0.001	0.002	0.002	0.004	0.002	0.002	0.002	0.001	0.002	0.001
Th	0.001	0.002	0.001	0.002	0.000	0.003	0.006	0.001	0.001	0.001
Ti	0.955	0.954	0.966	0.938	0.967	0.963	0.957	0.950	0.905	0.953
Ba	0.000	0.000	0.000	0.000	0.000	0.000	0.000	0.000	0.000	0.000
Ce	0.020	0.044	0.020	0.039	0.019	0.036	0.039	0.024	0.016	0.022
Nd	0.008	0.019	0.008	0.016	0.007	0.016	0.018	0.010	0.006	0.009
Na	0.013	0.046	0.030	0.039	0.027	0.037	0.043	0.016	0.054	0.014
Mg	0.000	0.000	0.000	0.000	0.000	0.000	0.000	0.000	0.000	0.000
Al	0.000	0.000	0.000	0.000	0.000	0.000	0.000	0.000	0.000	0.000
Ta	0.000	0.000	0.000	0.000	0.000	0.000	0.000	0.000	0.000	0.000
Cations	2.006	1.993	2.006	1.995	2.004	1.994	1.995	2.006	2.023	2.006
<i>lueshite</i>	0.00	0.01	0.01	0.02	0.01	0.01	0.01	0.00	0.00	0.00
<i>loparite</i>	0.02	0.07	0.05	0.05	0.04	0.06	0.07	0.03	0.07	0.02
<i>REEFeO₃</i>	0.03	0.03	0.02	0.04	0.02	0.02	0.02	0.03	0.00	0.03
<i>tausonite</i>	0.00	0.00	0.00	0.00	0.00	0.00	0.00	0.00	0.00	0.00
<i>REE₂Ti₂O₇</i>	0.00	0.01	0.00	0.01	0.00	0.01	0.01	0.00	0.00	0.00
<i>lakargiite</i>	0.00	0.00	0.00	0.00	0.00	0.00	0.00	0.00	0.00	0.00
<i>perovskite</i>	0.94	0.88	0.93	0.89	0.93	0.90	0.88	0.93	0.92	0.94
<i>Fe/Nb</i>	17.24	2.09	3.04	2.26	3.23	3.59	3.02	15.59	13.26	11.40
<i>ANNO</i>	2.82	-2.69	-3.08	-0.30	-2.91	-2.27	-2.53	2.99	5.40	2.06

TABELA B03 – Cont. Major element compositions and endmembers for perovskite from all samples. Structural formula calculated on the basis of 3 oxygens. C - core; R - rim; I - intermediated.

Sample Grain/Analysis Location	LMIC1 33/67 R	LMIC1 34/68 C	LMIC1 34/69 R	LMIC1 35/70 C	LMIC1 35/71 R	LMIC1 36/72 C	LMIC1 36/73 R	LMIC1 37/74 C	LMIC1 37/75 R	LMIC1 38/76 C
SiO ₂	0.00	0.26	0.01	0.01	0.02	0.11	0.01	0.00	0.04	0.17
Fe ₂ O ₃	2.26	2.59	2.45	2.48	2.60	2.45	2.34	2.39	2.64	2.35
La ₂ O ₃	0.94	0.82	1.02	1.10	0.92	0.87	0.96	1.04	0.84	0.93
Sm ₂ O ₃	0.11	0.10	0.11	0.13	0.11	0.10	0.10	0.12	0.08	0.10
Pr ₂ O ₃	0.25	0.21	0.30	0.33	0.22	0.22	0.26	0.31	0.18	0.27
CaO	37.82	37.84	37.51	36.99	38.00	37.89	37.81	37.27	38.08	36.64
Nb ₂ O ₅	0.34	0.30	0.24	0.30	0.28	0.34	0.29	0.28	0.35	0.28
SrO	0.18	0.22	0.17	0.19	0.20	0.20	0.17	0.18	0.28	0.18
ZrO ₂	0.11	0.08	0.09	0.09	0.09	0.11	0.11	0.10	0.14	0.07
ThO ₂	0.11	0.09	0.18	0.28	0.14	0.10	0.13	0.19	0.06	0.15
TiO ₂	53.68	52.54	53.13	52.87	53.45	53.58	53.79	53.25	53.53	52.14
BaO	0.00	0.00	0.00	0.00	0.00	0.00	0.00	0.00	0.00	0.00
Ce ₂ O ₃	2.23	2.00	2.54	2.92	2.16	1.91	2.26	2.64	1.70	2.32
Nd ₂ O ₃	0.90	0.82	1.03	1.22	0.87	0.70	0.85	1.03	0.63	0.89
Na ₂ O	0.29	0.28	0.30	0.37	0.26	0.34	0.27	0.34	0.29	0.32
MgO	0.00	0.00	0.00	0.00	0.00	0.00	0.00	0.00	0.00	0.00
Al ₂ O ₃	0.00	0.00	0.00	0.00	0.00	0.00	0.00	0.00	0.00	0.00
Ta ₂ O ₅	0.00	0.00	0.00	0.00	0.00	0.00	0.00	0.00	0.00	0.00
Total	99.24	98.16	99.07	99.29	99.31	98.93	99.35	99.12	98.84	96.81
Si	0.000	0.006	0.000	0.000	0.001	0.003	0.000	0.000	0.001	0.004
Fe	0.040	0.046	0.044	0.044	0.046	0.043	0.041	0.043	0.047	0.043
La	0.008	0.007	0.009	0.010	0.008	0.008	0.008	0.009	0.007	0.008
Sm	0.001	0.001	0.001	0.001	0.001	0.001	0.001	0.001	0.001	0.001
Pr	0.002	0.002	0.003	0.003	0.002	0.002	0.002	0.003	0.002	0.002
Ca	0.956	0.965	0.953	0.943	0.960	0.957	0.954	0.947	0.962	0.950
Nb	0.004	0.003	0.003	0.003	0.003	0.004	0.003	0.003	0.004	0.003
Sr	0.002	0.003	0.002	0.003	0.003	0.003	0.002	0.002	0.004	0.003
Zr	0.001	0.001	0.001	0.001	0.001	0.001	0.001	0.001	0.002	0.001
Th	0.001	0.001	0.001	0.002	0.001	0.001	0.001	0.001	0.000	0.001
Ti	0.953	0.941	0.948	0.946	0.948	0.950	0.953	0.950	0.949	0.949
Ba	0.000	0.000	0.000	0.000	0.000	0.000	0.000	0.000	0.000	0.000
Ce	0.019	0.017	0.022	0.025	0.019	0.016	0.019	0.023	0.015	0.021
Nd	0.008	0.007	0.009	0.010	0.007	0.006	0.007	0.009	0.005	0.008
Na	0.013	0.013	0.014	0.017	0.012	0.015	0.012	0.015	0.013	0.015
Mg	0.000	0.000	0.000	0.000	0.000	0.000	0.000	0.000	0.000	0.000
Al	0.000	0.000	0.000	0.000	0.000	0.000	0.000	0.000	0.000	0.000
Ta	0.000	0.000	0.000	0.000	0.000	0.000	0.000	0.000	0.000	0.000
Cations	2.008	2.013	2.009	2.008	2.010	2.009	2.007	2.007	2.011	2.007
<i>lueshite</i>	0.00	0.00	0.00	0.00	0.00	0.00	0.00	0.00	0.00	0.00
<i>loparite</i>	0.02	0.02	0.02	0.03	0.02	0.02	0.02	0.03	0.02	0.02
<i>REEFeO₃</i>	0.03	0.03	0.03	0.04	0.03	0.02	0.03	0.03	0.02	0.03
<i>tausonite</i>	0.00	0.00	0.00	0.00	0.00	0.00	0.00	0.00	0.00	0.00
<i>REE₂Ti₂O₇</i>	0.00	0.00	0.00	0.00	0.00	0.00	0.00	0.00	0.00	0.00
<i>lakargiite</i>	0.00	0.00	0.00	0.00	0.00	0.00	0.00	0.00	0.00	0.00
<i>perovskite</i>	0.94	0.95	0.94	0.93	0.95	0.95	0.95	0.94	0.95	0.94
Fe/Nb	11.12	14.44	17.08	13.71	15.53	11.82	13.54	14.39	12.62	14.11
ANNO	2.08	3.70	3.11	3.19	3.66	2.91	2.49	2.79	3.74	2.81

TABELA B03 – Cont. Major element compositions and endmembers for perovskite from all samples. Structural formula calculated on the basis of 3 oxygens. C - core; R - rim; I – intermediately.

Sample Grain/Analysis Location	LMIC1 38/77 R	LMIC1 39/78 C	LMIC1 39/79 R	LMIC1 40/80 C	LMIC1 40/87 R	LMIC2 41/88 R	LMIC2 41/88 C	LMIC2 42/89 C	LMIC2 42/90 R	LMIC2 42/91 R
SiO ₂	1.02	0.00	0.00	0.00	0.00	0.01	0.00	0.01	0.57	0.00
Fe ₂ O ₃	3.04	2.45	2.50	2.59	2.56	1.71	1.36	1.48	1.57	1.63
La ₂ O ₃	0.83	1.06	1.00	0.96	1.02	0.91	1.16	0.87	0.90	0.90
Sm ₂ O ₃	0.10	0.13	0.13	0.12	0.11	0.10	0.17	0.11	0.12	0.10
Pr ₂ O ₃	0.20	0.30	0.30	0.27	0.31	0.19	0.37	0.24	0.23	0.21
CaO	37.55	37.16	37.42	37.19	37.32	38.10	36.18	37.71	36.68	38.29
Nb ₂ O ₅	0.31	0.24	0.26	0.29	0.29	0.60	0.52	0.43	0.48	0.51
SrO	0.23	0.18	0.18	0.18	0.18	0.13	0.15	0.15	0.10	0.13
ZrO ₂	0.10	0.06	0.08	0.08	0.10	0.32	0.11	0.14	0.15	0.19
ThO ₂	0.10	0.18	0.19	0.17	0.19	0.00	0.16	0.00	0.00	0.00
TiO ₂	52.37	53.44	53.71	52.94	53.39	54.47	54.14	54.61	53.89	55.43
BaO	0.00	0.00	0.00	0.00	0.00	0.00	0.00	0.00	0.00	0.00
Ce ₂ O ₃	1.89	2.70	2.67	2.51	2.61	1.95	3.29	2.00	2.16	1.98
Nd ₂ O ₃	0.75	1.09	1.02	0.97	1.03	0.75	1.45	0.81	0.85	0.74
Na ₂ O	0.40	0.34	0.33	0.32	0.33	0.40	0.67	0.39	0.44	0.40
MgO	0.00	0.00	0.00	0.00	0.00	0.00	0.00	0.00	0.00	0.00
Al ₂ O ₃	0.00	0.00	0.00	0.00	0.00	0.00	0.00	0.00	0.00	0.00
Ta ₂ O ₅	0.00	0.00	0.00	0.00	0.00	0.00	0.00	0.00	0.00	0.00
Total	98.88	99.33	99.79	98.59	99.44	99.63	99.73	98.96	98.13	100.51
Si	0.024	0.000	0.000	0.000	0.000	0.000	0.000	0.000	0.014	0.000
Fe	0.054	0.044	0.044	0.046	0.046	0.030	0.024	0.026	0.028	0.028
La	0.007	0.009	0.009	0.008	0.009	0.008	0.010	0.008	0.008	0.008
Sm	0.001	0.001	0.001	0.001	0.001	0.001	0.001	0.001	0.001	0.001
Pr	0.002	0.003	0.003	0.002	0.003	0.002	0.003	0.002	0.002	0.002
Ca	0.946	0.943	0.944	0.949	0.945	0.954	0.917	0.950	0.930	0.949
Nb	0.003	0.003	0.003	0.003	0.003	0.006	0.006	0.005	0.005	0.005
Sr	0.003	0.002	0.002	0.003	0.002	0.002	0.002	0.002	0.001	0.002
Zr	0.001	0.001	0.001	0.001	0.001	0.004	0.001	0.002	0.002	0.002
Th	0.001	0.001	0.001	0.001	0.001	0.000	0.001	0.000	0.000	0.000
Ti	0.926	0.952	0.951	0.949	0.949	0.958	0.964	0.966	0.959	0.965
Ba	0.000	0.000	0.000	0.000	0.000	0.000	0.000	0.000	0.000	0.000
Ce	0.016	0.023	0.023	0.022	0.023	0.017	0.029	0.017	0.019	0.017
Nd	0.006	0.009	0.009	0.008	0.009	0.006	0.012	0.007	0.007	0.006
Na	0.018	0.016	0.015	0.015	0.015	0.018	0.031	0.018	0.020	0.018
Mg	0.000	0.000	0.000	0.000	0.000	0.000	0.000	0.000	0.000	0.000
Al	0.000	0.000	0.000	0.000	0.000	0.000	0.000	0.000	0.000	0.000
Ta	0.000	0.000	0.000	0.000	0.000	0.000	0.000	0.000	0.000	0.000
Cations	2.009	2.006	2.006	2.008	2.007	2.006	2.001	2.004	1.996	2.003
<i>lueshite</i>	0.00	0.00	0.00	0.00	0.00	0.01	0.01	0.00	0.01	0.01
<i>loparite</i>	0.03	0.03	0.03	0.02	0.02	0.02	0.05	0.03	0.03	0.03
<i>REEFeO₃</i>	0.02	0.03	0.03	0.03	0.03	0.02	0.02	0.02	0.02	0.02
<i>tausonite</i>	0.00	0.00	0.00	0.00	0.00	0.00	0.00	0.00	0.00	0.00
<i>REE₂Ti₂O₇</i>	0.00	0.00	0.00	0.00	0.00	0.00	0.00	0.00	0.00	0.00
<i>lakargiite</i>	0.00	0.00	0.00	0.00	0.00	0.00	0.00	0.00	0.00	0.00
<i>perovskite</i>	0.94	0.93	0.94	0.94	0.94	0.94	0.91	0.94	0.94	0.94
<i>Fe/Nb</i>	16.08	16.99	15.95	15.04	14.87	4.72	4.30	5.69	5.44	5.35
<i>ANNO</i>	5.53	3.09	3.23	3.72	3.50	-0.78	-2.17	-1.53	-1.15	-1.07

TABELA B03 – Cont. Major element compositions and endmembers for perovskite from all samples. Structural formula calculated on the basis of 3 oxygens. C - core; R - rim; I – intermediated.

Sample Grain/Analysis Location	LMIC2 44/93 C	LMIC2 44/94 R	LMIC2 45/95 C	LMIC2 45/96 R	LMIC2 45/97 C	LMIC2 45/98 R	LMIC2 46/99 C	LMIC2 46/100 R	LMIC2 47/101 C	LMIC2 47/102 R
SiO ₂	0.00	0.00	0.00	0.00	0.00	0.00	0.00	0.00	0.00	0.00
Fe ₂ O ₃	1.43	1.38	1.55	1.56	1.32	1.53	1.31	1.41	1.62	1.95
La ₂ O ₃	1.46	1.22	1.78	1.71	1.54	1.67	1.27	0.98	1.30	1.15
Sm ₂ O ₃	0.23	0.20	0.25	0.22	0.22	0.20	0.21	0.15	0.18	0.15
Pr ₂ O ₃	0.56	0.45	0.64	0.50	0.54	0.48	0.48	0.31	0.43	0.30
CaO	34.02	35.11	33.01	33.85	34.08	34.41	34.54	37.06	35.37	36.39
Nb ₂ O ₅	0.64	0.56	1.40	1.13	1.09	1.09	0.53	0.43	0.85	0.83
SrO	0.15	0.13	0.16	0.14	0.13	0.16	0.13	0.14	0.14	0.12
ZrO ₂	0.12	0.11	0.14	0.17	0.11	0.16	0.09	0.12	0.17	0.34
ThO ₂	1.13	0.43	0.37	0.03	0.36	0.01	0.66	0.07	0.04	0.10
TiO ₂	53.04	53.43	52.12	52.05	53.02	52.61	53.52	54.98	53.08	52.98
BaO	0.00	0.00	0.00	0.00	0.00	0.00	0.00	0.00	0.00	0.00
Ce ₂ O ₃	4.64	3.82	5.30	4.58	4.53	4.43	3.97	2.69	3.54	2.79
Nd ₂ O ₃	2.12	1.72	2.27	1.82	1.91	1.79	1.85	1.15	1.48	1.06
Na ₂ O	0.98	0.81	1.08	1.01	1.06	0.99	0.82	0.57	0.68	0.53
MgO	0.00	0.00	0.00	0.00	0.00	0.00	0.00	0.00	0.00	0.00
Al ₂ O ₃	0.00	0.00	0.00	0.00	0.00	0.00	0.00	0.00	0.00	0.00
Ta ₂ O ₅	0.00	0.00	0.00	0.00	0.00	0.00	0.00	0.00	0.00	0.00
Total	100.54	99.38	100.08	98.77	99.91	99.52	99.37	100.06	98.89	98.69
Si	0.000	0.000	0.000	0.000	0.000	0.000	0.000	0.000	0.000	0.000
Fe	0.026	0.025	0.028	0.028	0.024	0.028	0.024	0.025	0.029	0.035
La	0.013	0.011	0.016	0.015	0.014	0.015	0.011	0.008	0.011	0.010
Sm	0.002	0.002	0.002	0.002	0.002	0.002	0.002	0.001	0.001	0.001
Pr	0.005	0.004	0.006	0.004	0.005	0.004	0.004	0.003	0.004	0.003
Ca	0.874	0.900	0.855	0.880	0.875	0.886	0.887	0.929	0.908	0.930
Nb	0.007	0.006	0.015	0.012	0.012	0.012	0.006	0.005	0.009	0.009
Sr	0.002	0.002	0.002	0.002	0.002	0.002	0.002	0.002	0.002	0.002
Zr	0.001	0.001	0.002	0.002	0.001	0.002	0.001	0.001	0.002	0.004
Th	0.006	0.002	0.002	0.000	0.002	0.000	0.004	0.000	0.000	0.001
Ti	0.956	0.962	0.947	0.950	0.956	0.951	0.965	0.968	0.956	0.951
Ba	0.000	0.000	0.000	0.000	0.000	0.000	0.000	0.000	0.000	0.000
Ce	0.041	0.033	0.047	0.041	0.040	0.039	0.035	0.023	0.031	0.024
Nd	0.018	0.015	0.020	0.016	0.016	0.015	0.016	0.010	0.013	0.009
Na	0.045	0.038	0.051	0.047	0.049	0.046	0.038	0.026	0.032	0.024
Mg	0.000	0.000	0.000	0.000	0.000	0.000	0.000	0.000	0.000	0.000
Al	0.000	0.000	0.000	0.000	0.000	0.000	0.000	0.000	0.000	0.000
Ta	0.000	0.000	0.000	0.000	0.000	0.000	0.000	0.000	0.000	0.000
Cations	1.996	2.000	1.992	2.000	1.998	2.001	1.995	2.001	1.999	2.002
<i>lueshite</i>	0.01	0.01	0.02	0.01	0.01	0.01	0.01	0.00	0.01	0.01
<i>loparite</i>	0.08	0.06	0.07	0.07	0.08	0.07	0.07	0.04	0.05	0.03
<i>REEFeO₃</i>	0.03	0.03	0.03	0.03	0.02	0.03	0.02	0.02	0.03	0.03
<i>tausonite</i>	0.00	0.00	0.00	0.00	0.00	0.00	0.00	0.00	0.00	0.00
<i>REE₂Ti₂O₇</i>	0.01	0.00	0.01	0.01	0.01	0.01	0.01	0.00	0.00	0.00
<i>lakargiite</i>	0.00	0.00	0.00	0.00	0.00	0.00	0.00	0.00	0.00	0.00
<i>perovskite</i>	0.88	0.90	0.87	0.88	0.88	0.88	0.90	0.93	0.91	0.92
<i>Fe/Nb</i>	3.71	4.11	1.84	2.30	2.02	2.34	4.16	5.46	3.18	3.89
<i>ANNO</i>	-1.92	-2.05	-2.37	-1.93	-3.03	-2.06	-2.28	-1.88	-1.35	0.13

TABELA B03 – Cont. Major element compositions and endmembers for perovskite from all samples. Structural formula calculated on the basis of 3 oxygens. C - core; R - rim; I – intermediated.

Sample Grain/Analysis Location	LMIC2 48/103	LMIC2 48/104	LMIC2 49/105	LMIC2 49/106	LMIC2 50/107	LMIC2 50/108	LMIC2 51/109	LMIC2 51/110	LMIC2 52/111	LMIC2 52/112
	C	R	C	R	C	R	C	R	C	R
SiO ₂	0.00	0.00	0.00	0.03	0.09	0.04	0.00	0.00	0.00	0.00
Fe ₂ O ₃	1.50	1.50	1.59	1.77	1.69	1.75	1.34	1.34	1.38	1.34
La ₂ O ₃	1.37	1.10	1.21	0.85	1.26	0.98	1.22	1.16	1.19	1.03
Sm ₂ O ₃	0.22	0.17	0.20	0.09	0.21	0.12	0.19	0.17	0.20	0.16
Pr ₂ O ₃	0.49	0.37	0.46	0.18	0.49	0.27	0.45	0.39	0.42	0.34
CaO	34.94	36.73	35.07	38.22	34.38	37.20	35.65	36.28	35.77	36.55
Nb ₂ O ₅	0.65	0.56	0.86	0.51	0.65	0.54	0.55	0.54	0.55	0.47
SrO	0.13	0.13	0.13	0.13	0.18	0.14	0.12	0.11	0.16	0.12
ZrO ₂	0.15	0.16	0.19	0.31	0.27	0.26	0.14	0.13	0.12	0.13
ThO ₂	0.49	0.06	0.53	0.01	0.90	0.07	0.19	0.09	0.33	0.08
TiO ₂	53.40	54.61	52.76	54.40	52.37	54.02	53.92	54.51	53.62	54.78
BaO	0.00	0.00	0.00	0.00	0.00	0.00	0.00	0.00	0.00	0.00
Ce ₂ O ₃	4.21	3.09	3.67	1.68	4.19	2.40	3.54	3.19	3.57	2.86
Nd ₂ O ₃	1.85	1.31	1.68	0.63	1.88	1.00	1.59	1.42	1.62	1.29
Na ₂ O	0.83	0.64	0.77	0.35	0.90	0.57	0.73	0.65	0.74	0.61
MgO	0.00	0.00	0.00	0.00	0.00	0.00	0.00	0.00	0.00	0.00
Al ₂ O ₃	0.00	0.00	0.00	0.00	0.00	0.00	0.00	0.00	0.00	0.00
Ta ₂ O ₅	0.00	0.00	0.00	0.00	0.00	0.00	0.00	0.00	0.00	0.00
Total	100.23	100.42	99.13	99.18	99.47	99.36	99.63	99.99	99.68	99.77
Si	0.000	0.000	0.000	0.001	0.002	0.001	0.000	0.000	0.000	0.000
Fe	0.027	0.026	0.029	0.031	0.031	0.031	0.024	0.024	0.025	0.024
La	0.012	0.009	0.011	0.007	0.011	0.009	0.011	0.010	0.010	0.009
Sm	0.002	0.001	0.002	0.001	0.002	0.001	0.002	0.001	0.002	0.001
Pr	0.004	0.003	0.004	0.002	0.004	0.002	0.004	0.003	0.004	0.003
Ca	0.892	0.922	0.902	0.959	0.888	0.939	0.907	0.916	0.912	0.921
Nb	0.007	0.006	0.009	0.005	0.007	0.006	0.006	0.006	0.006	0.005
Sr	0.002	0.002	0.002	0.002	0.003	0.002	0.002	0.002	0.002	0.002
Zr	0.002	0.002	0.002	0.004	0.003	0.003	0.002	0.001	0.001	0.001
Th	0.003	0.000	0.003	0.000	0.005	0.000	0.001	0.000	0.002	0.000
Ti	0.957	0.963	0.953	0.959	0.949	0.957	0.964	0.966	0.960	0.969
Ba	0.000	0.000	0.000	0.000	0.000	0.000	0.000	0.000	0.000	0.000
Ce	0.037	0.027	0.032	0.014	0.037	0.021	0.031	0.028	0.031	0.025
Nd	0.016	0.011	0.014	0.005	0.016	0.008	0.013	0.012	0.014	0.011
Na	0.038	0.029	0.036	0.016	0.042	0.026	0.034	0.030	0.034	0.028
Mg	0.000	0.000	0.000	0.000	0.000	0.000	0.000	0.000	0.000	0.000
Al	0.000	0.000	0.000	0.000	0.000	0.000	0.000	0.000	0.000	0.000
Ta	0.000	0.000	0.000	0.000	0.000	0.000	0.000	0.000	0.000	0.000
Cations	1.998	2.002	2.000	2.006	2.000	2.007	1.999	1.999	2.003	1.999
<i>lueshite</i>	0.01	0.01	0.01	0.01	0.01	0.01	0.01	0.01	0.01	0.00
<i>loparite</i>	0.06	0.05	0.05	0.02	0.07	0.04	0.06	0.05	0.06	0.05
<i>REEFeO₃</i>	0.03	0.03	0.03	0.02	0.03	0.02	0.02	0.02	0.02	0.02
<i>tausonite</i>	0.00	0.00	0.00	0.00	0.00	0.00	0.00	0.00	0.00	0.00
<i>REE₂Ti₂O₇</i>	0.01	0.00	0.00	0.00	0.00	0.00	0.00	0.00	0.00	0.00
<i>lakargiite</i>	0.00	0.00	0.00	0.00	0.00	0.00	0.00	0.00	0.00	0.00
<i>perovskite</i>	0.89	0.92	0.90	0.95	0.88	0.93	0.91	0.92	0.90	0.92
<i>Fe/Nb</i>	3.82	4.49	3.09	5.73	4.30	5.42	4.08	4.15	4.14	4.77
<i>ANNO</i>	-1.66	-1.62	-1.48	-0.38	-0.73	-0.46	-2.25	-2.27	-2.08	-2.18

TABELA B03 – Cont. Major element compositions and endmembers for perovskite from all samples. Structural formula calculated on the basis of 3 oxygens. C - core; R - rim; I – intermediated.

Sample Grain/Analysis Location	LMIC2 53/113	LMIC2 53/114	LMIC2 54/115	LMIC2 54/116	LMIC2 54/117	LMIC2 54/118	LMIC2 54/119	LMIC2 55/120	LMIC2 57/122	TR-4 01/01
	C	R	R	R	C	R	C	C	C	C
SiO ₂	0.00	0.00	0.00	0.00	0.00	0.15	0.00	0.00	0.04	0.00
Fe ₂ O ₃	1.54	1.60	1.47	1.44	1.46	1.79	1.62	1.57	1.56	1.21
La ₂ O ₃	1.18	1.21	1.59	1.33	1.49	1.56	1.49	1.28	1.34	2.77
Sm ₂ O ₃	0.19	0.18	0.21	0.19	0.23	0.22	0.24	0.19	0.23	0.20
Pr ₂ O ₃	0.39	0.39	0.55	0.44	0.48	0.44	0.57	0.40	0.51	0.65
CaO	35.63	35.56	34.42	35.52	34.53	34.49	33.63	35.62	33.81	30.11
Nb ₂ O ₅	0.87	0.87	1.16	0.87	1.15	1.14	1.01	0.58	0.61	0.99
SrO	0.13	0.14	0.18	0.14	0.15	0.17	0.14	0.14	0.15	0.74
ZrO ₂	0.17	0.18	0.15	0.15	0.17	0.22	0.11	0.12	0.12	0.07
ThO ₂	0.02	0.01	0.45	0.36	0.13	0.01	0.83	0.14	0.96	0.67
TiO ₂	53.36	53.18	54.06	54.29	53.42	51.29	52.03	53.54	52.57	50.80
BaO	0.00	0.00	0.00	0.00	0.00	0.00	0.00	0.00	0.00	0.00
Ce ₂ O ₃	3.47	3.49	4.66	3.75	4.32	3.85	4.58	3.40	4.32	6.68
Nd ₂ O ₃	1.49	1.44	1.98	1.66	1.83	1.53	2.11	1.46	2.01	2.16
Na ₂ O	0.71	0.72	1.07	0.78	0.84	0.68	0.93	0.64	0.89	1.83
MgO	0.00	0.00	0.00	0.00	0.00	0.00	0.00	0.00	0.00	0.00
Al ₂ O ₃	0.00	0.00	0.00	0.00	0.00	0.00	0.00	0.00	0.00	0.00
Ta ₂ O ₅	0.00	0.00	0.00	0.00	0.00	0.00	0.00	0.00	0.00	0.00
Total	99.15	98.98	101.95	100.92	100.20	97.55	99.31	99.08	99.14	98.89
Si	0.000	0.000	0.000	0.000	0.000	0.004	0.000	0.000	0.001	0.000
Fe	0.028	0.029	0.026	0.025	0.026	0.033	0.030	0.028	0.028	0.023
La	0.010	0.011	0.014	0.012	0.013	0.014	0.013	0.011	0.012	0.025
Sm	0.002	0.001	0.002	0.002	0.002	0.002	0.002	0.002	0.002	0.002
Pr	0.003	0.003	0.005	0.004	0.004	0.004	0.005	0.003	0.004	0.006
Ca	0.911	0.911	0.867	0.895	0.881	0.902	0.874	0.911	0.877	0.803
Nb	0.009	0.009	0.012	0.009	0.012	0.013	0.011	0.006	0.007	0.011
Sr	0.002	0.002	0.002	0.002	0.002	0.002	0.002	0.002	0.002	0.011
Zr	0.002	0.002	0.002	0.002	0.002	0.003	0.001	0.001	0.001	0.001
Th	0.000	0.000	0.002	0.002	0.001	0.000	0.005	0.001	0.005	0.004
Ti	0.957	0.956	0.956	0.961	0.957	0.942	0.950	0.961	0.957	0.951
Ba	0.000	0.000	0.000	0.000	0.000	0.000	0.000	0.000	0.000	0.000
Ce	0.030	0.031	0.040	0.032	0.038	0.034	0.041	0.030	0.038	0.061
Nd	0.013	0.012	0.017	0.014	0.016	0.013	0.018	0.012	0.017	0.019
Na	0.033	0.034	0.049	0.035	0.039	0.032	0.044	0.030	0.042	0.088
Mg	0.000	0.000	0.000	0.000	0.000	0.000	0.000	0.000	0.000	0.000
Al	0.000	0.000	0.000	0.000	0.000	0.000	0.000	0.000	0.000	0.000
Ta	0.000	0.000	0.000	0.000	0.000	0.000	0.000	0.000	0.000	0.000
Cations	2.000	2.001	1.994	1.995	1.992	1.998	1.995	1.999	1.995	2.004
<i>lueshite</i>	0.01	0.01	0.01	0.01	0.01	0.01	0.01	0.01	0.01	0.01
<i>loparite</i>	0.05	0.05	0.07	0.05	0.05	0.04	0.07	0.05	0.07	0.16
<i>REEFeO₃</i>	0.03	0.03	0.03	0.03	0.03	0.03	0.03	0.03	0.03	0.02
<i>tausonite</i>	0.00	0.00	0.00	0.00	0.00	0.00	0.00	0.00	0.00	0.01
<i>REE₂Ti₂O₇</i>	0.00	0.00	0.01	0.01	0.01	0.01	0.01	0.00	0.01	0.01
<i>lakargiite</i>	0.00	0.00	0.00	0.00	0.00	0.00	0.00	0.00	0.00	0.00
<i>perovskite</i>	0.91	0.91	0.88	0.90	0.89	0.90	0.88	0.91	0.88	0.79
<i>Fe/Nb</i>	2.96	3.06	2.10	2.75	2.11	2.60	2.67	4.50	4.27	2.04
<i>ANNO</i>	-1.76	-1.48	-2.54	-2.29	-2.51	-0.86	-1.49	-1.23	-1.23	-3.21

TABELA B03 – Cont. Major element compositions and endmembers for perovskite from all samples. Structural formula calculated on the basis of 3 oxygens. C - core; R - rim; I – intermediated.

Sample Grain/Analysis Location	TR-4 01/02 R	TR-4 02/03 C	TR-4 02/04 R	TR-4 03/05 C	TR-4 03/06 R	TR-4 04/07 C	TR-4 04/08 R	TR-4 05/09 C	TR-4 05/10 R	TR-4 06/11 C	TR-4 06/12 R
SiO ₂	0.00	0.00	0.00	0.00	0.00	0.00	0.00	0.00	0.00	0.00	0.00
Fe ₂ O ₃	1.21	1.72	1.94	1.47	1.49	1.67	1.59	1.33	1.38	1.60	1.62
La ₂ O ₃	2.37	3.27	3.07	3.22	3.30	3.24	3.60	3.35	3.58	3.29	3.26
Sm ₂ O ₃	0.17	0.21	0.20	0.20	0.21	0.21	0.23	0.22	0.23	0.22	0.22
Pr ₂ O ₃	0.50	0.77	0.69	0.76	0.75	0.66	0.79	0.78	0.81	0.77	0.77
CaO	32.62	28.06	29.21	27.35	27.50	29.14	26.86	27.73	27.78	28.16	27.76
Nb ₂ O ₅	0.92	1.57	1.18	2.73	2.62	1.76	1.90	1.62	1.69	1.50	1.67
SrO	0.74	0.73	0.75	0.78	0.80	0.77	0.78	0.77	0.86	0.78	0.75
ZrO ₂	0.09	0.17	0.10	0.24	0.22	0.23	0.22	0.13	0.14	0.15	0.16
ThO ₂	0.21	1.32	0.65	1.19	1.27	0.17	0.71	0.80	0.78	1.33	1.49
TiO ₂	52.37	49.15	49.33	48.17	48.42	49.63	48.78	49.91	50.11	49.20	48.66
BaO	0.00	0.00	0.00	0.00	0.00	0.00	0.00	0.00	0.00	0.00	0.00
Ce ₂ O ₃	5.35	7.81	6.95	7.65	7.88	6.84	8.20	7.99	8.24	7.81	7.90
Nd ₂ O ₃	1.72	2.47	2.21	2.40	2.45	2.12	2.54	2.56	2.61	2.50	2.53
Na ₂ O	1.49	2.09	1.79	2.39	2.42	2.15	2.52	2.31	2.29	2.11	2.13
MgO	0.00	0.00	0.00	0.00	0.00	0.00	0.00	0.00	0.00	0.00	0.00
Al ₂ O ₃	0.00	0.00	0.00	0.00	0.00	0.00	0.00	0.00	0.00	0.00	0.00
Ta ₂ O ₅	0.00	0.00	0.00	0.00	0.00	0.00	0.00	0.00	0.00	0.00	0.00
Total	99.76	99.35	98.07	98.55	99.33	98.60	98.72	99.50	100.49	99.43	98.92
Si	0.000	0.000	0.000	0.000	0.000	0.000	0.000	0.000	0.000	0.000	0.000
Fe	0.022	0.033	0.037	0.028	0.028	0.031	0.030	0.025	0.026	0.030	0.031
La	0.021	0.030	0.029	0.030	0.031	0.030	0.034	0.031	0.033	0.031	0.031
Sm	0.001	0.002	0.002	0.002	0.002	0.002	0.002	0.002	0.002	0.002	0.002
Pr	0.004	0.007	0.006	0.007	0.007	0.006	0.007	0.007	0.007	0.007	0.007
Ca	0.847	0.759	0.790	0.746	0.746	0.782	0.732	0.746	0.742	0.761	0.756
Nb	0.010	0.018	0.013	0.031	0.030	0.020	0.022	0.018	0.019	0.017	0.019
Sr	0.010	0.011	0.011	0.011	0.012	0.011	0.012	0.011	0.012	0.011	0.011
Zr	0.001	0.002	0.001	0.003	0.003	0.003	0.003	0.002	0.002	0.002	0.002
Th	0.001	0.008	0.004	0.007	0.007	0.001	0.004	0.005	0.004	0.008	0.009
Ti	0.955	0.933	0.937	0.922	0.922	0.935	0.933	0.943	0.940	0.934	0.930
Ba	0.000	0.000	0.000	0.000	0.000	0.000	0.000	0.000	0.000	0.000	0.000
Ce	0.047	0.072	0.064	0.071	0.073	0.063	0.076	0.073	0.075	0.072	0.074
Nd	0.015	0.022	0.020	0.022	0.022	0.019	0.023	0.023	0.023	0.023	0.023
Na	0.070	0.102	0.088	0.118	0.119	0.104	0.124	0.112	0.111	0.103	0.105
Mg	0.000	0.000	0.000	0.000	0.000	0.000	0.000	0.000	0.000	0.000	0.000
Al	0.000	0.000	0.000	0.000	0.000	0.000	0.000	0.000	0.000	0.000	0.000
Ta	0.000	0.000	0.000	0.000	0.000	0.000	0.000	0.000	0.000	0.000	0.000
Cations	2.007	1.998	2.003	1.999	2.001	2.008	2.003	1.999	1.997	2.001	1.999
<i>lueshite</i>	0.01	0.02	0.01	0.03	0.03	0.02	0.02	0.02	0.02	0.02	0.02
<i>loparite</i>	0.12	0.17	0.15	0.18	0.18	0.17	0.21	0.19	0.19	0.18	0.18
<i>REE₂O₃</i>	0.02	0.03	0.04	0.03	0.03	0.03	0.03	0.03	0.03	0.03	0.03
<i>tausonite</i>	0.01	0.01	0.01	0.01	0.01	0.01	0.01	0.01	0.01	0.01	0.01
<i>REE₂Ti₂O₇</i>	0.00	0.01	0.00	0.01	0.01	0.00	0.00	0.01	0.01	0.01	0.01
<i>lakargiite</i>	0.00	0.00	0.00	0.00	0.00	0.00	0.00	0.00	0.00	0.00	0.00
<i>perovskite</i>	0.83	0.75	0.78	0.74	0.73	0.76	0.72	0.74	0.74	0.75	0.75
Fe/Nb	2.20	1.82	2.74	0.90	0.95	1.58	1.39	1.36	1.36	1.78	1.61
ANNO	-3.22	-1.57	0.03	-4.39	-4.15	-2.12	-2.62	-3.54	-3.43	-2.05	-2.15

TABELA B03 – Cont. Major element compositions and endmembers for perovskite from all samples. Structural formula calculated on the basis of 3 oxygens. C - core; R - rim; I – intermediated.

Sample Grain/Analysis	TR-4 07/13	TR-4 07/14	TR-4 08/15	TR-4 08/16	TR-4 09/17	TR-4 09/18	TR-4 10/19	TR-4 10/20	TR4-1 11/21	TR4-1 11/22	TR4-1 12/23
Location	C	R	C	R	C	R	C	R	C	R	C
SiO ₂	0.00	0.00	0.00	0.00	0.00	0.00	0.00	0.00	0.00	0.00	0.00
Fe ₂ O ₃	1.34	1.35	1.19	1.23	1.96	1.47	1.37	1.29	1.75	1.68	1.76
La ₂ O ₃	3.11	3.01	2.76	2.19	3.36	3.40	1.30	1.01	2.83	3.20	3.43
Sm ₂ O ₃	0.22	0.21	0.18	0.16	0.22	0.22	0.11	0.09	0.19	0.20	0.22
Pr ₂ O ₃	0.70	0.66	0.67	0.42	0.77	0.74	0.34	0.18	0.64	0.67	0.83
CaO	29.19	29.99	30.41	33.78	26.10	28.36	35.67	36.86	29.76	29.59	26.12
Nb ₂ O ₅	1.72	1.69	0.96	1.01	2.47	1.84	0.54	0.50	2.38	1.72	2.75
SrO	0.77	0.76	0.70	0.71	0.78	0.76	0.52	0.53	0.82	0.82	0.82
ZrO ₂	0.15	0.14	0.04	0.09	0.25	0.18	0.04	0.06	0.27	0.16	0.35
ThO ₂	0.49	0.30	0.78	0.08	1.51	0.56	0.21	0.05	0.28	0.15	2.21
TiO ₂	49.88	50.28	51.07	52.95	47.35	49.54	53.46	55.15	49.57	50.19	47.58
BaO	0.00	0.00	0.00	0.00	0.00	0.00	0.00	0.00	0.00	0.00	0.00
Ce ₂ O ₃	7.09	6.79	6.53	4.59	8.00	7.64	3.00	1.96	6.42	6.96	8.45
Nd ₂ O ₃	2.27	2.16	2.15	1.46	2.49	2.39	1.05	0.66	2.02	2.17	2.65
Na ₂ O	1.94	1.80	1.73	1.16	2.33	2.19	0.87	0.73	2.00	2.01	2.54
MgO	0.00	0.00	0.00	0.00	0.00	0.00	0.00	0.00	0.00	0.00	0.00
Al ₂ O ₃	0.00	0.00	0.00	0.00	0.00	0.00	0.00	0.00	0.00	0.00	0.00
Ta ₂ O ₅	0.00	0.00	0.00	0.00	0.00	0.00	0.00	0.00	0.00	0.00	0.00
Total	98.86	99.14	99.18	99.84	97.60	99.30	98.47	99.05	98.92	99.51	99.72
Si	0.000	0.000	0.000	0.000	0.000	0.000	0.000	0.000	0.000	0.000	0.000
Fe	0.025	0.025	0.022	0.022	0.038	0.028	0.025	0.023	0.033	0.031	0.034
La	0.029	0.028	0.025	0.019	0.032	0.031	0.011	0.009	0.026	0.029	0.032
Sm	0.002	0.002	0.002	0.001	0.002	0.002	0.001	0.001	0.002	0.002	0.002
Pr	0.006	0.006	0.006	0.004	0.007	0.007	0.003	0.002	0.006	0.006	0.008
Ca	0.783	0.799	0.807	0.869	0.723	0.763	0.915	0.928	0.793	0.787	0.715
Nb	0.019	0.019	0.011	0.011	0.029	0.021	0.006	0.005	0.027	0.019	0.032
Sr	0.011	0.011	0.010	0.010	0.012	0.011	0.007	0.007	0.012	0.012	0.012
Zr	0.002	0.002	0.001	0.001	0.003	0.002	0.000	0.001	0.003	0.002	0.004
Th	0.003	0.002	0.004	0.000	0.009	0.003	0.001	0.000	0.002	0.001	0.013
Ti	0.940	0.940	0.952	0.957	0.921	0.935	0.963	0.975	0.928	0.937	0.914
Ba	0.000	0.000	0.000	0.000	0.000	0.000	0.000	0.000	0.000	0.000	0.000
Ce	0.065	0.062	0.059	0.040	0.076	0.070	0.026	0.017	0.058	0.063	0.079
Nd	0.020	0.019	0.019	0.013	0.023	0.021	0.009	0.006	0.018	0.019	0.024
Na	0.094	0.087	0.083	0.054	0.117	0.107	0.040	0.033	0.096	0.097	0.126
Mg	0.000	0.000	0.000	0.000	0.000	0.000	0.000	0.000	0.000	0.000	0.000
Al	0.000	0.000	0.000	0.000	0.000	0.000	0.000	0.000	0.000	0.000	0.000
Ta	0.000	0.000	0.000	0.000	0.000	0.000	0.000	0.000	0.000	0.000	0.000
Cations	2.000	2.001	2.002	2.002	1.993	2.001	2.009	2.005	2.004	2.005	1.995
<i>lueshite</i>	0.02	0.02	0.01	0.01	0.03	0.02	0.01	0.01	0.03	0.02	0.03
<i>loparite</i>	0.15	0.14	0.15	0.09	0.18	0.18	0.07	0.06	0.14	0.16	0.19
<i>REEFeO₃</i>	0.03	0.03	0.02	0.02	0.04	0.03	0.02	0.01	0.03	0.03	0.03
<i>tausonite</i>	0.01	0.01	0.01	0.01	0.01	0.01	0.01	0.01	0.01	0.01	0.01
<i>REE₂Ti₂O₇</i>	0.01	0.01	0.01	0.01	0.01	0.01	0.00	0.00	0.00	0.01	0.01
<i>lakargiite</i>	0.00	0.00	0.00	0.00	0.00	0.00	0.00	0.00	0.00	0.00	0.00
<i>perovskite</i>	0.78	0.79	0.80	0.86	0.73	0.75	0.90	0.92	0.78	0.77	0.71
<i>Fe/Nb</i>	1.29	1.33	2.08	2.03	1.32	1.33	4.24	4.28	1.22	1.63	1.07
<i>ANNO</i>	-3.64	-3.58	-3.27	-3.30	-1.57	-3.17	-2.06	-2.45	-2.65	-2.07	-3.01

TABELA B03 – Cont. Major element compositions and endmembers for perovskite from all samples. Structural formula calculated on the basis of 3 oxygens. C - core; R - rim; I – intermediately.

Sample Grain/Analysis Location	TR4-1 12/24 R	TR4-1 13/25 C	TR4-1 13/25 C	TR4-1 13/26 R	TR4-1 14/27 C	TR4-1 14/28 R	TR4-1 15/29 C	TR4-1 16/30 C	TR4-1 16/31 R	TR4-1 17/32 C
SiO ₂	0.00	0.00	0.00	0.00	0.00	0.04	0.00	0.00	0.00	0.00
Fe ₂ O ₃	1.73	1.39	1.39	1.48	1.65	1.63	1.66	1.46	1.63	2.19
La ₂ O ₃	3.60	3.26	3.26	3.31	3.14	3.25	2.92	3.23	2.55	3.51
Sm ₂ O ₃	0.23	0.22	0.22	0.23	0.21	0.22	0.21	0.20	0.18	0.24
Pr ₂ O ₃	0.83	0.82	0.82	0.82	0.74	0.82	0.58	0.76	0.50	0.77
CaO	27.02	26.42	26.42	27.06	27.77	26.58	30.63	27.24	31.74	26.42
Nb ₂ O ₅	2.25	1.58	1.58	2.05	2.36	2.78	1.26	2.87	1.66	2.14
SrO	0.78	0.72	0.72	0.73	0.77	0.79	0.76	0.76	0.76	0.80
ZrO ₂	0.28	0.14	0.14	0.20	0.30	0.33	0.13	0.30	0.19	0.26
ThO ₂	1.34	2.60	2.60	2.11	0.99	1.90	0.25	1.45	0.11	0.95
TiO ₂	48.19	48.88	48.88	48.94	48.49	47.89	51.37	48.88	50.73	47.91
BaO	0.00	0.00	0.00	0.00	0.00	0.00	0.00	0.00	0.00	0.00
Ce ₂ O ₃	8.40	8.38	8.38	8.40	7.51	8.06	6.44	7.87	5.36	8.20
Nd ₂ O ₃	2.59	2.76	2.76	2.70	2.37	2.56	2.03	2.46	1.69	2.55
Na ₂ O	2.44	2.64	2.64	2.52	2.41	2.61	1.78	2.52	1.55	2.48
MgO	0.00	0.00	0.00	0.00	0.00	0.00	0.00	0.00	0.00	0.00
Al ₂ O ₃	0.00	0.00	0.00	0.00	0.00	0.00	0.00	0.00	0.00	0.00
Ta ₂ O ₅	0.00	0.00	0.00	0.00	0.00	0.00	0.00	0.00	0.00	0.00
Total	99.68	99.80	99.80	100.53	98.73	99.45	100.01	99.99	98.65	98.42
Si	0.000	0.000	0.000	0.000	0.000	0.001	0.000	0.000	0.000	0.000
Fe	0.033	0.027	0.027	0.028	0.031	0.031	0.031	0.028	0.030	0.042
La	0.034	0.031	0.031	0.031	0.029	0.030	0.026	0.030	0.023	0.033
Sm	0.002	0.002	0.002	0.002	0.002	0.002	0.002	0.002	0.002	0.002
Pr	0.008	0.008	0.008	0.008	0.007	0.008	0.005	0.007	0.005	0.007
Ca	0.735	0.720	0.720	0.730	0.754	0.725	0.804	0.733	0.837	0.725
Nb	0.026	0.018	0.018	0.023	0.027	0.032	0.014	0.033	0.018	0.025
Sr	0.011	0.011	0.011	0.011	0.011	0.012	0.011	0.011	0.011	0.012
Zr	0.003	0.002	0.002	0.002	0.004	0.004	0.001	0.004	0.002	0.003
Th	0.008	0.015	0.015	0.012	0.006	0.011	0.001	0.008	0.001	0.006
Ti	0.920	0.935	0.935	0.927	0.924	0.917	0.947	0.924	0.940	0.923
Ba	0.000	0.000	0.000	0.000	0.000	0.000	0.000	0.000	0.000	0.000
Ce	0.078	0.078	0.078	0.077	0.070	0.075	0.058	0.072	0.048	0.077
Nd	0.023	0.025	0.025	0.024	0.021	0.023	0.018	0.022	0.015	0.023
Na	0.120	0.130	0.130	0.123	0.118	0.129	0.085	0.123	0.074	0.123
Mg	0.000	0.000	0.000	0.000	0.000	0.000	0.000	0.000	0.000	0.000
Al	0.000	0.000	0.000	0.000	0.000	0.000	0.000	0.000	0.000	0.000
Ta	0.000	0.000	0.000	0.000	0.000	0.000	0.000	0.000	0.000	0.000
Cations	2.001	2.001	2.001	2.000	2.005	1.999	2.002	1.996	2.006	2.001
<i>lueshite</i>	0.03	0.02	0.02	0.03	0.03	0.01	0.03	0.02	0.02	0.02
<i>loparite</i>	0.19	0.23	0.20	0.19	0.20	0.14	0.18	0.11	0.20	0.18
<i>REEFeO₃</i>	0.03	0.03	0.03	0.03	0.03	0.03	0.03	0.03	0.04	0.03
<i>tausonite</i>	0.01	0.01	0.01	0.01	0.01	0.01	0.01	0.01	0.01	0.01
<i>REE₂Ti₂O₇</i>	0.01	0.00	0.01	0.00	0.01	0.00	0.01	0.00	0.00	0.01
<i>lakargiite</i>	0.00	0.00	0.00	0.00	0.00	0.00	0.00	0.00	0.00	0.00
<i>perovskite</i>	0.72	0.71	0.72	0.74	0.72	0.80	0.73	0.82	0.72	0.76
<i>Fe/Nb</i>	1.28	1.46	1.46	1.20	1.16	0.98	2.18	0.85	1.63	1.70
<i>ANNO</i>	-2.47	-3.12	-3.12	-3.40	-3.01	-3.70	-1.60	-4.67	-2.26	-0.05

TABELA B03 – Cont. Major element compositions and endmembers for perovskite from all samples. Structural formula calculated on the basis of 3 oxygens. C - core; R - rim; I – intermediated.

Sample Grain/Analysis Location	TR4-1 18/33	TR4-1 18/34	TR4-1 19/35	TR4-1 19/36	TR4-2 20/37	TR4-2 20/38	TR4-2 21/39	TR4-2 21/40	TR4-2 22/41	TR4-2 22/42	TR4-2 23/43
	C	R	C	R	C	R	C	R	C	R	C
SiO ₂	0.00	0.00	0.00	0.00	0.00	0.00	0.00	0.00	0.00	0.00	0.59
Fe ₂ O ₃	1.62	1.52	1.67	1.64	1.57	1.82	1.53	1.57	1.76	1.69	2.00
La ₂ O ₃	3.15	2.83	3.13	3.17	3.38	2.57	3.14	2.70	2.87	3.08	3.49
Sm ₂ O ₃	0.21	0.20	0.22	0.21	0.22	0.18	0.20	0.19	0.21	0.19	0.22
Pr ₂ O ₃	0.77	0.63	0.76	0.76	0.79	0.49	0.76	0.57	0.60	0.66	0.81
CaO	28.09	30.58	28.14	28.58	26.31	31.81	28.52	30.62	29.92	29.65	24.76
Nb ₂ O ₅	1.35	1.02	1.48	1.30	1.65	1.46	1.16	0.98	2.03	1.64	2.39
SrO	0.72	0.73	0.78	0.81	0.74	0.82	0.77	0.72	0.77	0.76	0.75
ZrO ₂	0.14	0.10	0.15	0.14	0.15	0.20	0.12	0.09	0.27	0.19	0.28
ThO ₂	1.22	0.54	1.30	1.18	1.18	0.06	1.13	0.30	0.14	0.13	2.07
TiO ₂	49.61	51.12	49.73	49.75	48.76	50.97	50.65	50.89	50.34	50.21	47.47
BaO	0.00	0.00	0.00	0.00	0.00	0.00	0.00	0.00	0.00	0.00	0.00
Ce ₂ O ₃	7.64	6.49	7.74	7.58	8.11	5.21	7.55	5.83	6.55	6.80	8.48
Nd ₂ O ₃	2.49	2.11	2.50	2.45	2.60	1.67	2.42	1.85	2.08	2.16	2.66
Na ₂ O	2.09	1.83	2.14	2.07	2.64	1.46	2.20	1.77	2.08	1.99	2.78
MgO	0.00	0.00	0.00	0.00	0.00	0.00	0.00	0.00	0.00	0.00	0.00
Al ₂ O ₃	0.00	0.00	0.00	0.00	0.00	0.00	0.00	0.00	0.00	0.00	0.00
Ta ₂ O ₅	0.00	0.00	0.00	0.00	0.00	0.00	0.00	0.00	0.00	0.00	0.00
Total	99.08	99.69	99.75	99.63	98.10	98.74	100.15	98.09	99.61	99.14	98.75
Si	0.000	0.000	0.000	0.000	0.000	0.000	0.000	0.000	0.000	0.000	0.015
Fe	0.031	0.028	0.032	0.031	0.030	0.034	0.029	0.029	0.033	0.032	0.039
La	0.029	0.026	0.029	0.029	0.032	0.023	0.029	0.025	0.026	0.028	0.033
Sm	0.002	0.002	0.002	0.002	0.002	0.002	0.002	0.002	0.002	0.002	0.002
Pr	0.007	0.006	0.007	0.007	0.007	0.004	0.007	0.005	0.005	0.006	0.008
Ca	0.759	0.807	0.756	0.767	0.722	0.837	0.759	0.815	0.791	0.789	0.680
Nb	0.015	0.011	0.017	0.015	0.019	0.016	0.013	0.011	0.023	0.018	0.028
Sr	0.010	0.010	0.011	0.012	0.011	0.012	0.011	0.010	0.011	0.011	0.011
Zr	0.002	0.001	0.002	0.002	0.002	0.002	0.002	0.001	0.003	0.002	0.003
Th	0.007	0.003	0.007	0.007	0.007	0.000	0.006	0.002	0.001	0.001	0.012
Ti	0.941	0.947	0.938	0.938	0.940	0.942	0.947	0.951	0.934	0.939	0.916
Ba	0.000	0.000	0.000	0.000	0.000	0.000	0.000	0.000	0.000	0.000	0.000
Ce	0.071	0.059	0.071	0.070	0.076	0.047	0.069	0.053	0.059	0.062	0.080
Nd	0.022	0.019	0.022	0.022	0.024	0.015	0.021	0.016	0.018	0.019	0.024
Na	0.102	0.087	0.104	0.101	0.131	0.070	0.106	0.085	0.099	0.096	0.138
Mg	0.000	0.000	0.000	0.000	0.000	0.000	0.000	0.000	0.000	0.000	0.000
Al	0.000	0.000	0.000	0.000	0.000	0.000	0.000	0.000	0.000	0.000	0.000
Ta	0.000	0.000	0.000	0.000	0.000	0.000	0.000	0.000	0.000	0.000	0.000
Cations	1.998	2.006	1.998	2.002	2.003	2.004	2.001	2.007	2.006	2.005	1.989
<i>lueshite</i>	0.01	0.02	0.02	0.02	0.02	0.01	0.01	0.02	0.02	0.03	0.02
<i>loparite</i>	0.15	0.18	0.18	0.23	0.11	0.19	0.15	0.15	0.16	0.22	0.15
<i>REEFeO₃</i>	0.03	0.03	0.03	0.03	0.03	0.03	0.03	0.03	0.03	0.04	0.03
<i>tausonite</i>	0.01	0.01	0.01	0.01	0.01	0.01	0.01	0.01	0.01	0.01	0.01
<i>REE₂Ti₂O₇</i>	0.00	0.01	0.01	0.00	0.00	0.00	0.00	0.00	0.00	0.00	0.00
<i>lakargiite</i>	0.00	0.00	0.00	0.00	0.00	0.00	0.00	0.00	0.00	0.00	0.00
<i>perovskite</i>	0.79	0.75	0.76	0.71	0.83	0.75	0.80	0.77	0.78	0.69	0.77
<i>Fe/Nb</i>	2.00	2.49	1.88	2.10	1.58	2.07	2.19	2.68	1.44	1.72	1.39
<i>ANNO</i>	-1.74	-1.87	-1.72	-1.60	-2.32	-1.12	-1.98	-1.53	-2.16	-1.90	-1.32

TABELA B03 – Cont. Major element compositions and endmembers for perovskite from all samples. Structural formula calculated on the basis of 3 oxygens. C - core; R - rim; I – intermediately.

Sample Grain/Analysis Location	TR4-2 24/45 C	TR4-2 24/46 R	TRIV-5 25/47 C	TRIV-5 25/48 R	TRIV-5 26/49 C	TRIV-5 26/50 R	TRIV-5 27/51 C	TRIV-5 27/52 R	TRIV-5 28/53 C
SiO ₂	0.00	0.00	0.00	0.72	0.00	0.00	0.01	0.00	0.00
Fe ₂ O ₃	1.59	1.48	2.22	2.54	1.61	1.56	1.62	1.62	1.78
La ₂ O ₃	3.46	3.12	2.31	2.11	2.99	2.76	1.60	1.52	2.65
Sm ₂ O ₃	0.24	0.21	0.17	0.14	0.21	0.19	0.13	0.12	0.18
Pr ₂ O ₃	0.86	0.74	0.40	0.34	0.66	0.58	0.37	0.33	0.54
CaO	25.37	28.11	33.13	33.12	30.13	31.47	35.40	34.86	31.26
Nb ₂ O ₅	2.24	1.70	1.10	1.18	1.10	1.09	0.45	0.43	1.07
SrO	0.76	0.70	0.29	0.32	0.29	0.25	0.22	0.21	0.27
ZrO ₂	0.21	0.14	0.17	0.26	0.11	0.12	0.05	0.03	0.16
ThO ₂	2.46	0.79	0.03	0.02	0.21	0.14	0.30	0.27	0.05
TiO ₂	47.91	49.51	52.12	51.12	51.27	52.31	53.85	53.52	51.74
BaO	0.00	0.00	0.00	0.00	0.00	0.00	0.00	0.00	0.00
Ce ₂ O ₃	8.56	7.41	4.45	3.72	6.69	6.18	3.38	3.31	5.65
Nd ₂ O ₃	2.72	2.38	1.33	1.08	2.05	1.87	1.20	1.16	1.78
Na ₂ O	2.84	2.16	1.36	1.14	1.88	1.77	0.88	0.96	1.69
MgO	0.00	0.00	0.00	0.00	0.00	0.00	0.00	0.00	0.00
Al ₂ O ₃	0.00	0.00	0.00	0.00	0.00	0.00	0.00	0.00	0.00
Ta ₂ O ₅	0.00	0.00	0.00	0.00	0.00	0.00	0.00	0.00	0.00
Total	99.22	98.46	99.09	97.80	99.21	100.29	99.45	98.33	98.83
Si	0.000	0.000	0.000	0.017	0.000	0.000	0.000	0.000	0.000
Fe	0.031	0.028	0.040	0.046	0.030	0.028	0.029	0.029	0.033
La	0.033	0.029	0.021	0.019	0.027	0.025	0.014	0.013	0.024
Sm	0.002	0.002	0.001	0.001	0.002	0.002	0.001	0.001	0.002
Pr	0.008	0.007	0.004	0.003	0.006	0.005	0.003	0.003	0.005
Ca	0.698	0.761	0.858	0.861	0.797	0.817	0.902	0.897	0.821
Nb	0.026	0.019	0.012	0.013	0.012	0.012	0.005	0.005	0.012
Sr	0.011	0.010	0.004	0.005	0.004	0.004	0.003	0.003	0.004
Zr	0.003	0.002	0.002	0.003	0.001	0.001	0.001	0.000	0.002
Th	0.014	0.005	0.000	0.000	0.001	0.001	0.002	0.001	0.000
Ti	0.926	0.941	0.948	0.933	0.952	0.954	0.964	0.967	0.954
Ba	0.000	0.000	0.000	0.000	0.000	0.000	0.000	0.000	0.000
Ce	0.081	0.069	0.039	0.033	0.060	0.055	0.029	0.029	0.051
Nd	0.025	0.021	0.011	0.009	0.018	0.016	0.010	0.010	0.016
Na	0.141	0.106	0.064	0.054	0.090	0.083	0.040	0.045	0.080
Mg	0.000	0.000	0.000	0.000	0.000	0.000	0.000	0.000	0.000
Al	0.000	0.000	0.000	0.000	0.000	0.000	0.000	0.000	0.000
Ta	0.000	0.000	0.000	0.000	0.000	0.000	0.000	0.000	0.000
Cations	1.999	1.999	2.01	2.00	2.001	2.002	2.004	2.004	2.002
<i>lueshite</i>	0.03	0.02	0.01	0.01	0.01	0.01	0.00	0.00	0.01
<i>loparite</i>	0.23	0.18	0.10	0.08	0.16	0.14	0.07	0.08	0.14
<i>REE₂O₃</i>	0.03	0.03	0.03	0.03	0.03	0.03	0.02	0.02	0.03
<i>tausonite</i>	0.01	0.01	0.00	0.00	0.00	0.00	0.00	0.00	0.00
<i>REE₂Ti₂O₇</i>	0.00	0.01	0.00	0.00	0.00	0.00	0.00	0.00	0.00
<i>lakargiite</i>	0.00	0.00	0.00	0.00	0.00	0.00	0.00	0.00	0.00
<i>perovskite</i>	0.69	0.76	0.85	0.87	0.79	0.81	0.90	0.89	0.82
Fe/Nb	1.18	1.45	3.36	3.59	2.43	2.39	6.00	6.33	2.76
ΔANNO	-3.07	-2.89	1.09	2.48	-1.57	-1.87	-0.85	-0.76	-0.78

TABELA B03 – Cont. Major element compositions and endmembers for perovskite from all samples. Structural formula calculated on the basis of 3 oxygens. C - core; R - rim; I – intermediated.

Sample Grain/Analysis Location	TRIV-5 29/54 C	TRIV-5 29/55 R	TRIV-5 30/56 C	TRIV-5 30/57 R	TRIV-5 31/58 C	TRIV-5 31/59 R	TRIV-5 32/60 C	TRIV-5 32/61 R	TRIV-5 33/62 C
SiO ₂	0.21	1.20	0.00	0.09	0.00	0.00	0.00	0.00	0.00
Fe ₂ O ₃	2.00	2.72	1.79	2.32	1.57	1.99	1.58	1.74	1.81
La ₂ O ₃	3.06	2.51	3.51	2.87	2.92	2.36	2.66	2.38	2.53
Sm ₂ O ₃	0.20	0.15	0.23	0.19	0.19	0.16	0.18	0.16	0.18
Pr ₂ O ₃	0.66	0.43	0.80	0.56	0.62	0.43	0.58	0.45	0.50
CaO	28.50	32.53	27.31	30.64	30.52	33.47	31.43	32.71	32.37
Nb ₂ O ₅	1.45	1.68	1.65	1.45	1.00	1.11	0.86	0.87	1.00
SrO	0.29	0.36	0.28	0.27	0.29	0.32	0.29	0.28	0.30
ZrO ₂	0.15	0.59	0.19	0.35	0.10	0.16	0.09	0.09	0.12
ThO ₂	0.35	0.04	0.87	0.03	0.34	0.04	0.19	0.04	0.13
TiO ₂	49.68	50.57	49.48	50.01	51.46	52.44	52.18	52.15	52.50
BaO	0.00	0.00	0.00	0.00	0.00	0.00	0.00	0.00	0.00
Ce ₂ O ₃	6.97	4.56	8.21	5.71	6.47	4.68	5.87	4.88	5.40
Nd ₂ O ₃	2.12	1.34	2.59	1.75	2.08	1.43	1.87	1.52	1.69
Na ₂ O	2.11	1.29	2.38	1.54	1.78	1.28	1.68	1.40	1.54
MgO	0.00	0.00	0.00	0.00	0.00	0.00	0.00	0.00	0.00
Al ₂ O ₃	0.00	0.00	0.00	0.00	0.00	0.00	0.00	0.00	0.00
Ta ₂ O ₅	0.00	0.00	0.00	0.00	0.00	0.00	0.00	0.00	0.00
Total	97.76	99.99	99.28	97.79	99.33	99.86	99.45	98.66	100.07
Si	0.005	0.029	0.000	0.002	0.000	0.000	0.000	0.000	0.000
Fe	0.038	0.049	0.034	0.043	0.029	0.036	0.029	0.032	0.033
La	0.028	0.022	0.033	0.026	0.027	0.021	0.024	0.021	0.023
Sm	0.002	0.001	0.002	0.002	0.002	0.001	0.002	0.001	0.002
Pr	0.006	0.004	0.007	0.005	0.006	0.004	0.005	0.004	0.004
Ca	0.768	0.835	0.737	0.817	0.805	0.862	0.821	0.853	0.837
Nb	0.016	0.018	0.019	0.016	0.011	0.012	0.009	0.010	0.011
Sr	0.004	0.005	0.004	0.004	0.004	0.005	0.004	0.004	0.004
Zr	0.002	0.007	0.002	0.004	0.001	0.002	0.001	0.001	0.001
Th	0.002	0.000	0.005	0.000	0.002	0.000	0.001	0.000	0.001
Ti	0.940	0.911	0.938	0.936	0.953	0.948	0.957	0.955	0.953
Ba	0.000	0.000	0.000	0.000	0.000	0.000	0.000	0.000	0.000
Ce	0.064	0.040	0.076	0.052	0.058	0.041	0.052	0.043	0.048
Nd	0.019	0.011	0.023	0.016	0.018	0.012	0.016	0.013	0.015
Na	0.103	0.060	0.116	0.074	0.085	0.060	0.079	0.066	0.072
Mg	0.000	0.000	0.000	0.000	0.000	0.000	0.000	0.000	0.000
Al	0.000	0.000	0.000	0.000	0.000	0.000	0.000	0.000	0.000
Ta	0.000	0.000	0.000	0.000	0.000	0.000	0.000	0.000	0.000
Cations	1.999	1.992	1.997	1.998	2.000	2.004	2.002	2.005	2.003
<i>lueshite</i>	0.02	0.02	0.02	0.02	0.01	0.01	0.01	0.01	0.01
<i>loparite</i>	0.17	0.09	0.20	0.12	0.15	0.10	0.14	0.11	0.12
<i>REEFeO₃</i>	0.03	0.04	0.03	0.04	0.03	0.03	0.03	0.03	0.03
<i>tausonite</i>	0.00	0.01	0.00	0.00	0.00	0.00	0.00	0.00	0.00
<i>REE₂Ti₂O₇</i>	0.00	0.00	0.00	0.00	0.00	0.00	0.00	0.00	0.00
<i>lakargiite</i>	0.00	0.01	0.00	0.00	0.00	0.00	0.00	0.00	0.00
<i>perovskite</i>	0.77	0.85	0.74	0.82	0.80	0.85	0.82	0.84	0.83
Fe/Nb	2.30	2.69	1.81	2.66	2.62	2.99	3.07	3.32	3.01
ΔNNO	-0.10	2.48	-1.36	1.32	-1.62	-0.01	-1.43	-0.73	-0.65

TABELA B03 – Cont. Major element compositions and endmembers for perovskite from all samples. Structural formula calculated on the basis of 3 oxygens. C - core; R - rim; I – intermediately.

Sample Grain/Analysis Location	TRIV-5 33/63 R	TRIV-5 34/64 R	TRIV-5-3 35/65 C	TRIV-5-3 35/66 R	TRIV-5-3 36/67 C	TRIV-5-3 36/68 R	TRIV-5-3 37/69 C	TRIV-5-3 37/70 R
SiO ₂	0.00	0.00	0.00	0.00	0.00	0.00	0.00	0.00
Fe ₂ O ₃	1.97	1.85	1.79	1.85	1.53	1.81	1.39	1.55
La ₂ O ₃	2.45	2.90	3.51	3.20	3.41	2.65	2.76	2.15
Sm ₂ O ₃	0.17	0.19	0.23	0.20	0.23	0.17	0.19	0.15
Pr ₂ O ₃	0.46	0.62	0.79	0.69	0.78	0.53	0.66	0.41
CaO	32.75	29.79	27.53	29.41	27.46	32.57	30.25	33.45
Nb ₂ O ₅	1.08	1.19	1.46	1.33	1.34	1.11	0.86	0.84
SrO	0.30	0.29	0.26	0.30	0.29	0.28	0.26	0.27
ZrO ₂	0.14	0.15	0.17	0.18	0.14	0.17	0.09	0.10
ThO ₂	0.04	0.13	0.57	0.21	1.11	0.03	0.63	0.03
TiO ₂	51.95	51.03	49.56	50.88	49.87	51.92	51.74	52.80
BaO	0.00	0.00	0.00	0.00	0.00	0.00	0.00	0.00
Ce ₂ O ₃	4.90	6.51	7.97	7.12	8.06	5.21	6.71	4.47
Nd ₂ O ₃	1.54	2.03	2.48	2.23	2.53	1.61	2.15	1.41
Na ₂ O	1.39	1.91	2.23	2.07	2.34	1.44	1.88	1.29
MgO	0.00	0.00	0.00	0.00	0.00	0.00	0.00	0.00
Al ₂ O ₃	0.00	0.00	0.00	0.00	0.00	0.00	0.00	0.00
Ta ₂ O ₅	0.00	0.00	0.00	0.00	0.00	0.00	0.00	0.00
Total	99.14	98.57	98.55	99.67	99.08	99.50	99.58	98.93
Si	0.000	0.000	0.000	0.000	0.000	0.000	0.000	0.000
Fe	0.036	0.034	0.034	0.034	0.029	0.033	0.026	0.028
La	0.022	0.027	0.033	0.029	0.032	0.024	0.025	0.019
Sm	0.001	0.002	0.002	0.002	0.002	0.001	0.002	0.001
Pr	0.004	0.006	0.007	0.006	0.007	0.005	0.006	0.004
Ca	0.852	0.791	0.746	0.778	0.742	0.847	0.797	0.866
Nb	0.012	0.013	0.017	0.015	0.015	0.012	0.010	0.009
Sr	0.004	0.004	0.004	0.004	0.004	0.004	0.004	0.004
Zr	0.002	0.002	0.002	0.002	0.002	0.002	0.001	0.001
Th	0.000	0.001	0.003	0.001	0.006	0.000	0.004	0.000
Ti	0.949	0.951	0.943	0.945	0.946	0.948	0.957	0.959
Ba	0.000	0.000	0.000	0.000	0.000	0.000	0.000	0.000
Ce	0.044	0.059	0.074	0.064	0.074	0.046	0.060	0.040
Nd	0.013	0.018	0.022	0.020	0.023	0.014	0.019	0.012
Na	0.065	0.092	0.109	0.099	0.114	0.068	0.090	0.060
Mg	0.000	0.000	0.000	0.000	0.000	0.000	0.000	0.000
Al	0.000	0.000	0.000	0.000	0.000	0.000	0.000	0.000
Ta	0.000	0.000	0.000	0.000	0.000	0.000	0.000	0.000
Cations	2.004	1.999	1.996	2.001	1.997	2.004	2.000	2.004
<i>lueshite</i>	0.01	0.01	0.02	0.01	0.02	0.01	0.01	0.01
<i>loparite</i>	0.11	0.16	0.19	0.17	0.20	0.11	0.16	0.10
<i>REEFeO₃</i>	0.03	0.03	0.03	0.03	0.03	0.03	0.03	0.02
<i>tausonite</i>	0.00	0.00	0.00	0.00	0.00	0.00	0.00	0.00
<i>REE₂Ti₂O₇</i>	0.00	0.00	0.01	0.00	0.01	0.00	0.00	0.00
<i>lakargiite</i>	0.00	0.00	0.00	0.00	0.00	0.00	0.00	0.00
<i>perovskite</i>	0.84	0.79	0.75	0.77	0.74	0.84	0.79	0.86
Fe/Nb	3.03	2.59	2.04	2.31	1.90	2.70	2.70	3.08
ΔANNO	0.01	-0.54	-1.07	-0.76	-2.16	-0.77	-2.27	-1.60

TABELA B03 – Cont. Major element compositions and endmembers for perovskite from all samples. Structural formula calculated on the basis of 3 oxygens. C - core; R - rim; I – intermediated.

Sample Grain/Analysis Location	TRIV-5-3 38/71 C	TRIV-5-3 38/72 R	TRIV-5-3 39/73 R	TRIV-5-3 39/74 C	TRIV-5-3 41/77 C	TRIV-5-3 42/78 C	TRIV-5-3 42/79 R	TRIV-5-3 43/80 C
SiO ₂	0.05	0.00	0.00	0.00	0.00	0.04	0.00	0.00
Fe ₂ O ₃	1.90	1.78	1.69	1.16	1.96	1.62	1.60	1.64
La ₂ O ₃	2.46	2.52	3.70	1.44	3.04	3.45	3.21	3.20
Sm ₂ O ₃	0.16	0.18	0.24	0.12	0.19	0.23	0.21	0.22
Pr ₂ O ₃	0.45	0.47	0.84	0.32	0.59	0.77	0.68	0.69
CaO	32.91	32.71	26.00	35.44	30.76	27.75	28.90	29.05
Nb ₂ O ₅	1.17	1.09	1.80	0.66	1.54	1.51	1.30	1.13
SrO	0.28	0.31	0.30	0.24	0.36	0.30	0.30	0.28
ZrO ₂	0.16	0.13	0.24	0.05	0.29	0.13	0.13	0.13
ThO ₂	0.02	0.04	1.51	0.12	0.07	0.76	0.33	0.27
TiO ₂	52.01	52.49	48.38	55.05	50.35	49.82	50.88	50.48
BaO	0.00	0.00	0.00	0.00	0.00	0.00	0.00	0.00
Ce ₂ O ₃	4.90	5.18	8.61	3.08	6.26	7.89	7.33	7.12
Nd ₂ O ₃	1.50	1.65	2.55	0.99	1.90	2.43	2.30	2.23
Na ₂ O	1.24	1.45	2.45	1.21	1.52	2.23	2.23	2.00
MgO	0.00	0.00	0.00	0.00	0.00	0.00	0.00	0.00
Al ₂ O ₃	0.00	0.00	0.00	0.00	0.00	0.00	0.00	0.00
Ta ₂ O ₅	0.00	0.00	0.00	0.00	0.00	0.00	0.00	0.00
Total	99.23	99.99	98.30	99.86	98.83	98.93	99.40	98.43
Si	0.001	0.000	0.000	0.000	0.000	0.001	0.000	0.000
Fe	0.035	0.032	0.033	0.020	0.037	0.031	0.030	0.031
La	0.022	0.022	0.035	0.012	0.028	0.032	0.029	0.030
Sm	0.001	0.001	0.002	0.001	0.002	0.002	0.002	0.002
Pr	0.004	0.004	0.008	0.003	0.005	0.007	0.006	0.006
Ca	0.854	0.845	0.716	0.893	0.816	0.748	0.768	0.779
Nb	0.013	0.012	0.021	0.007	0.017	0.017	0.015	0.013
Sr	0.004	0.004	0.005	0.003	0.005	0.004	0.004	0.004
Zr	0.002	0.002	0.003	0.001	0.003	0.002	0.002	0.002
Th	0.000	0.000	0.009	0.001	0.000	0.004	0.002	0.002
Ti	0.948	0.952	0.935	0.974	0.937	0.943	0.950	0.950
Ba	0.000	0.000	0.000	0.000	0.000	0.000	0.000	0.000
Ce	0.043	0.046	0.081	0.027	0.057	0.073	0.067	0.065
Nd	0.013	0.014	0.023	0.008	0.017	0.022	0.020	0.020
Na	0.058	0.068	0.122	0.055	0.073	0.109	0.107	0.097
Mg	0.000	0.000	0.000	0.000	0.000	0.000	0.000	0.000
Al	0.000	0.000	0.000	0.000	0.000	0.000	0.000	0.000
Ta	0.000	0.000	0.000	0.000	0.000	0.000	0.000	0.000
Cations	1.999	2.002	1.992	2.006	1.997	1.995	2.002	1.999
<i>lueshite</i>	0.01	0.01	0.02	0.01	0.02	0.02	0.01	0.01
<i>loparite</i>	0.09	0.11	0.21	0.10	0.11	0.19	0.19	0.17
<i>REEFeO₃</i>	0.03	0.03	0.03	0.00	0.04	0.03	0.03	0.03
<i>tausonite</i>	0.00	0.00	0.00	0.00	0.01	0.00	0.00	0.00
<i>REE₂Ti₂O₇</i>	0.00	0.00	0.01	0.00	0.01	0.01	0.00	0.00
<i>lakargiite</i>	0.00	0.00	0.00	0.00	0.00	0.00	0.00	0.00
<i>perovskite</i>	0.85	0.84	0.72	0.89	0.82	0.75	0.76	0.78
<i>Fe/Nb</i>	2.69	2.71	1.56	2.93	2.12	1.79	2.04	2.42
<i>Anno</i>	-0.45	-0.92	-1.95	-3.26	-0.53	-1.98	-1.86	-1.37

TABELA B03 – Cont. Major element compositions and endmembers for perovskite from all samples. Structural formula calculated on the basis of 3 oxygens. C - core; R - rim; I – intermediately.

Sample Grain/Analysis Location	TRIV-5-3 43/81 R	TRIV-5-3 44/82 C	TRIV-5-3 45/83 R	TRIV-5-3 46/84 C	TRIV-5-3 46/85 R	TRIV-5-3 47/86 C	TRIV-5-3 47/87 R	TRIV-5-3 48/88 C
SiO ₂	0.00	2.67	0.00	0.00	0.90	0.00	0.00	0.50
Fe ₂ O ₃	1.81	2.76	1.41	1.53	2.14	1.19	1.37	1.76
La ₂ O ₃	2.99	2.49	2.62	3.27	2.29	2.54	1.79	2.57
Sm ₂ O ₃	0.22	0.17	0.17	0.21	0.15	0.19	0.14	0.19
Pr ₂ O ₃	0.66	0.48	0.59	0.73	0.41	0.65	0.33	0.56
CaO	31.31	29.76	32.31	28.41	31.72	30.55	34.34	30.99
Nb ₂ O ₅	1.13	1.18	0.78	1.12	1.02	0.78	0.75	0.80
SrO	0.31	0.31	0.31	0.31	0.28	0.27	0.26	0.26
ZrO ₂	0.15	0.35	0.08	0.10	0.17	0.07	0.06	0.08
ThO ₂	0.16	0.20	0.40	0.89	0.05	0.99	0.04	0.24
TiO ₂	51.49	47.20	52.09	50.15	49.88	52.34	53.14	51.10
BaO	0.00	0.00	0.00	0.00	0.00	0.00	0.00	0.00
Ce ₂ O ₃	6.67	4.96	5.97	7.65	4.36	6.51	3.54	5.63
Nd ₂ O ₃	2.16	1.55	1.94	2.37	1.34	2.16	1.10	1.82
Na ₂ O	1.80	1.20	1.48	2.17	1.37	1.92	1.16	1.44
MgO	0.00	0.00	0.00	0.00	0.00	0.00	0.00	0.00
Al ₂ O ₃	0.00	0.00	0.00	0.00	0.00	0.00	0.00	0.00
Ta ₂ O ₅	0.00	0.00	0.00	0.00	0.00	0.00	0.00	0.00
Total	100.86	95.27	100.16	98.90	96.09	100.16	98.00	97.93
Si	0.000	0.067	0.000	0.000	0.022	0.000	0.000	0.012
Fe	0.033	0.052	0.026	0.029	0.040	0.022	0.025	0.033
La	0.027	0.023	0.023	0.030	0.021	0.023	0.016	0.023
Sm	0.002	0.001	0.001	0.002	0.001	0.002	0.001	0.002
Pr	0.006	0.004	0.005	0.007	0.004	0.006	0.003	0.005
Ca	0.815	0.799	0.841	0.764	0.844	0.799	0.888	0.819
Nb	0.012	0.013	0.009	0.013	0.012	0.009	0.008	0.009
Sr	0.004	0.005	0.004	0.004	0.004	0.004	0.004	0.004
Zr	0.002	0.004	0.001	0.001	0.002	0.001	0.001	0.001
Th	0.001	0.001	0.002	0.005	0.000	0.005	0.000	0.001
Ti	0.942	0.890	0.952	0.947	0.932	0.962	0.965	0.948
Ba	0.000	0.000	0.000	0.000	0.000	0.000	0.000	0.000
Ce	0.059	0.045	0.053	0.070	0.040	0.058	0.031	0.051
Nd	0.019	0.014	0.017	0.021	0.012	0.019	0.009	0.016
Na	0.085	0.058	0.070	0.106	0.066	0.091	0.054	0.069
Mg	0.000	0.000	0.000	0.000	0.000	0.000	0.000	0.000
Al	0.000	0.000	0.000	0.000	0.000	0.000	0.000	0.000
Ta	0.000	0.000	0.000	0.000	0.000	0.000	0.000	0.000
Cations	2.007	1.977	2.004	2.000	2.000	2.000	2.006	1.993
<i>lueshite</i>	0.01	0.01	0.01	0.01	0.01	0.01	0.01	0.01
<i>loparite</i>	0.15	0.09	0.12	0.19	0.11	0.17	0.09	0.12
<i>REEFeO₃</i>	0.03	0.05	0.03	0.03	0.02	0.02	0.01	0.03
<i>tausonite</i>	0.00	0.00	0.00	0.00	0.00	0.00	0.00	0.00
<i>REE₂Ti₂O₇</i>	0.00	0.00	0.01	0.00	0.00	0.00	0.00	0.00
<i>lakargiite</i>	0.00	0.00	0.00	0.00	0.00	0.00	0.00	0.00
<i>perovskite</i>	0.80	0.84	0.83	0.76	0.85	0.80	0.88	0.83
Fe/Nb	2.68	3.90	3.03	2.27	3.48	2.55	3.05	3.67
ΔANNO	-0.77	3.84	-2.12	-1.86	1.06	-3.09	-2.30	-0.44

TABELA B03 – Cont. Major element compositions and endmembers for perovskite from all samples. Structural formula calculated on the basis of 3 oxygens. C - core; R - rim; I – intermediated.

Sample Grain/Analysis Location	TRIV-5-3 49/89 C	TRIV-5-3 49/90 R	TR-02 01/01 C	TR-02 01/02 I	TR-02 01/03 R	TR-02 02/04 C	TR-02 02/05 R	TR-02 03/06 C
SiO ₂	0.00	0.07	0.02	0.00	0.01	0.00	0.00	0.00
Fe ₂ O ₃	1.59	1.97	1.45	1.50	1.67	1.34	1.49	1.03
La ₂ O ₃	2.86	2.51	3.55	3.07	2.58	3.29	2.56	1.97
Sm ₂ O ₃	0.18	0.17	0.31	0.28	0.24	0.30	0.22	0.19
Pr ₂ O ₃	0.58	0.47	0.80	0.61	0.48	0.77	0.42	0.40
CaO	31.08	32.44	25.14	29.61	32.12	28.06	32.12	33.93
Nb ₂ O ₅	1.13	1.28	2.36	1.70	1.67	1.86	1.50	0.78
SrO	0.30	0.31	0.78	0.74	0.79	0.76	0.78	0.62
ZrO ₂	0.13	0.20	0.25	0.23	0.24	0.18	0.16	0.09
ThO ₂	0.22	0.05	2.45	0.38	0.04	1.12	0.09	0.25
TiO ₂	51.95	50.94	48.03	50.53	51.30	49.60	51.25	53.15
BaO	0.00	0.00	0.10	0.11	0.11	0.10	0.11	0.15
Ce ₂ O ₃	6.11	4.85	8.85	7.00	5.19	7.85	5.27	4.50
Nd ₂ O ₃	1.97	1.49	2.77	2.17	1.58	2.44	1.60	1.49
Na ₂ O	1.72	1.34	3.05	2.17	1.57	2.38	1.56	1.26
MgO	0.00	0.00	0.08	0.06	0.07	0.05	0.06	0.03
Al ₂ O ₃	0.00	0.00	0.00	0.00	0.00	0.00	0.00	0.01
Ta ₂ O ₅	0.00	0.00	0.45	0.11	0.04	0.22	0.02	0.11
Total	99.82	98.09	100.43	100.27	99.70	100.30	99.23	99.94
Si	0.000	0.002	0.000	0.000	0.000	0.000	0.000	0.000
Fe	0.029	0.036	0.028	0.031	0.025	0.027	0.019	0.022
La	0.026	0.023	0.028	0.023	0.030	0.023	0.017	0.008
Sm	0.002	0.001	0.002	0.002	0.003	0.002	0.002	0.001
Pr	0.005	0.004	0.006	0.004	0.007	0.004	0.004	0.001
Ca	0.812	0.854	0.782	0.837	0.752	0.841	0.872	0.946
Nb	0.012	0.014	0.019	0.018	0.021	0.017	0.008	0.011
Sr	0.004	0.004	0.011	0.011	0.011	0.011	0.009	0.009
Zr	0.002	0.002	0.003	0.003	0.002	0.002	0.001	0.002
Th	0.001	0.000	0.002	0.000	0.006	0.001	0.001	0.000
Ti	0.953	0.942	0.937	0.939	0.933	0.942	0.960	0.963
Ba	0.000	0.000	0.001	0.001	0.001	0.001	0.001	0.001
Ce	0.055	0.044	0.063	0.046	0.072	0.047	0.040	0.012
Nd	0.017	0.013	0.019	0.014	0.022	0.014	0.013	0.003
Na	0.081	0.064	0.104	0.074	0.115	0.074	0.058	0.029
Mg	0.000	0.000	0.002	0.003	0.002	0.002	0.001	0.001
Al	0.000	0.000	0.000	0.000	0.000	0.000	0.000	0.000
Ta	0.000	0.000	0.001	0.000	0.002	0.000	0.001	0.000
Cations	1.999	2.004	2.007	2.007	2.003	2.009	2.007	2.010
<i>lueshite</i>	0.01	0.01	0.03	0.02	0.02	0.02	0.02	0.01
<i>loparite</i>	0.14	0.10	0.25	0.17	0.11	0.19	0.12	0.10
<i>REEFeO₃</i>	0.03	0.04	0.03	0.03	0.03	0.03	0.03	0.02
<i>tausonite</i>	0.00	0.00	0.01	0.01	0.01	0.01	0.01	0.01
<i>REE₂Ti₂O₇</i>	0.00	0.00	0.00	0.00	0.00	0.01	0.00	0.00
<i>lakargiite</i>	0.00	0.00	0.00	0.00	0.00	0.00	0.00	0.00
<i>perovskite</i>	0.81	0.84	0.68	0.76	0.82	0.74	0.82	0.86
Fe/Nb	2.35	2.57	1.47	1.20	1.66	2.20	2.07	0.74
ΔANNO	-1.76	-0.17	-2.91	-2.14	-3.83	-2.71	-3.91	-3.36

TABELA B03 – Cont. Major element compositions and endmembers for perovskite from all samples. Structural formula calculated on the basis of 3 oxygens. C - core; R - rim; I – intermediately.

Sample Grain/Analysis Location	TR-02 03/07 R	TR-02 04/08 C	TR-02 04/09 R	TR-07 05/10 C	TR-07 05/11 R	TR-07 06/12 C	TR-07 06/13 R	TR-07 07/14 C	TR-07 07/15 R	TR-18 08/16 C
SiO ₂	0.00	0.00	0.01	0.00	0.41	0.00	0.09	0.00	0.00	0.00
Fe ₂ O ₃	1.25	1.26	1.59	1.19	1.39	1.07	1.21	1.58	1.22	1.58
La ₂ O ₃	0.99	3.36	2.70	3.29	2.76	2.28	2.08	1.80	1.57	3.27
Sm ₂ O ₃	0.10	0.27	0.21	0.26	0.24	0.21	0.18	0.15	0.13	0.28
Pr ₂ O ₃	0.13	0.68	0.42	0.66	0.46	0.45	0.37	0.27	0.19	0.76
CaO	37.95	27.21	31.96	28.52	30.64	32.78	33.66	34.64	36.60	26.47
Nb ₂ O ₅	1.00	2.85	1.94	2.16	1.93	0.96	0.97	0.90	1.08	4.35
SrO	0.67	0.78	0.85	0.78	0.79	0.68	0.65	0.67	0.74	0.81
ZrO ₂	0.14	0.28	0.24	0.18	0.20	0.08	0.09	0.08	0.15	0.61
ThO ₂	0.00	1.17	0.09	0.60	0.09	0.27	0.09	0.07	0.02	1.70
TiO ₂	55.01	48.73	50.77	49.79	49.65	51.33	53.22	53.04	54.67	46.71
BaO	0.13	0.12	0.11	0.12	0.08	0.09	0.14	0.12	0.09	0.14
Ce ₂ O ₃	1.40	8.07	5.49	7.55	5.78	5.20	4.36	3.69	2.73	7.99
Nd ₂ O ₃	0.39	2.39	1.67	2.34	1.80	1.74	1.37	1.14	0.85	2.34
Na ₂ O	0.65	2.64	1.47	2.40	1.85	1.54	1.35	1.12	0.85	2.78
MgO	0.04	0.05	0.08	0.04	0.50	0.03	0.16	0.05	0.03	0.06
Al ₂ O ₃	0.00	0.00	0.00	0.00	0.02	0.00	0.01	0.01	0.00	0.00
Ta ₂ O ₅	0.01	0.33	0.06	0.15	0.07	0.13	0.06	0.04	0.03	0.60
Total	99.83	100.19	99.65	100.03	98.64	98.84	100.05	99.34	100.95	100.46
Si	0.000	0.000	0.000	0.010	0.000	0.002	0.000	0.000	0.000	0.015
Fe	0.024	0.029	0.022	0.026	0.020	0.022	0.029	0.021	0.030	0.032
La	0.031	0.024	0.030	0.025	0.021	0.018	0.016	0.013	0.031	0.028
Sm	0.002	0.002	0.002	0.002	0.002	0.002	0.001	0.001	0.002	0.002
Pr	0.006	0.004	0.006	0.004	0.004	0.003	0.002	0.002	0.007	0.005
Ca	0.733	0.837	0.761	0.811	0.861	0.862	0.889	0.915	0.718	0.776
Nb	0.032	0.021	0.024	0.021	0.011	0.010	0.010	0.011	0.050	0.026
Sr	0.011	0.012	0.011	0.011	0.010	0.009	0.009	0.010	0.012	0.012
Zr	0.003	0.003	0.002	0.002	0.001	0.001	0.001	0.002	0.008	0.004
Th	0.007	0.001	0.003	0.001	0.001	0.000	0.000	0.000	0.010	0.001
Ti	0.921	0.933	0.933	0.923	0.947	0.957	0.955	0.960	0.890	0.910
Ba	0.001	0.001	0.001	0.001	0.001	0.001	0.001	0.001	0.001	0.001
Ce	0.074	0.049	0.069	0.052	0.047	0.038	0.032	0.023	0.074	0.059
Nd	0.021	0.015	0.021	0.016	0.015	0.012	0.010	0.007	0.021	0.017
Na	0.129	0.070	0.116	0.088	0.073	0.063	0.052	0.038	0.136	0.090
Mg	0.002	0.003	0.001	0.018	0.001	0.006	0.002	0.001	0.002	0.027
Al	0.000	0.000	0.000	0.000	0.000	0.000	0.000	0.000	0.000	0.000
Ta	0.002	0.000	0.001	0.000	0.001	0.000	0.000	0.000	0.004	0.000
Cations	2.001	2.004	2.006	2.013	2.016	2.007	2.009	2.006	1.997	2.005
<i>lueshite</i>	0.01	0.03	0.02	0.02	0.02	0.01	0.01	0.01	0.01	0.05
<i>loparite</i>	0.04	0.20	0.10	0.19	0.14	0.13	0.11	0.09	0.05	0.18
<i>REEFeO₃</i>	0.01	0.02	0.03	0.02	0.03	0.02	0.02	0.02	0.02	0.03
<i>tausonite</i>	0.01	0.01	0.01	0.01	0.01	0.01	0.01	0.01	0.01	0.01
<i>REE₂Ti₂O₇</i>	0.00	0.01	0.01	0.01	0.00	0.00	0.00	0.00	0.00	0.01
<i>lakargiite</i>	0.00	0.00	0.00	0.00	0.00	0.00	0.00	0.00	0.00	0.01
<i>perovskite</i>	0.93	0.72	0.82	0.74	0.79	0.83	0.85	0.87	0.90	0.71
<i>Fe/Nb</i>	1.37	0.91	1.20	1.85	2.08	2.94	1.89	0.60	1.23	1.33
<i>ANNO</i>	-5.60	-2.87	-4.98	-3.73	-3.89	-3.38	-1.58	-3.56	-6.20	-2.80

TABELA B03 – Cont. Major element compositions and endmembers for perovskite from all samples. Structural formula calculated on the basis of 3 oxygens. C - core; R - rim; I – intermediated.

Sample Grain/Analysis	TR-18 08/17	TR-03 09/18	TR-03 09/19	TR-03 10/20	TR-03 10/21	TR-03 10/22	TR-03 11/23	TR-03 11/24	TR-03 12/25	TR-03 12/26
Location	R	C	R	C	I	R	C	R	C	R
SiO ₂	0.60	0.00	0.05	0.00	0.00	0.45	0.00	0.15	0.00	0.00
Fe ₂ O ₃	1.71	1.43	1.67	1.27	1.25	1.66	1.49	1.94	1.96	1.65
La ₂ O ₃	3.11	3.26	2.34	3.12	2.69	2.09	2.69	2.33	2.84	2.91
Sm ₂ O ₃	0.28	0.28	0.21	0.27	0.24	0.17	0.23	0.21	0.26	0.25
Pr ₂ O ₃	0.53	0.71	0.42	0.74	0.60	0.34	0.50	0.33	0.58	0.56
CaO	29.48	28.31	32.52	28.64	31.12	33.90	32.03	33.46	30.61	30.56
Nb ₂ O ₅	2.30	1.80	1.34	1.38	1.09	1.32	1.29	1.54	1.45	1.67
SrO	0.84	0.76	0.73	0.73	0.72	0.80	0.76	0.81	0.77	0.82
ZrO ₂	0.31	0.24	0.21	0.13	0.11	0.21	0.15	0.24	0.18	0.19
ThO ₂	0.24	1.30	0.07	1.17	0.37	0.03	0.20	0.04	0.40	0.64
TiO ₂	49.24	49.31	51.33	50.17	51.54	52.44	51.66	51.72	50.80	50.61
BaO	0.09	0.11	0.08	0.13	0.08	0.10	0.11	0.13	0.12	0.12
Ce ₂ O ₃	6.61	7.70	4.76	7.62	6.18	3.88	5.74	4.22	6.42	6.39
Nd ₂ O ₃	1.98	2.47	1.46	2.44	1.97	1.13	1.76	1.33	1.95	2.01
Na ₂ O	1.88	2.29	1.62	2.21	1.86	1.19	1.74	1.29	1.80	1.80
MgO	0.74	0.08	0.16	0.05	0.05	0.68	0.04	0.11	0.14	0.06
Al ₂ O ₃	0.00	0.00	0.01	0.00	0.00	0.00	0.01	0.00	0.01	0.00
Ta ₂ O ₅	0.01	0.31	0.08	0.22	0.09	0.03	0.09	0.04	0.12	0.15
Total	99.96	100.34	99.04	100.28	99.96	100.40	100.47	99.90	100.40	100.39
Si	0.000	0.001	0.000	0.000	0.011	0.000	0.004	0.000	0.000	0.001
Fe	0.027	0.031	0.024	0.023	0.030	0.027	0.035	0.036	0.030	0.032
La	0.030	0.021	0.029	0.024	0.018	0.024	0.021	0.026	0.026	0.027
Sm	0.002	0.002	0.002	0.002	0.001	0.002	0.002	0.002	0.002	0.002
Pr	0.007	0.004	0.007	0.005	0.003	0.004	0.003	0.005	0.005	0.005
Ca	0.759	0.849	0.765	0.816	0.861	0.832	0.862	0.803	0.804	0.803
Nb	0.020	0.015	0.015	0.012	0.014	0.014	0.017	0.016	0.019	0.022
Sr	0.011	0.010	0.010	0.010	0.011	0.011	0.011	0.011	0.012	0.012
Zr	0.003	0.003	0.002	0.001	0.002	0.002	0.003	0.002	0.002	0.004
Th	0.007	0.000	0.007	0.002	0.000	0.001	0.000	0.002	0.004	0.001
Ti	0.928	0.941	0.940	0.949	0.935	0.943	0.936	0.935	0.935	0.929
Ba	0.001	0.001	0.001	0.001	0.001	0.001	0.001	0.001	0.001	0.001
Ce	0.070	0.042	0.070	0.055	0.034	0.051	0.037	0.058	0.057	0.057
Nd	0.022	0.013	0.022	0.017	0.010	0.015	0.011	0.017	0.018	0.017
Na	0.111	0.077	0.107	0.088	0.055	0.082	0.060	0.086	0.086	0.085
Mg	0.003	0.006	0.002	0.002	0.024	0.002	0.004	0.005	0.002	0.005
Al	0.000	0.000	0.000	0.000	0.000	0.000	0.000	0.000	0.000	0.000
Ta	0.002	0.001	0.001	0.001	0.000	0.001	0.000	0.001	0.001	0.000
Cations	2.004	2.014	2.003	2.009	2.010	2.011	2.008	2.006	2.004	2.004
<i>lueshite</i>	0.03	0.02	0.02	0.02	0.01	0.01	0.01	0.02	0.02	0.02
<i>loparite</i>	0.13	0.19	0.13	0.19	0.16	0.08	0.14	0.09	0.14	0.14
<i>REEFeO₃</i>	0.03	0.03	0.02	0.02	0.02	0.03	0.03	0.03	0.04	0.03
<i>tausonite</i>	0.01	0.01	0.01	0.01	0.01	0.01	0.01	0.01	0.01	0.01
<i>REE₂Ti₂O₇</i>	0.01	0.01	0.00	0.01	0.00	0.00	0.00	0.00	0.00	0.01
<i>lakargiite</i>	0.00	0.00	0.00	0.00	0.00	0.00	0.00	0.00	0.00	0.00
<i>perovskite</i>	0.78	0.74	0.82	0.75	0.79	0.86	0.81	0.85	0.79	0.79
<i>Fe/Nb</i>	2.08	1.54	1.90	2.09	1.93	2.10	2.25	1.64	1.47	1.66
<i>ΔNNO</i>	-3.29	-1.69	-3.48	-3.25	-1.87	-2.46	-0.82	-0.47	-2.21	-2.19

TABELA B03 – Cont. Major element compositions and endmembers for perovskite from all samples. Structural formula calculated on the basis of 3 oxygens. C - core; R - rim; I – intermediated.

Sample Grain/Analysis Location	TR-03 13/27 C	TR-03 13/28 R	TR-04a 14/29 C	TR-04a 14/30 R	TR-04a 15/31 C	TR-04a 15/32 R	TR-04b 16/33 C	TR-04b 16/34 I	TR-04b 16/35 R
SiO ₂	0.06	0.14	0.00	0.00	0.00	0.00	0.00	0.00	0.00
Fe ₂ O ₃	1.75	2.18	1.33	1.50	1.43	1.45	1.30	1.34	1.31
La ₂ O ₃	3.02	2.82	2.56	2.08	3.11	3.18	3.40	3.16	3.22
Sm ₂ O ₃	0.26	0.24	0.26	0.18	0.27	0.27	0.28	0.27	0.26
Pr ₂ O ₃	0.59	0.49	0.55	0.33	0.62	0.69	0.73	0.62	0.62
CaO	30.66	31.99	31.93	34.52	29.27	29.71	27.44	28.89	28.84
Nb ₂ O ₅	1.97	2.18	1.13	1.30	1.48	1.44	3.21	2.64	2.44
SrO	0.82	0.84	0.72	0.81	0.79	0.77	0.81	0.76	0.78
ZrO ₂	0.32	0.55	0.12	0.21	0.16	0.16	0.30	0.25	0.22
ThO ₂	0.15	0.02	0.20	0.02	0.76	0.62	1.27	0.63	0.63
TiO ₂	50.55	50.59	52.38	52.60	49.90	49.11	47.65	49.32	49.11
BaO	0.11	0.11	0.12	0.13	0.11	0.14	0.11	0.11	0.09
Ce ₂ O ₃	6.33	5.31	5.53	3.68	7.22	7.14	7.84	7.14	7.18
Nd ₂ O ₃	1.95	1.57	1.78	1.16	2.37	2.32	2.45	2.24	2.23
Na ₂ O	1.79	1.54	1.59	1.09	2.17	2.03	2.62	2.27	2.28
MgO	0.14	0.26	0.03	0.05	0.05	0.05	0.06	0.05	0.05
Al ₂ O ₃	0.01	0.01	0.00	0.00	0.00	0.00	0.00	0.00	0.01
Ta ₂ O ₅	0.06	0.02	0.10	0.01	0.22	0.13	0.32	0.17	0.14
Total	100.54	100.85	100.34	99.66	99.93	99.20	99.79	99.84	99.38
Si	0.003	0.000	0.000	0.000	0.000	0.000	0.000	0.000	0.000
Fe	0.040	0.024	0.027	0.027	0.027	0.025	0.025	0.025	0.023
La	0.025	0.023	0.018	0.029	0.029	0.032	0.029	0.030	0.026
Sm	0.002	0.002	0.001	0.002	0.002	0.002	0.002	0.002	0.002
Pr	0.004	0.005	0.003	0.006	0.006	0.007	0.006	0.006	0.006
Ca	0.827	0.828	0.886	0.781	0.799	0.745	0.771	0.774	0.780
Nb	0.024	0.012	0.014	0.017	0.016	0.037	0.030	0.028	0.031
Sr	0.012	0.010	0.011	0.011	0.011	0.012	0.011	0.011	0.012
Zr	0.006	0.001	0.002	0.002	0.002	0.004	0.003	0.003	0.003
Th	0.000	0.001	0.000	0.004	0.004	0.007	0.004	0.004	0.003
Ti	0.919	0.954	0.948	0.935	0.927	0.908	0.925	0.925	0.927
Ba	0.001	0.001	0.001	0.001	0.001	0.001	0.001	0.001	0.001
Ce	0.047	0.049	0.032	0.066	0.066	0.073	0.065	0.066	0.061
Nd	0.014	0.015	0.010	0.021	0.021	0.022	0.020	0.020	0.019
Na	0.072	0.075	0.051	0.105	0.099	0.129	0.109	0.111	0.110
Mg	0.009	0.001	0.002	0.002	0.002	0.002	0.002	0.002	0.002
Al	0.000	0.000	0.000	0.000	0.000	0.000	0.000	0.000	0.000
Ta	0.000	0.001	0.000	0.002	0.001	0.002	0.001	0.001	0.001
Cations	2.006	2.003	2.008	2.009	2.015	2.007	2.004	2.007	2.005
<i>lueshite</i>	0.02	0.02	0.01	0.01	0.02	0.02	0.04	0.03	0.03
<i>loparite</i>	0.13	0.10	0.13	0.07	0.18	0.17	0.19	0.16	0.17
<i>REEFeO₃</i>	0.03	0.04	0.02	0.03	0.03	0.03	0.03	0.03	0.03
<i>tausonite</i>	0.01	0.01	0.01	0.01	0.01	0.01	0.01	0.01	0.01
<i>REE₂Ti₂O₇</i>	0.01	0.00	0.00	0.00	0.00	0.01	0.01	0.01	0.01
<i>lakargiite</i>	0.00	0.01	0.00	0.00	0.00	0.00	0.00	0.00	0.00
<i>perovskite</i>	0.79	0.82	0.82	0.87	0.76	0.76	0.72	0.76	0.75
Fe/Nb	1.97	1.92	1.61	1.68	0.67	0.84	0.89	0.74	1.70
ΔANNO	-0.58	-2.98	-2.48	-2.87	-2.67	-5.92	-4.96	-4.80	-5.68

TABELA B03 – Cont. Major element compositions and endmembers for perovskite from all samples. Structural formula calculated on the basis of 3 oxygens. C - core; R - rim; I – intermediated.

Sample Grain/Analysis Location	TR-04b 17/36	TR-07 17/37	TR-07 18/38	TR-18 19/39	TR-18 19/40	TR-18 19/41	TR-18 22/44	TR-03 11/23	TR-03 11/24
	C	R	C	C	I	R	C	C	R
SiO ₂	0.00	0.00	0.00	0.00	0.25	0.05	0.00	0.00	0.15
Fe ₂ O ₃	1.22	1.30	1.64	1.43	1.42	1.70	4.00	1.49	1.94
La ₂ O ₃	2.80	1.80	2.87	3.14	3.27	2.97	2.60	2.69	2.33
Sm ₂ O ₃	0.27	0.16	0.25	0.27	0.29	0.25	0.23	0.23	0.21
Pr ₂ O ₃	0.61	0.31	0.56	0.69	0.63	0.48	0.40	0.50	0.33
CaO	29.28	34.69	31.02	27.50	28.29	30.94	29.96	32.03	33.46
Nb ₂ O ₅	2.75	1.27	2.02	4.38	2.50	2.31	1.19	1.29	1.54
SrO	0.81	0.77	0.79	0.82	0.77	0.83	0.73	0.76	0.81
ZrO ₂	0.27	0.16	0.33	0.58	0.23	0.34	0.12	0.15	0.24
ThO ₂	0.62	0.01	0.05	1.42	0.81	0.24	0.20	0.20	0.04
TiO ₂	49.57	53.00	49.98	46.75	48.10	50.39	49.87	51.66	51.72
BaO	0.11	0.12	0.12	0.12	0.10	0.12	0.09	0.11	0.13
Ce ₂ O ₃	6.66	3.59	5.93	7.61	7.49	6.29	5.58	5.74	4.22
Nd ₂ O ₃	2.10	1.13	1.79	2.29	2.31	1.91	1.80	1.76	1.33
Na ₂ O	2.29	1.36	1.86	2.75	2.25	1.76	1.86	1.74	1.29
MgO	0.04	0.03	0.04	0.06	0.35	0.10	0.18	0.04	0.11
Al ₂ O ₃	0.01	0.01	0.01	0.01	0.01	0.00	0.00	0.01	0.00
Ta ₂ O ₅	0.18	0.04	0.05	0.00	0.17	0.03	0.11	0.09	0.04
Total	99.58	99.74	99.30	99.80	99.22	100.70	98.90	100.47	99.90
Si	0.000	0.000	0.000	0.006	0.001	0.000	0.002	0.004	0.000
Fe	0.023	0.030	0.027	0.027	0.031	0.028	0.028	0.035	0.036
La	0.016	0.026	0.029	0.030	0.027	0.030	0.031	0.021	0.026
Sm	0.001	0.002	0.002	0.003	0.002	0.002	0.003	0.002	0.002
Pr	0.003	0.005	0.006	0.006	0.004	0.006	0.007	0.003	0.005
Ca	0.887	0.820	0.746	0.763	0.809	0.774	0.747	0.862	0.803
Nb	0.014	0.023	0.050	0.028	0.026	0.027	0.019	0.017	0.016
Sr	0.011	0.011	0.012	0.011	0.012	0.012	0.011	0.011	0.011
Zr	0.002	0.004	0.007	0.003	0.004	0.003	0.002	0.003	0.002
Th	0.000	0.000	0.008	0.005	0.001	0.003	0.004	0.000	0.002
Ti	0.952	0.928	0.890	0.911	0.925	0.922	0.935	0.936	0.935
Ba	0.001	0.001	0.001	0.001	0.001	0.001	0.001	0.001	0.001
Ce	0.031	0.054	0.070	0.069	0.056	0.069	0.069	0.037	0.058
Nd	0.010	0.016	0.021	0.021	0.017	0.020	0.022	0.011	0.017
Na	0.063	0.089	0.135	0.110	0.083	0.105	0.126	0.060	0.086
Mg	0.001	0.001	0.002	0.013	0.004	0.003	0.004	0.004	0.005
Al	0.000	0.000	0.000	0.000	0.000	0.000	0.000	0.000	0.000
Ta	0.000	0.000	0.000	0.001	0.000	0.000	0.001	0.000	0.001
Cations	2.015	2.012	2.008	2.008	2.003	2.006	2.010	2.008	2.006
<i>lueshite</i>	0.03	0.01	0.02	0.05	0.03	0.03	0.02	0.01	0.02
<i>loparite</i>	0.16	0.10	0.14	0.18	0.17	0.12	0.12	0.16	0.22
<i>REEFeO₃</i>	0.02	0.01	0.03	0.03	0.03	0.03	0.02	0.02	0.02
<i>tausonite</i>	0.01	0.01	0.01	0.01	0.01	0.01	0.01	0.01	0.01
<i>REE₂Ti₂O₇</i>	0.01	0.00	0.00	0.01	0.01	0.01	0.00	0.00	0.00
<i>lakargiite</i>	0.00	0.00	0.00	0.01	0.00	0.00	0.00	0.00	0.00
<i>perovskite</i>	0.76	0.86	0.79	0.71	0.75	0.80	0.82	0.79	0.72
<i>Fe/Nb</i>	1.35	0.54	0.95	1.22	1.05	5.87	1.66	2.25	1.64
<i>ΔNNO</i>	-3.38	-2.71	-6.97	-4.31	-2.91	-3.76	-3.02	-0.82	-0.47

TABELA B04 – Major element compositions for spinel from TRIV. Structural formula calculated on the basis of 32 oxygens. C - core; R - rim; I - intermediated; macro- macrocryst; micro- microcryst.

Sample	TR-4	TR4-1	TR4-1	TR4-1							
Grain/Analysis	01/01	01/02	02/03	02/04	03/05	03/06	04/07	04/08	05/09	05/10	06/11
Location	C	R	C	R	C	R	R	C	C	R	C
Crystal type	macro	macro	matr	matr	macro	macro	matr	matr	macro	macro	macro
Al ₂ O ₃	40.98	40.75	27.35	2.62	17.83	18.21	0.00	0.00	15.82	0.59	18.74
SiO ₂	0.00	0.05	0.01	0.13	0.00	0.00	0.00	0.00	0.00	0.01	0.04
FeO	15.03	14.48	19.15	67.84	19.35	19.25	1.43	1.50	19.16	33.31	21.93
MnO	0.16	0.17	0.21	0.92	0.27	0.26	0.00	0.00	0.26	0.89	0.30
NiO	0.16	0.17	0.09	0.19	0.06	0.05	0.00	0.02	0.04	0.15	0.12
K ₂ O	0.00	0.01	0.00	0.02	0.02	0.00	0.19	0.07	0.02	0.01	0.02
CaO	0.00	0.00	0.02	0.03	0.02	0.02	29.41	31.53	0.02	0.00	0.01
Nb ₂ O ₅	0.00	0.03	0.00	0.02	0.02	0.05	1.43	1.55	0.00	0.00	0.04
TiO ₂	0.14	0.01	0.23	3.89	0.58	0.26	51.20	51.03	0.17	3.86	0.05
Cr ₂ O ₃	27.73	27.76	40.99	18.96	51.84	51.57	0.54	0.51	53.63	53.52	47.72
V ₂ O ₅	0.15	0.09	0.19	0.04	0.26	0.27	0.25	0.22	0.25	0.16	0.20
ZnO	0.26	0.25	0.20	0.17	0.14	0.18	0.00	0.00	0.20	0.20	0.09
MgO	16.82	16.80	13.35	6.15	11.47	10.95	0.00	0.00	11.12	8.03	11.98
Na ₂ O	0.01	0.02	0.00	0.02	0.01	0.02	1.77	1.42	0.01	0.00	0.01
Total:	101.43	100.58	101.79	100.99	101.85	101.10	86.24	87.86	100.70	100.73	101.24
Al	10.807	10.822	7.761	0.899	5.325	5.485	0.000	0.001	4.822	0.200	5.588
Si	0.000	0.011	0.002	0.038	0.000	0.000	0.000	0.000	0.001	0.003	0.011
Fe ³⁺	2.531	2.455	3.470	14.857	3.690	3.702	0.349	0.357	3.729	7.154	4.175
Fe ²⁺	0.000	0.000	0.000	0.000	0.000	0.000	0.000	0.000	0.000	0.000	0.000
Mn	0.031	0.031	0.043	0.228	0.057	0.057	0.000	0.000	0.056	0.214	0.064
Ni	0.029	0.030	0.017	0.043	0.013	0.011	0.001	0.006	0.009	0.033	0.024
K	0.000	0.003	0.000	0.007	0.005	0.000	0.080	0.029	0.007	0.005	0.005
Ca	0.000	0.000	0.004	0.008	0.005	0.006	10.228	10.687	0.004	0.001	0.002
Nb	0.000	0.004	0.000	0.003	0.002	0.007	0.239	0.252	0.000	0.000	0.005
Ti	0.023	0.002	0.042	0.852	0.110	0.051	12.502	12.145	0.034	0.829	0.010
Cr	4.906	4.945	7.803	4.362	10.386	10.420	0.140	0.128	10.966	12.077	9.546
V	0.027	0.017	0.036	0.010	0.053	0.056	0.065	0.055	0.052	0.037	0.040
Zn	0.042	0.042	0.035	0.037	0.026	0.034	0.000	0.000	0.038	0.042	0.018
Mg	5.611	5.643	4.792	2.668	4.333	4.172	0.000	0.000	4.287	3.417	4.519
Na	0.003	0.007	0.000	0.009	0.004	0.009	1.114	0.871	0.003	0.000	0.006
Cations:	24.009	24.013	24.004	24.021	24.009	24.007	24.716	24.533	24.008	24.011	24.012

TABELA B04 – Cont. Major element compositions for spinel from TRIV. Structural formula calculated on the basis of 32 oxygens. C - core; R - rim; I - intermediated; macro- macrocryst; micro- microcryst.

Sample Grain/Analysis	TR4-1 06/12	TR4-1 07/13	TR4-1 07/14	TR4-1 08/15	TR4-1 08/16	TR4-2 09/17	TR4-2 08/18	TR4-2 09/19	TR4-2 10/20	TR4-2 11/21	TR4-2 11/22
Location	R	C	R	C	R	C	C	C	C	C	R
Crystal type	macro	macro	macro	macro	macro	-	-	-	-	-	-
Al ₂ O ₃	8.73	34.25	34.31	36.95	36.91	24.87	11.77	17.22	24.97	12.47	0.65
SiO ₂	0.02	0.00	0.01	0.04	0.03	0.00	0.00	0.01	0.01	0.00	0.00
FeO	37.15	15.69	15.79	14.74	15.05	18.32	22.85	21.38	18.21	21.01	34.63
MnO	0.38	0.18	0.18	0.18	0.18	0.23	0.30	0.31	0.26	0.32	0.88
NiO	0.23	0.12	0.12	0.13	0.11	0.09	0.09	0.10	0.09	0.09	0.17
K ₂ O	0.00	0.01	0.00	0.00	0.00	0.00	0.00	0.00	0.00	0.02	0.00
CaO	0.00	0.00	0.01	0.01	0.01	0.01	0.01	0.00	0.01	0.00	0.04
Nb ₂ O ₅	0.02	0.00	0.03	0.00	0.04	0.00	0.00	0.03	0.02	0.01	0.03
TiO ₂	1.44	0.00	0.16	0.08	0.05	0.37	0.20	0.01	0.00	0.17	4.21
Cr ₂ O ₃	44.13	33.92	33.55	31.48	31.62	43.62	55.54	51.71	43.96	56.42	51.62
V ₂ O ₅	0.21	0.14	0.15	0.16	0.17	0.15	0.23	0.21	0.18	0.25	0.15
ZnO	0.09	0.26	0.21	0.22	0.21	0.21	0.10	0.10	0.20	0.15	0.16
MgO	8.96	15.32	15.59	15.82	15.97	13.08	10.95	11.51	13.24	11.37	8.10
Na ₂ O	0.01	0.00	0.00	0.00	0.02	0.00	0.00	0.01	0.00	0.00	0.01
Total:	101.38	99.89	100.09	99.81	100.37	100.94	102.04	102.62	101.15	102.27	100.64
Al	2.796	9.464	9.447	10.074	10.015	7.186	3.618	5.125	7.190	3.799	0.217
Si	0.006	0.000	0.002	0.010	0.006	0.000	0.000	0.003	0.003	0.000	0.000
Fe ³⁺	7.597	2.768	2.776	2.566	2.607	3.380	4.484	4.063	3.348	4.087	7.443
Fe ²⁺	0.000	0.000	0.000	0.000	0.000	0.000	0.000	0.000	0.000	0.000	0.000
Mn	0.088	0.036	0.035	0.035	0.035	0.047	0.065	0.067	0.054	0.070	0.213
Ni	0.050	0.022	0.022	0.024	0.021	0.017	0.019	0.020	0.018	0.018	0.038
K	0.000	0.003	0.000	0.000	0.000	0.000	0.000	0.001	0.000	0.005	0.000
Ca	0.001	0.000	0.001	0.003	0.002	0.002	0.004	0.000	0.003	0.001	0.013
Nb	0.003	0.000	0.003	0.000	0.005	0.000	0.000	0.004	0.003	0.001	0.004
Ti	0.295	0.000	0.028	0.014	0.009	0.069	0.039	0.002	0.000	0.034	0.905
Cr	9.481	6.288	6.197	5.758	5.755	8.455	11.452	10.324	8.492	11.532	11.657
V	0.046	0.026	0.028	0.030	0.031	0.029	0.048	0.043	0.035	0.051	0.035
Zn	0.018	0.044	0.036	0.038	0.036	0.038	0.020	0.019	0.036	0.028	0.034
Mg	3.630	5.355	5.430	5.456	5.481	4.780	4.257	4.333	4.822	4.382	3.449
Na	0.004	0.001	0.000	0.000	0.009	0.001	0.000	0.004	0.002	0.000	0.003
Cations:	24.014	24.008	24.005	24.006	24.010	24.005	24.005	24.008	24.005	24.008	24.011

TABELA B04 – Cont. Major element compositions for spinel from TRIV. Structural formula calculated on the basis of 32 oxygens. C - core; R - rim; I - intermediated; macro- macrocryst; micro- microcryst.

Sample	TR4-2	TR4-2	TR4-2	TR4-2	TR-04A	TR-04A	TR-03	TR-03	TR-03	TR-03
Grain/Analysis	11/23	12/24	12/25	13/26	01/01	01/02	02/03	02/04	02/05	03/06
Location	R_reac	C	R	C	C	R	C	I	R	C
Crystal type	-	-	-	-	macro	macro	macro	macro	macro	micro
Al ₂ O ₃	0.27	17.04	1.10	0.18	13.70	0.47	20.57	20.08	0.32	21.03
SiO ₂	0.11	0.05	0.00	0.06	0.01	1.82	0.01	0.00	1.06	0.03
FeO	89.11	20.69	37.64	74.87	17.53	69.08	15.59	15.90	69.89	15.26
MnO	1.00	0.30	0.83	1.17	0.09	0.78	0.00	0.00	0.97	0.03
NiO	0.23	0.08	0.15	0.20	0.00	0.00	0.00	0.00	0.00	0.00
K ₂ O	0.00	0.00	0.01	0.00	0.00	0.00	0.00	0.00	0.00	0.00
CaO	0.07	0.01	0.06	0.01	0.00	0.00	0.00	0.00	0.00	0.00
Nb ₂ O ₅	0.00	0.00	0.01	0.00	0.00	0.00	0.00	0.00	0.00	0.00
TiO ₂	6.43	0.21	5.84	4.11	0.26	6.27	0.16	0.21	4.76	0.16
Cr ₂ O ₃	1.18	51.58	47.67	16.56	55.22	7.54	49.72	49.84	9.25	50.97
V ₂ O ₅	0.07	0.23	0.08	0.04	0.00	0.00	0.00	0.00	0.00	0.00
ZnO	0.07	0.13	0.12	0.15	0.00	0.00	0.00	0.00	0.00	0.00
MgO	4.16	11.73	8.20	4.28	10.97	5.94	13.06	13.49	5.97	12.99
Na ₂ O	0.00	0.00	0.01	0.00	0.00	0.00	0.00	0.00	0.00	0.00
Total:	102.71	102.07	101.72	101.63	97.77	91.88	99.10	99.54	92.21	100.48
Al	0.096	5.088	0.366	0.062	4.323	0.178	6.132	5.960	0.119	6.190
Si	0.034	0.014	0.000	0.018	0.003	0.585	0.002	0.001	0.339	0.008
Fe ³⁺	19.959	3.944	8.001	16.809	3.533	16.740	2.968	3.013	16.913	2.868
Fe ²⁺	0.000	0.000	0.000	0.000	0.000	0.000	0.000	0.000	0.000	0.000
Mn	0.251	0.065	0.198	0.296	0.019	0.212	0.000	0.000	0.264	0.007
Ni	0.055	0.017	0.033	0.049	0.000	0.000	0.000	0.000	0.000	0.000
K	0.000	0.000	0.005	0.000	0.000	0.000	0.000	0.000	0.000	0.000
Ca	0.022	0.003	0.019	0.003	0.000	0.000	0.000	0.000	0.000	0.000
Nb	0.000	0.000	0.001	0.000	0.000	0.000	0.000	0.000	0.000	0.000
Ti	1.440	0.041	1.241	0.922	0.053	1.518	0.029	0.041	1.152	0.029
Cr	0.278	10.331	10.647	3.906	11.691	1.918	9.945	9.922	2.351	10.062
V	0.017	0.048	0.019	0.010	0.000	0.000	0.000	0.000	0.000	0.000
Zn	0.016	0.025	0.025	0.032	0.000	0.000	0.000	0.000	0.000	0.000
Mg	1.846	4.430	3.453	1.904	4.378	2.849	4.924	5.064	2.861	4.837
Na	0.000	0.000	0.003	0.001	0.000	0.000	0.000	0.000	0.000	0.000
Cations:	24.014	24.004	24.014	24.013	24.000	24.000	24.000	24.000	24.000	24.000

TABELA B04 – Cont. Major element compositions for spinel from TRIV. Structural formula calculated on the basis of 32 oxygens. C - core; R - rim; I - intermediated; macro- macrocryst; micro- microcryst.

Sample Grain/Analysis	TR-03 03/07	TR-04B 04/08	TR-04B 04/09	TR-04B 05/10	TR-04B 05/11	TR-04B 06/12	TR-04B 06/13	TR-07 07/14	TR-07 07/15
Location	R	C	R	C	R	C	R	C	R
Crystal type	micro	micro	micro	micro	micro	micro	micro	micro	micro
Al ₂ O ₃	15.02	38.53	28.10	13.78	10.87	4.64	0.44	10.93	9.83
SiO ₂	0.13	0.01	0.39	0.07	0.05	0.01	0.09	0.04	0.12
FeO	21.78	13.56	23.43	18.06	22.52	23.19	77.16	19.86	21.63
MnO	0.39	0.00	0.22	0.07	0.08	0.12	0.71	0.02	0.06
NiO	0.00	0.00	0.00	0.00	0.00	0.00	0.00	0.00	0.00
K ₂ O	0.00	0.00	0.00	0.00	0.00	0.00	0.00	0.00	0.00
CaO	0.00	0.00	0.00	0.00	0.00	0.00	0.00	0.00	0.00
Nb ₂ O ₅	0.00	0.00	0.00	0.00	0.00	0.00	0.00	0.00	0.00
TiO ₂	1.01	0.02	1.39	0.20	0.42	0.10	6.86	0.17	0.13
Cr ₂ O ₃	46.92	32.20	28.38	54.99	53.40	61.67	1.80	56.54	53.47
V ₂ O ₅	0.00	0.00	0.00	0.00	0.00	0.00	0.00	0.00	0.00
ZnO	0.00	0.00	0.00	0.00	0.00	0.00	0.00	0.00	0.00
MgO	11.40	16.27	16.35	12.14	11.33	7.56	4.81	10.84	11.04
Na ₂ O	0.00	0.00	0.00	0.00	0.00	0.00	0.00	0.00	0.00
Total:	96.65	100.59	98.26	99.30	98.66	97.30	91.87	98.40	96.28
Al	4.752	10.346	8.013	4.252	3.443	1.579	0.170	3.479	3.200
Si	0.035	0.003	0.094	0.017	0.013	0.003	0.031	0.011	0.032
Fe ³⁺	4.400	2.324	4.266	3.558	4.554	5.038	19.083	4.036	4.498
Fe ²⁺	0.000	0.000	0.000	0.000	0.000	0.000	0.000	0.000	0.000
Mn	0.088	0.000	0.045	0.015	0.018	0.030	0.197	0.005	0.014
Ni	0.000	0.000	0.000	0.000	0.000	0.000	0.000	0.000	0.000
K	0.000	0.000	0.000	0.000	0.000	0.000	0.000	0.000	0.000
Ca	0.000	0.000	0.000	0.000	0.000	0.000	0.000	0.000	0.000
Nb	0.000	0.000	0.000	0.000	0.000	0.000	0.000	0.000	0.000
Ti	0.204	0.003	0.253	0.038	0.085	0.021	1.695	0.034	0.028
Cr	9.959	5.800	5.430	11.381	11.347	14.074	0.468	12.071	11.679
V	0.000	0.000	0.000	0.000	0.000	0.000	0.000	0.000	0.000
Zn	0.000	0.000	0.000	0.000	0.000	0.000	0.000	0.000	0.000
Mg	4.563	5.524	5.899	4.738	4.539	3.254	2.356	4.364	4.548
Na	0.000	0.000	0.000	0.000	0.000	0.000	0.000	0.000	0.000
Cations:	24.000	24.000	24.000	24.000	24.000	24.000	24.000	24.000	24.000

TABELA B04 – Cont. Major element compositions for spinel from TRIV. Structural formula calculated on the basis of 32 oxygens. C - core; R - rim; I - intermediated; macro- macrocryst; micro- microcryst.

Sample	TR-07	TR-07	TR-07	TR-07	TR-07	TR-04A	TR-04A	TR-04B	TR-04B	TR-02A
Grain/Analysis	08/16	08/17	08/18	09/19	09/20	10/21	10/22	11/23	11/24	12/25
Location	C	I	R	C	R	C	R	C	R	C
Crystal type	micro	micro	micro	micro	micro	mfc	mfc	mfc	mfc	mt
Al ₂ O ₃	32.10	31.51	0.59	12.20	0.76	9.71	0.74	0.96	0.42	35.57
SiO ₂	0.02	0.11	1.86	0.08	0.39	0.03	0.03	0.03	0.53	0.00
FeO	14.51	14.30	71.76	17.61	74.75	17.83	27.04	27.52	39.30	13.60
MnO	0.03	0.02	0.95	0.00	0.98	0.00	0.23	0.12	0.86	0.03
NiO	0.00	0.00	0.00	0.00	0.00	0.00	0.00	0.00	0.00	0.00
K ₂ O	0.00	0.00	0.00	0.00	0.00	0.00	0.00	0.00	0.00	0.00
CaO	0.00	0.00	0.00	0.00	0.00	0.00	0.00	0.00	0.00	0.00
Nb ₂ O ₅	0.00	0.00	0.00	0.00	0.00	0.00	0.00	0.00	0.00	0.00
TiO ₂	0.26	0.39	5.96	0.07	6.84	0.30	3.37	3.78	20.28	0.04
Cr ₂ O ₃	36.60	36.93	1.58	56.62	1.22	59.51	54.83	53.21	13.01	35.78
V ₂ O ₅	0.00	0.00	0.00	0.00	0.00	0.00	0.00	0.00	0.00	0.00
ZnO	0.00	0.00	0.00	0.00	0.00	0.00	0.00	0.00	0.00	0.00
MgO	14.76	14.83	7.79	10.48	4.80	10.89	9.95	9.95	6.13	16.18
Na ₂ O	0.00	0.00	0.00	0.00	0.00	0.00	0.00	0.00	0.00	0.00
Total:	98.28	98.09	90.47	97.06	89.74	98.26	96.19	95.57	80.53	101.20
Al	9.086	8.948	0.224	3.916	0.300	3.107	0.256	0.332	0.181	9.617
Si	0.004	0.026	0.596	0.021	0.131	0.007	0.010	0.008	0.192	0.000
Fe ³⁺	2.622	2.593	17.352	3.607	18.846	3.643	5.943	6.082	10.753	2.347
Fe ²⁺	0.000	0.000	0.000	0.000	0.000	0.000	0.000	0.000	0.000	0.000
Mn	0.007	0.003	0.258	0.000	0.279	0.000	0.056	0.029	0.265	0.006
Ni	0.000	0.000	0.000	0.000	0.000	0.000	0.000	0.000	0.000	0.000
K	0.000	0.000	0.000	0.000	0.000	0.000	0.000	0.000	0.000	0.000
Ca	0.000	0.000	0.000	0.000	0.000	0.000	0.000	0.000	0.000	0.000
Nb	0.000	0.000	0.000	0.000	0.000	0.000	0.000	0.000	0.000	0.000
Ti	0.046	0.070	1.440	0.015	1.723	0.061	0.740	0.836	5.547	0.006
Cr	6.949	7.034	0.400	12.187	0.322	12.775	12.663	12.355	3.740	6.489
V	0.000	0.000	0.000	0.000	0.000	0.000	0.000	0.000	0.000	0.000
Zn	0.000	0.000	0.000	0.000	0.000	0.000	0.000	0.000	0.000	0.000
Mg	5.286	5.326	3.731	4.254	2.398	4.407	4.332	4.358	3.323	5.534
Na	0.000	0.000	0.000	0.000	0.000	0.000	0.000	0.000	0.000	0.000
Cations:	24.000									

TABELA B04 – Cont. Major element compositions for spinel from TRIV. Structural formula calculated on the basis of 32 oxygens. C - core; R - rim; I - intermediated; macro- macrocryst; micro- microcryst.

Sample Grain/Analysis	TR-02A 12/26	TR-02A 12/27	TR-02A 13/28	TR-02A 13/29	TR-03 14/30	TR-03 15/31	TR-03 15/32
Location	I	R	C	R	C	C	R
Crystal type	mt	mt	mt	mt	mt	mt.eud.	mt.eud.
Al ₂ O ₃	0.82	0.44	6.83	0.31	0.63	1.17	0.20
SiO ₂	0.18	0.99	0.00	0.50	0.09	0.11	0.04
FeO	29.15	61.61	21.41	53.98	33.31	30.61	78.10
MnO	0.75	1.02	0.04	0.99	0.92	0.51	0.92
NiO	0.00	0.00	0.00	0.00	0.00	0.00	0.00
K ₂ O	0.00	0.00	0.00	0.00	0.00	0.00	0.00
CaO	0.00	0.00	0.00	0.00	0.00	0.00	0.00
Nb ₂ O ₅	0.00	0.00	0.00	0.00	0.00	0.00	0.00
TiO ₂	3.45	4.72	0.11	11.18	4.57	4.62	7.59
Cr ₂ O ₃	55.06	16.46	59.38	17.39	46.76	51.83	0.80
V ₂ O ₅	0.00	0.00	0.00	0.00	0.00	0.00	0.00
ZnO	0.00	0.00	0.00	0.00	0.00	0.00	0.00
MgO	8.44	6.04	10.19	4.85	7.44	8.91	4.43
Na ₂ O	0.00	0.00	0.00	0.00	0.00	0.00	0.00
Total:	97.85	91.28	97.95	89.19	93.72	97.76	92.07
Al	0.283	0.168	2.235	0.122	0.228	0.400	0.077
Si	0.052	0.319	0.000	0.166	0.028	0.032	0.013
Fe ³⁺	6.387	14.976	4.474	13.595	7.695	6.685	19.385
Fe ²⁺	0.000	0.000	0.000	0.000	0.000	0.000	0.000
Mn	0.184	0.280	0.010	0.280	0.240	0.124	0.258
Ni	0.000	0.000	0.000	0.000	0.000	0.000	0.000
K	0.000	0.000	0.000	0.000	0.000	0.000	0.000
Ca	0.000	0.000	0.000	0.000	0.000	0.000	0.000
Nb	0.000	0.000	0.000	0.000	0.000	0.000	0.000
Ti	0.756	1.148	0.023	2.816	1.055	1.009	1.883
Cr	12.675	4.204	13.041	4.603	11.348	11.893	0.208
V	0.000	0.000	0.000	0.000	0.000	0.000	0.000
Zn	0.000	0.000	0.000	0.000	0.000	0.000	0.000
Mg	3.664	2.906	4.217	2.418	3.406	3.856	2.177
Na	0.000	0.000	0.000	0.000	0.000	0.000	0.000
Cations:	24.000	24.000	24.000	24.000	24.000	24.000	24.000

TABELA B05 - Major element compositions of ilmenite from LM-I all samples. Structural formula calculated on the basis of 6 oxygens. C - core; R - rim; I - intermediately..

Sample Grain/Analysis	LM-2 01/01	LM-2 01/02	LM-2 02/03	LM-2 02/04	LM-2 03/05	LM-2 03/06	LM-2 04/07	LM-2 04/08	LM-2 05/09	LM-2 05/10	LM-2 06/11	LM-2 06/12	LM-2 07/13	LM-2 07/14	LM-2 08/15	LM-2 08/16	LM-2 09/17	LM-2 09/18
Location	C	R	C	R	C	R	C	R	C	R	C	R	C	R	C	R	C	R
SiO ₂	0.02	0.02	0.05	0.00	0.01	0.02	0.02	0.03	0.02	0.06	0.02	0.04	0.01	0.03	0.02	0.03	0.02	0.03
FeO	31.17	29.87	31.54	30.48	31.70	30.87	37.03	34.46	39.73	37.85	28.63	28.45	32.01	31.44	29.90	29.62	31.95	31.17
MnO	0.39	0.44	0.32	0.43	0.34	0.45	0.47	0.59	0.45	0.56	0.71	0.72	0.44	0.51	0.80	0.78	0.38	0.43
NiO	0.21	0.21	0.19	0.22	0.22	0.20	0.08	0.10	0.07	0.07	0.16	0.15	0.16	0.15	0.15	0.13	0.20	0.18
K ₂ O	0.00	0.01	0.00	0.03	0.01	0.02	0.00	0.02	0.04	0.02	0.01	0.01	0.02	0.01	0.00	0.00	0.00	0.00
CaO	0.00	0.05	0.01	0.00	0.01	0.04	0.04	0.12	0.01	0.11	0.06	0.12	0.02	0.02	0.05	0.17	0.03	0.05
Nb ₂ O ₅	0.17	0.15	0.20	0.20	0.09	0.13	0.15	0.19	0.40	0.34	0.15	0.16	0.17	0.19	0.23	0.13	0.15	0.11
TiO ₂	50.01	50.72	49.65	50.40	50.08	50.02	47.84	49.14	46.75	47.34	50.61	51.20	49.77	49.65	50.96	51.01	50.58	50.86
Cr ₂ O ₃	4.02	3.73	4.16	4.11	3.94	3.85	1.55	1.59	1.10	1.15	3.79	4.19	4.13	4.22	3.10	3.21	3.85	3.84
ZnO	0.02	0.01	0.03	0.00	0.01	0.00	0.00	0.00	0.00	0.01	0.03	0.07	0.05	0.03	0.00	0.04	0.02	0.00
MgO	12.29	12.65	11.86	12.26	11.96	12.32	10.35	11.49	8.61	10.15	13.65	14.07	11.70	12.16	13.01	13.19	12.01	12.62
Na ₂ O	0.03	0.04	0.00	0.02	0.00	0.00	0.02	0.04	0.01	0.03	0.05	0.04	0.02	0.01	0.01	0.03	0.00	0.00
Total:	98.50	97.97	98.12	98.21	98.45	97.99	97.64	97.82	97.18	97.72	97.94	99.31	98.54	98.51	98.25	98.35	99.28	99.36
Al	0.009	0.005	0.005	0.003	0.004	0.004	0.005	0.004	0.000	0.001	0.003	0.005	0.003	0.003	0.003	0.001	0.001	0.003
Si	0.001	0.001	0.002	0.000	0.001	0.001	0.001	0.001	0.001	0.003	0.001	0.001	0.002	0.000	0.001	0.001	0.001	0.001
Fe ³⁺	0.000	0.000	0.000	0.000	0.000	0.000	0.000	0.000	0.000	0.000	0.000	0.000	0.000	0.000	0.000	0.000	0.000	0.000
Fe ²⁺	1.213	1.166	1.236	1.191	1.237	1.207	1.469	1.355	1.606	1.503	1.109	1.085	1.251	1.225	1.161	1.146	1.237	1.200
Mn	0.015	0.017	0.013	0.017	0.014	0.018	0.019	0.023	0.018	0.023	0.028	0.028	0.017	0.020	0.032	0.031	0.015	0.017
Ni	0.008	0.008	0.007	0.008	0.008	0.008	0.003	0.004	0.003	0.003	0.006	0.005	0.006	0.006	0.005	0.005	0.007	0.007
K	0.000	0.000	0.000	0.002	0.001	0.001	0.000	0.000	0.001	0.002	0.001	0.000	0.001	0.001	0.000	0.000	0.000	0.000
Ca	0.000	0.003	0.001	0.000	0.001	0.002	0.002	0.006	0.000	0.006	0.003	0.006	0.001	0.001	0.002	0.009	0.001	0.003
Nb	0.004	0.003	0.005	0.005	0.002	0.003	0.004	0.005	0.010	0.008	0.003	0.004	0.004	0.005	0.006	0.003	0.004	0.003
Ti	1.751	1.781	1.750	1.772	1.758	1.759	1.708	1.738	1.700	1.691	1.764	1.756	1.749	1.740	1.780	1.776	1.761	1.762
Cr	0.148	0.138	0.154	0.152	0.145	0.142	0.058	0.059	0.042	0.043	0.139	0.151	0.153	0.155	0.114	0.117	0.141	0.140
Zn	0.001	0.000	0.001	0.000	0.000	0.000	0.000	0.000	0.000	0.001	0.002	0.002	0.001	0.001	0.001	0.001	0.001	0.000
Mg	0.852	0.880	0.828	0.854	0.832	0.859	0.732	0.805	0.620	0.719	0.943	0.956	0.815	0.844	0.900	0.910	0.829	0.866
Na	0.002	0.003	0.000	0.002	0.000	0.000	0.002	0.003	0.001	0.003	0.005	0.004	0.002	0.001	0.001	0.003	0.000	0.000
Total	4.004	4.005	4.002	4.005	4.003	4.002	4.004	4.002	4.004	4.006	4.004	4.005	4.004	4.004	4.003	4.004	4.002	4.002

TABELA B05 – Cont. Major element compositions of ilmenite from LM-I all samples. Structural formula calculated on the basis of 6 oxygens. C - core; R - rim; I – intermediate.

Sample	LM3-1	LM3-2										
Grain/Analysis	10/19	10/20	11/21	11/22	12/23	12/24	13/25	13/26	14/27	14/28	15/30	16/31
Location	C	R	C	R	C	R	C	R	C	R	C	C
SiO ₂	0.00	0.03	0.02	0.02	0.01	0.03	0.02	0.03	0.02	0.02	0.03	0.00
FeO	33.83	32.08	39.09	38.56	32.04	31.29	31.02	31.54	32.29	30.09	17.78	42.81
MnO	0.58	0.69	0.46	0.51	0.55	0.62	0.36	0.37	0.36	0.55	1.70	0.34
NiO	0.14	0.11	0.09	0.10	0.16	0.13	0.21	0.21	0.22	0.17	0.07	0.10
K ₂ O	0.01	0.00	0.03	0.00	0.01	0.01	0.00	0.00	0.00	0.00	0.02	0.03
CaO	0.05	0.07	0.00	0.11	0.04	0.06	0.02	0.03	0.05	0.21	0.36	0.00
Nb ₂ O ₅	0.32	0.24	0.39	0.40	0.16	0.11	0.11	0.14	0.13	0.08	0.12	0.56
TiO ₂	50.70	45.57	46.19	51.07	50.22	49.90	50.25	49.27	49.93	58.29	58.26	45.91
Cr ₂ O ₃	1.75	1.77	2.68	2.70	3.40	3.32	4.26	4.41	4.25	5.11	0.02	4.00
ZnO	0.01	0.01	0.00	0.00	0.02	0.02	0.08	0.00	0.02	0.02	0.00	0.01
MgO	12.02	12.85	9.53	9.82	11.69	12.43	12.23	12.43	11.71	12.61	20.54	20.30
Na ₂ O	0.02	0.02	0.00	0.01	0.04	0.05	0.00	0.01	0.00	0.06	0.05	0.02
Total:	99.48	99.52	97.92	98.47	99.25	98.34	98.30	99.48	98.34	98.89	98.77	99.02
Al	0.003	0.004	0.003	0.004	0.003	0.005	0.003	0.003	0.002	0.008	0.000	0.005
Si	0.000	0.001	0.001	0.000	0.001	0.001	0.001	0.001	0.001	0.001	0.000	0.000
Fe ³⁺	0.000	0.000	0.000	0.000	0.000	0.000	0.000	0.000	0.000	0.000	0.000	0.000
Fe ²⁺	1.307	1.231	1.556	1.524	1.244	1.218	1.210	1.215	1.263	1.164	0.652	1.714
Mn	0.023	0.027	0.018	0.020	0.022	0.025	0.014	0.014	0.022	0.063	0.014	0.015
Ni	0.005	0.004	0.004	0.004	0.006	0.005	0.008	0.008	0.008	0.006	0.002	0.009
K	0.000	0.000	0.002	0.000	0.001	0.000	0.000	0.000	0.000	0.001	0.000	0.001
Ca	0.003	0.003	0.000	0.005	0.002	0.003	0.001	0.001	0.002	0.010	0.017	0.001
Nb	0.008	0.006	0.010	0.010	0.004	0.003	0.003	0.003	0.003	0.002	0.003	0.014
Ti	1.762	1.780	1.632	1.642	1.784	1.758	1.751	1.742	1.734	1.737	1.924	1.654
Cr	0.064	0.064	0.101	0.101	0.125	0.122	0.157	0.161	0.157	0.187	0.001	0.145
Zn	0.000	0.000	0.000	0.001	0.001	0.003	0.000	0.001	0.001	0.000	0.000	0.000
Mg	0.828	0.879	0.676	0.692	0.809	0.862	0.850	0.854	0.817	0.869	1.344	0.819
Na	0.002	0.002	0.000	0.001	0.003	0.005	0.000	0.001	0.000	0.004	0.000	0.002
Total	4.003	4.003	4.002	4.002	4.004	4.005	4.003	4.003	4.003	4.004	4.004	4.005

TABELA B05 – Cont. Major element compositions of ilmenite from LM-I all samples. Structural formula calculated on the basis of 6 oxygens. C - core; R - rim; I – intermediately.

Sample Grain/Analysis Location	LM3-2 18/33	LM3-2 18/34	LM3-2 19/35	LM3-2 C	LM3-2 R	LM3-2 C	LM3-2 R	LM3-2 C	LM3-2 R	LM3-2 R reac
SiO ₂	0.02	0.00	0.03	0.04	0.00	0.02	0.00	0.02	0.00	0.00
FeO	33.38	1.29	36.72	34.95	35.63	33.33	1.72			
MnO	0.57	0.02	0.52	0.56	0.37	0.56	0.04			
NiO	0.11	0.05	0.12	0.12	0.15	0.12	0.00			
K ₂ O	0.00	0.06	0.01	0.03	0.00	0.00	0.00	0.00	0.00	0.08
CaO	0.22	38.27	0.02	1.00	0.01	0.12	36.96			
Nb ₂ O ₅	0.19	0.47	0.16	0.10	0.27	0.16	0.98			
TiO ₂	50.56	54.59	50.31	49.13	48.25	49.12	52.98			
Cr ₂ O ₃	1.85	0.32	1.38	1.58	3.94	3.97	0.11			
ZnO	0.02	0.02	0.01	0.03	0.03	0.00	0.01			
MgO	12.02	0.00	10.31	11.03	10.36	11.73	0.00			
Na ₂ O	0.02	0.43	0.02	0.02	0.00	0.00	0.55			
Total:	99.06	95.56	99.66	98.65	99.06	99.20	93.49			
Al	0.006	0.002	0.003	0.003	0.003	0.003	0.003	0.003	0.003	0.003
Si	0.001	0.000	0.001	0.002	0.000	0.001	0.000	0.001	0.000	0.000
Fe ³⁺	0.000	0.000	0.000	0.000	0.000	0.000	0.000	0.000	0.000	0.000
Fe ²⁺	1.293	0.051	1.433	1.364	1.398	1.292	0.070			
Mn	0.022	0.001	0.021	0.022	0.015	0.022	0.002			
Ni	0.004	0.002	0.004	0.004	0.006	0.004	0.000			
K	0.000	0.003	0.001	0.002	0.000	0.000	0.005			
Ca	0.011	1.951	0.001	0.050	0.000	0.006	1.932			
Nb	0.005	0.012	0.004	0.002	0.007	0.004	0.025			
Ti	1.761	1.954	1.766	1.725	1.702	1.713	1.945			
Cr	0.068	0.012	0.051	0.058	0.146	0.145	0.004			
Zn	0.001	0.001	0.000	0.001	0.001	0.000	0.000			
Mg	0.830	0.000	0.717	0.767	0.724	0.811	0.000			
Na	0.002	0.040	0.002	0.002	0.000	0.000	0.052			
Total	4.003	4.029	4.004	4.004	4.002	4.001	4.038			

TABELA B06 - Major element compositions of clinopyroxene from TRIV and LMI all samples. Structural formula calculated on the basis of 6 oxygens. C - core; R - rim; I - intermediated; mt - matrix; mega - megacryst.

Sample Grain/Analysis	TR-02A 01/01	TR-02A 01/02	TR-02A 02/03	TR-02A 03/04	TR-07 04/05	TR-07 04/06	TR-07 05/07	TR-07 06/08	TR-07 07/09	TR-07 08/10
Location	C mt	R mt	C mt	C mt	C mt	R mt	C mt	C mt	C mt	C mt
Crystal type										
SiO ₂	51.72	53.46	51.76	51.76	52.92	51.30	51.25	48.45	50.97	50.41
TiO ₂	0.93	0.56	0.63	0.63	0.73	0.79	1.98	1.81	1.41	1.21
Al ₂ O ₃	0.13	0.19	0.16	0.16	0.13	0.15	0.41	0.41	0.26	0.21
FeO	4.86	2.77	3.27	3.27	4.77	3.00	4.51	4.26	3.82	3.67
MnO	0.11	0.04	0.07	0.07	0.13	0.07	0.11	0.17	0.08	0.08
MgO	15.47	16.07	16.81	16.81	15.84	17.45	15.63	15.60	16.13	16.47
CaO	22.91	23.29	24.10	24.10	23.58	24.88	23.02	23.06	23.28	23.65
Na ₂ O	1.34	0.53	0.87	0.87	1.01	0.67	1.31	1.18	1.11	0.94
K ₂ O	0.01	0.01	0.00	0.00	0.01	0.02	0.00	0.01	0.00	0.00
Cr ₂ O ₃	0.44	0.22	0.16	0.16	0.10	0.03	0.23	0.34	0.25	0.16
Total	97.91	97.13	97.83	97.83	99.22	98.36	98.45	95.29	97.31	96.80
Si (T)	1.928	2.007	1.919	1.919	1.948	1.889	1.902	1.854	1.907	1.892
Al (T)	0.006	0.000	0.007	0.007	0.005	0.007	0.018	0.019	0.011	0.009
Fe ₃ (T)	0.066	0.000	0.074	0.074	0.046	0.092	0.080	0.127	0.082	0.098
Σ (T)	2.000	2.007	2.000	2.000	2.000	1.988	2.000	2.000	2.000	2.000
Al (M1)	0.000	0.008	0.000	0.000	0.000	0.000	0.000	0.000	0.000	0.000
Ti (M1)	0.026	0.016	0.018	0.018	0.020	0.022	0.055	0.052	0.040	0.034
Fe ³⁺ (M1)	0.085	0.000	0.027	0.027	0.081	0.000	0.060	0.009	0.038	0.017
Cr (M1)	0.013	0.006	0.005	0.005	0.003	0.001	0.007	0.010	0.007	0.005
Mg (M1)	0.860	0.899	0.929	0.929	0.870	0.957	0.865	0.890	0.899	0.922
Fe ²⁺ (M1)	0.000	0.070	0.000	0.000	0.019	0.000	0.000	0.000	0.000	0.000
Mn (M1)	0.004	0.000	0.002	0.002	0.004	0.002	0.003	0.006	0.003	0.002
Σ (M1)	0.988	1.000	0.980	0.980	0.997	0.982	0.991	0.967	0.986	0.980
Mg (M2)	0.000	0.000	0.000	0.000	0.000	0.000	0.000	0.000	0.000	0.000
Fe ²⁺ (M2)	0.000	0.017	0.000	0.000	0.000	0.000	0.000	0.000	0.000	0.000
Mn (M2)	0.000	0.001	0.000	0.000	0.000	0.000	0.000	0.000	0.000	0.000
Ca (M2)	0.915	0.936	0.957	0.957	0.930	0.981	0.915	0.945	0.933	0.951
Na (M2)	0.097	0.038	0.062	0.062	0.072	0.048	0.094	0.088	0.081	0.069
K (M2)	0.000	0.001	0.000	0.000	0.001	0.001	0.000	0.000	0.000	0.000
Σ (M2)	1.012	0.993	1.020	1.020	1.003	1.030	1.009	1.033	1.014	1.020
Cations	4.000	4.000	4.000	4.000	4.000	4.000	4.000	4.000	4.000	4.000
Sum	90.54	97.18	93.90	93.90	92.19	94.27	89.60	90.23	91.69	92.32
Xen	0.51	0.48	0.51	0.51	0.50	0.51	0.51	0.51	0.51	0.51
Xwo	0.49	0.49	0.49	0.49	0.49	0.49	0.48	0.49	0.49	0.49
Xfs	0.00	0.03	0.00	0.00	0.01	0.00	0.00	0.00	0.00	0.00

TABELA B06 – Cont. Major element compositions of clinopyroxene from TRIV and LMI all samples. Structural formula calculated on the basis of 6 oxygens. C - core; R - rim; I - intermediated; mt - matrix; mega - megacryst.

Sample	TR-07	LMI-B2							
Grain/Analysis	09/11	10/12	11/13	11/14	12/15	12/16	13/17	13/18	01/01
Location	C	C	C	R	C	R	C	R	C
Crystal type	mt	mega							
SiO ₂	48.76	50.53	51.01	50.58	52.11	52.09	53.34	52.50	52.73
TiO ₂	2.10	1.05	2.12	1.13	0.50	0.85	0.57	0.60	0.32
Al ₂ O ₃	0.32	0.23	0.31	0.23	0.11	0.09	0.09	0.10	0.10
FeO	4.40	3.51	4.33	3.29	3.50	3.49	3.49	3.38	3.22
MnO	0.12	0.07	0.08	0.07	0.11	0.15	0.15	0.06	0.09
MgO	15.56	16.50	15.54	15.87	16.19	16.45	16.45	15.88	20.80
CaO	22.79	23.66	22.67	23.69	23.69	23.76	23.76	23.70	21.87
Na ₂ O	1.31	0.91	1.35	0.88	0.95	0.93	0.93	0.82	0.57
K ₂ O	0.01	0.08	0.01	0.01	0.00	0.03	0.03	0.02	0.21
Cr ₂ O ₃	0.27	0.27	0.28	0.24	0.47	0.39	0.39	0.38	0.10
Total	95.63	96.80	97.69	95.97	97.63	98.23	99.20	97.41	100.00
Si (T)	1.860	1.896	1.908	1.919	1.941	1.929	1.956	1.964	1.887
Al (T)	0.014	0.010	0.014	0.010	0.005	0.004	0.004	0.004	0.004
Fe ₃ (T)	0.126	0.094	0.079	0.071	0.054	0.067	0.040	0.031	0.096
Σ (T)	2.000	1.988							
Al (M1)	0.000	0.000	0.000	0.000	0.000	0.000	0.000	0.000	0.000
Ti (M1)	0.060	0.029	0.060	0.032	0.014	0.024	0.016	0.017	0.009
Fe ₃₊ (M1)	0.014	0.016	0.057	0.033	0.055	0.041	0.067	0.052	0.000
Cr (M1)	0.008	0.008	0.008	0.007	0.014	0.012	0.011	0.011	0.003
Mg (M1)	0.885	0.923	0.866	0.897	0.899	0.908	0.899	0.886	0.989
Fe ₂₊ (M1)	0.000	0.000	0.000	0.000	0.000	0.000	0.000	0.023	0.000
Mn (M1)	0.004	0.002	0.002	0.002	0.004	0.005	0.005	0.002	0.000
Σ (M1)	0.972	0.979	0.993	0.972	0.986	0.989	0.999	0.990	1.000
Mg (M2)	0.000	0.000	0.000	0.000	0.000	0.000	0.000	0.000	0.121
Fe ₂₊ (M2)	0.000	0.000	0.000	0.000	0.000	0.000	0.000	0.000	0.000
Mn (M2)	0.000	0.000	0.000	0.000	0.000	0.000	0.000	0.000	0.003
Ca (M2)	0.932	0.951	0.908	0.963	0.946	0.943	0.934	0.950	0.839
Na (M2)	0.097	0.066	0.098	0.064	0.069	0.067	0.066	0.060	0.040
K (M2)	0.000	0.004	0.000	0.000	0.000	0.001	0.001	0.001	0.010
Σ (M2)	1.028	1.021	1.007	1.028	1.014	1.011	1.001	1.010	1.012
Cations	4.000								
Sum	89.54	92.83	89.60	92.93	93.58	93.16	93.56	94.81	94.75
Xen	0.52	0.51	0.52	0.50	0.50	0.51	0.50	0.49	0.59
Xwo	0.48	0.49	0.48	0.50	0.50	0.49	0.49	0.50	0.41
Xfs	0.00	0.00	0.00	0.00	0.00	0.00	0.00	0.01	0.00

TABELA B06 – Cont. Major element compositions of clinopyroxene from TRIV and LMI all samples. Structural formula calculated on the basis of 6 oxygens. C - core; R - rim; I - intermediately; mt - matrix; mega – megacryst.

Sample Grain/Analysis	LMI-B2 01/02	LMI-B2 01/03	LMI-B2 01/04	LMI-A1 02/05	LMI-A1 02/06	LMI-A1 02/07	LMI-A1 02/08	LMI-A1 02/09
Location	R	C	R	C	R	R	C	C
Crystal type	mega	mega	mega	mega	macro	macro	macro	macro
SiO ₂	53.21	45.81	50.56	54.31	54.29	54.29	54.07	53.90
TiO ₂	0.36	0.18	0.26	0.15	0.14	0.23	0.18	0.21
Al ₂ O ₃	0.05	0.51	0.35	0.21	0.23	0.32	0.21	0.19
FeO	2.78	7.67	4.17	3.09	3.19	3.36	3.16	3.09
MnO	0.07	0.19	0.13	0.12	0.10	0.12	0.12	0.11
MgO	18.59	30.36	24.02	17.60	17.43	17.54	17.57	17.55
CaO	23.79	12.83	19.30	22.66	22.92	22.16	23.01	23.07
Na ₂ O	0.62	0.31	0.40	0.81	0.79	0.79	0.81	0.81
K ₂ O	0.10	0.21	0.14	0.00	0.00	0.01	0.01	0.03
Cr ₂ O ₃	0.16	0.13	0.13	0.88	0.92	1.02	0.97	1.08
Total	99.72	98.20	99.44	99.82	100.02	99.85	100.11	100.02
Si (T)	1.925	1.620	1.801	1.973	1.970	1.974	1.959	1.955
Al (T)	0.002	0.021	0.015	0.009	0.010	0.014	0.009	0.008
Fe ₃ (T)	0.073	0.227	0.124	0.018	0.020	0.012	0.032	0.037
Σ (T)	2.000	1.868	1.940	2.000	2.000	2.000	2.000	2.000
Al (M1)	0.000	0.000	0.000	0.000	0.000	0.000	0.000	0.000
Ti (M1)	0.010	0.005	0.007	0.004	0.004	0.006	0.005	0.006
Fe ₃₊ (M1)	0.011	0.000	0.000	0.051	0.051	0.040	0.061	0.056
Cr (M1)	0.005	0.004	0.004	0.025	0.027	0.029	0.028	0.031
Mg (M1)	0.975	0.992	0.989	0.920	0.919	0.924	0.907	0.907
Fe ₂₊ (M1)	0.000	0.000	0.000	0.000	0.000	0.000	0.000	0.000
Mn (M1)	0.000	0.000	0.000	0.000	0.000	0.000	0.000	0.000
Σ (M1)	1.000							
Mg (M2)	0.028	0.609	0.286	0.033	0.024	0.027	0.042	0.042
Fe ₂₊ (M2)	0.000	0.000	0.000	0.025	0.026	0.050	0.003	0.000
Mn (M2)	0.002	0.006	0.004	0.004	0.003	0.004	0.004	0.003
Ca (M2)	0.922	0.486	0.737	0.882	0.891	0.863	0.893	0.896
Na (M2)	0.043	0.021	0.027	0.057	0.055	0.056	0.057	0.057
K (M2)	0.005	0.010	0.006	0.000	0.000	0.000	0.000	0.001
Σ (M2)	1.000	1.132	1.060	1.000	1.000	1.000	1.000	1.000
Cations	4.000							
Sum	95.25	89.09	93.60	96.19	96.09	96.73	94.90	94.79
Xen	0.53	0.85	0.66	0.52	0.51	0.51	0.52	0.52
Xwo	0.47	0.15	0.33	0.47	0.47	0.46	0.47	0.47
Xfs	0.00	0.00	0.00	0.02	0.02	0.03	0.00	0.00

TABELA B07 - Major element compositions of garnet from TRIV all samples. Structural formula calculated on the basis of 24 oxygens. C - core; R - rim; I - intermediated.

Sample Grain/Analysis Location	TR-04A 01/01 C	TR-04A 01/02 I	TR-04A 01/03 R	TR-04A 02/04 C	TR-04A 02/06 R	TR-04B 03/07 C	TR-04B 03/08 I	TR-04B 03/09 R	TR-04B 04/10 C
SiO ₂	42.06	42.19	41.58	42.08	42.56	42.52	42.54	42.17	42.44
TiO ₂	0.22	0.21	0.22	0.26	0.12	0.06	0.09	0.05	0.23
Al ₂ O ₃	20.94	21.14	20.65	22.87	23.03	20.63	20.72	20.58	22.20
Cr ₂ O ₃	2.90	2.78	3.31	0.91	0.67	4.25	4.02	4.30	1.49
FeOT	9.22	9.44	8.99	9.38	9.20	7.49	7.34	7.63	9.56
MnO	0.40	0.39	0.41	0.35	0.32	0.39	0.37	0.43	0.42
MgO	19.38	19.34	19.15	20.26	19.43	21.19	21.04	20.07	19.62
CaO	4.81	4.82	4.81	3.99	4.05	4.41	4.66	5.16	4.59
Na ₂ O	0.04	0.03	0.07	0.04	0.04	0.05	0.02	0.04	0.08
Total	99.98	100.33	99.20	100.14	99.42	100.99	100.79	100.42	100.63
Si	3.000	3.000	3.000	2.988	3.000	3.000	3.000	3.000	3.000
Al ^{IV}	0.000	0.000	0.000	0.012	0.000	0.000	0.000	0.000	0.000
ΣT	3.000								
Si	0.021	0.021	0.013	0.000	0.049	0.004	0.011	0.009	0.014
Ti	0.012	0.011	0.012	0.014	0.006	0.003	0.005	0.003	0.012
Al ^{VI}	1.772	1.784	1.764	1.903	1.944	1.718	1.728	1.730	1.859
Cr	0.165	0.157	0.190	0.051	0.038	0.238	0.225	0.243	0.084
Fe ²⁺	0.006	0.006	0.003	0.000	0.000	0.000	0.002	0.000	0.001
Fe ³⁺	0.002	0.000	0.006	0.034	0.000	0.037	0.019	0.009	0.015
Mg	0.021	0.021	0.013	0.000	0.000	0.001	0.011	0.006	0.014
ΣA	2.000	2.000	2.000	2.002	2.038	2.000	2.000	2.000	2.000
Fe ²⁺	0.545	0.560	0.536	0.523	0.551	0.406	0.413	0.446	0.551
Mg	2.054	2.043	2.056	2.145	2.075	2.231	2.209	2.129	2.064
Mn	0.025	0.023	0.025	0.021	0.020	0.023	0.022	0.026	0.025
Ca	0.370	0.370	0.374	0.304	0.311	0.334	0.353	0.394	0.349
Na	0.006	0.004	0.009	0.005	0.006	0.007	0.003	0.005	0.011
ΣB	3.000	3.000	3.000	2.998	2.962	3.000	3.000	3.000	3.000
Uvarovite	0.08	0.08	0.09	0.03	0.02	0.11	0.11	0.12	0.04
Spessartine	0.01	0.01	0.01	0.01	0.01	0.01	0.01	0.01	0.01
Pyrope	0.66	0.66	0.67	0.72	0.69	0.73	0.73	0.70	0.67
Almandine	0.18	0.19	0.18	0.17	0.18	0.12	0.13	0.15	0.18
Grossular	0.03	0.04	0.02	0.06	0.08	0.00	0.00	0.00	0.06
Andradite	0.00	0.00	0.00	0.01	0.00	0.00	0.00	0.00	0.01

TABELA B07 – Cont. Major element compositions of garnet from TRIV all samples. Structural formula calculated on the basis of 24 oxygens. C - core; R - rim; I - intermediately.

Sample Grain/Analysis Location	TR-04B 04/11 I	TR-04B 04/12 R	TR-04B 05/13 C	TR-04B 05/14 I	TR-04B 05/15 R	TR-07 241 06/16 C	TR-07 241 07/17 C	TR-07 241 07/18 R
SiO ₂	42.68	42.25	42.53	42.17	42.74	41.91	41.51	43.23
TiO ₂	0.20	0.20	0.02	0.08	0.05	0.03	0.08	0.09
Al ₂ O ₃	22.38	22.32	20.59	20.55	20.66	21.24	21.08	21.80
Cr ₂ O ₃	1.34	1.37	4.26	4.34	4.39	2.86	2.95	2.92
FeO _T	9.44	9.74	7.62	7.48	7.55	8.79	8.42	8.61
MnO	0.42	0.36	0.38	0.37	0.43	0.42	0.41	0.40
MgO	19.68	19.71	20.71	20.81	20.55	19.97	19.78	18.83
CaO	4.50	4.59	4.72	4.68	4.80	4.78	4.76	4.86
Na ₂ O	0.07	0.05	0.03	0.02	0.04	0.02	0.02	0.01
Total	100.70	100.59	100.86	100.49	101.22	100.01	99.01	100.75
Si	3.000	3.000	3.000	2.998	3.000	2.997	2.998	3.000
Al ^{IV}	0.000	0.000	0.000	0.002	0.000	0.003	0.002	0.000
ΣT	3.000	3.000	3.000	3.000	3.000	3.000	3.000	3.000
Si	0.027	0.001	0.015	0.000	0.022	0.000	0.000	0.084
Ti	0.011	0.011	0.001	0.004	0.003	0.002	0.004	0.005
Al ^{VI}	1.870	1.868	1.720	1.720	1.721	1.788	1.792	1.833
Cr	0.075	0.077	0.239	0.244	0.246	0.162	0.169	0.165
Fe ²⁺	0.000	0.004	0.000	0.000	0.000	0.000	0.000	0.000
Fe ³⁺	0.000	0.038	0.013	0.032	0.000	0.052	0.034	0.000
Mg	0.017	0.001	0.012	0.000	0.008	0.000	0.000	0.000
ΣA	2.000	2.000	2.000	2.000	2.000	2.003	2.000	2.087
Fe ²⁺	0.560	0.536	0.439	0.413	0.446	0.474	0.474	0.514
Mg	2.063	2.086	2.176	2.205	2.158	2.129	2.130	2.003
Mn	0.025	0.022	0.023	0.022	0.026	0.026	0.025	0.024
Ca	0.342	0.350	0.359	0.356	0.364	0.366	0.368	0.371
Na	0.010	0.006	0.004	0.003	0.006	0.002	0.002	0.001
ΣB	3.000	3.000	3.000	3.000	3.000	2.997	3.000	2.913
Uvarovite	0.04	0.04	0.12	0.12	0.12	0.08	0.08	0.08
Spessartine	0.01	0.01	0.01	0.01	0.01	0.01	0.01	0.01
Pyrope	0.67	0.69	0.71	0.73	0.71	0.71	0.71	0.67
Almandine	0.19	0.18	0.14	0.12	0.14	0.16	0.16	0.17
Grossular	0.07	0.05	0.00	0.00	0.00	0.02	0.02	0.04
Andradite	0.00	0.02	0.00	0.00	0.00	0.02	0.02	0.00

TABELA B07 – Cont. Major element compositions of garnet from TRIV all samples. Structural formula calculated on the basis of 24 oxygens. C - core; R - rim; I - intermediately.

Sample Grain/Analysis Location	TR-07 241 07/18 R	TR-07 241 08/19 C	TR-07 241 08/20 R	TRIV-5-2 09/21 C	TRIV-5-2 09/22 R	TRIV-5-2 10/23 C	TRIV-5-2 11/24 R
SiO ₂	43.23	41.94	41.79	40.70	40.99	40.72	40.68
TiO ₂	0.09	0.05	0.06	0.13	0.04	0.10	0.06
Al ₂ O ₃	21.80	21.30	21.23	17.98	18.11	18.12	18.06
Cr ₂ O ₃	2.92	3.01	2.91	6.94	6.97	7.04	7.20
FeO _T	8.61	8.76	8.60	7.81	7.93	8.15	8.05
MnO	0.40	0.47	0.49	0.43	0.46	0.44	0.45
MgO	18.83	20.06	20.47	19.08	18.97	18.91	18.86
CaO	4.86	4.69	4.68	5.67	5.67	5.57	5.58
Na ₂ O	0.01	0.02	0.01	0.00	0.00	0.00	0.00
Total	100.75	100.30	100.22	98.75	99.15	99.06	98.94
Si	3.000	2.992	2.977	2.990	3.000	2.987	2.988
Al ^{IV}	0.000	0.008	0.023	0.010	0.000	0.013	0.012
ΣT	3.000	3.000	3.000	3.000	3.000	3.000	3.000
Si	0.084	0.000	0.000	0.000	0.001	0.000	0.000
Ti	0.005	0.003	0.003	0.007	0.002	0.006	0.003
Al ^{VI}	1.833	1.782	1.760	1.547	1.563	1.553	1.552
Cr	0.165	0.170	0.164	0.403	0.404	0.408	0.418
Fe ²⁺	0.000	0.000	0.000	0.000	0.002	0.000	0.000
Fe ³⁺	0.000	0.054	0.093	0.045	0.026	0.040	0.035
Mg	0.000	0.000	0.000	0.000	0.001	0.000	0.000
ΣA	2.087	2.009	2.020	2.003	2.000	2.007	2.008
Fe ²⁺	0.514	0.468	0.419	0.434	0.457	0.460	0.459
Mg	2.003	2.133	2.174	2.090	2.069	2.068	2.065
Mn	0.024	0.028	0.029	0.027	0.029	0.027	0.028
Ca	0.371	0.359	0.357	0.446	0.445	0.438	0.439
Na	0.001	0.003	0.001	0.000	0.000	0.000	0.000
ΣB	2.913	2.991	2.980	2.997	3.000	2.993	2.992
Uvarovite	0.08	0.08	0.08	0.15	0.15	0.14	0.14
Spessartine	0.01	0.01	0.01	0.01	0.01	0.01	0.01
Pyrope	0.67	0.71	0.72	0.64	0.63	0.63	0.62
Almandine	0.17	0.16	0.14	0.12	0.14	0.14	0.14
Grossular	0.04	0.01	0.01	0.00	0.00	0.00	0.00
Andradite	0.00	0.02	0.03	0.00	0.00	0.00	0.00

APPENDIX C

LA-ICP-MS DATA

TABELA C01 - Standards concentrations from LA-ICP-MS analyses.

Sample: LMI-B1 (ol) 22/01/18

Standard		Li	Na	Mg	Al	Si	P	Ca
BHVO-2G	Primary	4.3	17457.0	42185.1	70921.5	230427.9	1265.7	80508.0
BHVO-2G	Primary	4.4	17958.5	43799.9	72610.3	230428.0	1256.8	81991.9
BHVO-2G	Primary	4.6	18384.1	43302.5	73350.0	230427.9	1289.0	82621.1
BHVO-2G	Primary	4.4	17860.6	42750.8	71852.4	230427.9	1260.3	81832.3
BHVO-2G	Primary	4.2	17416.1	42974.5	71243.7	230427.9	1257.9	80428.4
Mean		4.4	17815.3	43002.6	71995.6	230427.9	1265.9	81476.3
SD		0.1	356.1	540.0	889.0	0.0	11.9	864.8
Average detection limit		0.2	1.6	1.0	0.4	320.7	11.8	197.2
<i>GeoRem</i>		4.4	16400.0	43600.0	71300.0	233000.0	1200.0	81700.0
<i>Uncertainty</i>		0.8	600.0	700.0	800.0	3000.0	100.0	1200.0

Standard

Nist-610	Secundary	505.8	118630.0	543.6	11551.9	325805.2	473.0	88837.0
Detection limit		0.2	2.1	1.1	0.5	425.0	16.1	260.9
<i>GeoRem</i>		468.0	97139.8	432.0	10489.8	331744.0	413.0	81763.4
<i>Uncertainty</i>		24.0	2603.1	29.0	258.5	6440.0	46.0	2128.4

Sample: LMI-C2 (ol) 22/01/18

Standard		Li	Na	Mg	Al	Si	P	Ca
BHVO-2G	Primary	4.5	17918.3	42631.0	72044.8	230427.9	1263.8	83272.8
BHVO-2G	Primary	4.3	17665.9	43312.0	71910.8	230427.9	1270.2	79835.1
BHVO-2G	Primary	4.5	18029.4	43317.9	72087.3	230427.9	1252.5	81018.7
BHVO-2G	Primary	4.3	17633.8	42676.4	71904.1	230428.0	1277.7	82093.9
Mean		4.4	17811.9	42984.3	71986.7	230427.9	1266.0	81555.1
SD		0.1	167.1	331.0	80.7	0.0	9.2	1273.5
Average detection limit		0.1	1.4	0.9	0.4	289.0	11.0	148.6
<i>GeoRem</i>		4.4	16400.0	43600.0	71300.0	233000.0	1200.0	81700.0
<i>Uncertainty</i>		0.8	600.0	700.0	800.0	3000.0	100.0	1200.0

Standard

Nist-610	Secundary	484.6	118493.6	543.5	11585.9	325805.2	456.8	88559.0
Detection limit		0.2	2.0	1.2	0.5	433.9	17.0	224.2
<i>GeoRem</i>		468.0	97139.8	432.0	10489.8	331744.0	413.0	81763.4
<i>Uncertainty</i>		24.0	2603.1	29.0	258.5	6440.0	46.0	2128.4

Sample: TRIV-5 (ol) 22/01/18

Standard		Li	Na	Mg	Al	Si	P	Ca
BHVO-2G	Primary	4.3	17863.3	43132.7	72456.1	230428.0	1254.7	82497.4
BHVO-2G	Primary	4.5	17703.9	42898.6	72106.6	230428.0	1293.4	80940.6
BHVO-2G	Primary	4.4	17938.6	42939.8	70833.1	230428.0	1235.0	80653.7
BHVO-2G	Primary	4.3	17615.7	42864.0	72033.0	230428.1	1265.0	80932.8
BHVO-2G	Primary	4.5	17937.4	43164.2	72601.3	230428.1	1282.5	82548.2
Mean		4.4	17811.8	42999.8	72006.0	230428.0	1266.1	81514.6
SD		0.1	130.1	124.1	623.5	0.0	20.6	829.9
Average detection limit		0.1	1.3	1.0	0.4	290.2	11.4	143.1
<i>GeoRem</i>		4.4	16400.0	43600.0	71300.0	233000.0	1200.0	81700.0
<i>Uncertainty</i>		0.8	600.0	700.0	800.0	3000.0	100.0	1200.0

Standard

Nist-610	Secundary	481.5	116984.4	529.7	11579.0	325805.3	471.9	89375.2
Detection limit		0.2	2.2	0.7	0.6	484.2	18.9	239.7
<i>GeoRem</i>		468.0	97139.8	432.0	10489.8	331744.0	413.0	81763.4
<i>Uncertainty</i>		24.0	2603.1	29.0	258.5	6440.0	46.0	2128.4

TABELA C01 – Cont. Standards concentrations from LA-ICP-MS analyses

Sample: LMI-B1 (ol) 22/01/18

Standard		Sc	Ti	V	Cr	Mn	Co	Ni
BHVO-2G	Primary	32.7	16070.4	303.5	287.7	1308.7	43.0	115.5
BHVO-2G	Primary	33.2	16459.5	310.6	295.4	1315.5	44.6	116.1
BHVO-2G	Primary	33.2	16509.5	313.3	301.3	1339.1	45.1	117.0
BHVO-2G	Primary	33.2	16381.1	308.8	293.6	1332.3	44.4	117.0
BHVO-2G	Primary	32.7	16090.5	303.9	287.4	1290.7	43.0	114.5
Mean		33.0	16302.2	308.0	293.1	1317.3	44.0	116.0
SD		0.2	185.7	3.8	5.2	17.2	0.9	1.0
Average detection limit		0.1	0.4	0.1	0.5	0.2	0.0	0.1
<i>GeoRem</i>		33.0	16300.0	308.0	293.0	1290.0	44.0	116.0
<i>Uncertainty</i>		2.0	900.0	19.0	12.0	40.0	2.0	7.0
Standard								
Nist-610	Secundary	515.1	494.6	449.1	380.6	483.6	412.5	461.9
Detection limit		0.1	0.5	0.1	0.6	0.3	0.0	0.2
<i>GeoRem</i>		455.0	452.0	450.0	408.0	444.0	410.0	458.7
<i>Uncertainty</i>		10.0	10.0	9.0	10.0	13.0	10.0	4.0

Sample: LMI-C2 (ol) 22/01/18

Standard		Sc	Ti	V	Cr	Mn	Co	Ni
BHVO-2G	Primary	34.0	16622.5	313.1	297.5	1340.7	45.6	119.1
BHVO-2G	Primary	32.1	16025.8	303.8	289.3	1297.2	42.6	113.3
BHVO-2G	Primary	32.9	16132.8	304.4	289.3	1301.2	44.1	114.9
BHVO-2G	Primary	33.2	16487.9	311.8	296.8	1334.2	44.1	117.3
Mean		33.1	16317.2	308.3	293.2	1318.3	44.1	116.2
SD		0.7	245.6	4.2	3.9	19.3	1.1	2.2
Average detection limit		0.1	0.4	0.1	0.4	0.2	0.0	0.2
<i>GeoRem</i>		33.0	16300.0	308.0	293.0	1290.0	44.0	116.0
<i>Uncertainty</i>		2.0	900.0	19.0	12.0	40.0	2.0	7.0

Standard

Nist-610	Secundary	525.9	479.8	446.5	426.7	482.1	430.5	483.7
Detection limit		0.1	0.5	0.1	0.6	0.3	0.0	0.3
<i>GeoRem</i>		455.0	452.0	450.0	408.0	444.0	410.0	458.7
<i>Uncertainty</i>		10.0	10.0	9.0	10.0	13.0	10.0	4.0

Sample: TRIV-5 (ol) 22/01/18

Standard		Sc	Ti	V	Cr	Mn	Co	Ni
BHVO-2G	Primary	32.7	16481.7	311.9	294.6	1319.3	44.5	118.0
BHVO-2G	Primary	33.2	16160.0	304.6	293.4	1319.6	43.9	115.4
BHVO-2G	Primary	33.1	16271.8	308.5	289.6	1311.3	43.5	114.0
BHVO-2G	Primary	32.8	16104.4	302.8	289.7	1293.2	42.4	113.3
BHVO-2G	Primary	33.1	16532.4	313.4	298.4	1345.6	46.1	120.2
Mean		33.0	16310.1	308.2	293.1	1317.8	44.1	116.2
SD		0.2	170.4	4.1	3.3	16.9	1.2	2.6
Average detection limit		0.1	0.4	0.1	0.4	0.2	0.0	0.1
<i>GeoRem</i>		33.0	16300.0	308.0	293.0	1290.0	44.0	116.0
<i>Uncertainty</i>		2.0	900.0	19.0	12.0	40.0	2.0	7.0

Standard

Nist-610	Secundary	521.1	494.4	447.9	443.8	492.3	425.8	496.8
Detection limit		0.1	0.8	0.1	0.7	0.4	0.0	0.4
<i>GeoRem</i>		455.0	452.0	450.0	408.0	444.0	410.0	458.7
<i>Uncertainty</i>		10.0	10.0	9.0	10.0	13.0	10.0	4.0

TABELA C01 – Cont. Standards concentrations from LA-ICP-MS analyses

Sample: LMI-B1 (ol) 22/01/18

Standard		Cu	Zn	Rb	Sr	Y	Zr	Nb
BHVO-2G	Primary	125.6	99.8	9.1	386.4	25.3	165.9	18.0
BHVO-2G	Primary	127.4	102.5	9.2	404.2	26.8	173.4	18.5
BHVO-2G	Primary	129.4	106.3	9.3	401.7	26.2	172.8	18.7
BHVO-2G	Primary	129.8	103.8	9.3	401.2	26.2	171.8	18.6
BHVO-2G	Primary	123.2	97.9	9.1	387.5	25.7	166.5	17.9
Mean		127.0	102.1	9.2	396.2	26.0	170.1	18.3
SD		2.5	2.9	0.1	7.6	0.5	3.2	0.3
Average detection limit		0.1	0.4	0.0	0.0	0.0	0.0	0.0
<i>GeoRem</i>		127.0	102.0	9.2	396.0	26.0	170.0	18.3
<i>Uncertainty</i>		11.0	6.0	0.0	0.0	2.0	7.0	0.8
Standard								
Nist-610	Secondary	611.4	371.9	435.6	556.1	565.4	523.7	529.2
Detection limit		0.1	0.6	0.1	0.0	0.0	0.0	0.0
<i>GeoRem</i>		441.0	460.0	425.7	515.5	462.0	448.0	465.0
<i>Uncertainty</i>		15.0	18.0	1.0	1.0	11.0	9.0	34.0

Sample: LMI-C2 (ol) 22/01/18

Standard		Cu	Zn	Rb	Sr	Y	Zr	Nb
BHVO-2G	Primary	128.3	101.5	9.4	397.2	26.0	170.5	18.6
BHVO-2G	Primary	125.9	102.2	9.1	395.5	26.1	169.9	18.1
BHVO-2G	Primary	126.0	103.8	9.1	391.9	25.8	167.7	18.0
BHVO-2G	Primary	128.1	100.5	9.3	399.8	26.2	172.1	18.6
Mean		127.1	102.0	9.2	396.1	26.0	170.0	18.3
SD		1.1	1.2	0.1	2.8	0.2	1.6	0.3
Average detection limit		0.1	0.3	0.0	0.0	0.0	0.0	0.0
<i>GeoRem</i>		127.0	102.0	9.2	396.0	26.0	170.0	18.3
<i>Uncertainty</i>		11.0	6.0	0.0	0.0	2.0	7.0	0.8
Standard								
Nist-610	Secondary	543.1	375.4	453.7	562.4	559.2	512.1	515.6
Detection limit		0.1	0.6	0.0	0.0	0.0	0.0	0.0
<i>GeoRem</i>		441.0	460.0	425.7	515.5	462.0	448.0	465.0
<i>Uncertainty</i>		15.0	18.0	1.0	1.0	11.0	9.0	34.0

Sample: TRIV-5 (ol) 22/01/18

Standard		Cu	Zn	Rb	Sr	Y	Zr	Nb
BHVO-2G	Primary	129.0	101.0	9.4	396.4	25.8	169.0	18.3
BHVO-2G	Primary	125.9	103.8	9.0	395.9	26.0	171.6	18.5
BHVO-2G	Primary	125.7	100.5	9.3	397.6	26.4	169.1	18.0
BHVO-2G	Primary	125.6	100.8	8.9	384.9	25.5	168.3	18.1
BHVO-2G	Primary	129.3	104.0	9.4	407.2	26.3	172.1	18.7
Mean		127.1	102.0	9.2	396.4	26.0	170.0	18.3
SD		1.7	1.5	0.2	7.1	0.4	1.5	0.3
Average detection limit		0.1	0.4	0.0	0.0	0.0	0.0	0.0
<i>GeoRem</i>		127.0	102.0	9.2	396.0	26.0	170.0	18.3
<i>Uncertainty</i>		11.0	6.0	0.0	0.0	2.0	7.0	0.8
Standard								
Nist-610	Secondary	535.1	405.8	456.6	581.0	553.2	501.3	515.8
Detection limit		0.1	0.5	0.0	0.0	0.0	0.0	0.0
<i>GeoRem</i>		441.0	460.0	425.7	515.5	462.0	448.0	465.0
<i>Uncertainty</i>		15.0	18.0	1.0	1.0	11.0	9.0	34.0

TABELA C01 – Cont. Standards concentrations from LA-ICP-MS analyses

Sample: LMI-B1 (ol) 22/01/18

Standard	Ba	La	Ce	Pr	Nd	Sm	Eu	Gd	Tb	Dy
BHVO-2G Primary	127.3	14.8	36.7	5.2	24.3	5.8	2.1	6.0	0.9	5.0
BHVO-2G Primary	133.9	15.4	38.4	5.5	24.5	6.4	2.1	6.3	0.9	5.6
BHVO-2G Primary	134.3	15.7	38.2	5.4	25.1	6.2	2.1	6.3	1.0	5.6
BHVO-2G Primary	129.4	15.5	37.7	5.4	24.1	6.2	2.1	6.1	0.9	5.3
BHVO-2G Primary	130.3	14.6	37.1	5.3	24.5	6.0	2.0	6.1	0.9	5.1
Mean	131.0	15.2	37.6	5.4	24.5	6.1	2.1	6.2	0.9	5.3
SD	2.7	0.4	0.7	0.1	0.3	0.2	0.0	0.1	0.0	0.2
Average detection limit	0.1	0.0	0.0	0.0	0.1	0.1	0.0	0.1	0.0	0.0
<i>GeoRem</i>	131.0	15.2	37.6	5.4	24.5	6.1	2.1	6.2	0.9	5.3
<i>Uncertainty</i>	2.0	0.2	0.2	0.2	0.2	0.0	0.0	0.1	0.0	0.1

Standard

Nist-610	Secundary	496.7	496.5	518.8	523.1	493.4	527.2	496.9	495.8	513.7	506.1
Detection limit		0.1	0.0	0.0	0.0	0.1	0.1	0.0	0.1	0.0	0.0
<i>GeoRem</i>		452.0	440.0	453.0	448.0	430.0	453.0	447.0	449.0	437.0	437.0
<i>Uncertainty</i>		9.0	10.0	8.0	7.0	8.0	11.0	12.0	12.0	9.0	11.0

Sample: LMI-C2 (ol) 22/01/18

Standard	Ba	La	Ce	Pr	Nd	Sm	Eu	Gd	Tb	Dy
BHVO-2G Primary	133.2	15.4	37.7	5.4	26.0	6.4	2.0	6.2	0.9	5.4
BHVO-2G Primary	129.4	15.1	37.6	5.4	23.3	5.9	2.1	6.1	0.9	5.3
BHVO-2G Primary	128.0	14.6	36.8	5.4	23.7	5.8	2.1	6.2	0.9	4.9
BHVO-2G Primary	134.0	15.8	38.4	5.3	25.5	6.4	2.1	6.2	0.9	5.6
Mean	131.1	15.2	37.6	5.4	24.6	6.1	2.1	6.2	0.9	5.3
SD	2.5	0.4	0.6	0.0	1.1	0.3	0.0	0.0	0.0	0.3
Average detection limit	0.1	0.0	0.0	0.0	0.1	0.1	0.0	0.0	0.0	0.0
<i>GeoRem</i>	131.0	15.2	37.6	5.4	24.5	6.1	2.1	6.2	0.9	5.3
<i>Uncertainty</i>	2.0	0.2	0.2	0.2	0.2	0.0	0.0	0.1	0.0	0.1

Standard

Nist-610	Secundary	483.8	468.8	496.7	496.7	486.1	506.1	492.9	501.9	495.5	519.7
Detection limit		0.1	0.0	0.0	0.0	0.1	0.1	0.0	0.1	0.0	0.1
<i>GeoRem</i>		452.0	440.0	453.0	448.0	430.0	453.0	447.0	449.0	437.0	437.0
<i>Uncertainty</i>		9.0	10.0	8.0	7.0	8.0	11.0	12.0	12.0	9.0	11.0

Sample: TRIV-5 (ol) 22/01/18

Standard	Ba	La	Ce	Pr	Nd	Sm	Eu	Gd	Tb	Dy
BHVO-2G Primary	131.7	15.2	37.6	5.3	23.7	6.2	2.1	6.1	0.9	5.2
BHVO-2G Primary	130.4	15.1	37.4	5.3	25.1	6.0	2.0	6.3	0.9	5.2
BHVO-2G Primary	131.6	15.5	38.3	5.5	24.9	6.1	2.1	6.1	0.9	5.6
BHVO-2G Primary	127.5	14.9	36.5	5.2	24.2	6.2	2.0	5.8	0.9	5.0
BHVO-2G Primary	134.5	15.3	38.4	5.4	24.6	6.0	2.2	6.6	1.0	5.4
Mean	131.1	15.2	37.6	5.4	24.5	6.1	2.1	6.2	0.9	5.3
SD	2.3	0.2	0.7	0.1	0.5	0.1	0.1	0.2	0.0	0.2
Average detection limit	0.1	0.0	0.0	0.0	0.1	0.1	0.0	0.1	0.0	0.0
<i>GeoRem</i>	131.0	15.2	37.6	5.4	24.5	6.1	2.1	6.2	0.9	5.3
<i>Uncertainty</i>	2.0	0.2	0.2	0.2	0.2	0.0	0.0	0.1	0.0	0.1

Standard	Ba	La	Ce	Pr	Nd	Sm	Eu	Gd	Tb	Dy	
Nist-610	Secundary	472.2	470.6	492.7	509.2	478.9	500.2	487.9	495.8	491.6	487.1
Detection limit		0.1	0.0	0.0	0.0	0.1	0.1	0.0	0.1	0.0	0.1
<i>GeoRem</i>		452.0	440.0	453.0	448.0	430.0	453.0	447.0	449.0	437.0	437.0
<i>Uncertainty</i>		9.0	10.0	8.0	7.0	8.0	11.0	12.0	12.0	9.0	11.0

TABELA C01 – Cont. Standards concentrations from LA-ICP-MS analyses

Sample: LMI-B1 (ol) 22/01/18

Standard		Ho	Er	Tm	Yb	Lu	Hf	Ta	Pb	Th	U
BHVO-2G	Primary	0.9	2.4	0.3	1.9	0.3	4.2	1.1	1.6	1.2	0.4
BHVO-2G	Primary	1.0	2.7	0.4	2.2	0.3	4.4	1.2	1.8	1.3	0.4
BHVO-2G	Primary	1.0	2.7	0.3	2.0	0.3	4.4	1.1	1.6	1.2	0.4
BHVO-2G	Primary	1.0	2.5	0.4	1.9	0.3	4.3	1.2	1.7	1.2	0.4
BHVO-2G	Primary	0.9	2.6	0.3	2.1	0.3	4.3	1.1	1.8	1.2	0.4
Mean		1.0	2.6	0.3	2.0	0.3	4.3	1.2	1.7	1.2	0.4
SD		0.1	0.1	0.0	0.1	0.0	0.1	0.0	0.1	0.0	0.0
Average detection limit		0.0	0.0	0.0	0.1	0.0	0.1	0.0	0.0	0.0	0.0
<i>GeoRem</i>		1.0	2.6	0.3	2.0	0.3	4.3	1.2	1.7	1.2	0.4
<i>Uncertainty</i>		0.0	0.0	0.0	0.0	0.0	0.2	0.1	0.2	0.1	0.0
Standard											
Nist-610	Secundary	511.3	516.1	519.9	530.4	504.0	479.3	522.7	378.1	515.4	480.9
Detection limit		0.0	0.0	0.0	0.1	0.0	0.1	0.0	0.0	0.0	0.0
<i>GeoRem</i>		449.0	455.0	435.0	450.0	439.0	435.0	446.0	426.0	457.2	461.5
<i>Uncertainty</i>		12.0	14.0	10.0	9.0	8.0	12.0	33.0	1.0	1.0	1.0

Sample: LMI-C2 (ol) 22/01/18

Standard		Ho	Er	Tm	Yb	Lu	Hf	Ta	Pb	Th	U
BHVO-2G	Primary	1.0	2.5	0.3	2.0	0.3	4.0	1.2	1.6	1.2	0.4
BHVO-2G	Primary	0.9	2.6	0.4	2.0	0.3	4.7	1.1	1.8	1.2	0.4
BHVO-2G	Primary	0.9	2.5	0.3	1.9	0.3	4.2	1.1	1.7	1.2	0.4
BHVO-2G	Primary	1.0	2.6	0.4	2.2	0.3	4.4	1.2	1.7	1.3	0.4
Mean		1.0	2.6	0.3	2.0	0.3	4.3	1.2	1.7	1.2	0.4
SD		0.1	0.1	0.0	0.1	0.0	0.2	0.0	0.0	0.0	0.0
Average detection limit		0.0	0.0	0.0	0.0	0.0	0.1	0.0	0.0	0.0	0.0
<i>GeoRem</i>		1.0	2.6	0.3	2.0	0.3	4.3	1.2	1.7	1.2	0.4
<i>Uncertainty</i>		0.0	0.0	0.0	0.0	0.0	0.2	0.1	0.2	0.1	0.0
Standard											
Nist-610	Secundary	510.5	514.8	541.3	510.4	521.1	465.3	504.0	372.0	506.9	482.9
Detection limit		0.0	0.0	0.0	0.1	0.0	0.1	0.0	0.0	0.0	0.0
<i>GeoRem</i>		449.0	455.0	435.0	450.0	439.0	435.0	446.0	426.0	457.2	461.5
<i>Uncertainty</i>		12.0	14.0	10.0	9.0	8.0	12.0	33.0	1.0	1.0	1.0

Sample: TRIV-5 (ol) 22/01/18

Standard		Ho	Er	Tm	Yb	Lu	Hf	Ta	Pb	Th	U
BHVO-2G	Primary	1.0	2.5	0.3	2.0	0.3	4.3	1.2	1.8	1.2	0.4
BHVO-2G	Primary	1.0	2.6	0.4	2.0	0.3	4.4	1.1	1.7	1.2	0.4
BHVO-2G	Primary	1.0	2.6	0.3	2.0	0.3	4.4	1.1	1.6	1.2	0.4
BHVO-2G	Primary	1.0	2.4	0.4	1.9	0.3	4.2	1.2	1.6	1.2	0.4
BHVO-2G	Primary	1.0	2.7	0.4	2.1	0.3	4.4	1.1	1.8	1.2	0.5
Mean		1.0	2.6	0.3	2.0	0.3	4.3	1.2	1.7	1.2	0.4
SD		0.0	0.1	0.0	0.1	0.0	0.1	0.0	0.1	0.0	0.0
Average detection limit		0.0	0.0	0.0	0.0	0.0	0.0	0.0	0.0	0.0	0.0
<i>GeoRem</i>		1.0	2.6	0.3	2.0	0.3	4.3	1.2	1.7	1.2	0.4
<i>Uncertainty</i>		0.0	0.0	0.0	0.0	0.0	0.2	0.1	0.2	0.1	0.0
Standard											
Nist-610	Secundary	510.3	513.3	515.6	509.8	502.2	446.3	508.7	380.9	500.5	482.2
Detection limit		0.0	0.0	0.0	0.1	0.0	0.1	0.0	0.0	0.0	0.0
<i>GeoRem</i>		449.0	455.0	435.0	450.0	439.0	435.0	446.0	426.0	457.2	461.5
<i>Uncertainty</i>		12.0	14.0	10.0	9.0	8.0	12.0	33.0	1.0	1.0	1.0

TABELA C01 – Cont. Standards concentrations from LA-ICP-MS analyses

Sample: TRIV-5-3 (ol) 22/01/18

Standard		Li	Na	Mg	Al	Si	P	Ca
BHVO-2G	Primary	4.5	17853.6	43071.5	71909.9	230428.0	1256.6	82443.2
BHVO-2G	Primary	4.4	17782.2	42967.6	71776.3	230428.0	1275.0	80263.0
BHVO-2G	Primary	4.3	17732.5	42920.6	72960.2	230428.0	1282.1	82303.0
BHVO-2G	Primary	4.5	17816.7	42637.7	71078.2	230428.0	1209.2	80076.4
BHVO-2G	Primary	4.4	17842.0	43375.0	72297.7	230428.0	1311.6	82417.0
Mean		4.4	17805.4	42994.5	72004.5	230428.0	1266.9	81500.5
SD		0.1	43.9	238.4	619.4	0.0	33.8	1089.2
Average detection limit		0.1	1.5	1.0	0.4	307.8	11.9	166.7
GeoRem		4.4	16400.0	43600.0	71300.0	233000.0	1200.0	81700.0
Uncertainty		0.8	600.0	700.0	800.0	3000.0	100.0	1200.0
Standard								
Nist-610	Secundary	488.1	113889.9	523.4	11258.6	325805.3	466.5	86974.3
Detection limit		0.2	2.1	0.9	0.5	447.9	18.0	245.9
GeoRem		468.0	97139.8	432.0	10489.8	331744.0	413.0	81763.4
Uncertainty		24.0	2603.1	29.0	258.5	6440.0	46.0	2128.4

Sample: LMI-C2 (pv) 22/01/18

Standard		Li7	Mg24	Al27	Si29	P31	Ca42	Ca44
Nist-610	Primary	506.6	483.3	10248.0	336373.8	374.3	81833.3	80298.1
Nist-610	Primary	464.3	449.4	9810.4	320333.6	293.2	81833.3	83769.0
Nist-610	Primary	479.8	460.0	9881.6	326070.2	343.9	81833.3	82141.6
Nist-610	Primary	453.0	451.5	9853.8	329082.6	430.1	81833.3	80487.5
Nist-610	Primary	488.8	469.6	10096.5	330156.3	343.4	81833.3	81557.0
Mean		478.5	462.7	9978.1	328403.3	357.0	81833.3	81650.6
SD		18.7	12.5	167.2	5246.5	44.9	0.0	1258.5
Average detection limit		325.2	32540.6	3565.2	115297.5	110710.8	27415.4	54859.7
GeoRem		468.0	97139.8	432.0	10489.8	331744.0	413.0	81763.4
Uncertainty		24.0	2603.1	29.0	258.5	6440.0	46.0	2128.4
Standard								
BHVO-2G	Secundary	4.9	37662.5	60740.9	247903.1	1133.3	81475.9	77710.5
Detection limit		1.0	0.7	2.8	1949.4	75.3	1358.0	194.6
GeoRem		4.4	16400.0	43600.0	71300.0	233000.0	1200.0	81700.0
Uncertainty		0.8	600.0	700.0	800.0	3000.0	100.0	1200.0

Sample: TRIV-5 (pv) 22/01/18

Standard		Li7	Mg24	Al27	Si29	P31	Ca42	Ca44
Nist-610	Primary	465.0	442.4	9569.9	324652.9	390.1	81833.3	77766.0
Nist-610	Primary	525.4	505.9	10898.5	335649.3	260.8	81833.3	91045.1
Nist-610	Primary	457.3	462.6	9804.3	321375.8	383.7	81833.3	77940.4
Nist-610	Primary	513.3	464.6	10160.0	335273.7	306.5	81833.3	85841.8
Mean		490.2	468.9	10108.2	329237.9	335.3	81833.3	83148.3
SD		29.6	23.1	502.3	6331.9	54.2	0.0	5605.9
Average detection limit		1.9	1.6	5.0	3466.3	115.2	2220.4	348.1
GeoRem		468.0	97139.8	432.0	10489.8	331744.0	413.0	81763.4
Uncertainty		24.0	2603.1	29.0	258.5	6440.0	46.0	2128.4

Standard		Li7	Mg24	Al27	Si29	P31	Ca42	Ca44
BHVO-2G	Secundary	6.0	41075.0	66800.9	258386.3	1063.7	81475.9	83356.2
Detection limit		1.0	0.8	2.7	1956.0	65.7	1234.3	196.7
GeoRem		4.4	16400.0	43600.0	71300.0	233000.0	1200.0	81700.0
Uncertainty		0.8	600.0	700.0	800.0	3000.0	100.0	1200.0

TABELA C01 – Cont. Standards concentrations from LA-ICP-MS analyses

Sample: TRIV-5-3 (ol) 22/01/18

Standard		Sc	Ti	V	Cr	Mn	Co	Ni
BHVO-2G	Primary	33.4	16411.7	309.2	294.5	1326.0	44.3	116.9
BHVO-2G	Primary	32.7	16171.9	306.1	291.2	1307.4	43.9	114.9
BHVO-2G	Primary	32.8	16364.9	310.6	294.9	1320.4	43.6	117.0
BHVO-2G	Primary	32.6	16122.1	304.5	287.0	1302.5	43.2	113.0
BHVO-2G	Primary	33.6	16439.9	309.9	297.8	1329.5	45.0	118.4
Mean		33.0	16302.1	308.0	293.1	1317.2	44.0	116.0
SD		0.4	129.8	2.3	3.7	10.5	0.6	1.9
Average detection limit		0.1	0.4	0.1	0.5	0.2	0.0	0.1
GeoRem		33.0	16300.0	308.0	293.0	1290.0	44.0	116.0
Uncertainty		2.0	900.0	19.0	12.0	40.0	2.0	7.0
Standard								
Nist-610	Secundary	501.0	488.5	441.0	437.9	478.3	414.2	453.4
Detection limit		0.1	0.4	0.1	0.6	0.3	0.0	0.2
GeoRem		455.0	452.0	450.0	408.0	444.0	410.0	458.7
Uncertainty		10.0	10.0	9.0	10.0	13.0	10.0	4.0

Sample: LMI-C2 (pv) 22/01/18

Standard		Sc45	Ti46	Ti49	V51	Cr52	Mn55	Fe56
Nist-610	Primary	430.7	407.4	403.7	419.4	381.9	409.6	429.2
Nist-610	Primary	455.1	478.2	473.4	481.1	448.3	488.2	518.6
Nist-610	Primary	442.1	421.8	433.6	437.2	400.7	418.8	440.6
Nist-610	Primary	431.7	431.4	425.6	419.3	391.8	397.2	431.3
Nist-610	Primary	439.8	438.8	431.9	442.6	406.1	440.5	465.1
Mean		439.9	435.5	433.6	439.9	405.7	430.8	457.0
SD		8.8	23.8	22.5	22.6	22.8	32.0	33.3
Average detection limit		301.2	304.9	301.5	291.1	291.0	294.1	319.1
GeoRem		455.0	452.0	450.0	408.0	444.0	410.0	458.7
Uncertainty		10.0	10.0	9.0	10.0	13.0	10.0	4.0
Standard								
BHVO-2G	Secundary	29.4	13254.9	14699.4	302.0	277.7	1193.1	73102.7
Detection limit		0.5	5.6	3.1	0.6	3.0	1.9	13.5
GeoRem		33.0	16300.0	308.0	293.0	1290.0	44.0	116.0
Uncertainty		2.0	900.0	19.0	12.0	40.0	2.0	7.0

Sample: TRIV-5 (pv) 22/01/18

Standard		Sc45	Ti46	Ti49	V51	Cr52	Mn55	Fe56
Nist-610	Primary	422.5	415.1	415.3	427.9	391.6	413.8	451.0
Nist-610	Primary	480.2	471.5	464.6	471.1	435.3	472.9	464.2
Nist-610	Primary	421.5	398.1	421.5	415.1	377.4	416.6	468.7
Nist-610	Primary	460.9	470.9	443.6	471.5	437.0	448.9	445.2
Mean		446.3	438.9	436.2	446.4	410.3	438.0	457.3
SD		25.2	32.8	19.5	25.3	26.3	24.4	9.5
Average detection limit		0.9	9.4	4.9	1.1	5.5	3.4	22.9
GeoRem		455.0	452.0	450.0	408.0	444.0	410.0	458.7
Uncertainty		10.0	10.0	9.0	10.0	13.0	10.0	4.0
Standard								
BHVO-2G	Secundary	32.0	13232.6	15862.4	333.3	297.6	1312.1	78429.1
Detection limit		0.5	5.5	3.5	0.6	3.2	1.9	12.8
GeoRem		33.0	16300.0	308.0	293.0	1290.0	44.0	116.0
Uncertainty		2.0	900.0	19.0	12.0	40.0	2.0	7.0

TABELA C01 – Cont. Standards concentrations from LA-ICP-MS analyses

Sample: TRIV-5-3 (ol) 22/01/18

Standard		Cu	Zn	Rb	Sr	Y	Zr	Nb
BHVO-2G	Primary	129.2	100.6	9.3	396.0	25.9	169.3	18.4
BHVO-2G	Primary	125.4	103.4	9.0	394.9	26.0	169.9	18.1
BHVO-2G	Primary	126.2	103.1	9.5	399.7	26.3	172.8	18.5
BHVO-2G	Primary	122.0	98.4	9.1	393.4	26.1	167.8	18.0
BHVO-2G	Primary	132.7	104.8	9.2	396.4	25.8	170.5	18.5
Mean		127.1	102.1	9.2	396.1	26.0	170.0	18.3
SD		3.6	2.3	0.2	2.1	0.2	1.6	0.2
Average detection limit		0.1	0.4	0.0	0.0	0.0	0.0	0.0
GeoRem		127.0	102.0	9.2	396.0	26.0	170.0	18.3
Uncertainty		11.0	6.0	0.0	0.0	2.0	7.0	0.8
Standard								
Nist-610	Secundary	520.5	385.5	438.7	546.5	535.1	496.9	517.5
Detection limit		0.1	0.6	0.0	0.0	0.0	0.0	0.0
GeoRem		441.0	460.0	425.7	515.5	462.0	448.0	465.0
Uncertainty		15.0	18.0	1.0	1.0	11.0	9.0	34.0

Sample: LMI-C2 (pv) 22/01/18

Standard		Co59	Sr88	Y89	Zr91	Nb93	Sn118	Sb121
Nist-610	Primary	384.1	473.8	431.2	416.1	409.6	396.0	371.0
Nist-610	Primary	449.4	560.2	500.2	490.9	448.7	409.0	393.9
Nist-610	Primary	393.3	476.3	431.3	420.3	403.3	379.6	335.6
Nist-610	Primary	381.2	455.7	414.5	410.0	371.0	352.3	329.1
Nist-610	Primary	410.5	509.5	460.8	449.8	429.2	406.7	392.1
Mean		403.7	495.1	447.6	437.4	412.4	388.7	364.3
SD		25.0	36.9	30.2	30.1	26.1	21.0	27.4
Average detection limit		292.2	335.5	305.6	331.8	305.8	291.9	294.8
GeoRem		441.0	460.0	425.7	515.5	462.0	448.0	465.0
Uncertainty		15.0	18.0	1.0	1.0	11.0	9.0	34.0
Standard								
BHVO-2G	Secundary	43.7	358.5	22.5	157.6	15.0	3.5	0.5
Detection limit		0.2	0.1	0.1	0.4	0.1	1.8	0.5
GeoRem		127.0	102.0	9.2	396.0	26.0	170.0	18.3
Uncertainty		11.0	6.0	0.0	0.0	2.0	7.0	0.8

Sample: TRIV-5 (pv) 22/01/18

Standard		Co59	Sr88	Y89	Zr91	Nb93	Sn118	Sb121
Nist-610	Primary	384.8	473.1	428.0	420.5	398.8	370.0	351.3
Nist-610	Primary	446.7	551.2	499.2	475.6	460.9	448.7	400.5
Nist-610	Primary	387.1	471.5	424.3	424.0	409.0	386.2	360.0
Nist-610	Primary	421.9	524.3	477.5	453.4	427.5	402.7	374.6
Mean		410.1	505.0	457.2	443.4	424.0	401.9	371.6
SD		25.7	34.1	32.0	22.6	23.6	29.4	18.6
Average detection limit		0.3	0.1	0.2	1.4	0.2	3.4	1.1
GeoRem		441.0	460.0	425.7	515.5	462.0	448.0	465.0
Uncertainty		15.0	18.0	1.0	1.0	11.0	9.0	34.0
Standard								
BHVO-2G	Secundary	48.2	387.3	25.1	178.2	17.4	4.3	<0.57
Detection limit		0.2	0.1	0.0	0.3	0.1	1.8	0.6
GeoRem		127.0	102.0	9.2	396.0	26.0	170.0	18.3
Uncertainty		11.0	6.0	0.0	0.0	2.0	7.0	0.8

TABELA C01 – Cont. Standards concentrations from LA-ICP-MS analyses

Sample: TRIV-5-3 (ol) 22/01/18

Standard	Ba	La	Ce	Pr	Nd	Sm	Eu	Gd	Tb	Dy
BHVO-2G Primary	129.4	15.3	37.4	5.4	24.1	6.3	2.1	6.1	0.9	5.5
BHVO-2G Primary	132.7	15.2	38.0	5.3	25.3	6.0	2.1	6.2	0.9	5.0
BHVO-2G Primary	131.8	15.0	37.3	5.3	24.1	5.9	2.0	6.3	0.9	5.6
BHVO-2G Primary	129.2	14.9	36.9	5.3	23.7	6.4	2.0	6.1	0.9	5.1
BHVO-2G Primary	132.1	15.6	38.5	5.5	25.6	6.0	2.2	6.2	1.0	5.3
Mean	131.0	15.2	37.6	5.4	24.5	6.1	2.1	6.2	0.9	5.3
SD	1.5	0.3	0.6	0.1	0.8	0.2	0.1	0.1	0.0	0.2
Average detection limit	0.1	0.0	0.0	0.0	0.1	0.1	0.0	0.1	0.0	0.0
GeoRem	131.0	15.2	37.6	5.4	24.5	6.1	2.1	6.2	0.9	5.3
Uncertainty	2.0	0.2	0.2	0.2	0.2	0.0	0.0	0.1	0.0	0.1
Standard										
Nist-610 Secundary	481.5	466.9	483.6	487.9	465.6	470.0	469.2	494.7	482.5	468.0
Detection limit	0.1	0.0	0.0	0.0	0.1	0.0	0.0	0.1	0.0	0.1
<i>GeoRem</i>	452.0	440.0	453.0	448.0	430.0	453.0	447.0	449.0	437.0	437.0
<i>Uncertainty</i>	9.0	10.0	8.0	7.0	8.0	11.0	12.0	12.0	9.0	11.0

Sample: LMI-C2 (pv)

22/01/18

Standard	Ba137	La139	Ce140	Pr141	Nd143	Sm147	Eu151	Gd157	Tb159	Dy161
Nist-610 Primary	432.7	465.3	451.7	436.6	438.4	448.4	458.6	418.6	443.8	428.0
Nist-610 Primary	443.1	477.8	474.8	453.5	445.4	472.7	477.0	427.4	450.4	428.1
Nist-610 Primary	385.0	425.2	415.0	397.2	398.7	424.6	446.9	411.8	432.5	421.7
Nist-610 Primary	366.0	415.6	396.9	399.6	397.9	387.4	422.2	372.8	401.3	382.8
Nist-610 Primary	451.2	480.9	471.7	453.9	452.0	466.6	469.7	424.5	449.2	429.4
Mean	415.6	453.0	442.0	428.1	426.5	440.0	454.9	411.0	435.4	418.0
SD	33.8	27.2	31.0	25.1	23.4	31.1	19.3	19.8	18.2	17.8
Average detection limit	312.3	316.0	318.6	309.0	301.8	316.9	312.0	297.8	301.5	294.7
<i>GeoRem</i>	452.0	440.0	453.0	448.0	430.0	453.0	447.0	449.0	437.0	437.0
<i>Uncertainty</i>	9.0	10.0	8.0	7.0	8.0	11.0	12.0	12.0	9.0	11.0
Standard										
BHVO-2G Secundary	109.9	16.0	37.3	5.1	24.9	5.6	2.1	6.3	0.9	5.1
Detection limit	0.5	0.1	0.1	0.1	0.4	0.5	0.1	0.3	0.1	0.3
<i>GeoRem</i>	131.0	15.2	37.6	5.4	24.5	6.1	2.1	6.2	0.9	5.3
<i>Uncertainty</i>	2.0	0.2	0.2	0.2	0.2	0.0	0.0	0.1	0.0	0.1

Sample: TRIV-5 (pv) 22/01/18

Standard	Ba137	La139	Ce140	Pr141	Nd143	Sm147	Eu151	Gd157	Tb159	Dy161
Nist-610 Primary	401.2	440.0	435.9	411.7	411.4	432.9	441.6	406.0	427.0	403.5
Nist-610 Primary	464.9	490.5	466.2	465.0	464.4	479.3	496.8	442.0	470.5	469.7
Nist-610 Primary	414.9	449.8	455.7	423.2	424.1	450.6	461.9	424.2	446.5	423.1
Nist-610 Primary	429.8	462.8	439.0	434.0	434.4	447.9	457.6	414.1	437.2	426.4
Mean	427.7	460.8	449.2	433.5	433.6	452.7	464.5	421.6	445.3	430.7
SD	23.8	19.0	12.4	19.8	19.6	16.8	20.1	13.4	16.1	24.2
Average detection limit	1.2	0.2	0.2	0.2	1.3	0.9	0.3	0.6	0.1	0.7
<i>GeoRem</i>	452.0	440.0	453.0	448.0	430.0	453.0	447.0	449.0	437.0	437.0
<i>Uncertainty</i>	9.0	10.0	8.0	7.0	8.0	11.0	12.0	12.0	9.0	11.0
Standard										
BHVO-2G Secundary	129.9	16.3	37.3	5.2	24.0	7.1	2.5	7.3	1.1	5.4
Detection limit	0.5	0.1	0.1	0.1	0.5	0.4	0.1	0.3	0.1	0.3
<i>GeoRem</i>	131.0	15.2	37.6	5.4	24.5	6.1	2.1	6.2	0.9	5.3

TABELA C01 – Cont. Standards concentrations from LA-ICP-MS analyses

Sample: TRIV-5-3 (ol) 22/01/18

Standard		Ho	Er	Tm	Yb	Lu	Hf	Ta	Pb	Th	U
BHVO-2G	Primary	1.0	2.7	0.3	2.0	0.3	4.4	1.2	1.7	1.2	0.4
BHVO-2G	Primary	0.9	2.5	0.3	2.1	0.3	4.3	1.1	1.7	1.2	0.5
BHVO-2G	Primary	1.0	2.5	0.3	1.9	0.3	4.2	1.1	1.6	1.2	0.4
BHVO-2G	Primary	1.0	2.5	0.3	2.1	0.3	4.2	1.1	1.6	1.2	0.4
BHVO-2G	Primary	1.0	2.7	0.3	2.0	0.3	4.5	1.2	1.8	1.3	0.4
Mean		1.0	2.6	0.3	2.0	0.3	4.3	1.2	1.7	1.2	0.4
SD		0.0	0.1	0.0	0.1	0.0	0.1	0.0	0.1	0.0	0.0
Average detection limit		0.0	0.0	0.0	0.1	0.0	0.1	0.0	0.0	0.0	0.0
GeoRem		1.0	2.6	0.3	2.0	0.3	4.3	1.2	1.7	1.2	0.4
Uncertainty		0.0	0.0	0.0	0.0	0.0	0.2	0.1	0.2	0.1	0.0
Standard											
Nist-610	Secondary	506.6	503.2	498.1	493.3	488.4	481.4	505.5	421.2	498.6	456.5
Detection limit		0.0	0.1	0.0	0.1	0.0	0.1	0.0	0.0	0.0	0.0
<i>GeoRem</i>		449.0	455.0	435.0	450.0	439.0	435.0	446.0	426.0	457.2	461.5
<i>Uncertainty</i>		12.0	14.0	10.0	9.0	8.0	12.0	33.0	1.0	1.0	1.0

Sample: LMI-C2 (pv) 22/01/18

Standard		Ho165	Er166	Tm169	Yb173	Lu175	Hf178	Ta181	Pb206	Pb207	Pb208
Nist-610	Primary	439.7	418.9	414.5	444.5	425.6	406.9	369.0	416.4	413.2	417.0
Nist-610	Primary	466.8	435.7	428.8	476.1	446.3	428.0	378.2	401.2	406.6	402.6
Nist-610	Primary	446.0	425.9	419.0	473.6	436.4	423.3	388.3	427.5	424.3	422.9
Nist-610	Primary	408.0	389.8	394.3	430.6	409.5	410.1	352.2	371.4	366.3	350.8
Nist-610	Primary	450.7	425.6	420.4	454.0	433.1	413.9	369.9	406.2	407.6	408.4
Mean		442.2	419.2	415.4	455.8	430.2	416.5	371.5	404.5	403.6	400.3
SD		19.3	15.6	11.5	17.3	12.3	8.0	11.9	18.9	19.7	25.7
Average detection limit		306.4	298.7	289.0	307.1	294.8	285.6	275.9	283.7	294.8	298.5
<i>GeoRem</i>		449.0	455.0	435.0	450.0	439.0	435.0	446.0	426.0	457.2	461.5
<i>Uncertainty</i>		12.0	14.0	10.0	9.0	8.0	12.0	33.0	1.0	1.0	1.0
Standard											
BHVO-2G	Secondary	0.9	2.6	0.3	1.8	0.3	4.2	0.9	2.0	1.3	1.8
Detection limit		0.1	0.2	0.0	0.4	0.1	0.2	0.0	0.3	0.3	0.2
<i>GeoRem</i>		1.0	2.6	0.3	2.0	0.3	4.3	1.2	1.7	1.2	0.4
<i>Uncertainty</i>		0.0	0.0	0.0	0.0	0.0	0.2	0.1	0.2	0.1	0.0

Sample: TRIV-5 (pv) 22/01/18

Standard		Ho165	Er166	Tm169	Yb173	Lu175	Hf178	Ta181	Pb206	Pb207	Pb208
Nist-610	Primary	428.6	405.4	401.6	438.7	421.4	404.7	368.6	398.5	398.9	403.5
Nist-610	Primary	489.2	465.4	457.1	506.6	462.7	442.2	394.1	439.2	439.1	432.1
Nist-610	Primary	451.0	421.9	413.2	443.3	415.8	403.4	357.9	404.6	400.4	398.9
Nist-610	Primary	445.0	427.2	424.7	477.6	454.9	431.0	397.8	419.8	424.5	427.6
Mean		453.4	430.0	424.1	466.6	438.7	420.3	379.6	415.5	415.7	415.5
SD		22.2	22.0	20.7	27.6	20.4	16.8	16.8	15.7	16.9	14.5
Average detection limit		0.2	0.4	0.1	0.8	0.2	0.5	0.2	0.7	0.7	0.4
<i>GeoRem</i>		449.0	455.0	435.0	450.0	439.0	435.0	446.0	426.0	457.2	461.5
<i>Uncertainty</i>		12.0	14.0	10.0	9.0	8.0	12.0	33.0	1.0	1.0	1.0

Standard		Ho165	Er166	Tm169	Yb173	Lu175	Hf178	Ta181	Pb206	Pb207	Pb208
BHVO-2G	Secondary	1.0	2.0	0.4	2.3	0.4	4.9	1.0	2.2	1.8	1.8
Detection limit		0.1	0.2	0.0	0.3	0.0	0.1	0.1	0.4	0.5	0.2
<i>GeoRem</i>		1.0	2.6	0.3	2.0	0.3	4.3	1.2	1.7	1.2	0.4
<i>Uncertainty</i>		0.0	0.0	0.0	0.0	0.0	0.2	0.1	0.2	0.1	0.0

TABELA C01 – Cont. Standards concentrations from LA-ICP-MS analyses

Sample: LMI-C2 (pv)

22/01/18

Standard		Th232	U238
Nist-610	Primary	454.5	467.4
Nist-610	Primary	441.6	445.0
Nist-610	Primary	456.4	457.0
Nist-610	Primary	395.2	402.7
Nist-610	Primary	447.6	457.9
Mean		439.1	446.0
SD		22.5	22.8
Average detection limit		235.1	240.3

GeoRem

Uncertainty

Standard

BHVO-

2G	Secundary	1.0	0.3
Detection limit		0.0	0.0

GeoRem

Uncertainty

Sample: TRIV-5 (pv)

22/01/18

Standard		Th232	U238
Nist-610	Primary	445.2	451.0
Nist-610	Primary	462.2	469.7
Nist-610	Primary	435.9	442.9
Nist-610	Primary	466.3	472.0
Mean		452.4	458.9
SD		12.4	12.3
Average detection limit		0.2	0.3

GeoRem

Uncertainty

Standard

BHVO-

2G	Secundary	1.4	0.6
Detection limit		0.0	0.0

GeoRem

Uncertainty

TABELA C01 – Cont. Standards concentrations from LA-ICP-MS analyses

Sample: TRIV-5-3 (pv) 22/01/18

Standard		Li7	Mg24	Al27	Si29	P31	Ca42	Ca44
Nist-610	Primary	506.7	479.3	10278.9	332487.8	339.6	81833.2	81454.3
Nist-610	Primary	464.8	452.0	9753.5	324290.1	345.5	81833.2	82227.5
Nist-610	Primary	502.7	513.6	10864.9	359154.4	421.9	81833.3	82327.0
Nist-610	Primary	487.4	467.1	10041.4	328868.9	342.1	81833.3	81781.0
Mean		490.4	478.0	10234.7	336200.3	362.3	81833.2	81947.5
SD		16.4	22.7	408.7	13567.2	34.5	0.0	351.2
Average detection limit		490.4	478.0	10234.7	336200.3	362.3	81833.2	81947.5
<i>GeoRem</i>		468.0	97139.8	432.0	10489.8	331744.0	413.0	81763.4
<i>Uncertainty</i>		24.0	2603.1	29.0	258.5	6440.0	46.0	2128.4

Standard

BHVO-2G	Secundary	4.1	39585.0	61627.8	259163.4	1173.9	81475.9	78906.4
Detection limit		1.3	0.6	2.7	1894.7	65.5	1378.4	193.6
<i>GeoRem</i>		4.4	16400.0	43600.0	71300.0	233000.0	1200.0	81700.0
<i>Uncertainty</i>		0.8	600.0	700.0	800.0	3000.0	100.0	1200.0

Sample: LMI-C1 (ol) 23/01/18

Standard		Li	Na	Mg	Al	Si	P	Ca
BHVO-2G	Primary	4.3	17407.8	42580.2	71549.0	230428.0	1256.3	82197.8
BHVO-2G	Primary	4.5	18138.6	43523.0	72658.5	230428.0	1284.6	81279.7
BHVO-2G	Primary	4.6	18053.6	42802.6	71460.0	230428.0	1243.9	80160.7
BHVO-2G	Primary	4.6	17941.7	43074.2	72423.0	230428.0	1288.4	82182.5
BHVO-2G	Primary	4.2	17517.4	42991.8	71839.2	230428.0	1256.9	81620.7
Mean		4.4	17811.8	42994.4	71985.9	230428.0	1266.0	81488.3
SD		0.2	294.0	314.4	475.9	0.0	17.4	749.5
Average detection limit		0.1	1.4	0.8	0.4	304.8	10.7	173.7
<i>GeoRem</i>		4.4	16400.0	43600.0	71300.0	233000.0	1200.0	81700.0
<i>Uncertainty</i>		0.8	600.0	700.0	800.0	3000.0	100.0	1200.0

Standard

Nist-610	Secundary	483.5	115797.1	535.0	11576.5	325805.3	468.3	90584.7
Detection limit		0.1	1.9	1.2	0.5	423.0	15.4	240.4
<i>GeoRem</i>		468.0	97139.8	432.0	10489.8	331744.0	413.0	81763.4
<i>Uncertainty</i>		24.0	2603.1	29.0	258.5	6440.0	46.0	2128.4

Standard

BIR	Secundary	3.0	14439.5	57487.9	84502.3	223295.8	99.5	96979.7
Detection limit		0.1	1.6	1.0	0.4	339.4	11.9	191.6
<i>GeoRem</i>		3.2	13131.0	57854.0	81813.0	228999.8	96.0	91688.2
<i>Uncertainty</i>		0.1	6.0	5.0	6.0	1.8	9.7	687.6

TABELA C01 – Cont. Standards concentrations from LA-ICP-MS analyses.

Sample: TRIV-5-3 (pv) 22/01/18

Standard		Sc45	Ti46	Ti49	V51	Cr52	Mn55	Fe56
Nist-610	Primary	437.7	429.9	436.5	443.3	404.7	438.0	476.9
Nist-610	Primary	444.7	438.3	431.4	440.0	405.8	428.7	438.5
Nist-610	Primary	430.8	449.1	406.0	445.0	437.9	472.9	512.8
Nist-610	Primary	440.6	433.5	434.3	441.9	405.1	433.9	459.6
Mean		438.5	437.7	427.1	442.6	413.3	443.4	472.0
SD		5.1	7.2	12.3	1.8	14.2	17.4	27.2
Average detection limit		438.5	437.7	427.1	442.6	413.3	443.4	472.0
<i>GeoRem</i>		455.0	452.0	450.0	408.0	444.0	410.0	458.7
<i>Uncertainty</i>		10.0	10.0	9.0	10.0	13.0	10.0	4.0
Standard								
BHVO-2G	Secundary	28.3	13640.6	14096.0	311.8	297.4	1326.4	81921.1
Detection limit		0.5	5.4	2.4	0.7	3.1	1.9	14.5
<i>GeoRem</i>		33.0	16300.0	308.0	293.0	1290.0	44.0	116.0
<i>Uncertainty</i>		2.0	900.0	19.0	12.0	40.0	2.0	7.0

Sample: LMI-C1 (ol) 23/01/18

Standard		Sc	Ti	V	Cr	Mn	Co	Ni
BHVO-2G	Primary	33.2	16438.3	306.7	295.5	1328.5	43.9	114.9
BHVO-2G	Primary	33.0	16317.3	310.2	291.5	1311.9	44.1	116.9
BHVO-2G	Primary	32.4	15941.0	306.3	291.4	1303.9	44.1	117.1
BHVO-2G	Primary	33.2	16309.4	307.3	289.2	1304.6	43.6	114.6
BHVO-2G	Primary	33.2	16516.1	309.6	297.9	1337.9	44.3	116.6
Mean		33.0	16304.4	308.0	293.1	1317.4	44.0	116.0
SD		0.3	197.5	1.6	3.1	13.6	0.2	1.1
Average detection limit		0.1	0.4	0.1	0.4	0.2	0.0	0.1
<i>GeoRem</i>		33.0	16300.0	308.0	293.0	1290.0	44.0	116.0
<i>Uncertainty</i>		2.0	900.0	19.0	12.0	40.0	2.0	7.0
Standard								
Nist-610	Secundary	517.1	489.8	457.1	449.5	493.1	422.4	460.3
Detection limit		0.1	0.5	0.1	0.6	0.3	0.0	0.1
<i>GeoRem</i>		455.0	452.0	450.0	408.0	444.0	410.0	458.7
<i>Uncertainty</i>		10.0	10.0	9.0	10.0	13.0	10.0	4.0
Standard								
BIR	Secundary	46.3	5817.4	322.6	414.4	1397.9	53.5	175.8
Detection limit		0.1	0.5	0.1	0.5	0.3	0.0	0.1
<i>GeoRem</i>		43.2	5423.8	320.6	392.9	1382.8	52.2	168.9
<i>Uncertainty</i>		0.6	99.3	2.9	3.9	23.7	0.6	1.9

TABELA C01 – Cont. Standards concentrations from LA-ICP-MS analyses.

Sample: TRIV-5-3 (pv) 22/01/18

Standard		Co59	Sr88	Y89	Zr91	Nb93	Sn118	Sb121
Nist-610	Primary	410.2	505.8	466.2	449.1	432.7	413.4	388.5
Nist-610	Primary	399.9	489.4	435.4	430.9	407.3	380.8	351.0
Nist-610	Primary	451.8	556.5	494.2	473.8	442.7	429.5	401.1
Nist-610	Primary	405.6	498.4	451.7	441.0	421.0	398.3	370.8
Mean		416.9	512.5	461.9	448.7	425.9	405.5	377.8
SD		20.5	26.0	21.6	15.8	13.2	18.0	18.9
Average detection limit		416.9	512.5	461.9	448.7	425.9	405.5	377.8
<i>GeoRem</i>		441.0	460.0	425.7	515.5	462.0	448.0	465.0
<i>Uncertainty</i>		15.0	18.0	1.0	1.0	11.0	9.0	34.0
Standard								
BHVO-2G	Secundary	50.4	405.3	26.1	170.1	17.8	4.8	<0.58
Detection limit		0.2	0.1	0.0	0.5	0.1	1.8	0.6
<i>GeoRem</i>		127.0	102.0	9.2	396.0	26.0	170.0	18.3
<i>Uncertainty</i>		11.0	6.0	0.0	0.0	2.0	7.0	0.8

Sample: LMI-C1 (ol) 23/01/18

Standard		Cu	Zn	Rb	Sr	Y	Zr	Nb
BHVO-2G	Primary	124.0	101.6	8.9	394.0	26.2	170.0	18.4
BHVO-2G	Primary	129.7	103.5	9.6	398.3	26.0	172.1	18.4
BHVO-2G	Primary	128.7	99.8	9.2	396.4	25.7	165.5	17.8
BHVO-2G	Primary	124.6	100.9	8.9	390.9	25.8	169.7	18.4
BHVO-2G	Primary	128.1	104.3	9.4	400.7	26.4	173.0	18.6
Mean		127.0	102.0	9.2	396.0	26.0	170.0	18.3
SD		2.3	1.7	0.3	3.4	0.3	2.6	0.3
Average detection limit		0.1	0.4	0.0	0.0	0.0	0.0	0.0
<i>GeoRem</i>		127.0	102.0	9.2	396.0	26.0	170.0	18.3
<i>Uncertainty</i>		11.0	6.0	0.0	0.0	2.0	7.0	0.8

Standard								
Nist-610	Secundary	503.9	383.0	459.1	560.6	551.4	513.5	519.8
Detection limit		0.1	0.5	0.0	0.0	0.0	0.0	0.0
<i>GeoRem</i>		441.0	460.0	425.7	515.5	462.0	448.0	465.0
<i>Uncertainty</i>		15.0	18.0	1.0	1.0	11.0	9.0	34.0
Standard								
BIR	Secundary	129.8	67.9	0.2	110.1	16.1	15.2	0.6
Detection limit		0.1	0.4	0.0	0.0	0.0	0.0	0.0
<i>GeoRem</i>		120.7	70.4	0.2	108.6	15.6	14.8	0.6
<i>Uncertainty</i>		1.6	1.1	0.0	0.7	0.2	0.2	0.0

TABELA C01 – Cont. Standards concentrations from LA-ICP-MS analyses

Sample: TRIV-5-3 (pv) 22/01/18

Standard	Ba137	La139	Ce140	Pr141	Nd143	Sm147	Eu151	Gd157	Tb159	Dy161
Nist-610 Primary	449.3	494.9	476.5	457.3	454.4	466.4	490.1	451.1	474.1	449.4
Nist-610 Primary	401.7	428.0	424.1	407.2	409.6	435.6	437.0	393.9	417.7	406.5
Nist-610 Primary	493.6	531.8	489.9	489.1	476.2	475.7	471.4	431.0	449.8	434.2
Nist-610 Primary	427.2	461.6	451.2	432.9	433.7	452.5	464.5	423.6	446.4	429.2
Mean	442.9	479.1	460.4	446.6	443.5	457.5	465.7	424.9	447.0	429.8
SD	33.8	38.6	25.2	30.2	24.6	15.1	19.1	20.5	20.0	15.4
Average detection limit	442.9	479.1	460.4	446.6	443.5	457.5	465.7	424.9	447.0	429.8
<i>GeoRem</i>	452.0	440.0	453.0	448.0	430.0	453.0	447.0	449.0	437.0	437.0
<i>Uncertainty</i>	9.0	10.0	8.0	7.0	8.0	11.0	12.0	12.0	9.0	11.0
Standard										
BHVO-2G Secundary	131.3	19.3	41.4	5.9	25.9	6.1	2.4	6.0	1.0	5.8
Detection limit	0.5	0.1	0.1	0.1	0.9	0.5	0.1	0.4	0.1	0.3
<i>GeoRem</i>	131.0	15.2	37.6	5.4	24.5	6.1	2.1	6.2	0.9	5.3
<i>Uncertainty</i>	2.0	0.2	0.2	0.2	0.2	0.0	0.0	0.1	0.0	0.1

Sample: LMI-C1 (ol) 23/01/18

Standard	Ba	La	Ce	Pr	Nd	Sm	Eu	Gd	Tb	Dy
BHVO-2G Primary	131.7	15.3	37.7	5.4	24.9	6.3	2.1	6.0	0.9	5.3
BHVO-2G Primary	130.6	15.1	37.8	5.3	24.2	6.0	2.2	6.3	0.9	5.3
BHVO-2G Primary	130.4	15.2	37.1	5.3	24.3	6.0	1.9	6.5	0.9	5.2
BHVO-2G Primary	130.2	15.0	37.0	5.3	24.2	6.1	2.0	5.9	0.9	5.2
BHVO-2G Primary	132.2	15.4	38.5	5.4	25.0	6.2	2.2	6.3	0.9	5.4
Mean	131.0	15.2	37.6	5.4	24.5	6.1	2.1	6.2	0.9	5.3
SD	0.8	0.1	0.6	0.1	0.4	0.1	0.1	0.2	0.0	0.1
Average detection limit	0.1	0.0	0.0	0.0	0.1	0.1	0.0	0.1	0.0	0.0
<i>GeoRem</i>	131.0	15.2	37.6	5.4	24.5	6.1	2.1	6.2	0.9	5.3
<i>Uncertainty</i>	2.0	0.2	0.2	0.2	0.2	0.0	0.0	0.1	0.0	0.1

Standard

Nist-610 Secundary	490.1	487.4	503.1	504.8	478.9	491.1	507.7	491.8	475.2	476.5
Detection limit	0.1	0.0	0.0	0.0	0.1	0.1	0.0	0.1	0.0	0.1
<i>GeoRem</i>	452.0	440.0	453.0	448.0	430.0	453.0	447.0	449.0	437.0	437.0

Uncertainty

Standard

BIR Secundary	7.3	0.6	2.0	0.4	2.6	1.2	0.5	1.7	0.4	2.7
Detection limit	0.1	0.0	0.0	0.0	0.1	0.1	0.0	0.0	0.0	0.0
<i>GeoRem</i>	6.8	0.6	1.9	0.4	2.4	1.1	0.5	1.8	0.4	2.5

Uncertainty

TABELA C01 – Cont. Standards concentrations from LA-ICP-MS analyses

Sample: TRIV-5-3 (pv) 22/01/18

Standard		Ho165	Er166	Tm169	Yb173	Lu175	Hf178	Ta181	Pb206	Pb207	Pb208
Nist-610	Primary	472.2	445.0	432.5	476.8	451.4	441.2	395.9	428.9	430.1	417.7
Nist-610	Primary	430.0	409.2	408.9	447.3	420.0	397.4	360.1	398.9	397.8	409.0
Nist-610	Primary	444.9	425.9	423.8	477.6	452.8	444.5	399.5	442.2	425.5	447.5
Nist-610	Primary	452.0	428.2	421.5	463.3	436.6	420.5	378.9	415.2	415.4	413.9
Mean		449.8	427.1	421.7	466.3	440.2	425.9	383.6	421.3	417.2	422.0
SD		15.2	12.7	8.4	12.3	13.3	18.9	15.7	16.1	12.4	15.0
Average detection limit		449.8	427.1	421.7	466.3	440.2	425.9	383.6	421.3	417.2	422.0
<i>GeoRem</i>		449.0	455.0	435.0	450.0	439.0	435.0	446.0	426.0	457.2	461.5
<i>Uncertainty</i>		12.0	14.0	10.0	9.0	8.0	12.0	33.0	1.0	1.0	1.0

Standard											
BHVO-2G	Secundary	1.0	2.8	0.3	2.5	0.2	5.2	1.1	1.7	2.0	2.3
Detection limit		0.0	0.1	0.0	0.3	0.0	0.3	0.1	0.3	0.4	0.3
<i>GeoRem</i>		1.0	2.6	0.3	2.0	0.3	4.3	1.2	1.7	1.2	0.4
<i>Uncertainty</i>		0.0	0.0	0.0	0.0	0.0	0.2	0.1	0.2	0.1	0.0

Sample: LMI-C1 (ol) 23/01/18

Standard		Ho	Er	Tm	Yb	Lu	Hf	Ta	Pb	Th	U
BHVO-2G	Primary	1.0	2.6	0.3	1.9	0.3	4.5	1.1	1.8	1.2	0.4
BHVO-2G	Primary	1.0	2.5	0.4	2.1	0.3	4.2	1.1	1.6	1.3	0.4
BHVO-2G	Primary	1.0	2.6	0.3	2.1	0.3	4.2	1.2	1.8	1.2	0.4
BHVO-2G	Primary	1.0	2.5	0.3	2.0	0.3	4.3	1.1	1.7	1.2	0.4
BHVO-2G	Primary	1.0	2.6	0.4	2.0	0.3	4.5	1.1	1.7	1.2	0.4
Mean		1.0	2.6	0.3	2.0	0.3	4.3	1.2	1.7	1.2	0.4
SD		0.0	0.0	0.0	0.1	0.0	0.1	0.0	0.1	0.0	0.0
Average detection limit		0.0	0.0	0.0	0.0	0.0	0.1	0.0	0.0	0.0	0.0
<i>GeoRem</i>		1.0	2.6	0.3	2.0	0.3	4.3	1.2	1.7	1.2	0.4
<i>Uncertainty</i>		0.0	0.0	0.0	0.0	0.0	0.2	0.1	0.2	0.1	0.0

Standard											
Nist-610	Secundary	518.6	516.0	516.5	496.0	510.7	450.6	517.3	429.5	494.2	443.2
Detection limit		0.0	0.0	0.0	0.1	0.0	0.1	0.0	0.0	0.0	0.0
<i>GeoRem</i>		449.0	455.0	435.0	450.0	439.0	435.0	446.0	426.0	457.2	461.5
<i>Uncertainty</i>		12.0	14.0	10.0	9.0	8.0	12.0	33.0	1.0	1.0	1.0

Standard											
BIR	Secundary	0.7	1.6	0.3	1.8	0.3	0.6	0.0	3.4	0.0	0.0
Detection limit		0.0									
<i>GeoRem</i>		0.6	1.7	0.3	1.6	0.2	0.6	0.0	3.0	0.0	0.0
<i>Uncertainty</i>		0.0	0.0	0.0	0.0	0.0	0.0	0.0	0.0	0.0	0.0

TABELA C01 – Cont. Standards concentrations from LA-ICP-MS analyses.

Sample: LMI-B1-2 (cpx)

23/01/18

Standard		Li7	Be9	B11	Mg25	Si28	Si29	P31
BHVO-2G	Primary	4.4	1.2	b.d	42660.5	228302.3	230428.0	1268.7
BHVO-2G	Primary	4.5	1.4	b.d	43235.3	231901.2	230427.9	1260.9
BHVO-2G	Primary	4.3	1.5	b.d	42947.9	233066.6	230427.9	1287.5
BHVO-2G	Primary	4.5	1.2	b.d	43570.7	229922.3	230428.0	1240.7
BHVO-2G	Primary	4.4	1.3	b.d	42575.8	229067.4	230428.0	1272.8
Mean		4.4	1.3	b.d	42998.0	230451.9	230428.0	1266.1
SD		0.1	0.1	b.d	368.5	1775.1	0.0	15.4
Average detection limit		0.1	0.3	b.d	2.0	184.2	398.8	25.9
<i>GeoRem</i>		4.4	16400.0	43600.0	71300.0	233000.0	1200.0	81700.0
<i>Uncertainty</i>		0.8	600.0	700.0	800.0	3000.0	100.0	1200.0
Standard								
Nist-610	Secundary	491.6	540.6	b.d	476.5	329448.1	325805.2	470.0
Detection limit		0.2	b.d	b.d	1.3	221.5	476.1	30.2
<i>GeoRem</i>		468.0	97139.8	432.0	10489.8	331744.0	413.0	81763.4
<i>Uncertainty</i>		24.0	2603.1	29.0	258.5	6440.0	46.0	2128.4

Sample: TRIV-5-2 (grt)

23/01/18

Standard		Li7	Na23	Mg25	Al27	Si29	P31	Ca42
Nist-610	Primary	483.2	94054.8	453.2	9964.5	328329.3	337.4	82119.2
Nist-610	Primary	486.6	96814.1	483.0	10062.6	328329.3	348.8	81454.5
Nist-610	Primary	484.2	94873.3	462.0	9994.6	328329.3	341.3	81908.4
Nist-610	Primary	75.3	14868.9	73.9	1568.3	53521.8	54.4	13837.9
Mean		382.3	75152.8	368.1	7897.5	259627.4	270.5	64830.0
SD		177.2	34819.3	170.2	3654.3	118995.1	124.8	29441.3
Average detection limit		0.2	4.5	1.3	1.0	595.0	27.3	318.4
<i>GeoRem</i>		468.0	97139.8	432.0	10489.8	331744.0	413.0	81763.4
<i>Uncertainty</i>		24.0	2603.1	29.0	258.5	6440.0	46.0	2128.4
Standard								
BHVO-2G	Secundary	4.9	14892.5	40858.7	63699.5	230447.7	909.2	82834.5
Detection limit		0.2	5.1	1.3	1.3	673.7	29.4	360.7
<i>GeoRem</i>		4.4	16400.0	43600.0	71300.0	233000.0	1200.0	81700.0
<i>Uncertainty</i>		0.8	600.0	700.0	800.0	3000.0	100.0	1200.0

TABELA C01 – Cont. Standards concentrations from LA-ICP-MS analyses

Sample: LMI-B1-2 (cpx)

23/01/18

Standard		Ca42	Sc45	Ti49	V51	Cr52	Mn55	Co59
BHVO-2G	Primary	81601.1	33.0	16245.1	308.5	290.9	1311.1	43.5
BHVO-2G	Primary	81665.7	32.8	16346.6	308.3	295.5	1327.1	44.8
BHVO-2G	Primary	80143.3	33.0	16108.3	304.2	291.5	1308.5	44.0
BHVO-2G	Primary	82451.6	33.7	16662.4	310.9	295.3	1319.8	43.2
BHVO-2G	Primary	81540.6	32.5	16151.0	308.1	291.9	1318.4	44.5
Mean		81480.5	33.0	16302.7	308.0	293.0	1317.0	44.0
SD		746.1	0.4	197.7	2.2	1.9	6.6	0.6
Average detection limit		239.7	0.1	1.5	0.1	0.8	0.5	0.0
<i>GeoRem</i>		33.0	16300.0	308.0	293.0	1290.0	44.0	116.0
<i>Uncertainty</i>		2.0	900.0	19.0	12.0	40.0	2.0	7.0
Standard								
Nist-610	Secundary	81545.5	493.2	474.3	439.5	427.8	469.2	422.3
Detection limit		290.6	0.1	1.0	0.1	1.0	0.5	0.0
<i>GeoRem</i>		455.0	452.0	450.0	408.0	444.0	410.0	458.7
<i>Uncertainty</i>		10.0	10.0	9.0	10.0	13.0	10.0	4.0

Sample: TRIV-5-2 (grt)

23/01/18

Standard		Ca44	Sc45	Ti49	V51	Cr52	Fe54	Mn55
Nist-610	Primary	81905.0	443.1	439.3	443.4	405.3	449.9	434.9
Nist-610	Primary	81735.9	438.5	426.9	439.4	405.1	465.1	431.1
Nist-610	Primary	81852.2	441.6	435.4	442.1	405.2	455.8	433.7
Nist-610	Primary	13428.4	70.8	65.9	70.7	62.7	70.8	66.0
Mean		64730.4	348.5	341.9	348.9	319.6	360.4	341.4
SD		29619.3	160.3	159.4	160.6	148.3	167.3	159.0
Average detection limit		57.0	0.2	0.7	0.2	1.2	41.2	0.6
<i>GeoRem</i>		455.0	452.0	450.0	408.0	444.0	410.0	458.7
<i>Uncertainty</i>		10.0	10.0	9.0	10.0	13.0	10.0	4.0
Standard								
BHVO-2G	Secundary	80320.4	30.5	14390.1	308.5	276.9	58979.1	1199.9
Detection limit		63.9	0.2	0.8	0.2	1.3	41.4	0.7
<i>GeoRem</i>		33.0	16300.0	308.0	293.0	1290.0	44.0	116.0
<i>Uncertainty</i>		2.0	900.0	19.0	12.0	40.0	2.0	7.0

TABELA C01 – Cont. Standards concentrations from LA-ICP-MS analyses

Sample: LMI-B1-2 (cpx)

23/01/18

Standard		Ni60	Cu65	Zn66	Ga71	Rb85	Sr88	Y89
BHVO-2G	Primary	116.4	128.5	100.7	22.0	9.4	394.4	25.9
BHVO-2G	Primary	116.2	125.0	103.6	22.2	9.1	396.9	26.0
BHVO-2G	Primary	115.3	128.1	101.2	22.1	9.2	394.7	26.2
BHVO-2G	Primary	115.1	126.5	103.0	21.2	9.1	401.2	26.0
BHVO-2G	Primary	117.1	127.1	101.5	22.5	9.3	392.9	25.9
Mean		116.0	127.0	102.0	22.0	9.2	396.0	26.0
SD		0.7	1.3	1.1	0.4	0.1	2.9	0.1
Average detection limit		0.2	0.3	0.7	0.1	0.1	0.1	0.0
<i>GeoRem</i>		127.0	102.0	9.2	396.0	26.0	170.0	18.3
<i>Uncertainty</i>		11.0	6.0	0.0	0.0	2.0	7.0	0.8
Standard								
Nist-610	Secundary	460.3	520.9	379.0	505.3	444.5	531.1	531.9
Detection limit		0.2	0.2	0.8	0.1	0.1	0.0	0.0
<i>GeoRem</i>		441.0	460.0	425.7	515.5	462.0	448.0	465.0
<i>Uncertainty</i>		15.0	18.0	1.0	1.0	11.0	9.0	34.0
Sample: TRIV-5-2 (grt) 23/01/18								
Standard		Fe57	Co59	Ni62	Cu65	Zn66	Ga71	Rb85
Nist-610	Primary	457.4	404.0	438.8	432.6	456.2	434.8	431.6
Nist-610	Primary	456.7	406.4	451.2	427.1	456.5	442.8	430.4
Nist-610	Primary	457.2	404.7	442.5	430.9	456.3	437.2	431.2
Nist-610	Primary	72.8	62.8	72.6	67.2	68.4	67.3	65.5
Mean		361.0	319.5	351.3	339.5	359.3	345.5	339.7
SD		166.4	148.2	161.0	157.2	168.0	160.7	158.3
Average detection limit		18.9	0.1	1.7	0.2	1.2	0.1	0.1
<i>GeoRem</i>		441.0	460.0	425.7	515.5	462.0	448.0	465.0
<i>Uncertainty</i>		15.0	18.0	1.0	1.0	11.0	9.0	34.0
Standard								
BHVO-2G	Secundary	72078.4	43.0	116.4	101.0	120.1	20.3	9.2
Detection limit		21.4	0.1	1.7	0.2	1.4	0.1	0.1
<i>GeoRem</i>		127.0	102.0	9.2	396.0	26.0	170.0	18.3
<i>Uncertainty</i>		11.0	6.0	0.0	0.0	2.0	7.0	0.8

TABELA C01 – Cont. Standards concentrations from LA-ICP-MS analyses

Sample: LMI-B1-2 (cpx) 23/01/18

Standard		Zr90	Nb93	Mo95	Sn118	Sb121	Cs133	Ba137	La139	Ce140	Pr141
BHVO-2G	Primary	170.8	18.3	4.0	2.5	b.d	0.1	128.5	15.0	37.3	5.3
BHVO-2G	Primary	168.9	18.3	3.5	2.6	0.5	0.1	134.5	15.5	37.9	5.5
BHVO-2G	Primary	170.3	18.6	4.0	2.6	b.d	0.1	128.7	14.9	37.6	5.2
BHVO-2G	Primary	170.3	18.1	3.8	2.8	0.3	0.1	133.1	15.6	38.0	5.3
BHVO-2G	Primary	169.8	18.3	3.8	2.5	0.4	0.1	130.3	15.1	37.3	5.4
Mean		170.0	18.3	3.8	2.6	0.4	0.1	131.0	15.2	37.6	5.4
SD		0.6	0.2	0.2	0.1	0.1	0.0	2.4	0.3	0.3	0.1
Average detection limit		0.1	0.0	0.1	0.4	0.3	0.0	0.2	0.0	0.0	0.0
<i>GeoRem</i>		131.0	15.2	37.6	5.4	24.5	6.1	2.1	6.2	0.9	5.3
<i>Uncertainty</i>		2.0	0.2	0.2	0.2	0.2	0.0	0.0	0.1	0.0	0.1
Standard											
Nist-610	Secundary	493.5	510.9	398.5	567.0	906.7	430.6	471.9	462.0	470.8	478.4
Detection limit		0.0	0.0	0.1	0.6	0.4	0.0	0.3	0.0	0.0	0.0
<i>GeoRem</i>		452.0	440.0	453.0	448.0	430.0	453.0	447.0	449.0	437.0	437.0
<i>Uncertainty</i>		9.0	10.0	8.0	7.0	8.0	11.0	12.0	12.0	9.0	11.0

Sample: TRIV-5-2 (grt) 23/01/18

Standard		Sr88	Y89	Zr90	Nb93	Sn118	Sb121	Cs133	Ba137	La139	Ce140
Nist-610	Primary	495.5	449.6	441.0	419.5	397.2	367.4	364.3	426.2	458.1	449.6
Nist-610	Primary	500.0	450.3	438.4	419.3	395.1	370.1	356.4	421.2	456.4	445.3
Nist-610	Primary	496.9	449.8	440.2	419.4	396.5	368.2	361.8	424.7	457.6	448.3
Nist-610	Primary	74.3	68.1	65.8	63.1	59.6	55.2	54.4	66.0	69.9	70.7
Mean		391.7	354.4	346.3	330.3	312.1	290.2	284.2	334.5	360.5	353.5
SD		183.3	165.4	162.0	154.3	145.8	135.7	132.7	155.0	167.8	163.3
Average detection limit		0.0	0.0	0.0	0.0	0.5	0.2	0.0	0.2	0.0	0.0
<i>GeoRem</i>		452.0	440.0	453.0	448.0	430.0	453.0	447.0	449.0	437.0	437.0
<i>Uncertainty</i>		9.0	10.0	8.0	7.0	8.0	11.0	12.0	12.0	9.0	11.0
Standard											
BHVO-2G	Secundary	373.2	23.5	157.6	15.0	1.9	<0.182	0.1	120.5	15.0	35.4
Detection limit		0.0	0.0	0.1	0.0	0.6	0.2	0.0	0.2	0.0	0.0
<i>GeoRem</i>		131.0	15.2	37.6	5.4	24.5	6.1	2.1	6.2	0.9	5.3
<i>Uncertainty</i>		2.0	0.2	0.2	0.2	0.2	0.0	0.0	0.1	0.0	0.1

TABELA C01 – Cont. Standards concentrations from LA-ICP-MS analyses

Sample: LMI-B1-2 (cpx) 23/01/18

Standard		Nd143	Sm147	Eu151	Gd157	Tb159	Dy161	Ho165	Er166	Tm169	Yb172
BHVO-2G	Primary	24.7	5.9	2.0	6.3	0.9	5.4	1.0	2.6	0.3	2.3
BHVO-2G	Primary	24.5	6.3	2.1	6.1	1.0	5.2	1.0	2.6	0.3	1.8
BHVO-2G	Primary	23.7	6.5	2.0	6.0	0.9	4.9	0.9	2.6	0.3	2.0
BHVO-2G	Primary	24.8	5.8	2.4	6.2	1.0	5.8	1.0	2.4	0.4	2.0
BHVO-2G	Primary	24.8	6.1	1.9	6.3	0.9	5.2	1.0	2.7	0.3	2.1
Mean		24.5	6.1	2.1	6.2	0.9	5.3	1.0	2.6	0.3	2.0
SD		0.4	0.2	0.2	0.1	0.0	0.3	0.0	0.1	0.0	0.1
Average detection limit		0.1	0.1	0.0	0.1	0.0	0.1	0.0	0.0	0.0	0.1
<i>GeoRem</i>		1.0	2.6	0.3	2.0	0.3	4.3	1.2	1.7	1.2	0.4
<i>Uncertainty</i>		0.0	0.0	0.0	0.0	0.0	0.2	0.1	0.2	0.1	0.0
Standard											
Nist-610	Secundary	440.4	486.9	463.7	447.6	495.0	468.7	455.3	471.6	486.0	455.4
Detection limit		0.2	0.1	0.0	0.1	0.0	0.1	0.0	0.1	0.0	0.1
<i>GeoRem</i>		449.0	455.0	435.0	450.0	439.0	435.0	446.0	426.0	457.2	461.5
<i>Uncertainty</i>		12.0	14.0	10.0	9.0	8.0	12.0	33.0	1.0	1.0	1.0

Sample: TRIV-5-2 (grt) 23/01/18

Standard		Pr141	Nd146	Sm149	Eu151	Gd157	Tb159	Dy161	Ho165	Er166	Tm169
Nist-610	Primary	431.4	429.7	450.4	457.4	414.8	438.7	420.8	451.0	421.7	420.9
Nist-610	Primary	427.7	432.4	450.7	466.4	427.2	448.7	434.7	447.3	432.1	419.1
Nist-610	Primary	430.2	430.5	450.5	460.1	418.5	441.7	425.0	449.8	424.8	420.3
Nist-610	Primary	66.8	66.5	66.6	69.2	62.8	66.5	63.7	67.2	64.6	64.3
Mean		339.0	339.8	354.5	363.3	330.8	348.9	336.0	353.8	335.8	331.1
SD		157.2	157.8	166.2	169.8	154.8	163.1	157.3	165.5	156.6	154.0
Average detection limit		0.0	0.1	0.1	0.0	0.1	0.0	0.1	0.0	0.1	0.0
<i>GeoRem</i>		449.0	455.0	435.0	450.0	439.0	435.0	446.0	426.0	457.2	461.5
<i>Uncertainty</i>		12.0	14.0	10.0	9.0	8.0	12.0	33.0	1.0	1.0	1.0
Standard											
BHVO-2G	Secundary	4.8	23.0	5.6	2.0	6.1	0.8	5.3	0.8	2.3	0.3
Detection limit		0.0	0.2	0.2	0.1	0.1	0.0	0.1	0.0	0.1	0.0
<i>GeoRem</i>		1.0	2.6	0.3	2.0	0.3	4.3	1.2	1.7	1.2	0.4
<i>Uncertainty</i>		0.0	0.0	0.0	0.0	0.0	0.2	0.1	0.2	0.1	0.0

TABELA C01 – Cont. Standards concentrations from LA-ICP-MS analyses

Sample: LMI-B1-2 (cpx) 23/01/18

Standard		Lu175	Hf179	Ta181	Pb206	Pb207	Pb208	Th232	U238
BHVO-2G	Primary	0.3	4.2	1.2	1.6	1.8	1.8	1.2	0.4
BHVO-2G	Primary	0.3	4.5	1.1	1.9	1.7	1.6	1.3	0.4
BHVO-2G	Primary	0.3	4.2	1.1	1.6	1.6	1.7	1.2	0.4
BHVO-2G	Primary	0.3	4.4	1.2	1.8	1.6	1.9	1.2	0.4
BHVO-2G	Primary	0.3	4.3	1.2	1.7	1.9	1.6	1.3	0.4
Mean		0.3	4.3	1.2	1.7	1.7	1.7	1.2	0.4
SD		0.0	0.1	0.0	0.1	0.1	0.1	0.0	0.0
Average detection limit		0.0	0.1	0.0	0.1	0.1	0.0	0.0	0.0

*GeoRem
Uncertainty*

Standard									
Nist-610	Secundary	487.1	459.0	479.7	351.4	381.7	364.5	474.2	440.0
Detection limit		0.0	0.1	0.0	0.1	0.1	0.1	0.1	0.1

*GeoRem
Uncertainty*

Sample: TRIV-5-2 (grt) 23/01/18

Standard		Yb172	Lu175	Hf179	Ta181	Pb206	Pb207	Pb208	Th232	U238
Nist-610	Primary	465.7	438.3	423.6	380.9	420.4	417.8	416.6	449.7	456.4
Nist-610	Primary	455.8	429.9	409.9	371.0	403.9	407.2	408.9	451.9	458.0
Nist-610	Primary	462.6	435.7	419.2	377.7	415.2	414.5	414.2	450.4	456.9
Nist-610	Primary	71.4	66.9	63.3	58.5	64.0	62.1	63.9	68.3	70.5
Mean		363.9	342.7	329.0	297.0	325.9	325.4	325.9	355.0	360.5
SD		168.9	159.3	153.5	137.7	151.3	152.1	151.3	165.6	167.4
Average detection limit		0.1	0.0	0.1	0.0	0.1	0.1	0.1	0.0	0.0

*GeoRem
Uncertainty*

Standard									
BHVO-									
2G	Secundary	1.8	0.3	3.8	1.0	2.1	1.5	2.0	1.1
Detection limit		0.1	0.0	0.1	0.0	0.1	0.2	0.0	0.0
									0.4
									b.d

*GeoRem
Uncertainty*

TABELLA C02 - Trace element concentration, limit of detection and uncertainties (2-sigma error) of olivine megacrysts from all samples. C - core; R - rim; I - intermediately
LOD - limit of detection; b.d - below detection.

Sample	Grain/Analyses	LMi-B1	2 σ error	LOD	LMi-B1	2 σ error	LOD										
Location		R	R	R	C	C	R	C	R	C	C	R	R	C	R	R	C
Li		1.67	0.60	0.14	1.09	0.26	0.12	1.87	0.40	0.14	1.39	0.42	0.15	1.69	0.38	0.14	
Na		38.88	5.50	1.23	34.07	3.54	1.09	17.84	2.66	1.13	12.61	2.90	1.39	28.24	3.42	1.21	
Al		108.15	9.68	0.32	6.21	0.80	0.28	1.03	0.56	0.30	1.24	0.76	0.36	7.34	1.04	0.33	
P	b.d	26.10	9.26	b.d	11.50	8.52	b.d	14.98	8.75	b.d	19.68	10.74	b.d	14.68	9.23		
Ca	b.d	409.72	160.66	b.d	183.96	141.02	b.d	233.88	145.10	b.d	301.20	177.14	b.d	223.76	153.11		
Sc	2.79	0.58	0.08	2.60	0.28	0.07	2.13	0.32	0.07	2.12	0.38	0.09	2.55	0.32	0.07		
Ti	17.11	5.72	0.39	15.87	2.54	0.25	16.24	3.28	0.29	19.25	4.38	0.30	17.00	3.12	0.31		
V	3.51	0.68	0.07	1.18	0.19	0.06	1.08	0.22	0.06	0.94	0.26	0.08	3.42	0.40	0.07		
Cr	33.79	3.62	0.38	20.92	1.94	0.33	23.72	2.32	0.35	21.08	2.28	0.42	77.86	7.12	0.37		
Mn	1254.86	94.08	0.19	1308.30	97.24	0.17	942.74	71.06	0.18	859.33	65.92	0.22	1197.92	92.86	0.19		
Co	136.00	12.52	0.01	122.74	10.90	0.02	129.84	11.82	0.01	123.36	11.60	0.02	134.22	12.74	0.02		
Ni	2476.16	173.98	0.05	2380.27	159.72	0.06	2817.17	191.28	0.09	2687.29	185.64	0.11	2932.5	201.36	0.12		
Cu	0.52	0.40	0.06	0.76	0.20	0.05	b.d	0.10	0.05	b.d	0.13	0.05	0.70	0.24	0.06		
Zn	103.17	15.26	0.32	82.70	10.10	0.27	49.40	6.92	0.29	40.61	6.54	0.37	87.49	11.70	0.30		
Sr	b.d	0.07	0.01	0.05	0.03	0.01	0.50	0.12	0.00	b.d	0.01	0.01	0.12	0.05	0.01		
Y	b.d	0.05	0.01	b.d	0.01	0.01	b.d	0.03	0.01	b.d	0.00	0.01	0.01	0.01	0.00		
Zr	0.19	0.17	0.02	0.15	0.06	0.01	0.06	0.05	0.01	b.d	0.05	0.02	0.17	0.08	0.01		
Nb	1.48	0.38	0.00	1.14	0.16	0.00	4.50	0.52	0.01	4.89	0.62	0.01	1.30	0.20	0.01		
Ba	b.d	0.36	0.04	b.d	0.12	0.05	0.36	0.26	0.05	b.d	0.13	0.06	b.d	0.19	0.07		
La	b.d	0.00	0.01	b.d	0.01	0.00	0.05	0.03	0.00	b.d	0.01	0.01	0.02	0.02	0.01		
Ce	b.d	0.01	0.01	b.d	0.01	0.01	b.d	0.01	0.01	b.d	0.02	0.01	b.d	0.01	0.01		

TABELA C02 – Cont. Trace element concentration, limit of detection and uncertainties (2-sigma error) of olivine megacrysts from all samples. C - core; R - rim; I - intermediated; LOD - limit of detection; b.d - below detection.

Sample	LMI-B1	2σ error	LOD	LMI-B1	2σ error	LOD												
Grain/Analyses	03/06	03/06	03/06	04/07	04/07	04/07	04/08	04/08	04/08	05/09	05/09	05/10	05/10	05/10	05/10	05/10	05/10	05/10
Location	C	C	C	R	R	R	C	C	C	R	R	C	R	C	C	C	C	C
Li	0.63	0.62	0.15	1.83	0.42	0.22	b.d	0.38	0.12	1.85	0.80	0.13	1.70	0.44	0.12			
Na	74.86	9.96	1.26	56.35	6.56	1.82	38.46	5.86	1.12	110.52	14.50	1.13	49.46	6.44	1.09			
Al	63.92	7.56	0.33	5.61	0.92	0.47	12.77	2.26	0.30	38.39	5.32	0.29	20.58	2.38	0.28			
P	b.d	36.16	9.78	128.77	25.80	14.16	b.d	23.62	8.62	b.d	31.94	8.82	b.d	16.28	8.37			
Ca	b.d	516.26	157.45	b.d	257.30	223.75	561.26	378.58	138.37	b.d	454.62	139.07	511.79	243.28	131.38			
Sc	2.79	0.76	0.08	2.30	0.30	0.11	2.39	0.54	0.07	2.73	0.72	0.07	2.06	0.34	0.06			
Ti	5.89	4.44	0.32	116.17	11.46	0.58	11.07	4.48	0.30	8.14	4.90	0.27	6.80	2.30	0.28			
V	0.63	0.42	0.07	3.31	0.40	0.10	1.90	0.48	0.06	4.72	0.98	0.06	3.95	0.54	0.05			
Cr	22.84	3.32	0.38	107.82	10.88	0.54	31.58	3.90	0.34	129.97	14.84	0.34	141.65	15.78	0.33			
Mn	1161.18	94.10	0.19	1181.98	99.60	0.28	968.53	84.64	0.17	1004.68	90.84	0.18	960.67	87.66	0.17			
Co	122.08	12.86	0.01	140.47	15.02	0.02	118.78	13.56	0.01	122.01	14.72	0.01	120.97	14.46	0.02			
Ni	2875.05	214.54	0.10	3112.21	222.84	0.19	2728.01	205.22	0.10	2727.36	213.76	0.12	2832.36	213.44	0.10			
Cu	1.55	0.86	0.05	1.21	0.30	0.07	0.38	0.34	0.06	4.48	1.42	0.05	1.54	0.44	0.05			
Zn	70.53	14.10	0.29	83.25	12.52	0.41	68.74	12.84	0.25	63.00	13.70	0.29	58.78	10.46	0.27			
Sr	2.11	0.56	0.00	b.d	0.01	0.01	0.17	0.11	0.01	9.14	1.46	0.01	0.05	0.04	0.00			
Y	b.d	0.00	0.00	b.d	0.02	0.01	b.d	0.05	0.01	b.d	0.08	0.01	0.03	0.03	0.01			
Zr	0.35	0.30	0.01	0.40	0.12	0.02	b.d	0.13	0.01	1.14	0.50	0.02	0.34	0.14	0.01			
Nb	1.22	0.44	0.01	0.16	0.06	0.01	1.98	0.44	0.01	3.02	0.70	0.01	0.34	0.11	0.01			
Ba	5.17	2.20	0.08	b.d	0.11	0.09	1.22	0.80	0.07	38.24	7.06	0.06	b.d	0.14	0.06			
La	b.d	0.05	0.01	b.d	0.01	0.01	b.d	0.05	0.01	0.66	0.26	0.01	b.d	0.02	0.01			
Ce	b.d	0.08	0.01	b.d	0.02	0.01	b.d	0.03	0.01	1.33	0.38	0.01	b.d	0.01	0.01			

TABELA C02 – Cont. Trace element concentration, limit of detection and uncertainties (2-sigma error) of olivine megacrysts from all samples. C - core; R - rim; I - intermediate; LOD - limit of detection; b.d - below detection.

Sample	LMI-CI	2σ error	LOD													
Grain/Analyses	06/11	06/11	R	C	C	R	C	C	R	C	C	R	C	C	R	R
Location	R	R	R	R	R	R	R	R	R	R	R	R	R	R	R	R
Li	2.21	0.54	0.09	1.84	0.46	0.15	1.58	0.52	0.07	1.87	0.34	0.10	1.22	0.46	0.09	
Na	30.91	4.00	1.19	485.21	41.58	1.91	39.91	5.02	0.96	28.58	2.88	1.32	25.17	3.88	1.17	
Al	7.21	1.36	0.33	34.28	3.08	0.53	5.98	1.44	0.27	75.70	5.16	0.37	12.38	2.06	0.31	
P	b.d	20.54	9.74	b.d	23.14	15.87	b.d	20.86	8.03	b.d	10.14	10.71	b.d	23.74	9.67	
Ca	b.d	306.92	152.09	b.d	349.08	249.43	b.d	316.14	121.08	b.d	155.04	169.06	b.d	302.82	127.95	
Sc	1.78	0.38	0.07	2.00	0.36	0.12	2.48	0.52	0.06	2.70	0.26	0.08	2.13	0.50	0.07	
Ti	102.40	13.14	0.35	91.32	10.86	0.64	63.18	11.24	0.34	57.36	5.30	0.42	9.98	4.24	0.36	
V	2.12	0.40	0.06	1.78	0.34	0.10	1.63	0.42	0.05	1.92	0.19	0.06	1.02	0.36	0.06	
Cr	44.85	3.78	0.38	44.00	3.60	0.62	21.87	2.38	0.31	21.86	1.72	0.42	21.34	2.42	0.37	
Mn	1286.33	90.54	0.20	1235.94	87.56	0.42	1365.15	98.84	0.17	1434.91	103.66	0.23	1154.43	90.44	0.19	
Co	123.92	8.38	0.01	141.63	9.34	0.11	117.67	8.30	0.01	131.65	8.42	0.01	121.85	12.68	0.01	
Ni	2753.53	193.12	0.13	3157.20	220.52	1.41	2139.69	156.38	0.06	2486.40	174.68	0.14	2678.36	240.44	0.14	
Cu	0.41	0.28	0.05	b.d	0.19	0.09	b.d	0.22	0.05	b.d	0.09	0.06	b.d	0.26	0.05	
Zn	81.77	9.72	0.33	86.66	9.42	0.57	72.58	10.10	0.26	78.00	7.28	0.31	66.49	9.02	0.27	
Sr	0.18	0.09	0.01	0.57	0.14	0.01	0.18	0.11	0.00	0.13	0.03	0.01	0.25	0.13	0.01	
Y	b.d	0.00	0.01	0.05	0.04	0.01	b.d	0.00	0.01	b.d	0.01	0.01	b.d	0.00	0.01	
Zr	0.32	0.17	0.01	0.67	0.20	0.02	0.23	0.17	0.01	0.28	0.06	0.02	0.50	0.24	0.01	
Nb	0.76	0.20	0.01	0.96	0.20	0.01	1.88	0.40	0.01	2.33	0.24	0.01	0.82	0.26	0.01	
Ba	b.d	0.26	0.06	1.17	0.52	0.09	0.50	0.48	0.05	b.d	0.08	0.10	b.d	0.22	0.07	
La	b.d	0.03	0.01	0.07	0.04	0.01	b.d	0.03	0.00	b.d	0.01	0.01	b.d	0.00	0.01	
Ce	0.05	0.05	0.01	0.05	0.04	0.01	b.d	0.00	0.01	b.d	0.01	0.01	b.d	0.05	0.01	

TABELA C02 – Cont. Trace element concentration, limit of detection and uncertainties (2-sigma error) of olivine megacrysts from all samples. C - core; R - rim; I - intermediated; LOD - limit of detection; b.d - below detection.

Sample	LMI-C2	2σ error	LOD	LMI-C2	2σ error	LOD	LMI-C2	2σ error	LOD	TRIV-5	2σ error	LOD	TRIV-5	2σ error	LOD
Grain/Analyses	08/16	08/16	08/16	09/17	09/17	09/17	09/18	09/18	01/01	01/01	01/01	01/02	01/02	01/02	01/02
Location	C	C	C	R	R	R	C	C	R	R	R	C	C	C	C
Li	1.34	0.26	0.08	0.98	0.52	0.07	1.64	0.44	0.07	2.26	0.44	0.08	2.57	0.62	0.07
Na	23.97	2.32	1.08	46.22	6.04	1.00	40.13	4.10	1.02	63.57	5.16	1.08	57.51	5.50	0.95
Al	3.19	0.58	0.29	23.83	3.66	0.27	13.41	1.72	0.27	23.00	2.38	0.29	7.57	1.60	0.26
P	b.d	11.04	8.68	46.05	35.76	8.73	b.d	17.24	8.44	b.d	16.50	9.24	b.d	22.22	8.08
Ca	b.d	144.10	115.33	b.d	379.84	112.44	b.d	224.52	111.11	b.d	205.98	114.81	b.d	268.28	103.13
Sc	2.65	0.34	0.06	1.78	0.60	0.06	1.92	0.40	0.06	0.87	0.24	0.06	0.61	0.28	0.05
Ti	6.66	1.64	0.27	61.93	14.46	0.19	50.59	8.38	0.30	2.73	1.62	0.22	2.09	2.08	0.35
V	1.14	0.19	0.06	4.21	0.92	0.05	3.80	0.58	0.06	4.70	0.60	0.06	3.61	0.66	0.05
Cr	19.97	1.74	0.34	81.96	7.86	0.31	70.80	6.32	0.31	130.53	9.72	0.34	99.38	7.98	0.30
Mn	1113.55	88.46	0.18	1174.73	99.12	0.17	1264.57	109.52	0.17	937.92	69.54	0.18	884.59	66.92	0.16
Co	125.09	13.08	0.01	126.00	14.78	0.02	134.73	16.10	0.01	141.41	15.82	0.02	124.08	14.46	0.01
Ni	2822.44	255.48	0.18	2405.17	239.14	0.07	2690.79	272.02	0.14	3209.11	308.52	0.17	2971.54	294.30	0.06
Cu	b.d	0.11	0.06	0.69	0.56	0.04	0.72	0.34	0.05	0.37	0.22	0.04	b.d	0.24	0.05
Zn	55.51	5.18	0.30	84.11	13.06	0.24	88.22	9.70	0.23	60.77	7.16	0.29	53.59	8.20	0.25
Sr	0.04	0.02	0.01	0.31	0.19	b.d	0.10	0.06	0.01	0.70	0.17	0.01	0.14	0.10	0.01
Y	b.d	0.01	0.01	b.d	0.05	0.01	0.03	0.03	0.01	b.d	0.03	0.01	0.06	0.06	b.d
Zr	0.08	0.05	0.01	0.30	0.26	0.02	0.52	0.20	0.01	0.13	0.09	0.02	b.d	0.10	0.01
Nb	1.21	0.17	0.01	1.82	0.50	0.01	1.83	0.32	0.01	0.51	0.15	0.01	0.86	0.26	0.01
Ba	0.15	0.12	0.04	b.d	0.36	0.06	0.36	0.34	0.07	1.20	0.54	0.06	1.86	0.90	0.03
La	b.d	0.01	0.01	b.d	0.00	0.01	b.d	0.00	0.00	0.09	0.05	0.01	b.d	0.03	0.01
Ce	b.d	0.01	0.01	b.d	0.00	0.01	b.d	0.02	0.01	0.22	0.08	0.01	b.d	0.03	0.00

TABELA C02 – Cont. Trace element concentration, limit of detection and uncertainties (2-sigma error) of olivine megacrysts from all samples. C - core; R - rim; I - intermediate; LOD - limit of detection; b.d - below detection.

Sample	TRIV-5	2σ error	LOD																			
Grain/Analyses	02/03	02/03	02/03	02/04	02/04	02/04	03/05	03/05	03/05	03/06	03/06	03/06	04/07	04/07	04/07	04/07	04/07	04/07	04/07	04/07	04/07	
Location	R	R	R	C	C	C	R	R	R	C	C	C	R	R	R	R	R	R	R	R	R	R
Li	2.13	0.54	0.07	2.56	0.72	0.09	2.05	0.84	0.13	3.19	0.70	0.09	1.53	0.30	0.09	1.53	0.30	0.09	1.53	0.30	0.09	
Na	53.52	5.14	0.99	55.08	6.12	1.26	61.15	8.12	1.70	81.34	7.30	1.22	14.32	2.00	1.13	1.22	1.22	1.13	1.22	1.22	1.13	
Al	6.93	1.48	0.27	10.64	2.20	0.33	14.57	3.30	0.46	7.14	1.56	0.31	8.29	1.04	0.30	8.29	1.04	0.30	8.29	1.04	0.30	
P	b.d	20.48	8.56	b.d	29.14	11.26	68.77	50.04	14.06	b.d	26.10	10.37	b.d	13.34	9.90	b.d	13.34	9.90	b.d	13.34	9.90	
Ca	b.d	256.04	107.53	443.36	355.30	133.13	b.d	494.48	171.49	b.d	289.32	129.92	b.d	158.46	117.47	b.d	158.46	117.47	b.d	158.46	117.47	
Sc	0.60	0.26	0.06	0.40	0.30	0.08	1.15	0.56	0.10	1.99	0.46	0.07	0.62	0.16	0.06	0.62	0.16	0.06	0.62	0.16	0.06	
Ti	b.d	1.52	0.23	b.d	2.32	0.38	5.16	4.56	0.44	84.65	13.24	0.38	6.61	1.86	0.39	6.61	1.86	0.39	6.61	1.86	0.39	
V	2.70	0.54	0.05	2.59	0.64	0.07	1.33	0.60	0.10	2.24	0.50	0.07	5.38	0.60	0.06	5.38	0.60	0.06	5.38	0.60	0.06	
Cr	92.98	7.50	0.32	97.42	8.32	0.40	84.78	8.38	0.53	87.59	7.74	0.38	142.00	11.82	0.35	142.00	11.82	0.35	142.00	11.82	0.35	
Mn	854.59	65.42	0.17	940.80	73.88	0.21	1459.11	123.68	0.28	1616.63	138.10	0.20	810.96	70.74	0.19	810.96	70.74	0.19	810.96	70.74	0.19	
Co	125.32	14.94	0.01	141.45	17.60	0.02	134.57	19.24	0.03	141.46	20.50	0.01	138.17	20.68	0.02	138.17	20.68	0.02	138.17	20.68	0.02	
Ni	3067.45	309.60	0.10	3240.70	339.46	0.07	2555.60	303.04	0.09	2729.85	327.36	0.16	3042.63	375.16	0.12	3042.63	375.16	0.12	3042.63	375.16	0.12	
Cu	1.04	0.48	0.03	1.16	0.64	0.06	0.67	0.66	0.09	0.50	0.36	0.05	1.06	0.28	0.06	1.06	0.28	0.06	1.06	0.28	0.06	
Zn	46.43	7.22	0.26	63.63	10.40	0.33	97.36	16.78	0.44	86.03	11.84	0.30	49.44	5.94	0.29	49.44	5.94	0.29	49.44	5.94	0.29	
Sr	0.13	0.09	0.01	0.13	0.11	0.01	0.43	0.26	0.01	0.55	0.19	0.01	b.d	0.02	0.01	b.d	0.02	0.01	b.d	0.02	0.01	
Y	b.d	0.04	0.00	b.d	0.06	0.01	b.d	0.10	0.01	0.03	0.01	0.01	b.d	0.01	0.01	b.d	0.01	0.01	b.d	0.01	0.01	
Zr	b.d	0.05	0.01	0.20	0.18	0.01	b.d	0.13	0.02	0.57	0.26	0.01	b.d	0.02	0.01	b.d	0.02	0.01	b.d	0.02	0.01	
Nb	0.11	0.09	0.01	0.19	0.14	0.01	b.d	0.11	0.01	2.14	0.42	0.01	b.d	0.02	0.00	b.d	0.02	0.00	b.d	0.02	0.00	
Ba	b.d	0.04	0.06	b.d	0.40	0.09	1.95	1.38	0.11	1.46	0.78	0.08	b.d	0.08	0.05	b.d	0.08	0.05	b.d	0.08	0.05	
La	b.d	0.00	0.01	b.d	0.01	0.01	b.d	0.01	0.01	b.d	0.03	0.01	b.d	0.01	0.01	b.d	0.01	0.01	b.d	0.01	0.01	
Ce	b.d	0.00	0.01	b.d	0.05	0.01	b.d	0.01	0.02	b.d	0.02	0.01	b.d	0.01	0.01	b.d	0.01	0.01	b.d	0.01	0.01	

TABELA C02 – Cont. Trace element concentration, limit of detection and uncertainties (2-sigma error) of olivine megacrysts from all samples. C - core; R - rim; I - intermediated; LOD - limit of detection; b.d - below detection.

Sample	TRIV-5	2σ error	LOD	TRIV-5-3	2σ error	LOD	TRIV-5-3	2σ error	LOD	TRIV-5-3	2σ error	LOD
Grain/Analyses	04/08	04/08	04/08	05/09	05/09	05/09	05/10	05/10	05/10	06/11	06/11	06/11
Location	C	C	C	R	R	R	C	C	C	R	R	R
Li	1.34	0.24	0.09	3.13	0.52	0.09	3.52	0.60	0.09	0.94	0.66	0.12
Na	18.70	2.00	1.26	298.26	19.06	0.97	319.52	20.56	0.95	26.78	6.10	1.42
Al	8.29	0.90	0.32	143.10	10.44	0.25	165.49	12.20	0.25	78.16	8.86	0.36
P	b.d	11.38	10.86	73.57	22.34	7.64	62.94	22.92	7.63	b.d	44.00	12.33
Ca	b.d	136.36	128.94	b.d	214.80	109.72	653.21	242.16	107.98	b.d	548.24	165.55
Sc	0.58	0.12	0.06	1.68	0.32	0.06	2.05	0.38	0.05	0.58	0.46	0.08
Ti	b.d	0.58	0.39	224.53	20.12	0.27	222.36	21.02	0.26	4.99	4.58	0.20
V	4.73	0.50	0.06	8.11	0.82	0.05	8.95	0.94	0.05	1.28	0.60	0.08
Cr	133.60	11.32	0.39	128.14	9.78	0.29	136.57	10.60	0.29	58.22	6.22	0.43
Mn	782.88	70.26	0.20	1088.51	72.14	0.15	1111.99	74.26	0.15	737.12	52.16	0.23
Co	135.27	21.18	0.03	167.60	13.02	0.01	169.10	13.36	0.01	109.53	10.18	0.02
Ni	3143.08	403.14	0.17	2392.20	195.34	0.11	2431.98	202.24	0.09	2367.49	214.48	0.15
Cu	1.12	0.24	0.05	8.49	1.36	0.05	8.70	1.48	0.06	1.06	0.82	0.07
Zn	49.83	5.68	0.34	107.22	12.20	0.24	103.48	12.40	0.24	43.33	10.66	0.39
Sr	0.20	0.05	0.01	1.06	0.20	0.01	0.13	0.07	0.01	0.81	0.36	0.00
Y	b.d	0.00	0.00	b.d	0.02	0.00	b.d	0.03	0.01	b.d	0.00	0.01
Zr	b.d	0.02	0.02	0.55	0.19	0.01	0.14	0.10	0.01	b.d	0.01	0.02
Nb	b.d	0.01	0.00	0.15	0.08	0.01	0.05	0.05	0.01	b.d	0.01	0.01
Ba	b.d	0.06	0.05	2.42	0.74	0.03	b.d	0.22	0.04	2.05	1.48	0.06
La	b.d	0.01	0.01	0.17	0.07	0.01	b.d	0.02	0.00	0.12	0.13	0.01
Ce	b.d	0.01	0.00	0.32	0.09	0.00	b.d	0.00	0.01	b.d	0.09	0.01

TABELA C02 – Cont. Trace element concentration, limit of detection and uncertainties (2-sigma error) of olivine megacrysts from all samples. C - core; R - rim; I - intermediated; LOD - limit of detection; b.d - below detection.

Sample	TRIV-5-3	2σ error	LOD									
Grain/Analyses	06/12	06/12	06/12	07/13	07/13	07/13	07/14	07/14	07/14	08/15	08/15	08/15
Location	C	C	C	R	R	R	C	C	C	R	R	R
Li	1.37	0.26	0.09	1.02	0.42	0.09	1.33	0.44	0.09	0.78	0.38	0.10
Na	31.68	2.64	1.09	37.43	4.36	1.00	40.33	4.20	0.97	39.58	4.36	1.06
Al	7.39	0.90	0.29	11.00	1.98	0.27	8.51	1.58	0.26	21.93	2.82	0.29
P	b.d	11.54	9.36	b.d	24.20	8.50	b.d	21.78	8.22	b.d	22.04	8.56
Ca	b.d	158.96	124.69	b.d	306.84	116.59	b.d	274.08	113.05	b.d	305.90	124.66
Sc	1.14	0.19	0.07	0.98	0.34	0.06	0.63	0.26	0.06	2.66	0.54	0.06
Ti	7.05	1.70	0.20	1.98	1.94	0.22	b.d	1.22	0.24	3.28	2.32	0.23
V	1.49	0.22	0.05	4.73	0.76	0.05	4.44	0.68	0.05	1.26	0.38	0.06
Cr	60.47	4.78	0.34	91.38	7.94	0.32	84.65	7.40	0.30	32.39	3.40	0.33
Mn	801.15	53.90	0.18	742.92	51.62	0.17	813.59	56.86	0.16	955.96	68.80	0.17
Co	128.74	10.32	0.01	120.97	10.50	0.01	129.74	11.32	0.01	135.10	12.48	0.02
Ni	2872.86	245.32	0.09	2601.43	234.60	0.13	2878.95	265.24	0.08	2734.17	270.12	0.10
Cu	1.26	0.30	0.05	1.21	0.58	0.04	0.99	0.46	0.04	b.d	0.24	0.05
Zn	42.61	5.20	0.31	50.17	8.62	0.26	49.82	8.18	0.24	44.01	7.98	0.28
Sr	b.d	0.01	0.01	0.25	0.13	0.01	17.35	1.48	0.02	0.75	0.22	0.01
Y	b.d	0.00	0.00	b.d	0.00	0.01	b.d	0.05	0.01	b.d	0.03	0.01
Zr	b.d	0.02	0.01	0.24	0.18	0.01	b.d	0.07	b.d	0.13	0.12	0.01
Nb	0.04	0.03	0.01	0.18	0.12	0.01	b.d	0.00	0.00	b.d	0.06	0.01
Ba	b.d	0.12	0.07	0.51	0.50	0.05	1.90	0.84	0.06	2.43	1.00	0.03
La	0.01	0.01	0.00	b.d	0.00	0.00	b.d	0.02	0.01	b.d	0.02	0.01
Ce	b.d	0.01	0.01	b.d	0.00	0.01	0.07	0.06	0.01	b.d	0.05	0.01

TABELA C02 – Cont. Trace element concentration, limit of detection and uncertainties (2-sigma error) of olivine megacrysts from all samples. C - core; R - rim; I - intermediated; LOD - limit of detection; b.d - below detection.

Sample Grain/Analyses	TRIV-5-3 08/16	2σ error 08/16	LOD 08/16
Location	C	C	C
Li	0.60	0.24	0.11
Na	48.94	4.00	1.33
Al	28.08	2.64	0.36
P	b.d	17.16	11.30
Ca	1061.72	250.24	151.84
Sc	2.74	0.40	0.08
Ti	1.21	0.94	0.25
V	1.73	0.30	0.07
Cr	48.13	4.44	0.41
Mn	953.15	68.90	0.23
Co	149.07	13.74	0.02
Ni	3506.16	353.70	0.21
Cu	0.34	0.20	0.07
Zn	38.03	5.90	0.32
Sr	0.24	0.08	0.01
Y	b.d	0.01	0.01
Zr	b.d	0.02	0.01
Nb	b.d	0.02	0.01
Ba	b.d	0.05	0.09
La	b.d	0.02	0.01
Ce	0.05	0.03	0.01

TABELA C03 - Trace element concentration, limit of detection and uncertainties (2-sigma error) of perovskite from all samples. C - core; LOD - limit of detection; b.d - below detection.

Sample	LMI-C2 01/01	2σ error 01/01	LOD 01/01	LMI-C2 02/02	2σ error 02/02	LOD 02/02	LMI-C2 03/03	2σ error 03/03	LOD 03/03
Grain/Analyses	C	C	C	C	C	C	C	C	C
Location									
Mg	9219.63	980.64	0.38	1530.24	166.46	0.38	6811.59	748.54	0.38
Al	367.23	37.06	1.13	319.63	31.94	1.25	818.72	79.24	1.29
Sc	5.83	1.14	0.19	5.27	0.96	0.21	21.05	2.46	0.24
V	144.21	22.82	0.27	130.40	20.88	0.32	269.38	43.78	0.29
Mn	221.60	44.32	0.79	219.59	44.68	0.87	961.66	200.22	0.94
Fe	10924.46	2329.02	5.77	9768.59	2117.38	6.23	68475.43	15222.16	6.63
Sr	3336.73	661.04	0.11	3124.18	631.70	0.03	2930.42	610.68	0.06
Y	332.13	60.80	0.05	393.11	73.20	0.04	377.69	72.46	0.03
Zr	1291.36	257.28	0.35	1240.11	252.10	0.22	2122.53	444.48	0.26
Nb	4736.98	644.70	0.17	5178.63	716.40	0.02	7207.96	1023.66	0.10
Ba	31.96	8.78	0.26	20.12	5.78	0.24	16.63	5.24	0.39
La	8686.76	1479.80	0.27	10516.87	1833.46	0.04	10626.62	1913.84	0.07
Ce	22978.16	4175.06	0.55	28511.54	5303.34	0.04	29099.32	5593.12	0.08
Pr	3250.54	604.86	0.20	3913.39	746.24	0.02	3832.44	755.98	0.04
Nd	12462.24	2012.10	1.12	14642.16	2420.80	0.29	13847.76	2368.52	0.29
Sm	1563.64	221.78	0.50	1729.42	249.16	0.15	1539.25	228.88	0.21
Eu	346.12	34.28	0.12	362.07	36.06	0.05	315.67	32.30	0.07
Gd	786.63	62.02	0.46	802.06	62.60	0.13	675.59	53.98	0.15
Tb	73.52	6.34	0.07	67.06	5.72	0.03	58.87	5.16	0.02
Dy	245.19	19.02	0.35	229.31	17.14	0.11	204.59	15.76	0.15
Ho	25.66	2.66	0.05	25.71	2.56	0.02	24.36	2.50	0.03
Er	37.04	3.96	0.11	41.57	4.00	0.08	41.03	4.06	0.07
Tm	3.15	0.54	0.02	3.15	0.48	0.02	3.16	0.48	0.03
Yb	11.42	2.68	0.16	12.35	2.48	0.15	14.04	2.80	0.15
Lu	0.88	0.28	0.02	1.23	0.28	0.01	0.99	0.26	0.03
Hf	59.89	7.02	0.16	63.44	6.88	0.07	93.61	9.74	0.15
Ta	557.86	50.14	0.27	703.33	63.58	0.02	416.05	38.58	0.03
Pb	31.75	4.02	0.14	33.90	3.90	0.12	37.21	4.30	0.11
Th	2114.28	154.62	0.77	2314.00	169.34	0.02	1931.47	143.22	0.03
U	189.31	15.78	0.19	241.60	19.80	b.d	134.41	11.46	0.01

TABELA C03 – Cont. Trace element concentration, limit of detection and uncertainties (2-sigma error) of perovskite from all samples. C - core; LOD - limit of detection; b.d - below detection.

Sample Grain/Analyses	LMI-C2 04/04	2σ error 04/04	LOD 04/04	LMI-C2 05/05	2σ error 05/05	LOD 05/05	LMI-C2 06/06	2σ error 06/06	LOD 06/06
Location	C	C	C	C	C	C	C	C	C
Mg	248.86	29.84	0.31	819.04	97.16	0.28	228.01	31.58	0.28
Al	275.26	28.24	1.05	391.51	40.62	0.98	205.97	24.00	1.22
Sc	3.76	0.78	0.19	4.54	0.98	0.18	6.85	1.32	0.24
V	113.56	19.40	0.21	118.09	21.14	0.23	153.18	31.14	0.30
Mn	132.91	29.04	0.73	190.02	43.20	0.70	153.26	40.14	0.85
Fe	7503.51	1721.82	5.29	10863.76	2586.42	4.95	9217.09	2487.82	5.88
Sr	2841.73	614.06	0.04	2921.37	658.32	0.05	3087.88	799.76	0.03
Y	290.18	57.70	0.02	294.79	61.14	0.03	343.49	81.58	0.02
Zr	906.97	198.08	0.17	849.62	194.36	0.21	1836.10	483.20	0.22
Nb	4789.32	702.02	0.04	3860.21	587.62	0.05	7885.10	1359.92	0.03
Ba	17.10	5.22	0.29	20.39	6.52	0.14	20.29	7.16	0.12
La	10534.31	1971.22	0.05	8189.69	1601.44	0.08	12664.83	2865.92	0.04
Ce	30563.22	6106.54	0.10	24145.33	5042.96	0.16	36864.10	8919.94	0.06
Pr	4182.15	858.42	0.03	3506.55	753.22	0.06	5111.41	1276.28	0.04
Nd	16894.11	3005.32	0.30	14508.41	2701.46	0.38	19520.27	4222.46	0.40
Sm	1868.77	287.00	0.19	1635.85	262.56	0.16	2270.27	416.90	0.26
Eu	365.46	38.16	0.05	353.77	38.36	0.05	460.83	55.52	0.06
Gd	787.42	63.00	0.12	713.45	59.08	0.12	947.58	83.02	0.13
Tb	66.13	5.80	0.02	57.81	5.32	0.02	83.38	8.10	0.03
Dy	208.56	15.74	0.09	189.12	15.18	0.13	269.14	21.18	0.16
Ho	21.71	2.26	0.02	19.54	2.20	0.02	29.51	3.42	0.03
Er	33.01	3.34	0.08	29.84	3.36	0.06	44.88	4.84	0.05
Tm	2.11	0.36	0.02	1.86	0.38	0.01	3.16	0.54	0.02
Yb	7.93	1.86	0.14	8.43	2.18	0.15	14.37	3.24	0.13
Lu	0.76	0.22	0.02	0.71	0.24	0.02	1.27	0.34	0.03
Hf	45.39	5.32	0.14	43.77	5.62	0.09	103.85	12.16	0.13
Ta	994.91	93.60	0.03	870.91	84.50	0.12	900.28	96.20	0.03
Pb	81.88	8.18	0.05	60.09	6.66	0.12	61.18	7.24	0.09
Th	7838.06	585.14	0.06	5195.31	395.16	0.57	5133.68	413.12	b.d
U	217.50	18.36	0.01	172.09	15.10	0.12	159.49	15.08	b.d

TABELA C03 – Cont. Trace element concentration, limit of detection and uncertainties (2-sigma error) of perovskite from all samples. C - core; LOD - limit of detection; b.d - below detection.

Sample	LMI-C2 07/07	2σ error 07/07	LOD 07/07	LMI-C2 08/08	2σ error 08/08	LOD 08/08	LMI-C2 09/09	2σ error 09/09	LOD 09/09
Grain/Analyses	C	C	C	C	C	C	C	C	C
Location									
Mg	284.49	40.96	0.26	701.17	98.64	0.51	414.02	61.10	0.37
Al	289.38	34.26	1.08	266.29	31.26	0.98	209.29	25.48	1.06
Sc	9.00	1.74	0.21	4.32	1.00	0.19	3.64	0.88	0.19
V	144.24	31.02	0.21	129.67	29.00	0.23	137.94	32.24	0.24
Mn	145.34	40.10	0.76	152.31	43.82	0.70	172.67	51.96	0.74
Fe	11400.31	3215.90	5.20	8906.89	2623.08	4.78	8345.01	2565.30	4.97
Sr	3888.94	1056.96	0.03	3201.86	911.84	0.04	3177.16	947.70	0.04
Y	432.23	107.66	b.d	309.22	80.64	0.02	347.36	94.76	0.02
Zr	2207.42	611.00	0.08	1004.78	292.48	0.19	1432.34	436.82	0.22
Nb	10141.74	1828.72	0.07	4535.48	853.24	0.03	5607.11	1100.60	0.04
Ba	23.30	8.78	0.22	13.06	5.30	0.25	16.73	6.54	0.17
La	15314.18	3647.02	0.07	10294.13	2576.28	0.06	10948.69	2879.26	0.05
Ce	41712.41	10623.44	0.11	30294.74	8110.00	0.09	30162.46	8485.38	0.11
Pr	5133.87	1350.98	0.04	4207.20	1165.24	0.04	4134.08	1204.86	0.04
Nd	21113.63	4813.50	0.24	16342.56	3919.92	0.32	16448.37	4150.78	0.32
Sm	2294.09	442.86	0.18	1802.74	364.20	0.14	1864.02	394.38	0.18
Eu	462.90	58.36	0.06	354.10	46.28	0.04	386.29	52.46	0.05
Gd	1050.98	95.38	0.13	776.73	71.80	0.11	846.67	79.96	0.11
Tb	87.59	8.88	0.02	66.94	6.92	0.02	74.50	7.86	0.02
Dy	288.97	23.74	0.08	207.13	16.94	0.11	256.68	20.46	0.11
Ho	32.16	3.92	0.02	24.18	3.00	0.02	27.54	3.46	0.02
Er	52.50	5.94	0.06	38.19	4.32	0.06	44.68	4.92	0.06
Tm	3.41	0.64	0.02	3.10	0.52	0.02	3.12	0.52	0.01
Yb	15.79	3.86	0.09	9.89	2.54	0.16	11.70	2.82	0.14
Lu	1.16	0.38	0.03	1.16	0.32	0.02	0.93	0.26	0.01
Hf	129.00	15.70	0.07	61.41	8.10	0.08	70.97	9.28	0.05
Ta	801.86	89.20	0.03	1035.40	118.70	0.04	679.43	80.88	0.03
Pb	49.28	6.56	0.10	77.75	9.24	0.06	45.02	5.84	0.07
Th	3945.71	326.36	0.04	6773.23	568.84	0.09	3400.31	292.36	0.06
U	182.34	17.86	b.d	195.11	19.20	0.01	241.19	24.22	0.01

TABELA C03 – Cont. Trace element concentration, limit of detection and uncertainties (2-sigma error) of perovskite from all samples. C - core; LOD - limit of detection; b.d - below detection.

Sample Grain/Analyses Location	LMI-C2 10/10 C	2σ error 10/10 C	LOD 10/10 C	LMI-C2 11/11 C	2σ error 11/11 C	LOD 11/11 C	TRIV-5 01/01 C	2σ error 01/01 C	LOD 01/01 C
Mg	1387.47	207.62	0.29	2182.95	337.28	0.46	771.16	128.92	0.35
Al	229.00	28.16	0.99	523.07	62.54	1.15	199.22	35.14	1.00
Sc	5.14	1.06	0.19	3.05	0.72	0.22	6.38	1.62	0.18
V	132.31	32.36	0.22	117.72	30.04	0.30	38.46	8.28	0.23
Mn	173.49	54.62	0.68	156.52	51.46	0.79	91.09	17.38	0.72
Fe	7763.10	2488.84	4.66	7358.99	2457.48	5.29	8993.24	874.24	4.63
Sr	2437.82	760.84	0.04	2528.02	824.22	0.05	6112.51	1343.90	0.03
Y	318.05	90.72	0.03	262.23	78.08	0.03	185.61	42.86	0.03
Zr	1166.80	373.16	0.19	890.01	297.88	0.22	1485.25	252.80	0.22
Nb	5149.99	1053.98	0.05	3940.22	839.58	0.03	11720.19	2087.66	0.02
Ba	11.88	5.04	0.16	27.09	10.10	0.32	83.06	17.92	0.15
La	8906.64	2458.98	0.07	9079.98	2628.22	0.06	25408.83	3496.78	0.02
Ce	26218.47	7743.40	0.11	27453.06	8500.48	0.07	53633.45	5668.94	0.03
Pr	3438.42	1053.56	0.05	3848.53	1238.04	0.03	5262.64	781.34	0.02
Nd	13709.46	3636.66	0.28	15731.23	4379.74	0.31	18143.84	2708.94	0.28
Sm	1532.60	339.66	0.20	1739.55	402.48	0.21	1615.06	210.06	0.18
Eu	330.09	46.72	0.05	354.72	52.02	0.04	309.68	44.48	0.05
Gd	678.51	66.08	0.12	760.78	75.20	0.15	774.80	91.10	0.14
Tb	61.16	6.68	0.02	65.30	7.24	0.03	54.79	7.12	0.02
Dy	223.08	18.08	0.09	204.14	16.22	0.10	155.33	28.60	0.11
Ho	22.88	3.00	0.02	23.10	3.04	0.02	14.63	2.54	0.02
Er	41.42	4.64	0.05	36.60	4.04	0.05	23.72	4.54	0.08
Tm	3.00	0.50	0.02	2.57	0.40	0.02	1.52	0.42	0.02
Yb	13.15	3.04	0.07	9.81	2.28	0.13	4.67	1.82	0.10
Lu	1.00	0.28	0.02	0.67	0.19	0.02	0.53	0.24	0.02
Hf	63.14	8.54	0.06	53.82	7.28	0.09	68.71	11.00	0.10
Ta	590.77	72.96	0.04	841.73	107.46	0.03	1564.97	251.04	0.02
Pb	42.74	5.66	0.06	67.10	8.34	0.08	120.74	16.62	0.10
Th	3852.60	338.86	0.11	5737.75	515.26	0.05	7477.90	827.30	0.02
U	147.22	15.36	0.02	192.99	20.38	0.02	212.98	23.84	b.d

TABELA C03 – Cont. Trace element concentration, limit of detection and uncertainties (2-sigma error) of perovskite from all samples. C - core; LOD - limit of detection; b.d - below detection.

Sample	TRIV-5	2σ error	LOD	TRIV-5	2σ error	LOD	TRIV-5-3	2σ error	LOD
Grain/Analyses	02/02	02/02	02/02	03/03	03/03	03/03	04/04	04/04	04/04
Location	C	C	C	C	C	C	C	C	C
Mg	875.84	152.28	0.35	2022.66	392.06	0.52	4005.62	405.04	0.26
Al	313.65	56.36	1.14	236.93	47.56	1.21	620.84	63.22	1.03
Sc	4.66	1.34	0.21	4.28	1.28	0.24	9.22	1.22	0.18
V	37.65	8.44	0.26	43.39	10.66	0.27	37.06	3.66	0.27
Mn	164.83	32.30	0.76	252.99	55.76	0.85	198.28	14.70	0.68
Fe	9828.50	982.78	5.25	8307.99	904.22	5.60	11549.50	1354.20	5.28
Sr	6815.82	1577.70	0.06	6205.63	1646.60	0.06	6623.87	484.48	0.04
Y	235.20	56.96	0.03	217.08	60.04	0.02	199.14	20.62	0.03
Zr	1177.58	210.82	0.26	813.87	166.04	0.32	2151.43	172.36	0.18
Nb	9184.22	1717.88	0.07	7316.96	1560.04	0.07	11794.30	1110.64	0.05
Ba	110.66	23.70	0.25	70.37	17.08	0.24	290.17	44.52	0.18
La	24859.72	3561.10	0.11	22397.19	3590.66	0.12	21709.87	3883.70	0.06
Ce	52774.90	5765.30	0.19	50530.84	6078.84	0.13	45697.62	6756.08	0.09
Pr	5304.20	820.42	0.07	5653.26	980.54	0.05	4779.28	705.64	0.03
Nd	20046.45	3121.20	0.48	19790.77	3464.80	0.35	17839.40	2401.04	0.21
Sm	1729.38	233.74	0.26	1806.90	272.42	0.15	1553.68	157.98	0.15
Eu	357.17	53.28	0.05	340.16	56.68	0.05	295.86	43.54	0.04
Gd	885.74	107.68	0.16	794.49	107.02	0.14	687.93	116.44	0.11
Tb	63.82	8.52	0.03	56.70	8.32	0.03	48.65	7.86	0.02
Dy	192.96	36.72	0.11	170.52	36.38	0.11	148.48	20.52	0.10
Ho	18.32	3.22	0.02	15.69	3.04	0.03	14.50	2.02	0.01
Er	28.25	5.44	0.04	28.51	5.92	0.09	27.72	3.80	0.05
Tm	1.74	0.46	0.03	1.59	0.42	0.03	1.38	0.30	0.01
Yb	6.44	2.24	0.13	7.40	2.44	0.18	6.83	1.64	0.11
Lu	0.61	0.26	0.02	0.62	0.24	0.03	0.51	0.18	0.02
Hf	53.13	9.06	0.10	40.99	7.66	0.08	93.90	13.72	0.07
Ta	1227.51	205.92	0.07	1193.75	226.18	0.05	871.68	109.84	0.03
Pb	77.02	11.32	0.13	89.20	13.94	0.11	66.62	5.80	0.06
Th	5572.01	636.90	0.20	5711.78	718.16	0.16	3808.97	316.38	0.06
U	186.25	21.58	0.05	197.59	24.98	0.02	213.96	17.76	0.02

TABELA C03 – Cont. Trace element concentration, limit of detection and uncertainties (2-sigma error) of perovskite from all samples. C - core; LOD - limit of detection; b.d - below detection.

Sample Grain/Analyses	TRIV-5-3 05/05	2σ error 05/05	LOD 05/05
Location	C	C	C
Mg	5256.41	602.90	0.30
Al	1586.65	176.98	1.05
Sc	2.49	0.66	0.20
V	46.35	4.32	0.25
Mn	168.37	13.20	0.72
Fe	8592.28	1264.36	5.47
Sr	4918.99	396.78	0.02
Y	161.72	20.32	0.03
Zr	463.47	45.02	0.21
Nb	5616.00	631.22	0.02
Ba	74.62	15.82	0.21
La	18922.63	4341.50	0.03
Ce	43498.28	8128.98	0.02
Pr	5149.95	965.08	0.03
Nd	18398.01	3093.02	0.30
Sm	1506.56	182.18	0.18
Eu	280.17	52.00	0.03
Gd	670.60	144.08	0.14
Tb	42.88	8.76	0.01
Dy	129.99	22.34	0.10
Ho	11.70	2.00	0.01
Er	20.54	3.44	0.06
Tm	1.15	0.28	0.02
Yb	4.07	1.30	0.13
Lu	0.35	0.15	0.02
Hf	21.18	4.38	0.08
Ta	1147.64	180.04	0.03
Pb	101.95	8.50	0.07
Th	8123.66	771.52	0.01
U	147.78	13.98	b.d

TABELA C04 - Trace element concentration, limit of detection and uncertainties (2-sigma error) of clinopyroxene from all samples. *C* - core; *R* - rim; *LOD* - limit of detection; *b.d* - below detection.

Sample	LMI-B1-2 01/01	2σ error 01/01	LOD 01/01	LMI-B1-2 01/02	2σ error 01/02	LOD 01/02
Grain/Analyses			R	C	C	C
Location	R	R	R	C	C	C
Sc	5.61	1.00	0.14	6.22	1.00	0.15
V	52.69	4.46	0.12	52.80	4.54	0.12
Cr	950.30	63.62	0.89	833.68	60.36	0.95
Mn	1613.22	103.52	0.53	1009.26	68.30	0.50
Co	67.45	6.22	0.06	40.21	4.46	0.04
Ni	930.36	66.58	0.44	351.23	28.82	0.30
Zn	56.37	10.30	0.63	48.90	8.76	0.79
Rb	9.02	1.32	0.05	17.71	2.08	0.08
Sr	2223.24	147.72	0.02	2647.87	193.32	0.10
Y	2.90	0.56	0.02	7.19	0.86	0.02
Zr	10.66	1.52	0.04	87.16	6.60	0.03
Nb	11.99	1.42	0.02	18.19	1.86	0.02
Cs	b.d	0.52	0.02	b.d	0.28	0.01
Ba	81.07	10.34	0.12	110.90	15.10	0.17
La	16.74	1.88	0.02	15.65	2.10	0.02
Ce	32.19	2.70	0.01	34.99	3.02	0.02
Pr	4.21	0.68	0.02	5.01	0.84	0.02
Nd	10.99	2.68	0.19	16.77	3.30	0.11
Sm	2.47	1.18	0.13	3.39	1.40	0.12
Eu	0.89	0.42	0.04	0.75	0.42	0.03
Gd	1.25	0.74	0.09	2.83	1.02	0.08
Tb	0.19	0.13	0.02	0.26	0.14	0.02
Dy	b.d	0.32	0.06	1.55	0.82	0.10
Ho	b.d	0.07	0.02	0.17	0.10	0.01
Er	b.d	0.14	0.04	0.57	0.34	0.04
Tm	b.d	0.07	0.01	b.d	0.05	0.02
Yb	b.d	0.26	0.09	b.d	0.24	0.05
Lu	b.d	0.04	0.02	b.d	0.05	0.02
Hf	b.d	0.32	0.13	1.49	0.84	0.13
Ta	0.67	0.22	0.02	1.52	0.36	0.02
Th	1.49	0.36	b.d	1.98	0.46	0.01
U	0.16	0.11	0.01	0.17	0.10	b.d

TABELA C05 - Trace element concentration, limit of detection and uncertainties (2-sigma error) of garnet from all samples. *C* - core; *R* - rim; *LOD* - limit of detection; *b.d* - below detection.

Sample	TRIV-5-2	2σ error	LOD	TRIV-5-2	2σ error	LOD
Grain/Analyses	01/01	01/01	01/01	01/02	01/02	01/02
Location	R	R	R	C	C	C
Li	b.d	0.54	0.31	b.d	0.60	0.31
Sc	124.64	9.74	0.26	122.10	9.28	0.23
Ti	319.92	45.44	1.60	645.10	69.74	1.15
V	321.12	22.70	0.22	311.37	21.68	0.23
Co	42.87	4.68	0.06	41.48	4.26	0.06
Ni	49.22	23.80	1.54	36.15	18.82	2.58
Zn	14.86	8.24	1.82	11.32	6.42	1.48
Ga	7.50	2.04	0.10	8.37	1.96	0.06
Rb	b.d	0.32	0.13	b.d	0.24	0.09
Sr	47.34	4.26	0.03	5.11	0.94	0.03
Y	1.95	0.58	0.02	3.00	0.66	0.04
Zr	3.30	1.06	0.06	29.35	3.32	0.06
Nb	b.d	0.17	0.04	0.38	0.26	0.04
Cs	b.d	0.09	0.04	b.d	0.07	0.03
Ba	b.d	0.64	0.24	b.d	0.88	0.24
La	b.d	0.12	0.04	b.d	0.16	0.04
Ce	b.d	0.12	0.04	1.32	0.42	0.03
Pr	b.d	0.09	0.03	0.29	0.18	0.03
Nd	b.d	0.56	0.17	1.38	0.98	0.19
Sm	b.d	0.08	0.13	b.d	0.84	0.20
Eu	b.d	0.28	0.05	b.d	0.19	0.02
Gd	b.d	0.40	0.15	b.d	0.54	0.16
Tb	b.d	0.11	0.03	b.d	0.11	0.03
Dy	b.d	0.48	0.16	b.d	0.28	0.14
Ho	b.d	0.11	0.03	b.d	0.05	0.02
Er	b.d	0.26	0.07	0.40	0.36	0.06
Tm	b.d	0.06	0.03	b.d	0.07	0.02
Yb	b.d	0.60	0.10	0.68	0.64	0.16
Lu	b.d	0.09	0.04	b.d	0.09	0.03
Hf	b.d	0.14	0.22	b.d	0.60	0.21
Ta	b.d	0.02	0.03	b.d	0.05	0.02
Th	b.d	0.07	b.d	b.d	0.08	0.02
U	b.d	b.d	b.d	b.d	0.06	b.d

APPENDIX D

XRF AND ICP-MPS DATA

TABELA D01 - Whole rock major element concentration in mass.% for Três Ranchos IV and Limeira I kimberlite.

	LM-3	LMI-B1	LMI-C1	TR-4	TRIV-5	TRIV-9	TRIV-9
SiO ₂	29.19	29.79	30.14	34.57	33.03	32.85	32.64
TiO ₂	2.41	2.33	2.37	1.05	1.29	1.22	1.13
Al ₂ O ₃	1.86	1.81	1.98	2.21	2.08	2.01	1.81
Fe ₂ O ₃	10.93	11.06	11.00	9.44	9.36	9.26	9.21
MnO	0.20	0.20	0.20	0.19	0.19	0.18	0.18
MgO	29.26	30.48	30.48	34.64	31.08	31.75	32.35
CaO	12.15	10.74	10.78	3.68	8.35	7.92	7.80
Na ₂ O	<0.02	<0.03	<0.04	<0.05	0.06	0.05	0.06
K ₂ O	1.16	0.97	0.88	0.69	1.18	1.07	0.96
P ₂ O ₅	2.27	2.43	2.47	1.10	1.40	1.38	1.36
Total	99.08	99.03	100.12	98.51	99.00	98.68	98.43
Mg#	73	73	73	79	77	77	78
LoI	9.64	9.22	9.82	10.94	10.98	10.99	10.92

TABELA D02 - Whole rock trace element concentration in ppm for Três Ranchos IV and Limeira I kimberlite. Analyses performed by ¹ICP-MS e ²XRF.

	LM-3	LMI-B1	LMI-C1	TR-4	TRIV-5	TRIV-9	TRIV-9
Rb ¹	124	106	103	60.9	104	95.5	94.2
Rb ²	120	102	99	60	106	105	96
Sr ¹	2221	2245	2304	2055	2174	2060	2039
Sr ²	2281	2307	2353	2152	2295	2263	2143
Y ¹	34.1	33.7	33.8	23	22.4	22.8	21.5
Zr ¹	629	688	658	342	362	363	358
Zr ²	542	571	574	319	341	337	337
Co ²	84	86	85	94	88	90	86
Cr ²	1390	1523	1408	1754	1727	1750	1617
Nb ¹	209	221	227	311	323	325	324
Nb ²	187	191	195	272	288	285	281
Ga ²	9	9	9	9	9	9	9
Cu ²	50	40	42	18	32	32	22
Ni ²	1216	1256	1250	1634	1469	1469	1491
Cs ¹	2.1	1.6	1.6	1.6	1.9	1.8	1.8
Ba ¹	2476	2342	2417	3422	4863	4706	4709
Ba ²	2623	2512	2543	3224	4831	4993	4657
La ¹	277	288	298	389	400	406	407
La ²	258	268	278	369	397	423	394
Ce ¹	559	575	596	664	695	700	708
Ce ²	461	446	472	529	558	556	548
Zn ²	87	81	79	75	70	71	70
Sc ²	28	29	28	16	23	24	20
Pr ¹	62.6	65	67.8	66.1	67.9	67.7	69.2
Nd ¹	197	205	209	181	185	186	185
Nd ²	194	197	196	164	180	180	165
Sm ¹	31.2	32.7	33.2	23.7	24.1	24.1	23.8
Eu ¹	7.6	7.8	8.1	5.5	5.8	5.9	5.8
Gd ¹	21.3	22.2	23	16.8	17.3	16.8	17.1
Tb ¹	2.1	2.2	2.2	1.4	1.5	1.4	1.5
Dy ¹	9.7	9.9	10.3	6.8	6.8	6.8	7.0
Ho ¹	1.3	1.3	1.4	0.9	0.8	0.9	0.9
Er ¹	2.9	3.0	3.1	2.1	2.0	2.0	2.1
Tm ¹	0.3	0.3	0.3	0.2	0.2	0.2	0.2
Yb ¹	1.7	1.7	1.7	1.2	1.1	1.1	1.2
Lu ¹	0.2	0.2	0.2	0.2	0.2	0.2	0.2
Hf ¹	11.8	13.1	12.5	6.1	6.3	6.4	6.4
Pb ¹	10.1	9.8	9.3	15	15.3	15	15.2
Pb ²	15	15	15	15	18	15	17
Th ¹	19.8	20.9	21.5	31.6	32.3	33	32.5
Th ²	36	35	37	45	51	49	51
V ²	164	155	153	31	140	143	103
Y ²	33	33	33	22	23	22	22
U ²	26	25	26	24	28	26	26
U ¹	4.9	5.0	5.2	7.3	7.8	7.5	7.5
F	1407	1712	2357	2155	2339	2098	2386
Cl	500	500	500	500	500	500	500
S	785	550	550	550	700	718	619

APPENDIX E

THERMOBAROMETRY DATA

TABELA E01 - Thermobarometry data obtained in this work from Três Ranchos IV and Limeira I kimberlite and compiled from APAP.

Intrusion	Reference (author)	Lithotype	Wells (1977)	Finnerty and Boyd (1986)	Balhaus (1991)	Brey & Koehler (1990)	MacGregor (1974)	Brey et al. (2008)	Nimis and Taylor (2000)	Canil (1999)	Bussweiler et al. (2017)	Read et al. (2004)	Grütter et al. (2006)
Três Ranchos IV	This work	peridotitic to lherzolitic garnet xenocryst	-	-	-	-	-	-	-	-	975 ± 19°C- 24°C	1270 ± 13°C	18- 34Kbar
	Costa (2008)	garnet lherzolite	974°C	1065°C/50Kbar	-	-	-	51Kbar	43Kbar	1007°C/59Kbar	-	-	-
		spinel phlogopite lherzolite	1037°C	1139°C/40Kbar	-	-	-	45Kbar	36Kbar	1082°C/49Kbar	-	-	-
	Leonardos et al. (1993)	garnet lherzolite	743 ± 18°C	-	890 ± 30 °C	855 ± 60°C	-	-	-	-	-	-	-
Limeira I	This work	garnet-facies clinopyroxene xenocryst	977- 1120°C	1273°C/57- 57Kbar	-	-	-	55-72Kbar	-	-	-	-	-
	Almeida (2009)	spinel lherzolite	822°C	-	638°C	854°C	-	-	-	-	718-986°C	-	985 ± 13°C- 47Kbar

TABELA E01 – Cont. Thermobarometry data obtained in this work from Três Ranchos IV and Limeira I kimberlite and compiled from APAP.

Intrusion	Reference (author)	Lithotype	Wells (1977)	Finnerty and Boyd (1986)	Balhaus (1991)	Brey & Koehler (1990)	MacGregor (1974)	Nimis and Brey et al. (2008)	Taylor (2000)	Canil (1999)	Bussweiler et al. (2017)	Read et al. (2004)	Grütter et al. (2006)
Indaiá	Nannini et al. (2011)	Cromite harzburgite	901°C	908°C	-	-	-	36Kbar	-	-	-	-	-
		Spinel harzburgite	656- 724°C	529-650°C	-	-	-	26Kbar	-	-	-	-	-
Canastra 1	Costa (2008)	garnet lherzolite	-	1255- 1282°C/59 -66Kbar	-	1141- 1168°C	57-58Kbar	57- 60Kbar	57- 60Kbar	57- 60Kbar	1232- 1257°C/51 -59Kbar	-	-
		Thomaz (2009)	garnet lherzolite	1053° C	-	-	1350°C/ 32Kbar	-	40Kbar	41Kbar	-	-	-
APAP	Read et al. (2004)	Spinel- facies cli- nopyroxen es	-	-	-	-	-	-	-	625-875°C	-	-	-
		xenocrysts	Garnet- facies	-	-	-	-	-	-	700-1000 °C	-	-	-